UNIVERSITY OF SOUTHAMPTON

FACULTY OF NATURAL AND ENVIRONMENTAL SCIENCES

Chemistry

Biochemical Characterisation and Exploitation of the

Enzyme RelA from Biothreat Agents

by

Rachael Claire Wilkinson

Thesis for the degree of Doctor of Philosophy

October 2015

UNIVERSITY OF SOUTHAMPTON

ABSTRACT

FACULTY OF NATURAL AND ENVIRONMENTAL SCIENCES

Chemistry

Thesis for the degree of Doctor of Philosophy

BIOCHEMICAL CHARACTERISATION AND EXPLOITATION OF THE ENZYME RELA FROM BIOTHREAT AGENTS

Rachael Claire Wilkinson

Recent years have seen a rise in bacterial resistance to clinically available antibiotics in tandem with a decrease in the discovery of novel antimicrobials. Consequently this has renewed concern over pathogenic bacteria, for which treatment has previously been available. One method of overcoming antibacterial resistance is the identification of new inhibitors against novel targets within bacteria. The stringent response is essential to bacterial survival during unfavourable conditions and is underpinned by the actions of the signalling molecules guanosine penta- and tetra-phosphate. In β- and γ-proteobacteria the synthesis of these molecules is predominantly catalysed by the enzyme RelA. Knockouts of genes encoding RelA result in reduced virulence within several pathogenic bacteria. The focus of this project was to characterise the RelA enzymes from the biothreat agents *Francisella tularensis* (*F. tularensis*), *Yersinia pestis* (*Y. pestis*) and *Burkholderia pseudomallei* (*B. pseudomallei*) and develop a method for identifying inhibitors of RelA.

F. tularensis RelA purified as a stable dimer that could be concentrated to 10 mg/mL, which is higher than that reported for other RelA enzymes. *F. tularensis* RelA demonstrated strict specificity for GTP as a pyrophosphate acceptor, except in the presence of methanol. Substrate specificity was not observed for the other RelA enzymes investigated. Steady state kinetic characterisation of *F. tularensis* RelA consistently generated data that fitted a sigmoidal function (R^2 = 0.95). Kinetic parameters calculated for *F. tularensis* RelA gave a V_{max} of 12.27 (± 0.37) × 10^{-3} s^{-1} and 14.02 (± 0.90) × 10^{-3} s^{-1} and $K_{1/2}$ values of 351.5 ± 15 μM and 1072 ± 84 μM for ATP and GTP respectively. *F. tularensis*

RelA was shown to be activated by stalled ribosomal complexes from *Escherichia coli* (11 fold) and to a lesser extent those from *F. philomiragia* (1.39 fold). Activation of RelA was observed upon the addition of ppGpp, EC_{50} of 60 ± 1.9 μM, which demonstrated that the ACT domain is not involved in this process.

A high throughput method for the screening of inhibitors of *F. tularensis* RelA was developed. This method demonstrated a good screening window with a high Z' factor. The high throughput method was validated against a small library of focussed molecules.

Table of Contents

List of Tables

List of Figures

DECLARATION OF AUTHORSHIP

I, Rachael Claire Wilkinson declare that this thesis entitled 'Biochemical characterisation and exploitation of the enzyme RelA from biothreat agents' and the work presented in it are my own and has been generated by me as the result of my own original research.

I confirm that:

1. This work was done wholly or mainly while in candidature for a research degree at this University;
2. Where any part of this thesis has previously been submitted for a degree or any other qualification at this University or any other institution, this has been clearly stated;
3. Where I have consulted the published work of others, this is always clearly attributed;
4. Where I have quoted from the work of others, the source is always given. With the exception of such quotations, this thesis is entirely my own work;
5. I have acknowledged all main sources of help;
6. Where the thesis is based on work done by myself jointly with others, I have made clear exactly what was done by others and what I have contributed myself;
7. Parts of this work have been published as: Wilkinson, R. C., Batten, L. E., Wells, N. J., Oyston, P. C., & Roach, P. L. (2015). Biochemical studies on Francisella tularensis RelA in (p) ppGpp Biosynthesis. Bioscience reports.

Signed: .....

Date: .....

Acknowledgements

I first would like to acknowledge the work by Dr. L. Batten and Miss C. Frankling which is mentioned within this thesis. I would like to thank my supervisor Prof. P. Roach and collaborative supervisor Prof. P. Oyston for devising the project in which I have completed my PhD. The work has been fascinating, even if it has been largely unpredictable. I would like to thank Dr. N. Wells for his assistance with all the NMR experiments described within this thesis. I thank DTRA for the funding they have provided throughout my PhD. Finally, I would like to thank the members of the Roach group and Level 5 who have made the time during my PhD more enjoyable, and tea filled.

Definitions and Abbreviations

2 × YT – 2 × Yeast extract Tryptone

A site – Acceptor site

aa – amino acids

ABTS - 2,2’-azino-bis(3-ethylbenzthiazoline-6-sulfonic acid)

ACP – Acyl Carrier Protein

ACT – Aspartate kinase, Chorismate mutase, TyrA

AMP – adenosine monophosphate

AMPCPP – α, β-Methyleneadenosine 5’-triphosphate

AMPPNP – β, γ-imidoadenosine 5’ triphosphate

ATP – adenosine triphosphate

A_{xxx} – absorbance at a specified wavelength

B. pseudomallei – *Burkholderia pseudomallei*

B. subtilis – *Bacillus subtilis*

BIT - Bronopol and 1,2-benziothiazolin-3-one

BSA – Bovine Serum Albumin

Bsa – *Burkholderia* secretion apparatus

CC – conserved cysteine

CDC – Centers for Disease Control and Prevention

CFU – Colony Forming Unit

Cryo-EM – cryo-electron microscopy

CTD – C-terminal domain

CTP – cytosine triphosphate

D_2O – deuterium oxide

ddGTP – dideoxy guanosine triphosphate

DFMO - α-difluoromethylornithine

DMHA – dimethylhexylamine

DMSO – dimethyl sulfoxide

DNA – deoxyribose nucleic acid

DNA-Ag - deoxyribose nucleic acid silver

DTT – dithiothreitol

E site – Exit site

E. coli – *Escherichia coli*

EC_{50} – half maximal effective concentration

EHEC - Enterohemorrhagic *Escherichia coli*

ELISA - Enzyme-Linked Immunosorbent Assay

EMSA - Electrophoretic Mobility Shift Assay

ESI – Electrospray Ionisation

F. philomiragia – *Francisella philomiragia*

FDA – US Food and Drug Administration

FPI – *Francisella* Pathogenicity Island

FRET – Fluorescence Resonance Energy Transfer

GDP – guanosine diphosphate

GST - Glutathione S-Transferase

GTP – guanosine triphosphate

h – Hill coefficient

HD – Hydrolase Domain

HEPES - 4-(2-hydroxyethyl)-1-piperazineethanesulfonic acid

HFIP – hexafluoroisopropanol

HGT – Horizontal Gene Transfer

HPLC – high performance liquid chromatography

HQNO - 4-hydroxy-2-heptylquinoline-*N*-oxide

HSL – 3-oxo-C_{12}-homoserine lactone

HTS – High Throughput Screening

iNOS – inducible nitric oxide synthase

iNTP – initiating nucleotide triphosphate

IPTG – isopropyl β-D-1-thiogalactopyranoside

ITC – Isothermal Titration Calorimetry

$K_{1/2}$ – concentration of substrate required to give half maximal velocity

K_{cat} – catalytic turnover

kDa – kilodalton

K_M – Michaelis-Menten constant

LB – Luria Broth

LCMS – Liquid Chromatography Mass Spectrometry

LEE - locus of enterocyte effacement

LVS – *Francisella tularensis* live vaccine strain

M. tuberculosis – *Mycobacterium tuberculosis*

MAD – multiple wavelength anomalous diffraction

MBP – Maltose-Binding Protein

MESG - 2-amino-6-mercapto-7-methylpurine riboside

MGNC – Multinucleated Giant Cell

MIC – Minimal Inhibitory Concentration

mRNA – messenger ribonucleic acid

NDP – nucleotide diphosphate

Ni-IDA – nickel iminodiacetic acid

NMR – Nuclear Magnetic Resonance

NTD – N-terminal domain

NTP – nucleotide triphosphate

OD_{XXX} – optical density at a specified wavelength

P site – Peptidyl transferase site

PCR – Polymerase Chain Reaction

PEI - polyethylenimine

PKIS - Published Kinase Inhibitor Set

PNP – Purine Nucleoside Phosphorylase

PO_4^{3-}/ Pi – inorganic phosphate

ppApp – adenosine tetraphosphate

ppGpp – guanosine tetraphosphate

ppm – parts per million

pppGpp – guanosine pentaphosphate

(p)ppGpp – guanosine penta-/tetra-phosphate

RAC – RelA Activating Complex

RNA – Ribose Nucleic Acid

RNAP – ribonucleic acid polymerase

rrn – ribosomal ribonucleic acid promoter

rRNA – ribosomal ribonucleic acid

RSH – RelA/ SpoT Homologue

SAH – Small Alarmone Hydrolase

SAS – Small Alarmone Synthetase

SDS-PAGE – sodium dodecyl sulphate polyacrylamide gel electrophoresis

SOC – Super Optimal broth with Catabolite repression

T3SS – Type Three Secretion System

TBF – Transformation Buffer

TGS – Threonyl-tRNA synthetase, GTPase and SpoT

TLC – Thin Layer Chromatography

tRNA – transfer ribonucleic acid

$tRNA^{fmet}$ – N-formylmethionine charged transfer ribonucleic acid

$tRNA^{val}$ – valine charged transfer ribonucleic acid

TSB – Trypticase Soy Broth

US – United States

USSR – Union of Soviet Socialist Republics

vHTS – virtual High Throughput Screening

V_{max} – maximum velocity

WT – Wild Type

Y. pestis – *Yersinia pestis*

α-MG – α-methylglucoside

β-Me – β-mercaptoethanol

Chapter 1: **Introduction**

1.1 Antibiotic Resistance and Drug Discovery

1.1.1 Antibiotics

Antibacterial agents are compounds capable of either killing (bactericidal) or stunting the growth (bacteriostatic) of bacteria [1]. Clinical use of antibacterial agents have been reported since the 1930s with the use of Sulfa drugs [2]. The following decade saw the introduction of penicillin, one of the most widely used antibiotics to date [3]. The so called golden era of antibiotic drug discovery spanned the 1940s to the 1960s, with the discovery of only a few new classes of antibiotic since then (Figure 1.1.2). However, in January 2015 the discovery of teixobactin, via the novel method of isolation Chip (iChip), from the previously uncultured and undescribed soil bacterium *Eleftheria terrae* was published [4, 5]. Teixobactin is a cyclic depsipeptide containing the unusual amino acid enduracididine (Figure 1.1.1) [4]. It inhibits cell wall synthesis by binding to a highly conserved non-peptide motif in the peptidoglycan precursor (lipid II) and teichoic acid precursor (lipid III) [4].

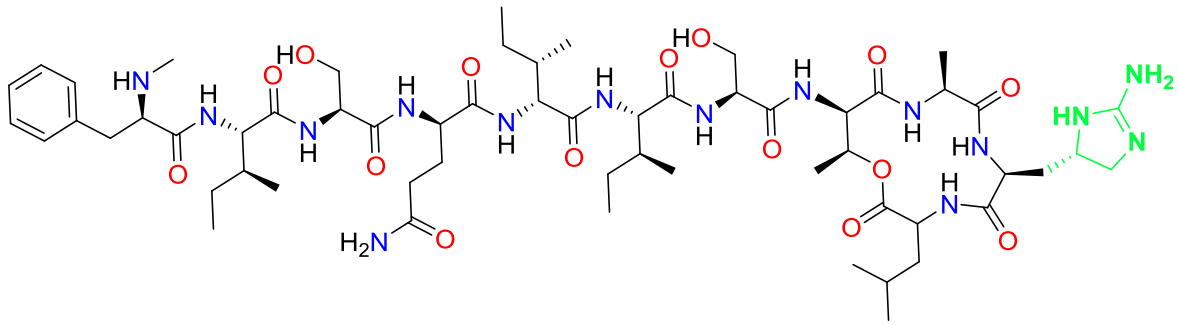

Figure1.1.1. Chemical structure of the new antibiotic teixobactin, with the unusual amino acid enduracididine highlighted in green.

Comparison of death rates resulting from infectious disease following widespread deployment of antibiotics showed a 20 fold reduction between 1900 and 1980 [6]. Antibiotic discovery can be generally approached by one of two means; the isolation of

natural products with antibacterial properties [7] or the purposeful synthesis of antibacterial agents by medicinal chemists [8].

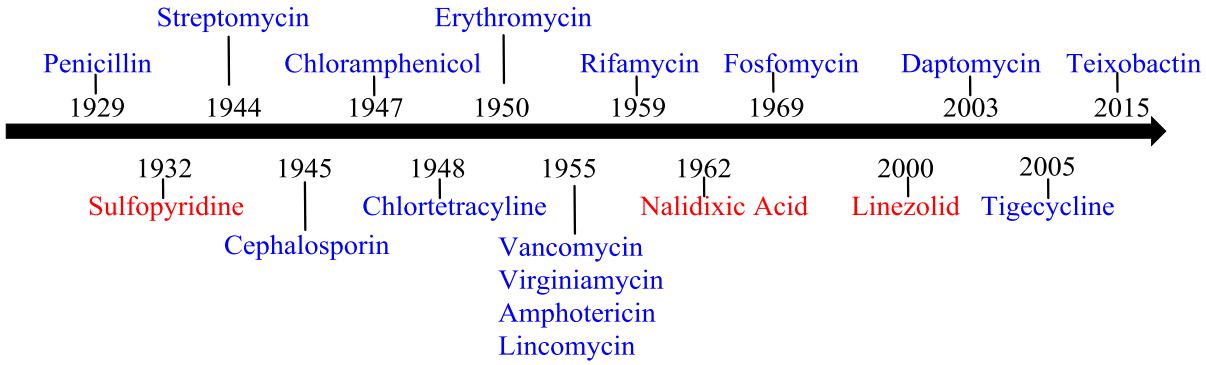

Figure 1.1.2. Outline of antibacterial drug discovery since the 1930s to present day, with listed antibiotics either of synthetic origin (red) or natural product origin (blue). Compiled from [4, 6, 9].

1.1.2 Rise in Bacterial Resistance to Antibiotics

The introduction of antibiotics into clinical use has shown a strong correlation with the rise of resistant bacterial species. The last 50 years have consequently seen an emerging battle between the rise in antibacterial resistance and the pharmaceutical companies and healthcare systems. Bacterial infections are still of significant importance to human morbidity: for example *E. coli* contamination of vegetables in Germany saw 5000 people infected and 50 deaths in the absence of reported antibacterial resistance [10]. Posing the worrying question of how many deaths would be caused by such an infection if caused by an antibacterial resistant strain? In 2007 within the US, 400 000 infections were recorded to have been caused by multidrug resistant strains, of which there were 25 000 attributable deaths [10].

The emergence of bacterial resistance has been accelerated by many aspects of antibiotic use, including the use in agriculture [11] and the sale of non-prescription antibiotics [12, 13]. In 2011 50% of the antibiotic produced were reported to be used in animal feeds to promote growth [10]. Misuse of antibiotics however does not account for all the emerging problems with antibacterial resistance. In part the rise in resistance seen within

clinical cases can be attributed to the limited number of targets which most current antibacterial classes are active against (Figure 1.1.3). In 2005 Walsh *et al.* detailed only four 'robust' targets for antibiotics in clinical use; bacterial cell wall biosynthesis, bacterial protein biosynthesis, DNA replication and repair, and folate coenzyme biosynthesis [6].

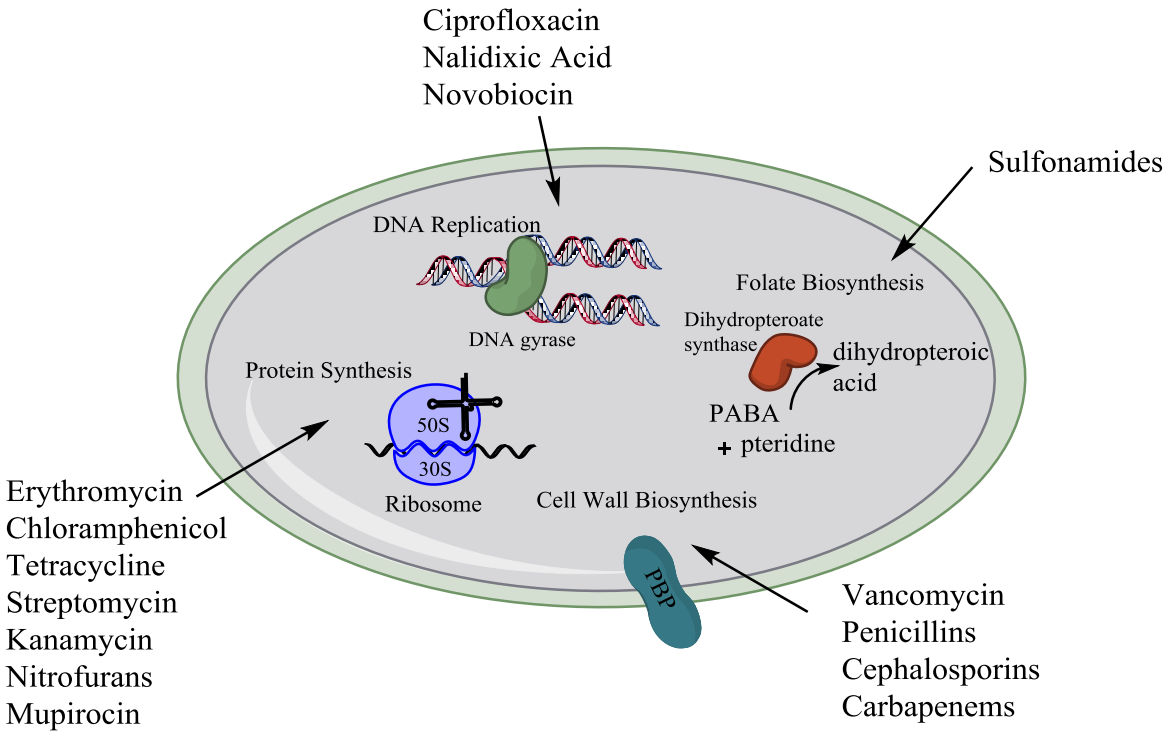

Figure 1.1.3. Illustration representing four of the targets within the bacterial cell currently exploited by clinically available antibiotics. The four targets depicted are: DNA replication, protein synthesis, cell wall biosynthesis and folate biosynthesis [14, 15].

Resistance to an antibiotic can arise within a bacterium by several means and these can be intrinsic to the bacterium, acquired by chromosomal mutation or acquired by horizontal gene transfer (HGT). Intrinsic resistance is resultant from natural characteristics of the bacterium which render it either resistant or less susceptible to an antibiotic. An example of intrinsic resistance is the reduced permeability of Gram-negative cell walls to lipophilic or amphiphilic antibiotics, due to the charge properties and pore construction within their outer membranes [16]. Gram-negative bacteria are resistant to treatment with the new antibiotic teixobactin for this reason [4].

Acquired bacterial resistance to antibiotics can result from chromosomal mutation rendering a target ineffective or the acquisition of a gene encoding a mechanism of

resistance. Chromosomal mutations can include insertions, deletions or substitutions which may lead to an altered antibacterial target. For example, a point mutation in the *mprF* gene and insertion within the *yycG* gene of *Staphylococcus aureus* have been implicated in the decreased susceptibility of this organism to the antibiotic daptomycin [17]. Finally, horizontal gene transfer (HGT) can result in antibiotic resistance by the dissemination of resistance genes across a bacterial population. Horizontal gene transfer can occur by one of three methods; conjugation, transduction or transformation [1] (Figure 1.1.4). Acquisition of a gene by HGT can facilitate the spread of resistance mechanisms such as the expression of alternative penicillin binding proteins (PBP2) throughout a bacterial population [18].

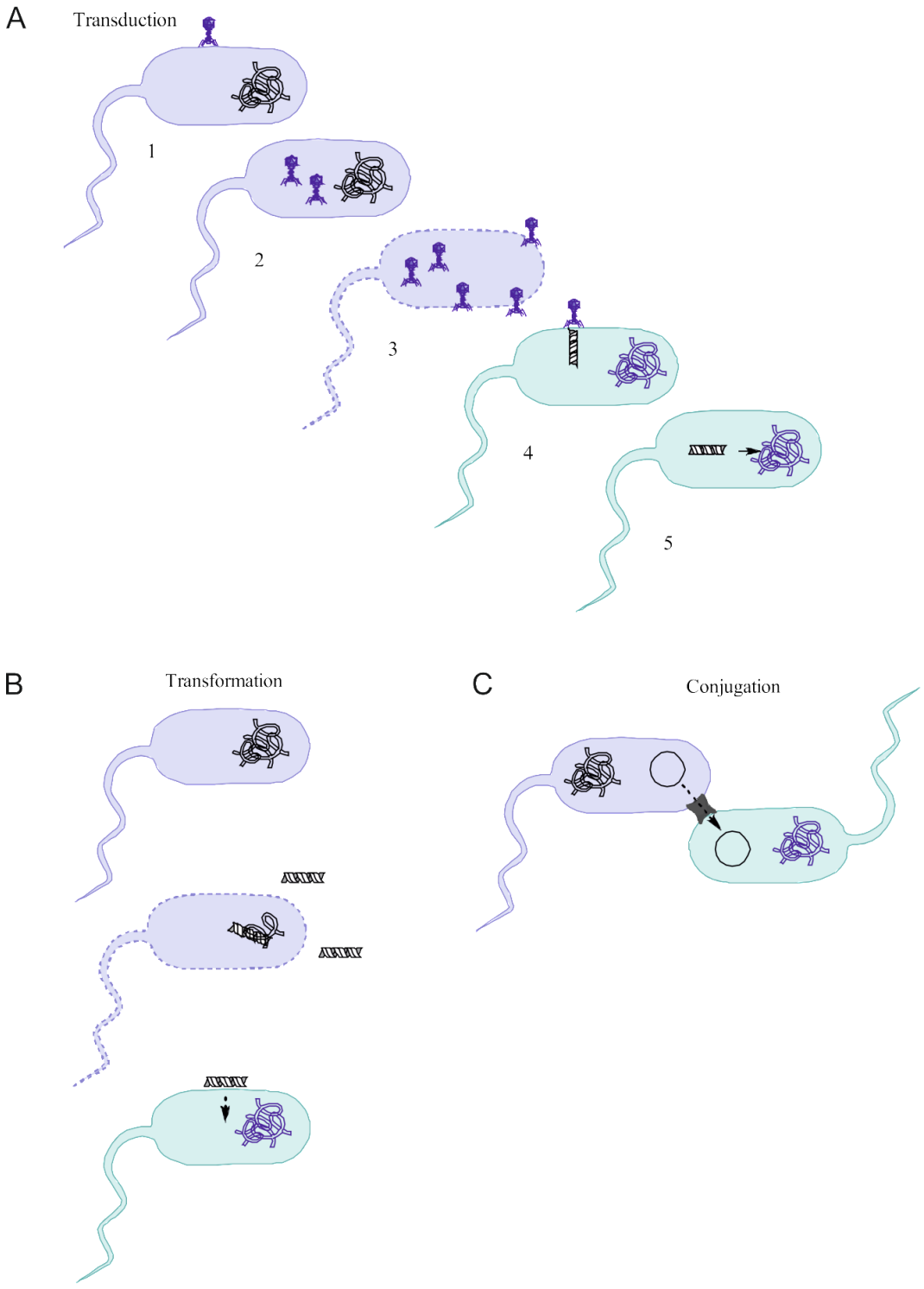

Figure 1.1.4. Processes of horizontal gene transfer. (A) Transduction, the process of genetic transfer by bacteriophage infection of bacteria and can be specific (excision of a gene directly adjacent to the viral DNA) or generic (inclusion of random DNA into the viral capsid). (B) Transformation, the uptake of DNA from the environment. (C) Conjugation, specific pili-mediated transfer of plasmids from one bacterium to another (usually species specific). Compiled from information in [1].

1.1.3 Mechanisms of Resistance

There are many mechanisms by which a bacterium can become resistant to an antibiotic. Potential mechanisms include; alteration of the target site, removal of the antibiotic, or inactivation of the antibiotic (Figure 1.1.5).

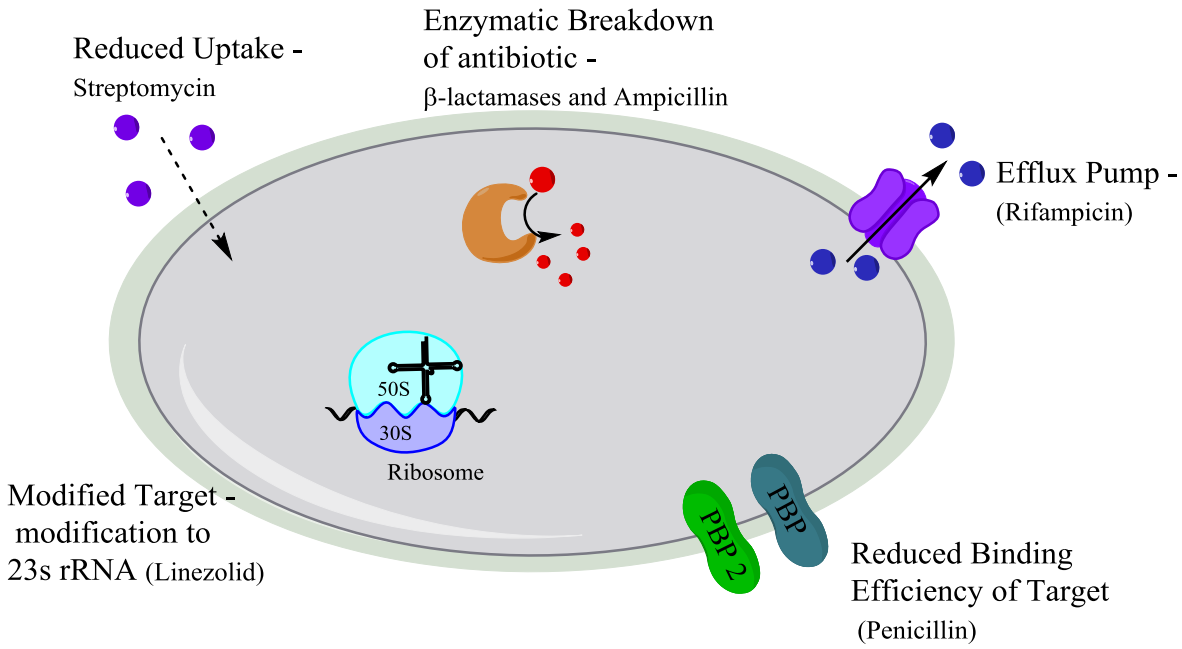

Figure 1.1.5. Examples of various methods of antibacterial resistance within a bacterial cell. Methods depicted include: reduced antibiotic uptake, enzymatic degradation of the antibiotic, efflux pump-mediated removal of the antibiotic, reduced binding efficiency of the antibiotic target and the modification of the antibiotic target.

Resistance resulting from an altered antibacterial target site is typified by the acquired β-lactam resistance from the expression of the alternative penicillin binding protein II. β-Lactam antibiotics prevent the cross-linking of peptidoglycan by interacting with penicillin binding proteins [19]. The emergence of alternative penicillin binding proteins (II), which have a lower binding affinity for β-Lactam antibiotics, in some organisms (i.e.; *Staphylococcus aureus* [20]), has led to an increased resistance to these antibiotics .

Another method of resistance to β-lactam antibiotics is the presence of β-lactamases, which are enzymes capable of hydrolysing the active β-lactam ring (Figure 1.1.6) [21]. β-lactamases have been grouped into four classes (A-D) based on their hydrolytic spectrum,

susceptibility to inhibition and whether they are located on the chromosome or a plasmid [22]. *F. tularensis* and *B. pseudomallei* both encode a β-lactamase, facilitating the observed resistance of these organisms to β-lactam antibiotics [23, 24].

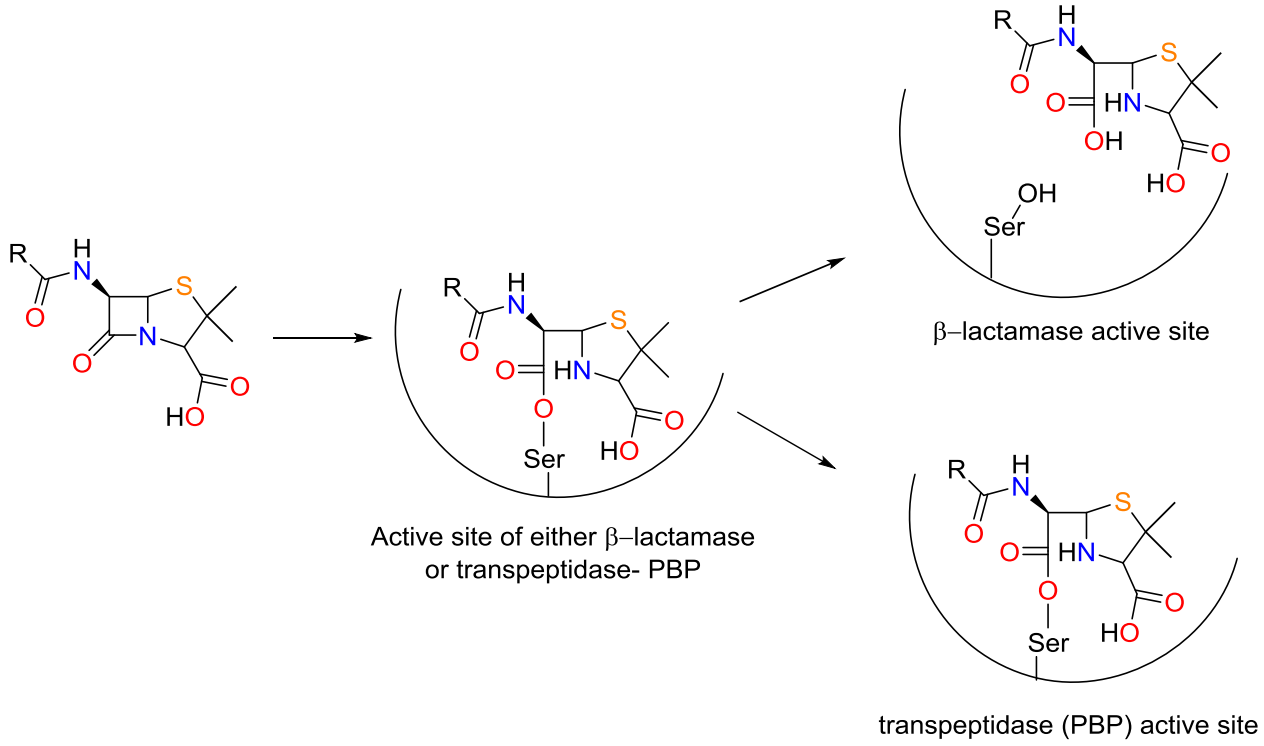

Figure 1.1.6. Illustration depicting the difference following the acylation of a β-lactam antibiotic in transpeptidases and β-lactamases. In transpeptidases the β-lactam remains bound, however the β-lactamase releases the hydrolysed β-lactam. Adapted from [25].

A widespread and more generic means of resistance is the increase in efflux pumps within a bacterial cell wall [26]. Efflux pumps can been found in both susceptible and resistant strains of bacteria, but overexpression or an increased efficiency of efflux pumps can lead to antibiotic resistance by facilitating active removal of the antibiotic from the cell [27]. Clinical isolates displaying resistance to at least one antimicrobial agent of *Burkholderia cepacia*, an organism capable of complex infection in individuals with cystic fibrosis, were analysed for efflux pump activity [28]. Of the 42 isolates shown to display antimicrobial resistance, 94.4% of those demonstrating Ceftazidime-resistance and 72.7% of those demonstrating chloramphenicol resistance, showed efflux pump activity [28]. Sequence analysis of efflux pump regulators within resistant strains suggested that mutations in the

RND-3 efflux pump regulator gene were responsible for efflux pump mediated removal of antimicrobials [28].

1.1.4 **Antibiotic Drug Development**

The drug discovery process is both long and expensive, a recent report (2014) by Tufts University (Boston, US) estimated that the current cost in the US to bring a drug to market is $2558 million [29]. The majority of antibiotics currently available are either derived directly from natural products or are synthetic derivatives of them [30]. Traditional means of sourcing such compounds include screening whole broth or extracts of microbial ferments against a specific set of bacterial strains [31]. The efficacy of isolated compounds are then assessed by measuring zones of inhibition, which are the areas surrounding the test compound absent of bacterial growth within an otherwise confluent plate [1].

Isolation of compounds from natural sources has yielded many important antibiotics, however recent years have seen a steep decline in antibiotic drug discovery with few new antibiotics discovered in the last 50 years (Figure 1.1.2). Advances in molecular biology and other experimental techniques have shifted focus to rational design of inhibitors of novel antibacterial targets. Novel targets can be identified using genomics to screen for potentially important pathways or targets [32]. Targets are required to be either essential for bacterial growth [33] or essential for bacterial virulence [34]. Genetic knockouts, wherein the gene encoding the particular target is typically subjected to cassette mutagenesis or gene disruption, can therefore be utilised for target validation [1]. The resultant mutant can then be tested for viability, phenotypic changes and most importantly attenuation within an animal model. Once a target is identified and validated, potential inhibitors can be identified or developed by either *in silico* or experimental screening, detailed below.

1.1.4.1 ***In silico* Screening**

In silico screening is dependent on the acquisition of 3D structural information for the target, typically achieved by protein crystallisation. The greatest difficulty to overcome with this method is determining the 3D protein structure. Automation of the process of

protein crystallography has provided two key improvements with increased throughput and miniaturisation. Miniaturisation has been beneficial in both reducing the cost per plate and in reducing the amount of protein required, which was previously a rate limiting step [35]. The introduction of MAD (Multiple Wavelength Anomalous Diffraction) phasing has improved the ability to solve new structures [36].

Once structural information is obtained there are three main methods to identify new ligands, these include; structure and known inhibitor design, *de novo* design, and virtual High Throughput Screening (vHTS) [37]. Structure and known inhibitor design is primarily used to increase the binding efficiency of a previously known inhibitor by building in structural modifications. New structures are scored and ranked based on their predicted binding affinity and synthetic accessibility. This method was utilised to derive chloramphenicol derivatives based on X-ray diffraction structures of a bacterial ribosome with chloramphenicol bound [38]. This method centred on the addition of different moieties to the chloramphenicol amine to improve binding to the peptidyl transferase centre or P-loop of the ribosome. The conjugation of a pyrene group to the chloramphenicol amine demonstrated enhanced binding to the chloramphenicol binding site [38].

De novo design of inhibitors is built upon the docking of virtual fragments into sub sites and subsequent joining to create a complete molecule [39]. Programs used to design these types of inhibitors initially analyse the target site of the protein for hydrogen bond donors and acceptors as well as hydrophobic residues. Once analysis is complete regions where favourable interactions could occur are found and docking of fragments can begin. Often this approach can lead to complex molecules which are difficult to synthesise, therefore these hits are also analysed for complexity and synthetic tractability [37]. Fragment screens have been used in the development of an inhibitor of an extended spectrum β-lactamase, yielding a hit rate of 14.5% (from 69 fragments tested) [40]. Many identified fragments contained tetrazole groups and this led to the analysis of larger analogues of identified fragments to develop potentially potent inhibitors [40].

Finally *in silico* methods can be used for vHTS, and are suggested to generate a hit rate of 20-30% over the <1% obtained by experimental screening [37]. This process works by using rapid docking algorithms to search databases of commercially available compounds for novel molecules which are predicted to bind to the target protein. It is often used as a

precursor to experimental screening as a means of focussing the compound library tested against the protein target. In 2013 vHTS was used to identify inhibitors of *F. tularensis* FabI, an enzyme essential in this organism for lipid biosynthesis [41]. From an initial screen of the ChemNavigator database (14 million compounds), those ranked within the top 2000 (alongside 1500 FDA approved drugs) were then screened using Glide (Schrödinger). The top 200 scoring compounds were then visually inspected and from this 65 commercially available compounds were chosen for experimental evaluation [41].

1.1.4.2 **Experimental Screening**

Experimental high throughput screening (HTS) utilises the miniaturisation of assays and automated detection of multiple well microtitre plates (96, 384, or even 1536 well) to simultaneously test large libraries of chemical compounds against a particular target. Whilst in the mid-1990s screens were designed to test thousands of compounds per day by the early 2000s screens were being designed to test hundreds of thousands of compounds per day [42]. The inherent requirement of HTS systems to be reproducible over time and experiments requires reagents to be stable over time, as well as resistant to automated equipment and not impacted by liquid dispensers [43]. HTS methods may be based on product formation, substrate depletion or the concentration of free enzyme (reviewed in [43]). When analysing either product formation or substrate depletion the use of positive controls, with enzyme activity, can be compared to negative controls, with no enzyme activity, to give a screening window.

Any compounds identified within the screening window are therefore classed as inhibitors, with the efficacy of the screening window determined by the statistical measurement referred to as a Z' value [44]. HTS methods can vary widely but can be broadly divided into either continuous (i.e.; Purine nucleoside phosphorylase (PNP) detection of free phosphate [45]) or quenched assays (i.e.; malachite green for free phosphate [46]), and either direct measurement (i.e.; mass spectrometry for post translation modifications [47, 48]) or indirect measurement (i.e.; Fluorescence Resonance Energy Transfer (FRET) [49]) assays. Quenched methods are typically preferred to continuous for ease of set up, as all assays can simultaneously be stopped and analysed. For many assays direct measurements are not possible or the throughput capacity is not sufficient [43]. Frequently enzyme coupled assays are employed for high throughput

screens, for example many kinases are coupled with firefly luciferase to test activity by luminescence in accordance to ATP concentration [50, 51].

In summary, the decline in antibiotics being brought to market in tandem with the rise in antibacterial resistance has heightened the importance in antibiotic drug discovery. Furthermore, the action of most clinically available antibiotics is limited to a restricted number of 'robust' targets. There is therefore a need for the identification, validation and discovery of inhibitors against a novel robust antibacterial target.

1.2 Biological Warfare

The application of biological agents in warfare has been documented throughout history and is reviewed by Barras *et al*. [52]. The advent of antibiotics and their widespread therapeutic application however has led to the reduction in the potential impact of bacterial biowarfare agents as weapons. This threat was renewed in recent years following a surge in the natural and manufactured antibiotic resistance of these organisms. In 1999 a classification system for biological warfare agents (categories A-C) was set up by the Centers for Disease Control and Prevention (CDC), with category A being given highest priority for prevention [53]. Category A agents are classed as high risk due to the ease of dissemination and transmission, resultant high mortality rates, and the potential to cause public panic [53]. The following have been noted as potential bacterial agents of concern; *Bacillus anthracis*, *Francisella tularensis*, *Yersinia pestis*, *Brucella melitensis*/*abortus*, and *Burkholderia pseudomallei*/*mallei*.

1.2.1 Intracellular Bacterial Biowarfare Agents

Intracellular bacteria are capable of invading and replicating within a host cell. When within host cells (typically macrophages) the bacteria are not readily recognised by antibodies and equally avoid humoral defence mechanisms [54]. This can reduce the efficiency of the host immune response to clear the infection. The price of this intracellular lifecycle however is that the pathogen must develop mechanisms for invasion of host cells, find a suitable niche for intracellular replication, and develop an exit strategy from host cells [15].

Phagocytosis by macrophages is the process of pathogen recognition and uptake into the macrophage by their engulfment into membrane-bound vesicles called phagosomes [55]. Within the host cell the usual course of action for the phagosome is to fuse with a lysosome, a membrane-bound compartment containing reactive oxygen species. The fusion of these two compartments forms a phagolysosome. The formation of a phagolysosome typically results in the destruction of the bacterium within it and allows the subsequent display of antigens corresponding to that pathogen on the surface of the host cell [1]. The pH within the phagolysosome is acidic, with a recorded average pH of 5.4 ± 0.4, twenty minutes after exposure to a microorganism [56]. Intracellular bacteria

have however developed methods to prevent their degradation by phagolysosomes. The four main routes include: (1) escape from the phagosome, (2) prevention of the fusion between the phagosome and lysosome, (3) prevention of phagosome acidification or (4) adaptation for survival within the phagolysosome (Figure 1.2.1) [57].

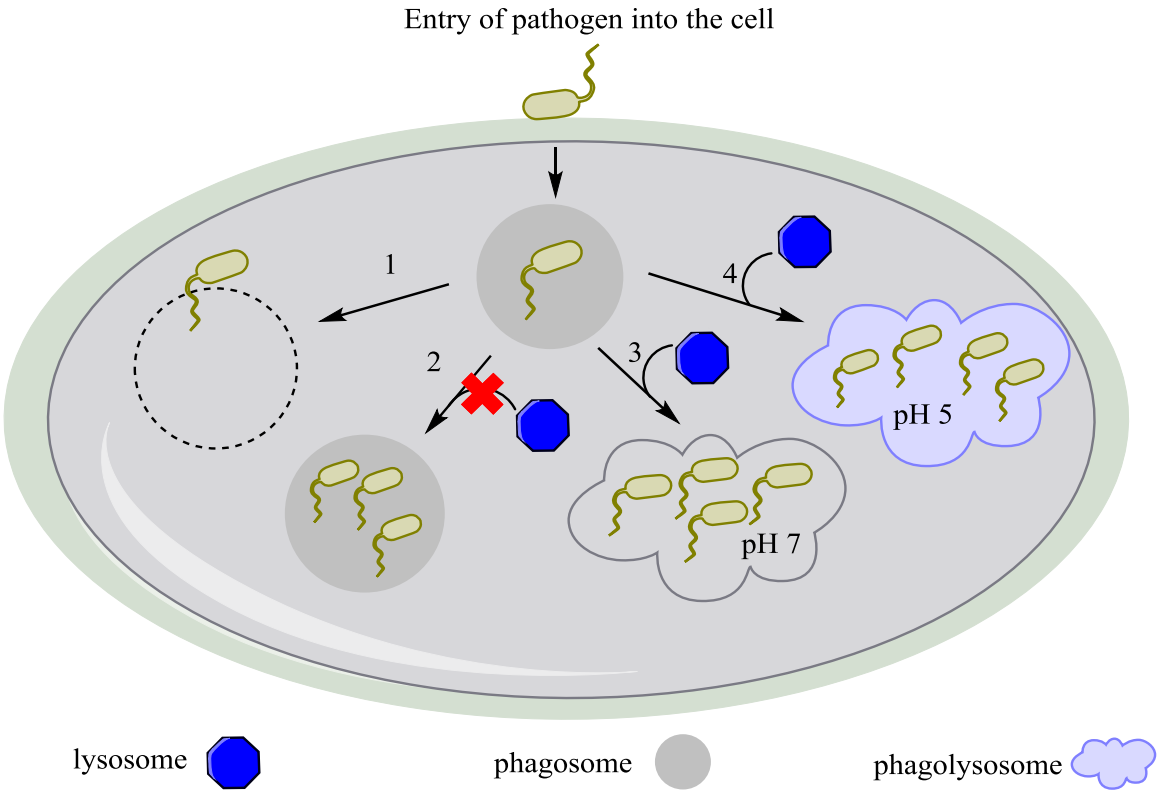

Figure 1.2.1. The mechanisms of survival for intracellular bacterial pathogens following phagocytosis. (1) Escape of the pathogen from the phagosome to replicate within the cell. (2) Prevention of the lysosome fusion with the phagosome, and replication within the phagosome. (3) Prevention of the acidification of the phagolysosome. (4) Adaptation to replicate in the unfavourable conditions within a phagolysosome.

All of the potential bacterial agents of concern listed previously are capable of intracellular survival [58-61]. This thesis will however focus on the following three; *Y. pestis*, *B. pseudomallei* and *F. tularensis*.

1.2.1.1 *Yersinia pestis*

Y. pestis, the causative agent of the plague, is a Gram-negative organism that belongs to the family *Enterobacteriaceae*. The disease plague can present in bubonic or pneumonic forms, and in a small percentage of cases septicaemic plague may develop [62] (Table 1.2.1). The classification of *Y. pestis* as a category A agent is largely based on the ease of respiratory infection and the severity of the disease associated with this route of transmission (pneumonic). The organism has caused three human pandemics; the Justinian plague (6-8th century), the Black Death (14-19th century), and modern plague (19th century– present day) [63, 64]. Plague is primarily a disease of rodents and other wild mammals and is principally transmitted by fleas.

Table 1.2.1. The three clinical presentations of the disease plague as caused by the pathogen *Yersinia pestis* [65]

Type of Plague	Incubation Period	Symptoms	Transmission	Mortality Rate (%)
Bubonic	2-6 days	Fever, headache, chills, and swollen, extremely tender lymph nodes	Bite by an infected flea	40 – 60 (untreated)
Septicaemic	1-4 days	Chills, headache, malaise, gastrointestinal disturbances, skin lesions, gangrene	Can arise from inhalation of infectious aerosol, or develop from bubonic plague	~100 (untreated)
Pneumonic	1-3 days	Flu-like symptoms progressing to pneumonia, coughing and bloody sputum	Inhalation of airborne droplets or person to person	~100 (untreated)

1.2.1.1.1 **Intracellular Lifecycle of *Y. pestis***

Y. pestis has a predominantly extracellular lifecycle, with human mortality relating to the septicaemia that results from the infection [59]. During extracellular growth the organism actively subverts uptake by phagocytosis into macrophages [66, 67]. It is now believed however that at early stages of its infectious lifecycle *Y. pestis* (Figure 1.2.2) is capable of intracellular infection [68]. Finegold *et al.* studied lung sections from Rhesus monkeys infected with wild type *Y. pestis* and identified intact bacteria within phagosomes of alveolar macrophages [69]. This observation was supported by Straley *et al*. [70]. Straley *et al*. used transmission electron microscopy analysis of infected mouse peritoneal macrophages to show *Y. pestis* cells closely surrounded by a membrane, both immediately and 4.5 hours post infection [70]. These membranes were identified as lysosomal compartments by the labelling of secondary lysosomes from macrophages with electron dense particles of thorium dioxide [70]. Collectively these data suggested that *Y. pestis* grows within the lysosomal compartment of the host cell. Survival of this organism within the phagolysosome is proposed to depend on its ability to prevent acidification of the vacuole, with reported pH values greater than 7.0 [71]. Intracellular *Y. pestis* are released by dying macrophages and then disseminate and replicate within the nearby tissues, in a process that is not reliant on autophagy [72]. The ability of *Y. pestis* to survive intracellularly is hypothesised to influence the degree of disease severity observed in the host [73]. The intracellular stage of its lifecycle is therefore of interest for antibacterial drug development.

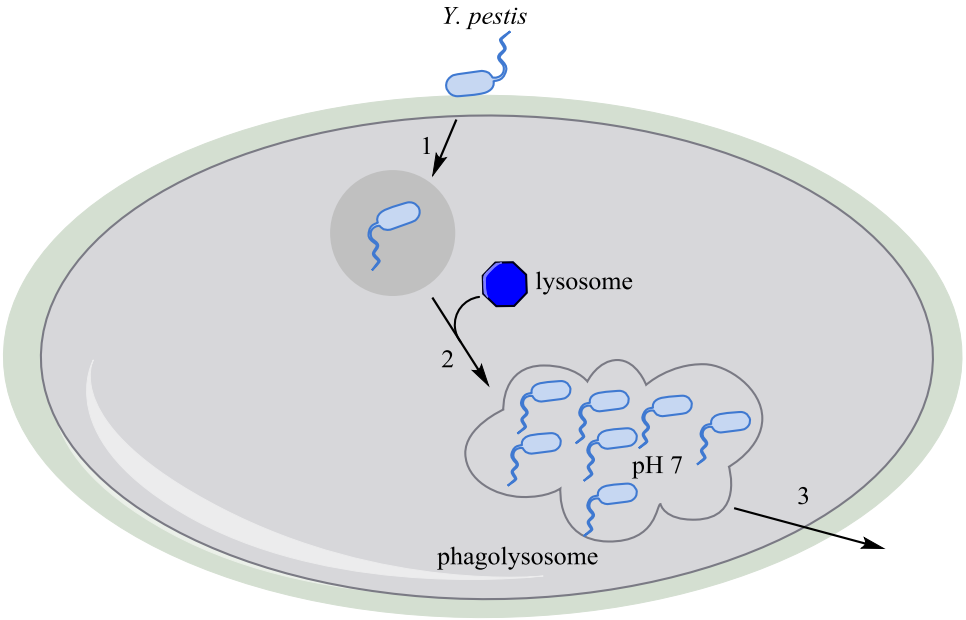

Figure 1.2.2. Intracellular lifecycle of *Y. pestis* in a monocyte. (1) Entry of *Y. pestis* into the host cell via phagocytosis, typically in the early stages of infection. (2) The *Yersinia* containing phagosome matures and fuses with the lysosome to form a phagolysosome. *Y. pestis* prevents the acidification of this compartment and replicates within it. (3) Release of *Y. pestis* cells follows the death the host cell.

1.2.1.1.2 **Treatment of Plague**

The antibiotics streptomycin, gentamicin, ciprofloxacin and doxycycline are considered for therapeutic treatment of plague [74, 75]. *Yersinia pestis* is largely known for being responsive to antibiotic treatment, however in 1995 a multidrug resistant strain was isolated from a patient with symptoms of bubonic plague in Madagascar [76]. Furthermore, in 1997 Galimand *et al.* reported high levels of resistance to many antibiotics commonly used for the treatment of plague, conferred by the conjugative plasmid pIP1202 [77].

1.2.1.2 ***Burkholderia pseudomallei***

The bacterium *Burkholderia pseudomallei* (*B. pseudomallei*), is the causative agent of the infectious disease melioidosis. The disease was first described in 1911 by the pathologist Alfred Whitmore and was only later termed melioidosis by Stanton and Fletcher [78]. Melioidosis is a febrile disease often resulting in septicaemia or abscesses. In north-eastern Thailand it has been reported to account for 20% of community acquired

septicaemias [79]. The main routes of infection include subcutaneous infection, inhalation, or ingestion of contaminated particles or aerosols [80]. This Gram-negative organism is capable of surviving in various hostile conditions including; prolonged nutrient starvation, acidic environments, dehydration, and a variety of temperatures [81].

B. pseudomallei has been classed as a potential biological warfare agent due to its contagious nature and its link with mortality rates of 50% (northeastern-Thailand) [82]. The absence of a licensed vaccine and the observed recurrence in patients treated with antibiotics (30%, when treatment is less than 8 weeks), which is fatal in 25% of cases [83-85], makes this organism of greater concern.

1.2.1.2.1 **Intracellular Lifecycle of *Burkholderia pseudomallei***

B. pseudomallei can invade and proliferate within both phagocytic and nonphagocytic cell lines (Figure 1.2.3) [60, 86]. The exact mechanism by which it invades the cells is still unclear. Once inside the host cell *B. pseudomallei* is able to escape from the phagosome and replicate within the cytoplasm [78, 87]. Following entry into the host cell cytoplasm, *B. pseudomallei* cells evade macrophage-based killing by repressing the induction of inducible nitric oxide synthase (iNOS) expression [88]. *B. pseudomallei rpoS* mutants defective for the stress-related RNA polymerase sigma factor, RpoS, induced higher levels of iNOS which resulted in limited intracellular growth [89]. Following sufficient intracellular replication, *B. pseudomallei* cells are able to escape the host cell by inducing cell lysis. Mutational analysis suggested this process is also partially dependent on RpoS [90]. *B. pseudomallei* is capable of spreading intracellularly via the formation of membrane protrusions between the infected and neighbouring cell, through which bacteria travel by actin-mediated motility (Figure 1.2.3b) [91]. This actin-mediated motility is reliant on the BimA protein from *B. pseudomallei*, with a *bimA* mutant incapable of forming actin tails [92]. One side effect of the intracellular spread of *B. pseudomallei* is cell fusion to form a multinuclear giant cell (MNGC). The formation of these MNGCs alongside the intracellular spread of *B. pseudomallei* is suggested to be important for the progression of the disease [78]. In 2001 a type three secretion system (T3SS) termed the *Burkholderia* secretion apparatus (Bsa) was identified in *B. pseudomallei* [93]. Mutational analysis has demonstrated the Bsa T3SS is important in the intracellular lifecycle of *B. pseudomallei* [94, 95]. The effector protein BopE induces the

rearrangement of the host cell cytoskeleton and is suggested to facilitate invasion of neighbouring cells [94]. Escape from the phagosome is also at least partially dependent on the Bsa T3SS, with *bsa2* and *bipD* mutants incapable of leaving the endocytic vacuoles [95]. Additionally, the Bsa T3SS effector protein BopA has been implicated in the active evasion of autophagy by *B. pseudomallei* [96].

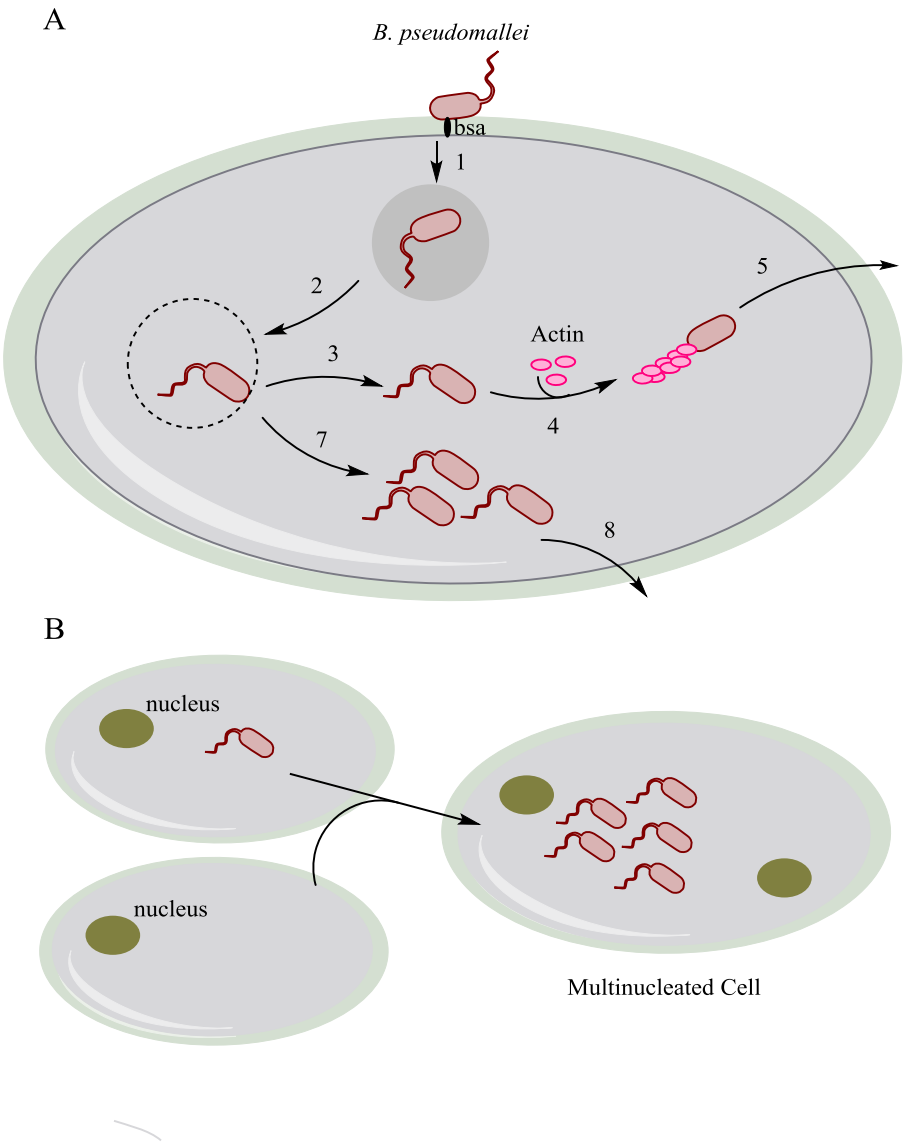

Figure 1.2.3. Intracellular lifecycle of *B. pseudomallei* within a phagocytic cell. (A) (1) Entry of *B. pseudomallei* into the host cell and (2) Escape from the phagosome are mediated by the *Burkholderia* secretion apparatus (bsa) system. (3-5) Cell to cell spread of *B. pseudomallei* mediated by the formation of actin-based membrane protrusion which is subsequently phagocytosed by the neighbouring cell. (7-8) Alternatively *B. pseudomallei* can replicate until it has reached 'sufficient' levels upon which it

induces cell lysis and thereby exits the cell. (B) *B. pseudomallei* can induce the formation of multinucleated cells following cell fusion. Adapted from [97].

1.2.1.2.2 **Treatment of Melioidosis**

B. pseudomallei has been shown to display resistance to a wide range of antibiotics ranging from penicillins to third-generation cephalosporins [98]. As a consequence choice in treatments is largely limited, with Ceftazidime as the current drug of choice for treatment and to a lesser extent amoxicillin-clavulanate (Figure 1.2.4). The recommended treatment for melioidosis is long term, with a potential 3-6 months course of antibacterial therapy [99]. Recent reports have found strains which are resistant to Ceftazidime [100]. Several β-lactamases, enzymes capable of degrading β-lactam antibiotics, have been identified in the genome of *B. pseudomallei* [23]. Of those found *blaA* is often described as the most functionally important, but this is readily inhibited by clavulanate (Figure 1.2.4b) [101].

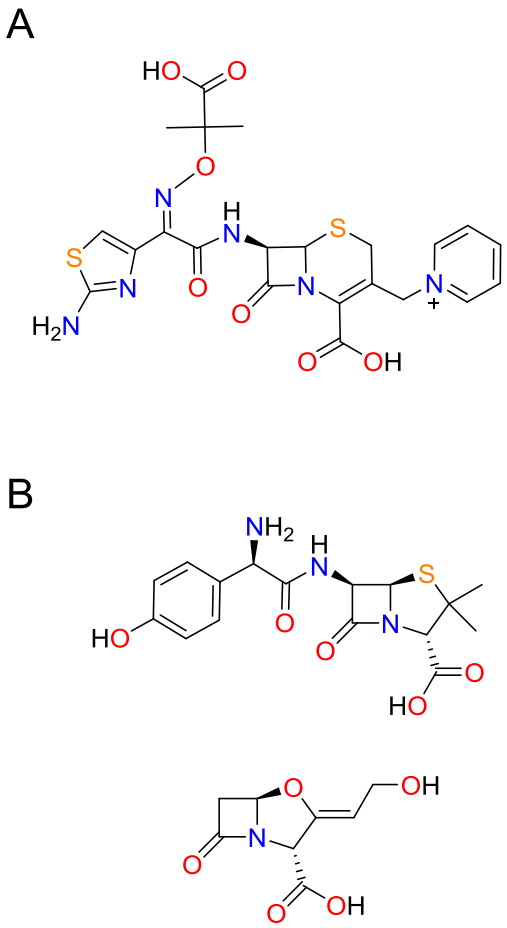

Figure 1.2.4. Antibiotics of choice for *B. pseudomallei* treatment. (A) Ceftazidime (B) Co-Amoxiclav.

1.2.1.3 ***Francisella tularensis***

Francisella tularensis, herein referred to as *F. tularensis*, is a member of the *Francisella* genus, the sole genus of the family *Francisellaceae* [102]. The organism was originally isolated in 1911 from ground squirrels (from Tulare, California) which were noted as dying from a plague-like disease [103]. Despite being known under several different names the organism was finally placed in a new genus, *Francisella*, so named in honour of Dr Edward Francis who pioneered early research on the organism [104]. Although characterisation of the genus *Francisella* has been varied over the years, in 2012 Sjödin *et al*. divided the genus into two main genetic clades [105]. Genome analysis suggested independently developed evolutionary paths of host adaptation could be observed for *F. tularensis* (infecting mammals) and *F. noatunensis subsp. noatunensis* (infecting fish) [105]. The transmission of *F. tularensis subspecies tularensis* associated with rabbits, ticks and sheep [106]. Alternatively the transmission of *F. tularensis subspecies holarctica* is associated with bodies of water (streams, ponds, lakes and rivers) as well as beavers, muskrats and

lemmings [106]. The organism is also highly resistant to freezing with cases of live bacteria being found in rabbit meat after 3 years of storage at -15 °C [106].

1.2.1.3.1 **Tularaemia**

F. tularensis is the causative agent of the disease tularaemia. This is a zoonotic disease capable of infecting a wide range of mammals, with particular prevalence amongst lagomorphs [107]. Outbreaks in man often occur in parallel with those of animal populations [103]. In man, tularaemia is caused most notably by two *F. tularensis* subspecies; *tularensis* and *holarctica* [105]. The subspecies *tularensis*, often referred to as Type A, is the most virulent and is almost exclusively found in North America. Subspecies *holarctica*, often referred to as Type B is less virulent and is more widely distributed in the Northern Hemisphere [105, 106]. Tularaemia in humans can range from localised illness to life-threatening septicaemia or pneumonia [106]. There are six forms of tularaemia which can be differentiated by the means of exposure or the severity of disease (Table 1.2.2). Although the incubation period can range from 1to 21 days, it is usually between 3 and 5 days [103]. Transmission of the organism has been linked to various methods including ingestion, inhalation, arthropod-borne transfer, and direct contact but as of yet no human-human transmission has been observed [106]. Respiratory (pneumonic) tularemia has the highest mortality rate of 30-60% if untreated [108]. Two outbreaks of primary pneumonic tularaemia were observed in Martha's Vineyards, Massachusetts [109]. Human activity (i.e. mowing the lawn) in areas with an environmental source of bacteria were linked to the outbreaks observed [109, 110]. The reasons behind the prevalence of the disease on this island and the pneumonic presentation commonly observed however are still largely unknown.

Table 1.2.2. The six clinical presentations of tularaemia. The six forms of tularaemia described are for infection by *F. tularensis subspecies tularensis* [106, 111].

Type of Tularaemia	Symptoms	Route of Transmission
Glandular	Initial flu-like symptoms, inflamed regional lymph nodes, no ulcer develops	Abrasions on skin or mucous membrane/ vector-borne
Ulceroglandular	Initial flu-like symptoms, inflamed papule which ulcerates upon point of entry, inflamed regional lymph nodes	Abrasions on skin or mucous membrane/ vector-borne
Oculoglandular	Unilateral, painful, purulent conjunctivitis with preauricular or cervical lymphadenopathy	Inoculation of the conjunctiva
Oropharyngeal	Pharyngitis, cervical lymphadenopathy, ulcers often develop	Ingestion of contaminated food or drink
Gastrointestinal	Mild to persistent diarrhoea, patients may develop ulceration of the bowel depending of the size of the inoculum	Ingestion of contaminated food or drink
Respiratory	Initial symptoms include cough, high fever, chill, malaise, chest pain, and dyspnea. Occasionally severe systemic symptoms develop without respiratory signs	Inhalation

The potential use of *F. tularensis* as a biological warfare agent has been recognised since the mid-twentieth century, with several outbreaks revealing its low infectious dose, ease of dissemination and ability to cause severe disease [112]. As with many organisms considered as biological warfare threats, the most likely means of weaponised

dissemination is aerosolisation. The use of airborne tularaemia would lead to an outbreak of acute, undifferentiated febrile disease [113]. This disease could then progress to result in pneumonia, pleuritis and hilar lymphadenopathy [113].

1.2.1.3.2 **Intracellular Lifecycle of *F. tularensis***

F. tularensis is described as a facultative intracellular organism, that once within a mammalian host becomes obligate in nature [114]. The use of the *F. tularensis* live vaccine strain (LVS), an attenuated *F. tularensis* subspecies *holarctica* strain [115, 116], is commonly used when studying *F. tularensis* due to safety considerations. The intracellular nature of *F. tularensis* was first observed by transmission electron microscopy and bacterial counts of LVS within macrophage monolayers from mice, guinea pigs and rats [117]. A further study showed that this strain could grow in a logarithmic fashion within murine macrophages, with a calculated doubling time of 4-6 hours [118]. Research into the intracellular lifecycle of *Francisella* species has been a topic of interest for many years. Although much is still unclear about the process, reviews published by Chong, A. and Celli, J. (2010) [61] and Celli, J. and Zhart, T.C. (2013) [119] detail the current understanding in this area (Figure 1.2.6).

Different *Francisella* species and strains have demonstrated the ability to enter, survive and proliferate within a range of host cells [120-122]. Although little is known about how they enter non-phagocytic cells research has highlighted a variety of receptors important in *Francisella* uptake by phagocytosis [123-127]. Research by Clemens *et al.* showed the invasion of macrophages by *F. tularensis* LVS potentially occurs via the use of a novel pseudopod loop mechanism in a complement dependent fashion [128]. The receptors involved in the uptake of *Francisella* species however vary across literature and appear to be dependent on the bacterium's opsonisation conditions (serum-opsonised or nonopsonic uptake) [119].

Following uptake *Francisella* species reside within a phagosome which follows the normal maturation process [129-131] but is prevented from fusing with the lysosome [130, 132]. Another key aspect to phagosome maturation is the acidification of the phagosomal lumen [133]. The acidification of the phagosome had a suggested role in iron uptake and consequently intracellular survival of *Francisella tularensis* [118]. This was shown by the use of lysosomotropic agents, which block endosome acidification, against macrophage culture prior to infection. Use of these agents prevented replication of *F. tularensis* LVS

within the macrophages with recovered cells dropping from 10^8 to 10^4 CFU (equivalent to the starting inoculum). This effect could be reversed by the washing of agents away from the macrophage culture, prior to re-infection with *F. tularensis* LVS [118]. These data were suggested to confer to the requirement of *F. tularensis* for acidic environment for the release of iron from transferrin, an iron binding blood plasma glycoprotein [118]. The observed acidification of *Francisella* containing phagosomes is not however universal [119] and as has been described for the uptake of *Francisella* species, the acidification of phagosomes is suggested to relate to the opsonisation state of the bacterium [119].

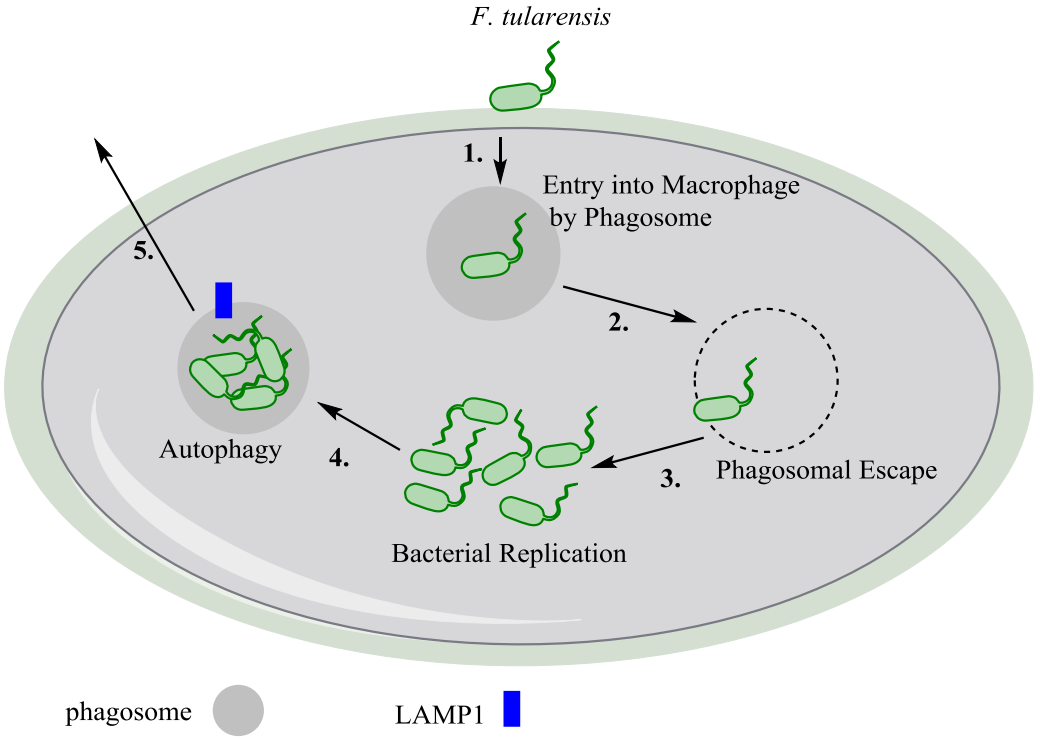

Figure 1.2.5. Suggested intracellular lifecycle of *F. tularensis*. (1) Entry of *F. tularensis* into a macrophage by phagocytosis. (2) Escape from the nutrient poor phagosome into the nutrient rich cytoplasm. (3) Replication of *F. tularensis* within the cytoplasm. (4) Return of *F. tularensis* into membrane bound vesicles by autophagy. (5) Release of *F. tularensis* from the macrophage. N.B. Autophagy is a process used by cells in the regulated lysosomal degradation of cellular material and LAMP-1 is a protein that is a major constituent of the lysosome membrane [134].

Francisella species replicate within the host cell cytoplasm [120], which consequently requires them to escape from the phagosome. Several genes encoded on the intracellular growth locus (*igl*) are known to be important in phagosomal escape (reviewed in [61]).The IglC, IglD and MglA proteins were demonstrated to contribute to the phagosomal escape of *F. tularensis* LVS strain in murine macrophage-like cell line J774.1 [132]. The identification of key genes involved in the intracellular replication of *Francisella* species is more difficult because of the prerequisite for phagosomal escape. Nonetheless, the following genes have been identified as important for cytosolic replication of *Francisella*: purine biosynthetic genes (*PurMCD*) [135, 136], γ-glutamyl transpeptidase (*ggt*) [137] and several genes of unknown function [119].

In 2006 Checroun *et al*. highlighted that *F. tularensis* escaped the phagosome 60 minutes post infection [129]. Replication was then shown to occur within the cytoplasm for 4 to 20 hours post infection [129], with a suggested 8-9 rounds of replication during this time. Of note perhaps, is the unusual observation that beyond 20 hours post infection the bacteria appeared to have re-entered into vacuoles. These vacuoles were found to contain LAMP-1, a lysosomal associated membrane protein [134], and were able to accumulate monodansylcadaverine, an autofluorescent dye used to label autophagic vacuoles [129]. An overview of *F. tularensis* replication within macrophages is detailed in Figure 1.2.6. It is possibly the first bacterial species shown to re-enter the endocytic pathway following replication within the cytoplasm. The exact nature by which *F. tularensis* leaves and spreads between host cells is still unclear. Collectively these data suggest that there is a high degree of novelty in the intracellular lifestyle of this pathogen.

1.2.1.3.3 **Treatment of Tularaemia**

With the disease tularaemia displaying undifferentiated symptoms of infection [113], detection of the causative agent is paramount. In 1993 Long *et al*. described a PCR reaction based assay for the detection of *F. tularensis*, both Type A and B, from blood samples [114]. Most cases of tularaemia are described as responding well to antibiotic treatment, with the mortality rates of even virulent strains reducing with treatment [103].

Antibiotics used in the treatment of tularaemia include: streptomycin, tetracycline ciprofloxacin and other fluoroquinolones [74]. This aside, *F. tularensis* strains have been

shown to be resistant to many other commonly used antibiotics, including all β-lactams and azithromycin [138]. The resistance of *F. tularensis* to β-lactams has been linked to the presence of a β-lactamase identified in fourteen *F. tularensis* strains [24]. The class A β-lactamase, FTU-1, is able to cleave penicillins and early generation cephalosporins with catalytic efficiencies of ~10^5 and ~10^2 M^{-1} s^{-1} respectively [24].

No licensed vaccine is available for *F. tularensis* currently. *F. tularensis* LVS was developed by the former USSR in the mid-20^{th} century [115, 116]. Identification of this strain was established by serial passage of *F. tularensis* subspecies *holarctica* on peptone cysteine agar which yielded two phenotypic variants, displaying differentiation by either a grey or blue colour [139]. Whilst the blue colony variant demonstrated an ability to induce protective immunity, the grey colony variant was unable to induce a similar response. Licensing of *F. tularensis* LVS has not been approved despite the successful immunisation of a number of people for several reasons including; contamination of a large scale preparations with the grey colony variant, a lack of knowledge on the method of attenuation, and observed residual virulence [139]. Further work has looked into the use of subunit vaccines or rationally attenuated strains (reviewed in [139, 140]). In the absence of a promising vaccine candidate the requirement for novel antibiotics for the treatment of tularaemia is of greater importance.

Resistance to multiple antibacterial compounds have been reported for the facultative intracellular pathogens; *Y. pestis*, *B. pseudomallei* and *F. tularensis* [76, 98, 138]. Antibiotic therapy for the diseases caused by these organisms is therefore limited and as such the requirement for a new antibacterial is imperative. The intracellular lifecycles for these organisms is also varied and often specialised; for example the unusual intracellular lifecycle of *F. tularensis* [119]. Given this individuality, the discovery of an inhibitor of a globally important target for intracellular bacteria would provide the potential for a broad spectrum antibiotic capable of targeting all of these intracellular bacterial pathogens.

1.3 The Stringent Response

The growth of heterotrophic bacteria is largely dependent on their environment and upon nutrient depletion growth rates can ultimately drop to almost zero [141]. Under these nutrient limiting conditions bacteria will employ a range of both physiological and phenotypic changes to improve the survival rate of cells. The stringent response is triggered by a lowering of many essential nutrients including amino acids, carbon, fatty acids and phosphorous (Figure 1.3.1) [142-145]. It subsequently involves a virtually immediate transcriptional switch which results in genes responsible for the rapid growth of cells being down-regulated and those involved in biosynthesis and survival being up-regulated [146] (Table 1.3.1).

Table 1.3.1. Processes which are upregulated or downregulated during the stress/stringent response by *E. coli*.

Upregulated Processes	Downregulated Processes
Amino acid biosynthesis [147]	Cell division [155]
σ^S synthesis [148]	Cell motility [156]
Universal stress protein synthesis [149]	DNA replication [157]
Carbohydrate metabolism [145]	Stable RNA synthesis [158]
Virulence gene expression [150]	Ribosome synthesis [159]
Toxin/ antitoxin systems [151]	Protein synthesis [160]
Antibiotic resistance [152]	Translation initiation and elongation [161]
Cyclopropane fatty acid synthesis [153]	Nucleotide biosynthesis [162]
Chaperones and proteolysis systems [154]	Metabolite transport [163]
	Phospholipid synthesis [164]
	Oxidative metabolism [165]

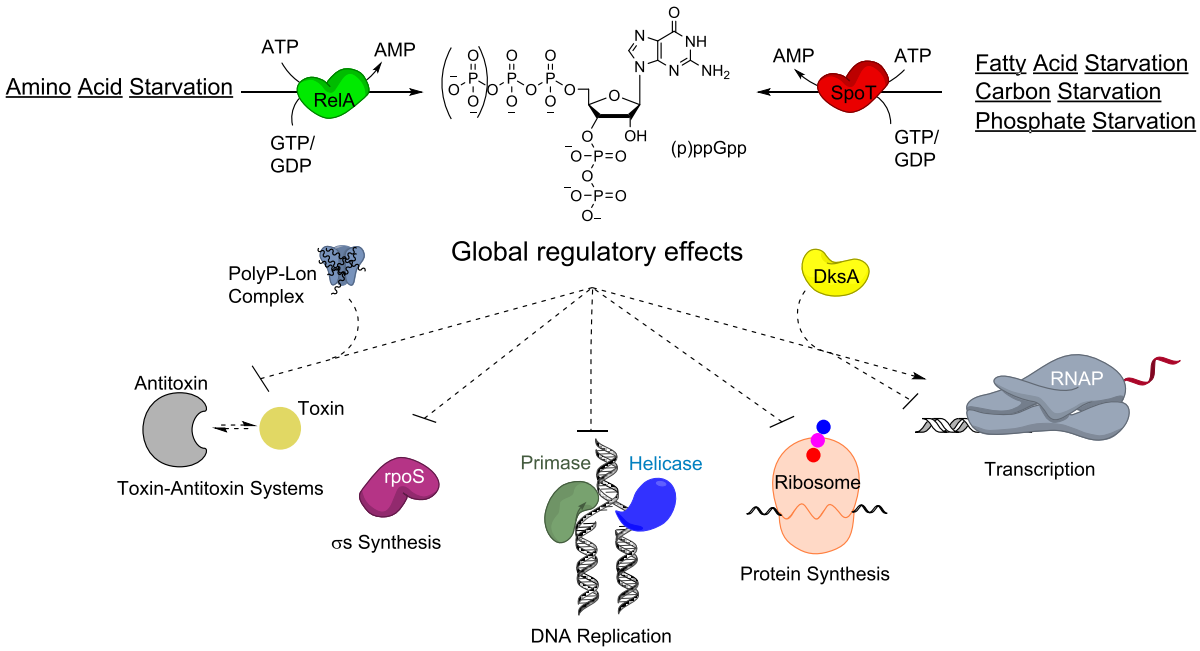

Figure 1.3.1. Cartoon schematic depicting the causes and outcomes of nutrient starvation in bacterial cells. RelA and SpoT enzymes respond to different environmental stresses to produce the signalling molecules (p)ppGpp. Examples of the effects of these molecules within the cell include the degradation of antitoxins to increase cellular toxin concentrations and downstream pleiotropic effects; decrease in stationary sigma factor (rpoS) concentrations; inhibition of DNA primase; inhibition of protein synthesis; and alteration to gene expression in co-ordination with transcription factor DksA [142-144, 146, 151, 160, 166-168].

In 2007 Durfee *et al.* were able to show using transcriptional profiling that flagellar and chemotaxis gene expression were also downregulated under the stringent response [146]. This suggests that upon entry into starvation mode *E. coli* cells become non-motile.

1.3.1 Activation of the Stringent Response

The stringent response can be triggered by a number of stressful environments for the bacteria as detailed above. The following section will detail the bacterial response to fatty acid, carbon and amino acid starvation.

1.3.1.1 The Stringent Response and Fatty Acid Starvation

Fatty acid starvation can be mimicked *in vitro* by the addition of the antibiotic cerulenin (Figure 1.3.2), an inhibitor of β-keto acyl thioester synthetase [169]. In 1993 Seyfzadeh *et*

al. demonstrated the rapid accumulation of (p)ppGpp during fatty acid starvation with a full complementation of amino acids and carbon source [142]. They further demonstrated that this accumulation of (p)ppGpp was SpoT-dependent. Following the observation that SpoT was also the primary enzyme responsible for ppGpp accumulation during carbon starvation [170], they proposed that carbon starvation induces fatty acid starvation and this then triggers SpoT-mediated (p)ppGpp synthesis. Fatty acid starvation was later shown to be mediated by the specific interaction between the TGS domain of SpoT and the deacylated acyl carrier protein (ACP) [171]. ACP is a central cofactor to fatty acid synthesis [172]. Cells containing SpoT mutants that are incapable of interacting with ACP, do not accumulate (p)ppGpp during fatty acid starvation [171].

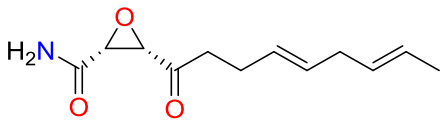

Figure 1.3.2. Chemical structure of the antibiotic cerulenin, which can be used to induce fatty acid starvation in cell culture.

1.3.1.2 **The Stringent Response and Carbon Starvation**

Bacterial cells encounter carbon starvation upon the limitation of their sugar source, *in vitro* this is commonly modelled with glucose deprivation [173, 174]. Carbon starvation results in the entry of cells into a resistant, non-growth state (stationary state): normal growth can be resumed however when conditions become favourable again. The transition into this state is dependent on the regulation of gene expression which can be mediated by signalling molecules such as (p)ppGpp [144, 145]. The inhibition of stable RNA synthesis during bacterial responses to stress conditions has previously been reported [175]. In 1983 Sarmientos *et al*. detailed the relationship between (p)ppGpp synthesis and transcription from ribosomal RNA (rrn) promoters. High levels of (p)ppGpp were linked to the inhibition of the upstream rrn promoter and subsequent reduction of ribosomal RNA synthesis [144]. Conversely a downstream promoter did not appear to be inhibited by (p)ppGpp levels, and was suggested to allow constitutive weak expression of ribosomal RNA throughout stringent conditions [144].

Carbon starvation can be mimicked *in vitro* by the addition of α-methylglucoside (α-MG), a glucose analogue (Figure 1.3.3) which competitively inhibits glucose uptake in *E. coli* [176]. The use of α-MG on *E. coli* cultures to cause a shift in growth rate, demonstrated that both stringent (*relA*$^+$) and relaxed (*relA*$^-$) strains of *E. coli* were able to accumulate ppGpp and rapidly curtail RNA synthesis [177]. This data was strongly supported by the results of Lazzarini *et al*. [178], which suggests that RelA is not responsible for the ppGpp accumulation in response to carbon starvation. Later research demonstrated that the enzyme SpoT was responsible for this accumulation of ppGpp during carbon starvation [170].

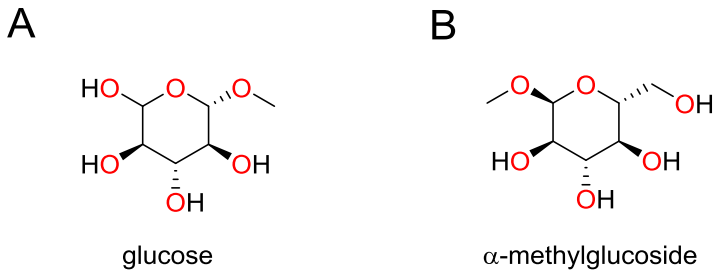

Figure 1.3.3. Chemical structures of glucose (A) and the glucose analogue α-methylglucoside (B).

In *V. cholerae* the rapid accumulation of (p)ppGpp levels within cells upon carbon starvation has also been noted [179]. Strains of *V. cholerae* with mutations in either the *relA* or the *csrS* gene resulted in the reduced expression of proteins usually upregulated during carbon starvation [173]. The *csrS* gene was suggested to encode a SpoT-like protein, however differences within its sequence implied the alterations in both the synthetase and hydrolase activity of this enzyme [179]. The *csrS* mutant strain demonstrated equal levels of (p)ppGpp accumulation to wild type (WT) upon carbon starvation, but interestingly higher absolute basal levels of (p)ppGpp (~4 fold higher than WT) [173]. This latter observation could suggest a weaker ability of this enzyme to hydrolyse (p)ppGpp.

1.3.1.3 **The Stringent Response and Amino Acid Starvation**

In 1973 Haseltine *et al.* showed the connection between the stringent response and an 'idling step' in protein synthesis [180]. Protein synthesis involves the ribosome-mediated

addition of individual amino acids to a peptide chain in an order determined by an mRNA sequence and the binding of a cognate aminoacylated-tRNA [181]. This process involves three sites within a ribosome designated A (Acceptor), P (Peptidyl) and E (Exit). The A-site accepts incoming cognate aminoacylated-tRNA, in the P-site the peptidyl transfer reaction occurs and finally the E-site contains unacylated-tRNA prior to its exit from the ribosome [181]. Protein synthesis relies on the movement of tRNA molecules through these three sites (Figure 1.3.4).

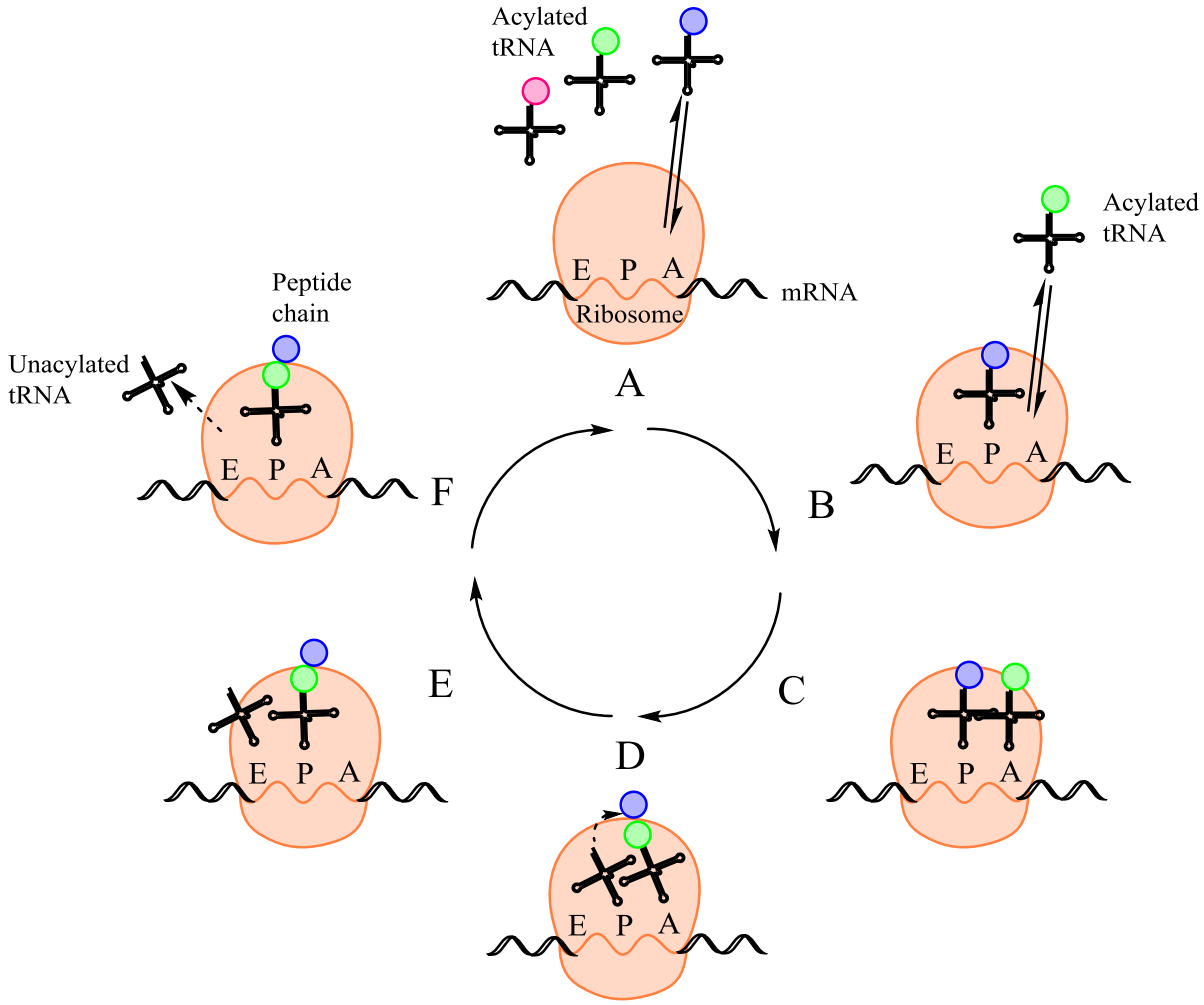

Figure 1.3.4. Cartoon illustration of ribosome-mediated protein synthesis. (A) Association and dissociation of charged tRNA moiety to the ribosomal A-site empty ribosomal complex (B) Transfer of charged tRNA to ribosomal P site and association of secondary charged tRNA to the ribosomal A site (C) Ribosome with occupied P and A sites (D) Formation of peptide bond within peptidyl transferase site. (E) Transfer of tRNA moieties to the neighbouring ribosomal sites, with the peptide chain remaining in the P site tRNA. (F) Dissociation of uncharged tRNA from ribosomal E site.

In 1973 Haseltine *et al.* uncovered the ribosome-bound stringent factor (RelA) and showed the synthesis of (p)ppGpp occurred when the A-site of the ribosome was unoccupied [182]. Later it was shown that the presence of unacylated-tRNA in the ribosomal A-site was responsible for triggering ppGpp synthesis in response to amino acid starvation [180]. During growth in nutrient rich conditions the intracellular levels of acylated-tRNA molecules are high and therefore the binding equilibrium at the ribosomal A-site (with the mRNA-encoded acylated tRNA, Figure 1.3.4b) correctly loads a higher proportion of ribosomal A sites [183]. This is due to rapid re-acylation of tRNA molecules following their dissociation from the ribosome. Entry into nutrient starvation however increases the intracellular pool of unacylated-tRNA molecules, and this in turn increases the probability that the A-site can bind a unacylated-tRNA. The presence of unacylated-tRNA in the ribosome leads to the stalling of protein synthesis and consequently ribosomes in this state are often referred to as 'stalled'. Entry into the stringent response caused by amino acid starvation is therefore highly reliant upon the ribosome-associated stringent factor RelA [168].

1.4 Signalling Molecules Guanosine Penta/Tetraphosphate (p)ppGpp

The signalling nucleotides guanosine 3', 5' bisphosphate (ppGpp) and guanosine 5'-triphosphate 3'diphosphate (pppGpp) are the main effectors of the stringent response [184] (Figure 1.4.1). Originally discovered as two unexpected spots from TLC analysis of cells under nutrient stress, these compounds were initially known as Magic spot I and II for ppGpp and pppGpp respectively [185]. Full chemical characterisation of these compounds was later aided by the use of ^{13}C nuclear magnetic resonance (NMR) analysis [186]. Once synthesised, pppGpp is often converted into ppGpp by members of the PPX/GppA superfamily [187]. Other enzymes responsible for the conversion of pppGpp to ppGpp include translational GTPases such as EF-G, EF-Tu or IF-2 (Figure 1.4.1) [188, 189]. The global regulator is therefore most often described as ppGpp due to its abundance over pppGpp in *E. coli* [190]. For certain Gram-positive species however the predominant signalling nucleotide is pppGpp [191, 192]. Collectively these molecules exert a plethora of downstream effects within the cell resulting in an alteration in cellular growth rate, virulence, persistence, antibiotic resistance and secondary metabolite regulation.

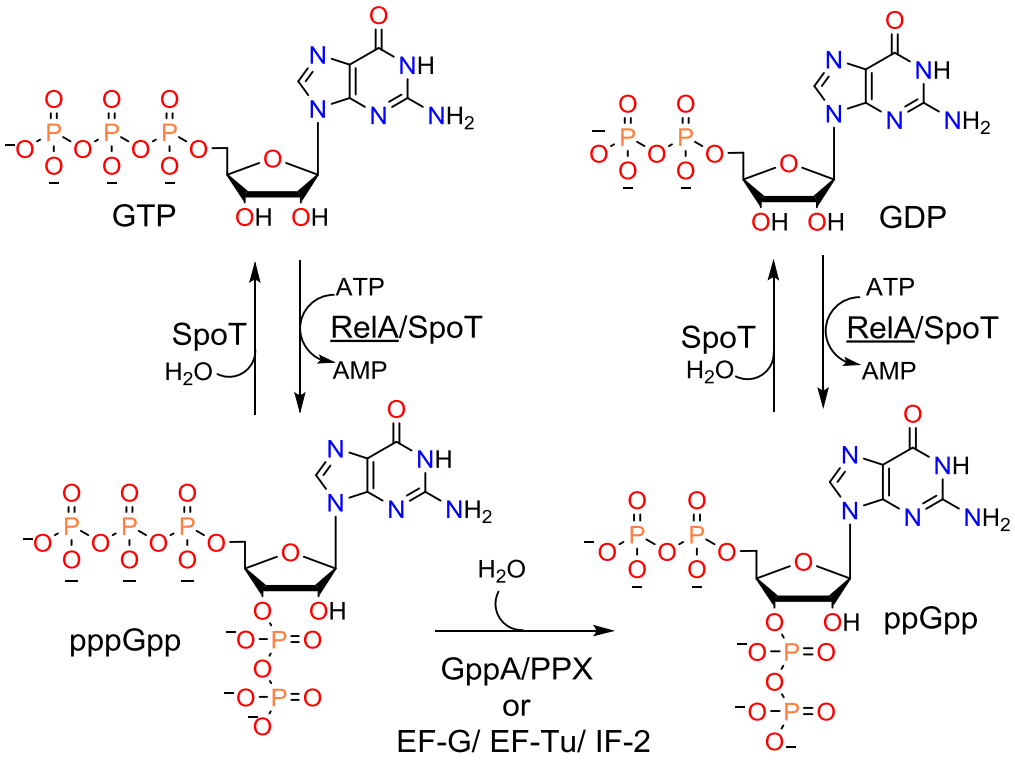

Figure 1.4.1. Metabolism of guanosine penta- and tetra-phosphate within bacterial cells. Synthesis of (p)ppGpp from GDP/GTP respectively is catalysed by the enzymes RelA and SpoT. The pppGpp can then be converted to ppGpp following hydrolysis of the 5' terminal phosphate by GppA/ PPX enzymes as well as a variety of GTPases. The enzyme SpoT catalyses the hydrolysis of the 3' pyrophosphate moiety to yield GDP/ GTP from ppGpp/ pppGpp respectively.

1.4.1 Transcriptional Regulation and (p)ppGpp

1.4.1.1 RNAP and (p)ppGpp

The outcome of the induced stringent response is largely reliant on the transcriptional regulation of genes. This transcriptional regulation has been linked to the interactions between the transcription factor DksA, ppGpp and the DeoxyriboseNucleic Acid (DNA)-dependent RiboNucleic Acid polymerase (RNAP). The nucleotide ppGpp has been shown to bind directly to a site within RNAP [147], and a recent 3D structure of RNAP co-crystallised with ppGpp shows it bound near the active site [193]. Furthermore, ppGpp directly interacts with the transcriptional factor DksA [194] and the DksA: ppGpp complex can then bind to the secondary channel of the RNAP [195]. The interaction causes the downregulation of several genes by reducing the half-life of the open complex of the

RNAP at a promoter [157]. This destabilisation is particularly effective for promoters with a GC rich region (discriminator) between the TATA box (-10) and the +1 position [184], and in those promoters with shorter linker regions between the -35 and -10 sequences (Figure 1.4.2) [184]. Conversely, genes with a AT rich discriminator are upregulated by the DksA: ppGpp: RNAP complex formation (Figure 1.4.2).

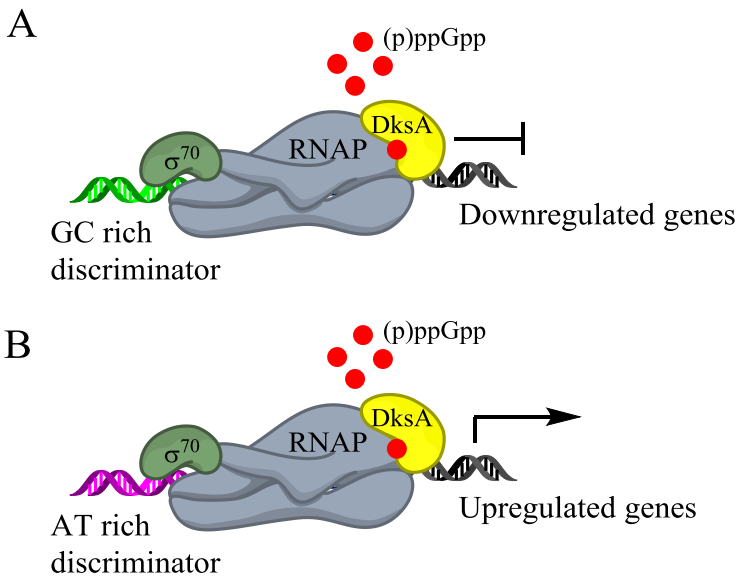

Figure 1.4.2. Cartoon schematic of the downregulation (A) and upregulation (B) of genes mediated by interaction between the transcription factor DksA and the signalling molecules (p)ppGpp. Adapted from [196].

1.4.1.2 Sigma Factor Regulation and (p)ppGpp

Indirectly both DksA and ppGpp regulate transcription of several genes by σ-factor competition. During the exponential phase of bacterial growth, when the population increases in a logarithmic fashion, the vegetative σ-factor (RpoD) will directly interact with the RNAP and support the transcription of genes fundamental to protein, lipid and DNA synthesis [197]. During the stringent response ppGpp is produced rapidly, this molecule has been shown to inhibit the binding of RNAP to strong σ-factor dependent promoters [198]. This inhibition leaves core polymerase free to bind alternative σ-factors which also accumulate during the stringent response. In *E. coli* it has been shown that the stationary sigma factor (RpoS), vital for stress resistance and expression of virulence factors, is controlled both directly and indirectly by ppGpp [166]. This is possible by

regulation at several levels; gene transcription [148], mRNA translation [199], protein stability [166] and protein activity [200]. The transcription of RpoS is consistent throughout the vegetative phase but during this phase the σ-factor is directed to the ClpXP proteasome by an adaptor protein, rssB [201]. By inducing the expression of anti-adapter proteins IraP [202] and IraD [203], which bind and therefore inhibit rssB, ppGpp is able to promote the stability of RpoS. The induction of IraP expression is related to phosphate stress and is dependent on the activity of SpoT specifically [197]. One hypothesis is that the precise intracellular concentration of ppGpp is responsible for regulating certain downstream effects, such as the upregulation of IraP expression. This hypothesis supports the observed requirement of the enzyme SpoT, as the hydrolase activity of this enzyme is important in maintaining cellular levels of ppGpp [184, 204].

1.4.1.3 **Initiating Nucleotide Levels and (p)ppGpp**

A broader, less specific, method of regulating transcription of genes from particular promoters is the limitation of available initiating nucleotides. Recent reviews have described a wide range of literature demonstrating a strong link between GTP metabolism and the stringent response in Gram-positive bacteria [205, 206]. In *Bacillus subtilis* the levels of the nucleotides GTP and ATP, which vary in a reciprocal manner, can regulate transcription, dependent on which is required as the initiating nucleotide for transcription (iNTP) [207]. In *B. subtilis* the inhibition of inosine monophosphate dehydrogenase, an enzyme which catalyses an early step in GTP biosynthesis, by (p)ppGpp results in an inhibition of GTP biosynthesis [196]. During the stringent response, the coupled turnover of GTP to pppGpp and inhibition of GTP biosynthesis results in a drop in GTP concentration [208]. The resultant low GTP level leads to the decreased transcription of operons requiring GTP as the iNTP [207]. A parallel mechanism of transcriptional regulation by GTP in *Firmicutes* occurs through the direct interaction between ppGpp and the transcription factor CodY [205, 209]. In *B. subtilis* these mechanisms can have many important downstream effects vital in eliciting the stringent response including preventing sporulation [210], inhibiting stable RNA synthesis [211] and promoting amino acid biosynthesis [212].

1.4.2 **Growth Arrest and (p)ppGpp**

The stringent response naturally occurs during the transition of a bacterial culture from logarithmic to stationary phase [200] (Figure 1.4.3) and has been well described for the cessation of growth in response to nutrient limitation [147]. This growth arrest is associated with several downstream effects of (p)ppGpp biosynthesis including: the downregulation of stable RNA biosynthesis, inhibition of DNA replication, downregulation of cell wall and phospholipid biosynthesis [184].

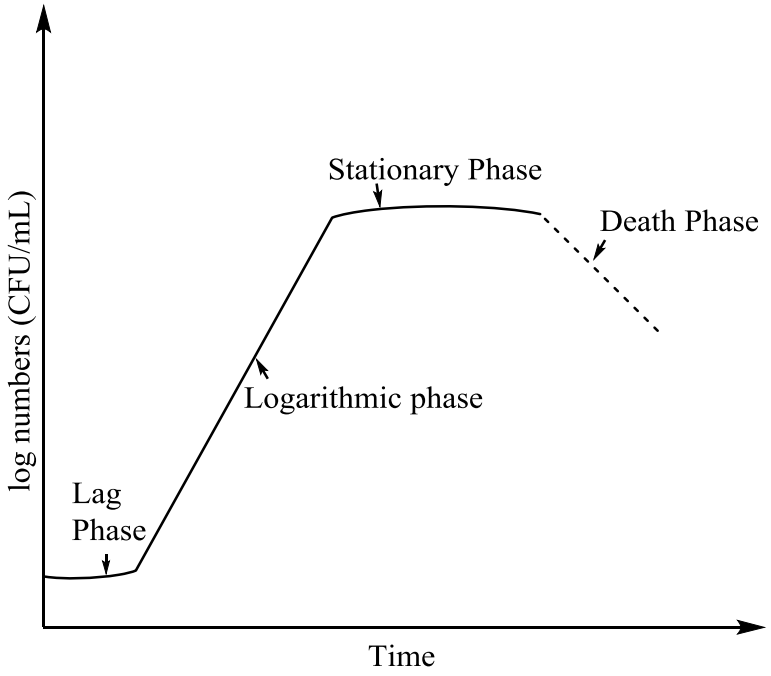

Figure 1.4.3. Generalised growth curve for bacteria including lag, exponential, stationary and death phase.

Despite early studies concluding that DNA replication was inhibited at the initiation stage at *oriC* further research elucidated that DNA primase was being directly inhibited by (p)ppGpp [167]. Conversely the downregulation of stable RNA molecules such as transfer RNA (tRNA) and ribosomal RNA (rRNA) in *E. coli* is primarily achieved by transcriptional regulation of these genes [206]. Upon entry into a growth arrest state cell wall biosynthesis is of reduced importance, in *E. coli* downregulation of both peptidoglycan and phospholipid biosynthesis occurs during the stringent response [213].

1.4.3 **Quorum Sensing, Biofilms and (p)ppGpp**

Quorum sensing is a process dependent on the release and detection of signalling molecules, such as N-acyl homoserine lactone (AHL), to sense the density of a cell population [214]. In *P. aeruginosa* full expression of the AHL quorum sensing systems are reliant on (p)ppGpp as shown by comparison of a (p)ppGpp null mutant with that of the wild type [215]. Previous work with *P. aeruginosa* has shown that the synthesis of autoinducers and particular virulence factors only occurs at a certain cell density. Previous work by Van Delden *et al*. demonstrated that induction of the stringent response by the addition of the serine analogue serine hydroxamate led to premature production of the autoinducer 3-oxo-C_{12}-homoserine lactone (HSL) [216]. Furthermore the overexpression of *relA* led to the premature accumulation of the virulence factor LasB elastase [216].

Biofilms can be defined as communities of microorganisms which are attached to a surface [217]. The formation of a biofilm is reliant on planktonic (free swimming) bacteria transitioning to a surface bound community [217], a process which is dependent on quorum sensing [214]. Given the observed link between the stringent response and quorum sensing [216], a subsequent link between the stringent response and biofilm formation was postulated. Within the species *Enterococcus faecalis*, mutant strains deficient in the stringent response (Δ*relA*/ Δ*relQ*/ Δ*relA*Δ*relQ*) were observed to possess a weaker ability to form biofilms [218]. Similar observations of reduced biofilm formation have been seen for stringent response mutants in *Escherichia coli* [219], *Streptococcus mutans* [220], and *Vibrio cholerae* [221]. For *E. faecalis* strains cell viability was also shown to deplete at a faster rate for the double mutant, with 57% survival recorded at 3 days compared to >95% survival recorded for the other mutants and wild type strain [218].

The relationship between the stringent response and biofilm formation was further unfolded when in 2014 Robert Hancock's group identified of the immunomodulatory peptide innate defence regulator (IDR)-1018, herein referred to as peptide 1018 [222]. The failure to accumulate ppGpp was noted for several bacterial strains upon treatment with peptide 1018 (5 μg/mL). Phosphorus NMR analysis of peptide 1018 and the nucleotides ppGpp and GTP showed a reduction of ppGpp signals following the addition of peptide 1018 [222]. This data was indicative of direct binding between ppGpp and the peptide, however subsequent work demonstrated an inability to release ppGpp from the

peptide following treatment with formic acid. TLC and NMR analysis of *in vivo* experiments elucidated that ppGpp was eliminated 30 minutes from the addition of peptide 1018 (20 µg/mL) to *P. aeruginosa* culture grown for 3 hours in the presence of serine hydroxamate, with similar observations following the overexpression of *relA* [222]. Fuente-Núñez *et al.* therefore suggested that peptide 1018 was binding ppGpp and targeting it for degradation (Figure 1.4.4). An alternative hypothesis would be that peptide 1018 is inhibiting the activity or activation of the RelA enzyme. The effect of peptide 1018 on RelA (p)ppGpp synthetase activity has however not currently been determined.

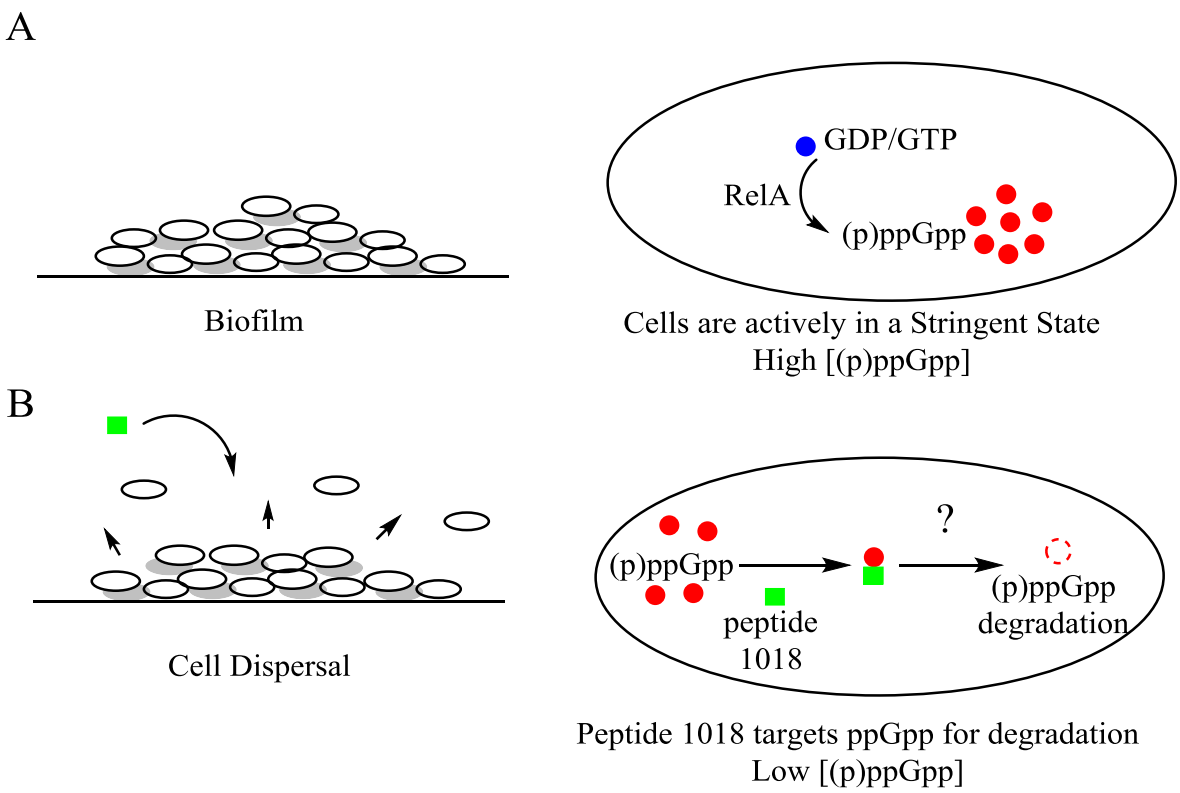

Figure 1.4.4. Cartoon schematic depicting the effect of peptide 1018 on biofilms. (A) Cells within a biofilm (left) have high levels of intracellular (p)ppGpp (right). (B) Following the addition of peptide 1018 (denoted by green square) cells begin to disperse from the biofilm (left) due to a reduction in intracellular (p)ppGpp concentration (left). The reduction in ppGpp is mediated by peptide 1018 but the mechanism of degradation is still unknown. Based on findings by Fuente-Núñez *et al.*[222].

The effect of this peptide on biofilm formation and dispersal was investigated with respect to its potential use for the treatment of bacterial biofilms. Dispersal of viable cells from a biofilm during an infection, can be particularly dangerous as these cells might result in the spread of infection to a secondary site or lead to sepsis [223]. Low concentrations of the peptide 1018 were shown to cause increased dispersal of viable cells from a *P. aeruginosa* biofilm [222], however when in combination with the antibiotic ciprofloxacin it showed reduced cell dispersal [224]. Further to this treatment of *P. aeruginosa* biofilms for 2 hours at the beginning of biofilm formation with peptide 1018 and ciprofloxacin completely inhibited biofilm formation leaving only a few aggregated cells. Treatment of pre-formed biofilms of this strain for 1 hour twice a day for 2 days virtually eradicated the biofilm [224].

1.4.4 **Antibiotic Resistance and (p)ppGpp**

The ppGpp-dependent increase in bacterial resistance to a wide range of antibiotics has been reported and is reviewed by Wu *et al*. [152]. In 1999 Greenway *et al*. investigated the level of antibiotic resistance for an *E. coli* ppGpp null mutant (CF1652) [225]. They analysed the sensitivity of the strain to a variety of different antibiotics including several beta-lactams, trimethoprim, gentamicin, polymixin B, Bronopol and 1,2-benziothiazolin-3-one (BIT) [225]. The ppGpp null mutant demonstrated reduced resistance to all the antibiotics tested, with measured minimal inhibitory concentrations (MICs) which were 4 to 16× lower than those measured for the wild type strain [225]. In addition, treatment of the wild type strain with the antibiotics concentrations lower than the MIC displayed a significant accumulation of ppGpp within 15 minutes of exposure [225].

Further work by Pomares *et al*. demonstrated a protective role of ppGpp against microcin J25 [226]. Microcin J25 is a peptide antibiotic known to function by binding to the secondary channel in RNA Polymerase β-subunit and preventing the binding of nucleotides [227]. The basis of this protection was therefore suggested to relate to the competitive binding of ppGpp to secondary channel of RNAP. Alternatively the molecule ppGpp was postulated to be exerting its effects from the upregulation of Yoj1, a protein transporter capable of keeping Microcin J25 levels below MIC within the cell [226]. Further work is required in this area to determine the precise nature by which ppGpp is conferring an increased resistance to the antimicrobial micrococin.

Penicillin, a β-lactam antibiotic discovered in the early 20th century, is still one of the most commonly prescribed antibiotics to date [228, 229]. β-lactam antibiotics work by inhibiting the final transpeptidase (cross-linking) reaction in the synthesis of peptidoglycan [230]. This results in a fragmented cell wall and renders the cell vulnerable to lysis by osmotic pressure [230]. Commonly autolysis of the existing peptidoglycan is observed in cells treated with a β-lactam antibiotic. Autolysins are enzymes capable of degrading components of the cell from which they are made, in bacteria a typical target is peptidoglycan [231]. The inhibition of the autolysin of *E. coli* [232] alongside the overall inhibition of peptidoglycan metabolism [213] observed in the presence of ppGpp results in increased resistance to these antibiotics.

These data collectively strongly support the hypothesis that the stringent response is important in antibiotic resistance in *E. coli* strains at least. An important corollary to these observations is that the development of an inhibitor of the stringent response as a potential conjugate for combined antibacterial therapy. In turn this might increase longevity in the medical use of current antibiotics.

1.4.5 **Persistence and (p)ppGpp**

Bacterial persistence was first discovered by Joseph Bigger. His work determined that following the treatment of bacterial culture with an antibiotic resulted in an initial increase in bacterial cell death that was followed by a reduction in death rate revealing rare persister cells which remained [233]. The persister cells were found to be few in number (~ 1 in every 100 000 cells), and were insensitive to antibiotics [233]. Persistence is reported for most bacterial species, and unsurprisingly has been shown to be prominent in chronic infections [234]. Initial work suggested that persister cells contained mutations which mapped to the *hipA* locus, whereby hip refers to high persister mutants [235]. Maisonneuve *et al.* determined that the cause of persister cells within a population arise following a momentary transition to a slow growth rate [151]. They attribute this transition to the occurrence of conditions inducing a micro-starvation state of small subpopulations within the overall population. This model suggested a potential role for the stringent response and subsequently ppGpp in persister cell formation. The importance of ppGpp in the HipA-mediated formation of persister cells was reported by Korch *et al*., with *relA/spoT* mutants demonstrating a drastically diminished capability to form persisters [236]. Work by Maisonneuve investigating the ability of *ppK*, *ppx*, *ppx/ppk*,

lon, and *relA/spoT* mutants to form persister cells, resulted in a proposed model for the stringent response induced persistence [151].

The *hipA* locus encodes a toxin: antitoxin system within *E. coli*. Overexpression of the HipA toxin results in the increase in persister cells [237], with the regulation of this toxin therefore postulated to determine persister formation. Toxin modules such as HipA are usually inactivated by the formation of a complex with their cognate antitoxin (i.e.; HipB) [237]. Furthermore the expression of antitoxin HipB results in the repression of the *hipA* gene. The degradation of antitoxins can therefore result in an increase in toxin concentration within the cell.

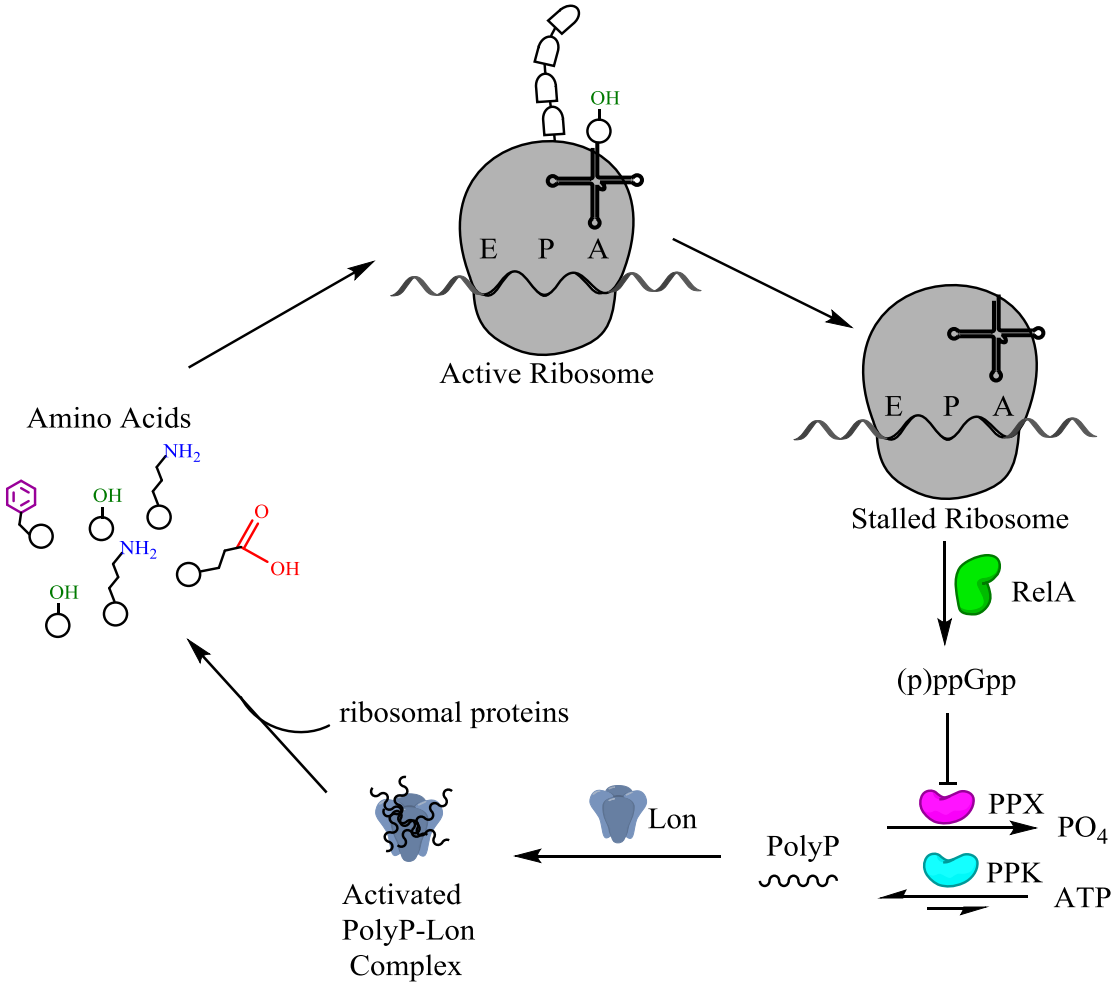

Figure 1.4.5. Cartoon schematic for the stringent response induced scavenging of amino acids via the PolyP-Lon degradation of ribosomal proteins. Upon amino acid deprivation, protein synthesis on the ribosome is stalled by the binding of unacylated tRNA to the ribosomal A site. The stalled ribosome activates RelA mediated (p)ppGpp synthesis. (p)ppGpp inhibits the exopolyphosphatase (PPX) activity, resulting in the accumulation of polyphosphate. Binding of polyphosphate to Lon activates the protease which degrades ribosomal proteins to generate a pool of amino acids. Adapted from [238].

Following from the initial proposal by Maisonneuve *et al.* the micro-starvation state was suggested to induce the stringent response within a small number of cells. The stringent response has been previously linked to the accumulation of polyphosphate (PolyP) [239].This accumulation of PolyP in turn results in the formation of a PolyP-Lon protease complex, capable of degrading a variety of short lived regulatory proteins including antitoxins (Figure 1.4.5) [238]. The proposed model therefore suggested that degradation of the antitoxin by the polyP-Lon complex resulted in a consequent increase in toxin

levels (Figure 1.4.6). The resultant increase in toxin levels subsequently allows the rapid accumulation of toxin by the increase in expression of both the toxin and antitoxin (Figure 1.4.6). In this model the degradation of antitoxin by the polyP-Lon complex is required to be more efficient than the expression of the antitoxin, and therefore denotes its regulation by the stringent response.

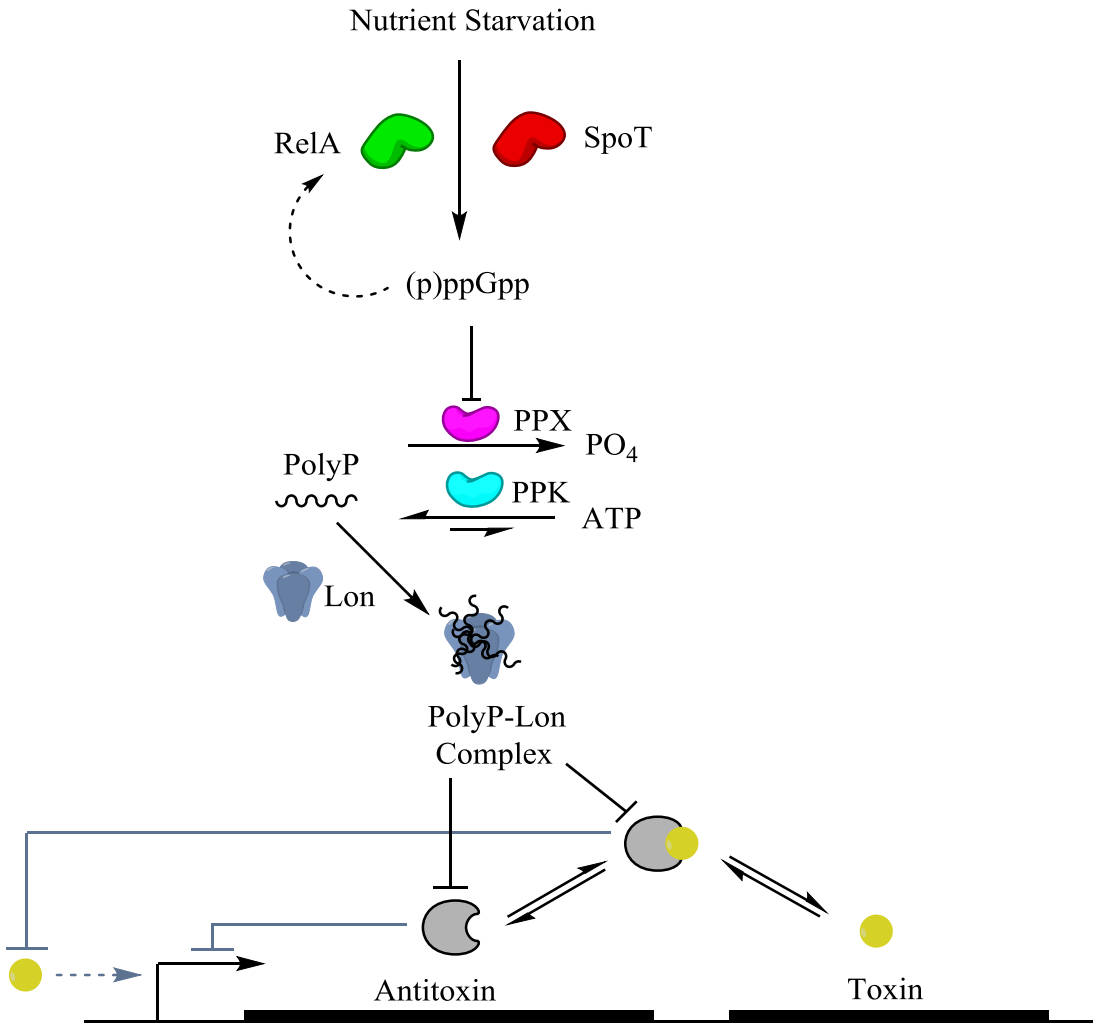

Figure 1.4.6. Cartoon schematic for the stringent response dependent accumulation of toxin required for the formation of persister cells. Nutrient starvation results in the synthesis of (p)ppGpp by the enzymes RelA and SpoT. The inhibition of PPX by (p)ppGpp results in the accumulation of polyphosphate. The binding of PolyP to the Lon protease, results in the degradation of the antitoxin. Increase in toxin concentration induces the expression of the antitoxin toxin operon. Adapted from **[151]**.

1.4.6 Secondary Metabolite Regulation and (p)ppGpp

Many bacteria will produce secondary metabolites during their lifecycle, which are non-essential but can yield beneficial results under certain environmental conditions. Examples include antibiotic production within *Streptomyces* strains, with 80% of antibiotics in clinical use derived from these species [240]. Antibiotic production within these strains has been shown to relate to the number of bacteria within the environment and the correlating reduction in nutrient availability [241]. It is not therefore a stretch to imagine the importance of the nutrient-dependent stringent response in regulating antibiotic production.

The production of the β-lactam cephamycin C (Figure 1.4.7a) and the β-lactamase inhibitor clavulanic acid (Figure 1.4.7b) in *Streptomyces clavuligerus* were shown to be negatively regulated by (p)ppGpp [242]. Biosynthesis of Cephamycin C and clavulanic acid in the wild type *S. clavuligerus* strain was compared to that of a *'relA'* knockout mutant, to show a 3-4 fold increase in clavulanic acid and 2.5 fold increase in cephamycin C production [242]. Complementation with wild type *'relA'* restored antibiotic levels to near that of wild type. Transcriptional analysis also demonstrated an increase in expression of genes involved in the production of these antibiotics within the mutant strain [242].

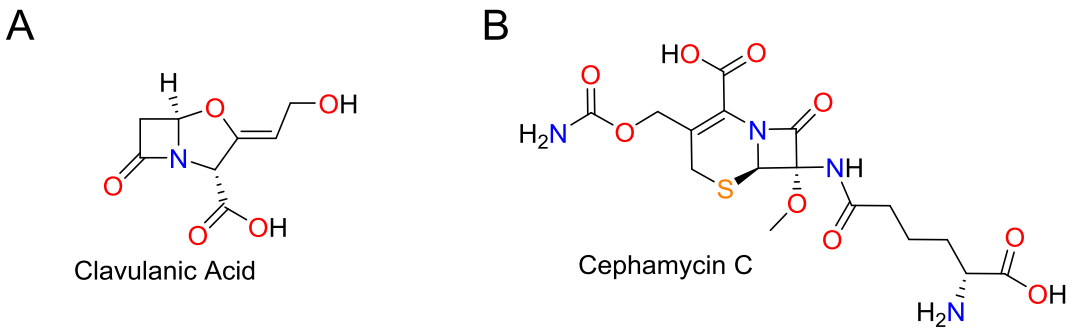

Figure 1.4.7. Chemical structures of secondary metabolites biosynthesised by *S. clavuligerus*. (A) The β-lactamase inhibitor Clavulanic acid. (B) The β-lactam Cephamycin C.

Another example lies within the biosynthesis of 4-hydroxy-2-alkylquinoline (HAQ) molecules in *Pseudomonas aeruginosa* (*P. aeruginosa*) [215]. HAQs are a family of secondary metabolites which share a common quinoline ring and have a wide range of biological indications [243]. The HAQ molecule 4-hydroxy-2-heptylquinoline-*N*-oxide

(HQNO) has been shown to induce biofilm formation in *Staphylococcus aureus*, which is often found to co-infect with *P. aeruginosa* in patients with cystic fibrosis [244]. Once again antibiotic production was monitored by comparison of that in a wild type strain with that in a *relA spoT* mutant strain. Conversely to what is described above for cephamycin C in *S. clavuligerus* however the *relA spoT* mutants of *P. aeruginosa* showed reduced biosynthesis of HQNO [215].

These data demonstrate that there is clearly a link between (p)ppGpp production and the regulation of secondary metabolite production, however this interplay appears to be variable across different species.

1.4.7 **Bacterial Virulence and (p)ppGpp**

Bacterial virulence and the alarmones (p)ppGpp have been described for a wide number of pathogens to date as reviewed by Dalebroux in 2010 [150]. These observations can be linked to the requirement of many pathogenic bacteria to survive inhospitable environments as part of their infectious lifecycle. A few examples are detailed below, including how ppGpp alters the virulence of *Francisella* species.

Enterohemorrhagic *Escherichia coli* (EHEC) is a strain of *E. coli* capable of causing gastrointestinal disease, but still retains a high level of similarity to the harmless K12 strain [245]. A key difference between these strains is the presence of the locus of enterocyte effacement (LEE) pathogenicity island which encodes a selection of virulence factors [246]. Nutrient deprivation induces the expression of the genes encoded on the LEE pathogenicity island and has been shown to encourage bacterial adherence [247]. Subsequent *in vitro* studies demonstrated that ppGpp and the transcription factor DksA are required for activation of the LEE1 promoter [247].

Yersinia pestis, the causative agent of plague (1.2.1.1), has a complicated infectious lifecycle in which it is capable of surviving and replicating within an insect (flea) and mammalian host [65]. A large variety of virulence factors are required for the intracellular survival of this organism within its two hosts and these are encoded on three plasmids [248]. Type III secretion systems (T3SS) are complicated structures utilised by bacteria to inject effector proteins directly into a host cell cytoplasm, and consequently play an important role in virulence [249]. The *Y. pestis* encoded type three secretion system (T3SS) is required for the bacteria to evade phagocytosis and also limit the host inflammatory

response [65]. The alarmone ppGpp has been shown to specifically induce the expression of the T3SS effectors YopE, YopH, both related to the disruption of host cell cytoskeleton and phagocytosis resistance, and LcrV which is linked to triggering IL-10 release and suppressing the pro-inflammatory cytokines TNF-α and IFN- γ [250]. *Y. pestis relA/ spoT* deletion mutants interestingly show a reduced mortality rate in murine model by subcutaneous infection with a 100 000 fold decrease in LD_{50} compared to the wild type strain [250]. This attenuation is not observed for the *relA* only deletion mutant, and can be reversed by the complementation of spoT alone. These data collectively suggest that *Y. pestis* requires ppGpp for efficient formation of bubonic disease in the mammalian host. The requirement for SpoT and not RelA under these conditions is still unclear but has been suggested to relate to a requirement of a specific basal concentration of ppGpp only achievable in the presence of the bifunctional RSH enzyme or the induction of expression from these virulence genes from low concentrations of ppGpp [150].

Francisella species are known to contain a so called *Francisella* pathogenicity island (FPI). The majority of genes on this pathogenicity island are positively regulated by the proteins MglA and SspA [251] with the exception of *ripA* [252]. MglA and SspA belong to the stringent starvation protein A family, and form a complex which binds to the DNA-dependent RNAP [253]. In 2009 Charity *et al*. were able to show that the putative DNA-binding protein in *Francisella novicida*, PigR, could bind to the MglA/SspA/RNAP complex and act to stabilise the interaction between RNAP and particular promoters [251]. Within this paper they show that the alarmone ppGpp promotes the interaction between PigR and this complex (Figure 1.4.8) [251]. This strongly supports the role of ppGpp in the virulence of *Francisella* species.

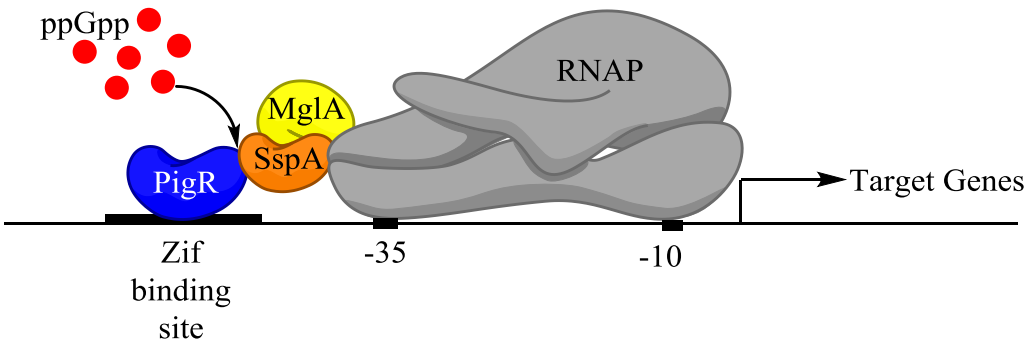

Figure 1.4.8. Cartoon schematic depicting the stabilisation of the putative DNA binding protein PigR complex formation with the transcription factors MglA, SspA and RNAP resulting in the upregulation of genes within *Francisella* species. Adapted from [251].

1.5 The RelA/ SpoT Homologue (RSH) Superfamily

RelA SpoT Homologue (RSH) enzymes are so named for their homology to the RelA and SpoT proteins in *E. coli* and constitute a family of enzymes that catalyse the synthesis and hydrolysis of (p)ppGpp [189]. Despite previous confusion over RSH protein nomenclature and phylogeny, a review by Atkinson *et al* in 2011 proposed division of the family into three groups: long RSH proteins, Small Alarmone Synthetases (SAS) and Small Alarmone Hydrolases (SAH) [189]. The main distinction between these groups is the differences in the domain structure of the enzymes (Figure 1.5.1). Aside from the long RSH enzymes, the other two groups are single domain proteins. The SAS group of proteins share homology with the synthetase domain of RelA and conversely the SAH group of proteins share homology with the hydrolase domain of SpoT [189].

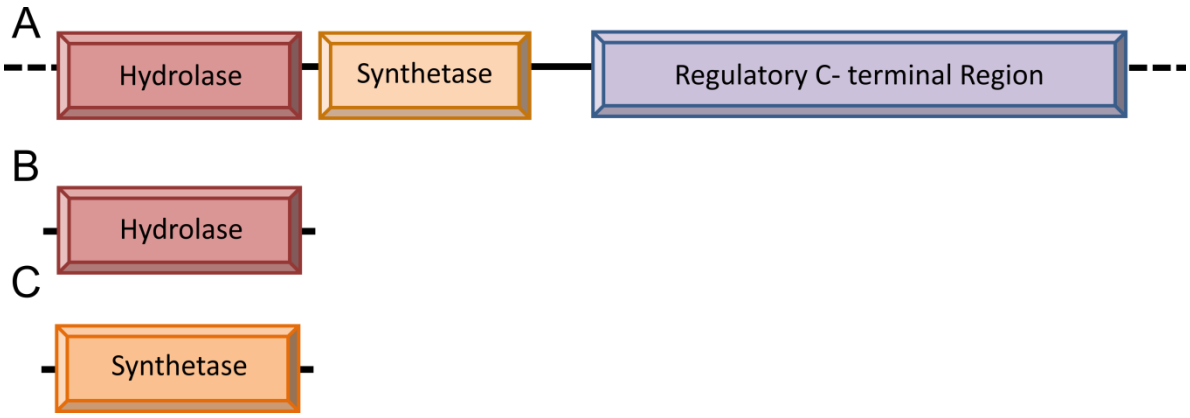

Figure 1.5.1. Schematic illustration for the difference in structure for the 3 classes of RSH enzymes; long RSH enzymes (A), small alarmone hydrolase (SAH) (B), small alarmone synthetase (SAS) (C). Adapted from [189].

1.5.1 Long RSH Enzymes

Long RSH proteins contain both hydrolase and synthetase domains and can be divided further into Rel, SpoT and RelA proteins (Figure 1.5.2). These enzymes contain a catalytic N-terminal region containing both the hydrolase and synthetase domains [189, 254, 255]. Within the regulatory C-terminal region, a further 4 domains have been identified: 'Threonyl-tRNA synthetase, GTPase and SpoT' (TGS), conserved cysteine (CC), 'Aspartate kinase, Chorismate mutase, TyrA' (ACT) and helical domain (Figure 1.5.2) [189]. Long RSH

enzymes can be further divided into bifunctional (Rel/SpoT) and monofunctional (RelA), dependent on their catalytic properties [256]. The protein sequences of RelA and SpoT from *E. coli* have been shown to share extensive homology, reflecting the similar domain structure they share [257].

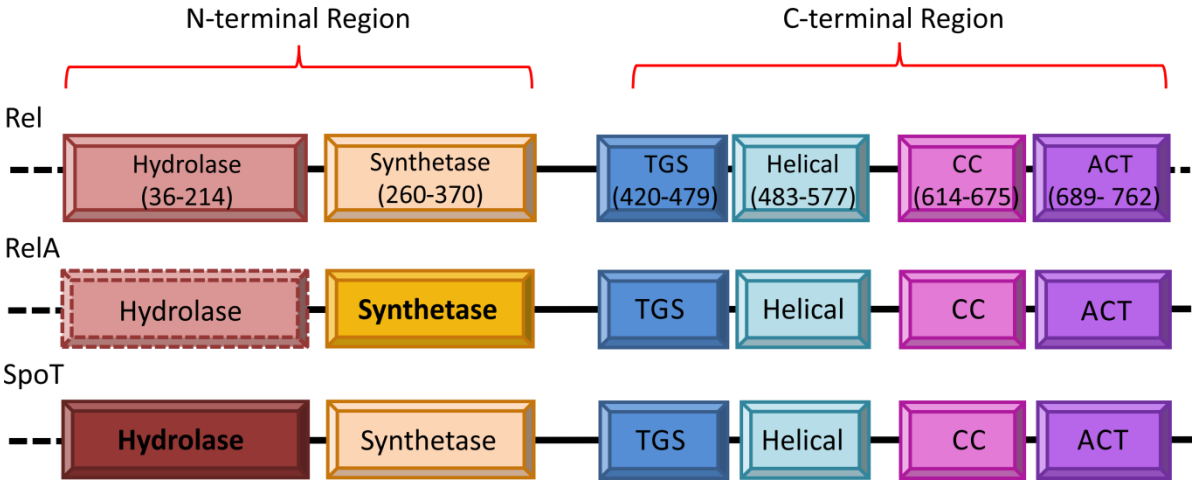

Figure 1.5.2. Illustration of the difference in domain structure for the N-terminal and C-terminal region of the long RSH enzymes: Rel, RelA and SpoT. Domains highlighted in bold indicate domains with greater activity. Dashed lines denote domains that are functionally inactive. Adapted from [189].

The long RSH proteins RelA and SpoT have only been identified in β- and γ-proteobacteria and are thought to have been derived from gene duplication [189]. Gene duplication relieves selective pressure on one or both of the duplicated genes. This allows sequence divergence (sub-functionalisation) and ultimately two more specialised gene products are generated [258]. Bacteria containing both RelA and SpoT proteins have a greater propensity to fine tune their levels of (p)ppGpp because of their independent hydrolase and synthetase activities.

Research into the potential pyrophosphate acceptors and donors for these enzymes demonstrated greatest activity with ATP as a pyrophosphate donor and GTP or GDP as a pyrophosphate acceptor (Table 1.5.1).

Table 1.5.1. List of potential pyrophosphate acceptors and donors for RSH enzymes, with respective percentage synthetase activity (100% activity in the presence of known substrates GTP and ATP) [259, 260]. Superscript numbers denotes nucleotides tested against the RSH enzyme from *E. coli* (1) or *B. subtilis* (2).

Pyrophosphate acceptor	Activity (% of maximal)	Pyrophosphate donor	Activity (% of maximal)
GTP[1]	100	ATP[1]	100
GDP[1]	92	GTP[1]	0
GDPCP[1]	32	UTP[1]	0
ITP[1]	20	CTP[1]	0
dGTP[1/2]	0	dGTP[1]	<3
dGDP[1/2]	0	dATP[1]	33
5'GMP[2]	2	dCTP[1]	0
GPPNP[2]	13	dTTP[1]	0
GPPPP[2]	8	ADP[2]	0
2'dGTP[2]	0	AMPPNP[2]	0

1.5.1.1 **The Rel Enzymes**

The most widespread of the long RSH proteins is the Rel protein, which has been identified in most bacterial species. Rel proteins are denoted by three letters corresponding to the organism it came from (first letter is the first letter of the genus, second and third letters are the first two letters of the species name) examples include the *M. tuberculosis* Rel protein, noted as Rel_{Mtb} [192], and *S. equisimilis* Rel protein, noted as Rel_{Seq} [191].

Rel proteins catalyse both (p)ppGpp synthesis and (p)ppGpp hydrolysis. Avarbock *et al.* demonstrated that for Rel_{Mtb}, in the absence of activating cofactors, both synthetase and hydrolase activities could occur simultaneously [262]. This suggested that these activities could be located to independent sites within the enzyme. Later work by Avarbock *et al.*

illustrated using mutational analysis that these activities mapped to different enzyme fragments: amino acid residues (aa) 87- 394 and aa 1-181 for the synthetase and hydrolase activity respectively [255]. Moreover, they demonstrated a simultaneous shift towards (p)ppGpp synthesis (20 fold increase in k_{cat}) and away from (p)ppGpp hydrolysis (2 fold reduction in k_{cat}) following the addition of stalled ribosomal complexes [255]. These data suggested an antagonistic mechanism of action between the respective active sites, an observation that is supported by research on other Rel proteins [191, 254].

Preliminary research has involved assessing the means by which this antagonism is regulated. Work by Mechold *et al*. on the Rel_{Seq} enzyme demonstrated a 12-fold increase in synthetase activity and 150-fold reduction in hydrolase activity for the C-terminal deletion (ΔCTD) mutant [191]. This led to the proposed model that the activities are mutually exclusive and the linker region between the N-terminal and C-terminal regions plays an important part in flexibility of this enzyme (Figure 1.5.3). Conversely, the equivalent mutation in Rel_{Mtb} failed to exert any alteration to either the hydrolase or synthetase activities of the enzyme compared to wild type [255]. The regulatory role of the C-terminal region in directing the switch from synthetase to hydrolase activity, or vice versa, is still therefore largely unknown and experimentally untested.

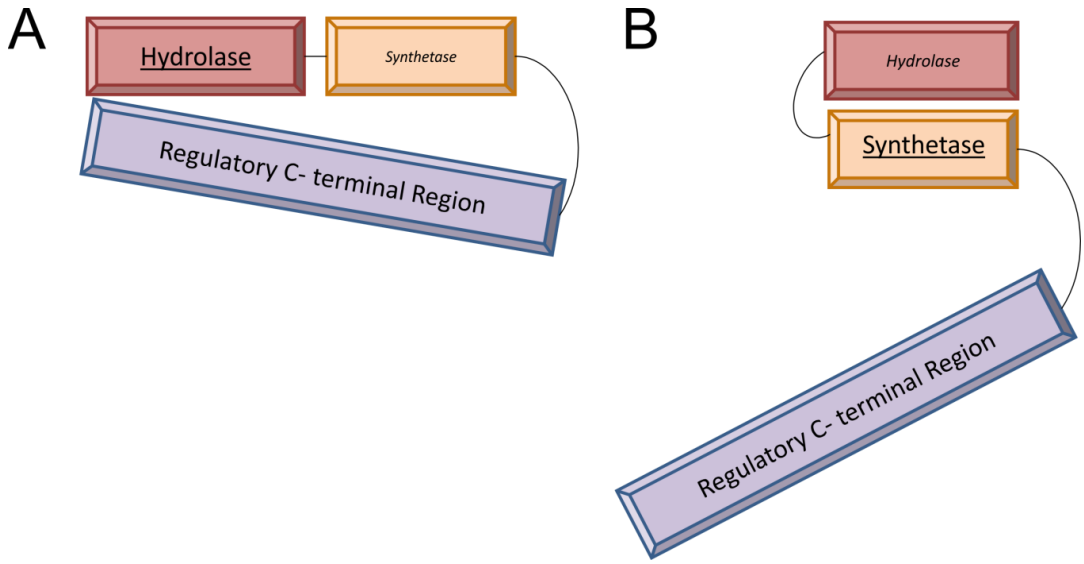

Figure 1.5.3. Illustration of the conformational antagonism responsible for RSH enzyme conformations induced by either hydrolase (A) or synthetase (B) activity. Underlined text indicates the active domains and smaller italicised text indicates inactive domains. Adapted from [191].

Alteration in an enzyme's multimeric state can result in a change in activity [263]. Wild type Rel_{Mtb} formed trimers *in vitro* (calculated molecular weight of 240 kDa) but both the C-terminal fragment (aa 395-738) and the N-terminal fragment (aa 1-203) alternatively remained as monomers [255]. This suggested that neither of these regions alone was sufficient for dimerization. Avarbock *et al.* went onto suggest that the trimeric state of the protein is its inactive form and the monomeric state could instead relate to its highly active state. Further work into the differences in activity upon changes in the multimeric state of the enzyme would be required to support this interesting hypothesis.

The transfer of a pyrophosphate group from the 5' β rather than α phosphate led to the expectation that Rel enzymes employed a dual divalent cation mechanism of reaction (Figure 1.5.4) [262, 264].

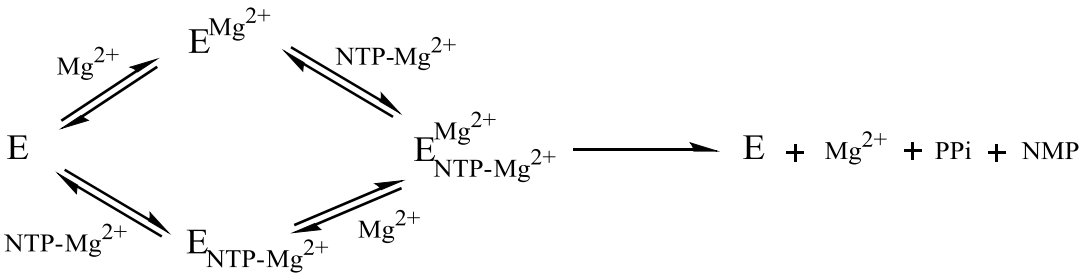

Figure 1.5.4. Scheme for dual divalent cation enzyme catalysed reaction with the release of pyrophosphate group from a nucleotide triphosphate (NTP). Adapted from [265].

The use of such a mechanism would require high levels of divalent cations, to ensure both substrate and enzyme were occupied. The (p)ppGpp synthetase activity by Rel_{Mtb} however was shown to diminish at higher concentrations of magnesium (Mg^{2+}) or manganese (Mn^{2+}) [262]. Optimal Mg^{2+} concentrations appeared to be stoichiometric to the substrate concentration and interestingly the optimal Mn^{2+} concentration was equivalent to half the substrate concentration [262]. This requirement for low levels of magnesium was later suggested to arise from an inability of the RXKD active site motif to co-ordinate a second magnesium ion [256]. These data collectively demonstrated that Rel enzymes did not use a dual divalent cation mechanism.

In 2004 Hogg *et al.* were the first to publish a 3D structure (to 2.1 Å resolution) for an RSH enzyme fragment (aa 1-385) [254]. This N-terminal fragment was observed to crystallise as one of two monomeric forms; a hydrolase-off/ synthetase-on monomer or a hydrolase-on/synthetase-off monomer. The hydrolase active site (aa 5-159) and synthetase active site (aa 176-371) were separated by 30Å with a 3 helix bundle domain (aa 135-195) between them (Figure 1.5.5) [254].

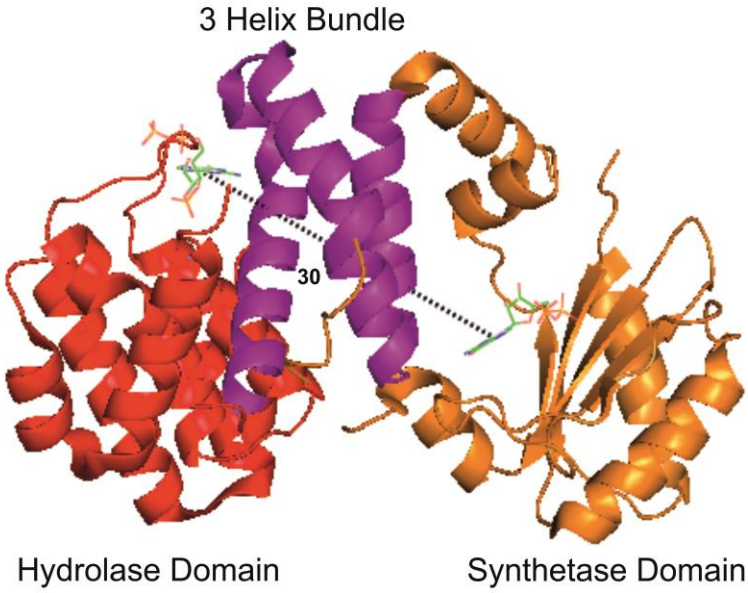

Figure 1.5.5. X-ray crystal structure of *S. dysgalactiae* subsp. *equisimilis* Rel protein N-terminal region (aa 1-385). This image details the joining of the hydrolase domain (aa 5-159) (red) with the synthetase domain (aa 176-371) (orange) via the 3 helix bundle (aa 135-195) (purple). Active sites of the hydrolase and synthetase domain are separated by 30 Å. PDB-1VJ7, visualised using Pymol.

Interestingly the hydrolase-on/synthetase-off monomer showed density attributable to the unusual ligand GDP- 2′:3′-cyclic monophosphate (ppG2′:3′p) (Figure 1.5.6b) [254]. This nucleotide was observed to fit within a cleft formed by residues 148-155 of the 3 helix bundle; nearby a hexa-coordinated Mn^{2+} (co-ordinated by H53, H77, D78, D144 and 2 H_2O) (Figure 1.5.6a) [254].

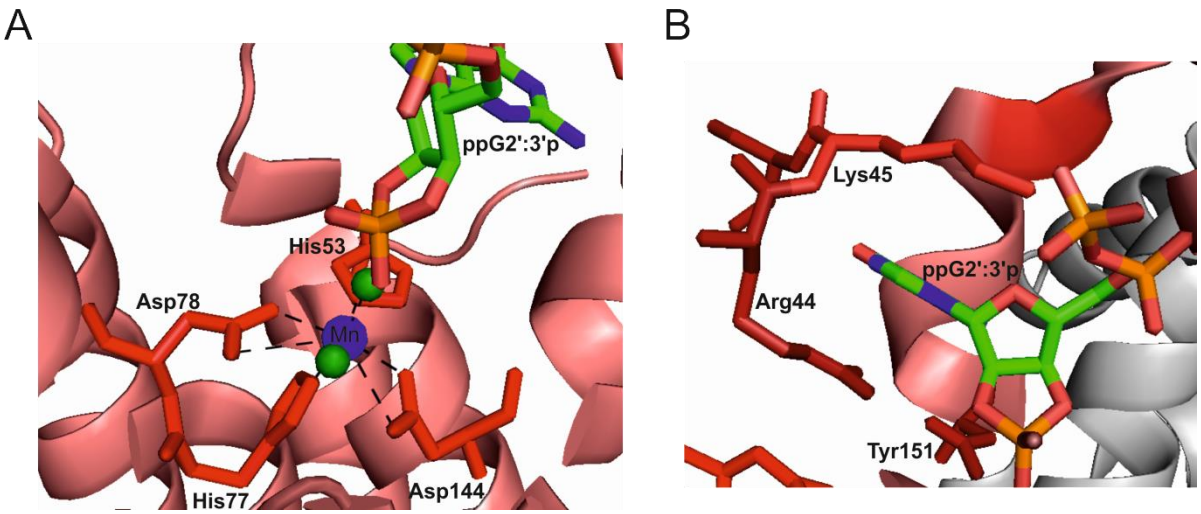

Figure 1.5.6. The hydrolase site within Rel enzyme from *S. equisimilis*. (A) Co-ordination of the manganese ion (Mn) by His53, His77, Asp78, Asp144 and 2 H_2O molecules. (B) The ppG2':3'p moiety within the hydrolase activity site, with the guanine base situated between the residues Arg44 and Lys45. PDB-1VJ7, visualised using Pymol.

Within the 3 helix bundle domain the α13/β4 loop containing Asp264 was termed the synthetase domain catalytic loop by Hogg *et al*. [254]. The importance of Asp264 for (p)ppGpp synthetase activity was established in part by comparison with the DNA pol β structure, which contains a similarly important aspartic acid residue in its active site [266]. Mutation of Asp264 to a glycine resulted in an inactive synthetase domain [254]. Comparison of the two monomer states suggested that this catalytic loop was vital in determining the enzymes activity. In the hydrolase-off/synthetase-on motif the Asp264 is situated within the synthetase active site and is directed towards Glu323 (Figure 1.5.7) [254]. In this conformation there is a small intercarboxylate distance (~4.6 Å), which Hogg *et al.* suggest is optimal for Mg^{2+} co-ordination upon ATP binding [254]. Conversely in the hydrolase-on/synthetase-off motif the Asp264 residue is removed from the synthetase active site and the intercaboxylate distance to Glu323 increases to ~14 Å [254]. This observation of an important overlapping section for the hydrolase and synthetase domains within Rel proteins had previously been noted. Analysis of Rel_{Mtb} fragments demonstrated an important overlapping region between the identified synthetase and hydrolase domains [255].

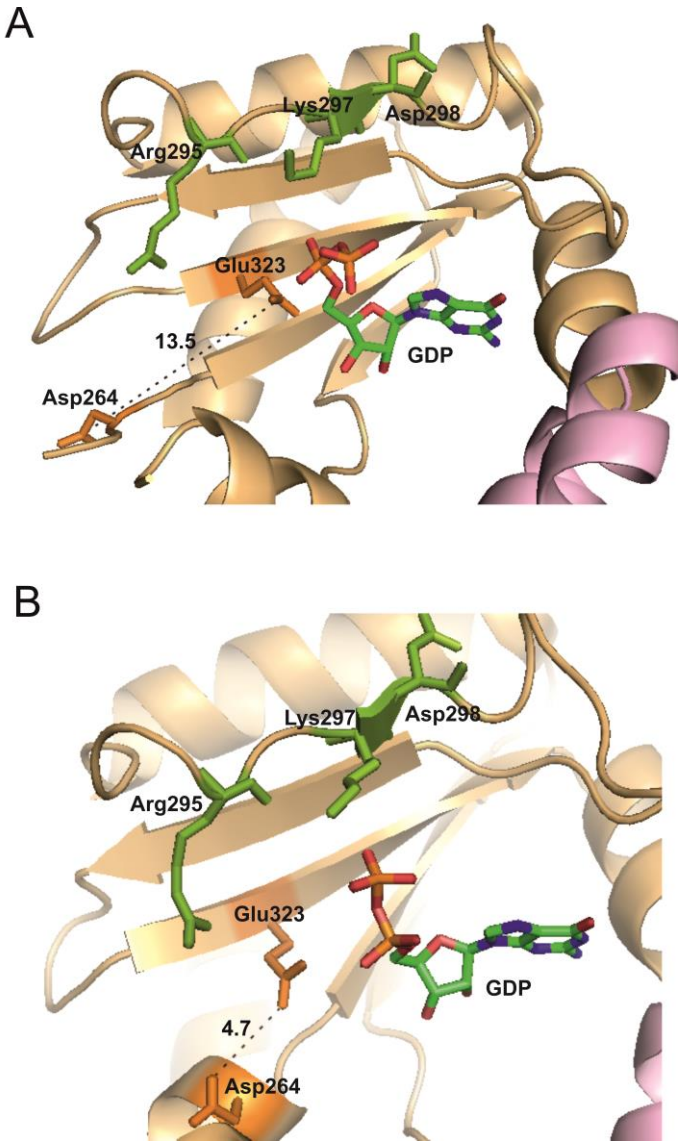

Figure 1.5.7. Proximity of Glu323 and Asp264 (highlighted in orange) within the synthetase active site for the hydrolase-on/ synthetase-off conformation (A) or the hydrolase-off/ synthetase-on conformation (B). Active site motif residues in the Rel_{Seq} synthetase site, Arg295, Lys297, and Asp298 are also highlighted in green. PDB-1VJ7, visualised using Pymol.

1.5.1.2 **The ppGpp Synthetase II, SpoT**

Initial analysis of the stringent response in *E. coli* showed that the enzyme RelA was capable of synthesising ppGpp [178]. Creation of *relA* null mutants however still retained residual levels of ppGpp production; this was shown to be eliminated by *spoT* null mutations [267]. Double *relA* and *spoT* mutants displayed increased auxotrophy and showed no accumulation of (p)ppGpp upon glucose exhaustion and chelation of manganese ions [267]. Mutational analysis detailed that this gene encoded a product

capable of (p)ppGpp hydrolysis and (p)ppGpp synthesis [268]. In *E. coli* the *spoT* gene was mapped to a new genetic locus, around 72 min on the chromosome [269], and was found to be the second gene in the *spo* operon [204]. Deletion mutants for *spoT* demonstrated greater (p)ppGpp stability following recovery from starvation conditions [269].

The *spoT* gene was originally thought to encode for an unstable (p)ppGpp synthetase and a stable (p)ppGpp hydrolase [270]. Subsequently acquired knowledge of the antagonistic nature of Rel enzymes revealed that these two activities were within the same enzyme [254, 255, 262]. Isolation of SpoT (as judged by its activity) showed that it was located within the cytoplasm [270, 271] and associated with ribosomes [272]. It was not however reliant on ribosomes for activity [272].

SpoT, like Rel proteins, contains an active synthetase domain and an active hydrolase domain. However, unlike Rel proteins, SpoT has a greater activity in its hydrolase domain than its synthetase domain [272, 273]. The enzyme SpoT has been shown to be part of a metal-dependent phosphohydrolase superfamily [274]. The identification of a novel superfamily of metal-dependent phosphohydrolases termed HD, identified three key amino acid motifs conserved across the whole family. Motif II contains two conserved histidine residues and was designated the HD signature. Secondary structure prediction of motif II suggested a complex α-β pattern [274]. Further conserved amino acids found in motifs I or V were either histidine or aspartate, suggesting that divalent cation co-ordination was a requirement for the activity of these enzymes. The hydrolysis of (p)ppGpp by SpoT is dependent on the presence of manganese [275].

The SpoT enzyme from *E. coli* is responsible for (p)ppGpp synthesis under carbon starvation [270], fatty acid starvation [276], iron starvation [277] and phosphate starvation [143]. The enzyme SpoT was shown to interact with the Acyl Carrier Protein (ACP), a fundamental co-factor in fatty acid synthesis, via its TGS domain [278]. Further analysis of the interaction has shown that it is the helix II of ACP that is involved in the direct interaction with SpoT [279].

1.6 The (p)ppGpp Synthetase I Enzyme, RelA

RelA, also known as (p)ppGpp synthetase I or stringent factor, was the first (p)ppGpp synthetase discovered [196]. The RelA enzyme catalyses the transfer of a 5' pyrophosphate moiety from a donor (typically ATP) to the 3' position of a pyrophosphate acceptor (typically GDP or GTP) yielding (p)ppGpp and AMP [168] (Figure 1.6.1). *E. coli* cells lacking the *relA* gene are described as displaying a 'relaxed' phenotype. This refers to the relaxed response to RNA accumulation under amino acid starvation conditions when compared to that of wild-type cells [280]. The *relA* gene was first described by Stent and Brenner, who noted the existence of a chromosomal locus in *E. coli* (referred to as RC), which in a different allelic state (RC^{rel}) allowed an impaired stringent response to amino acid starvation [281].

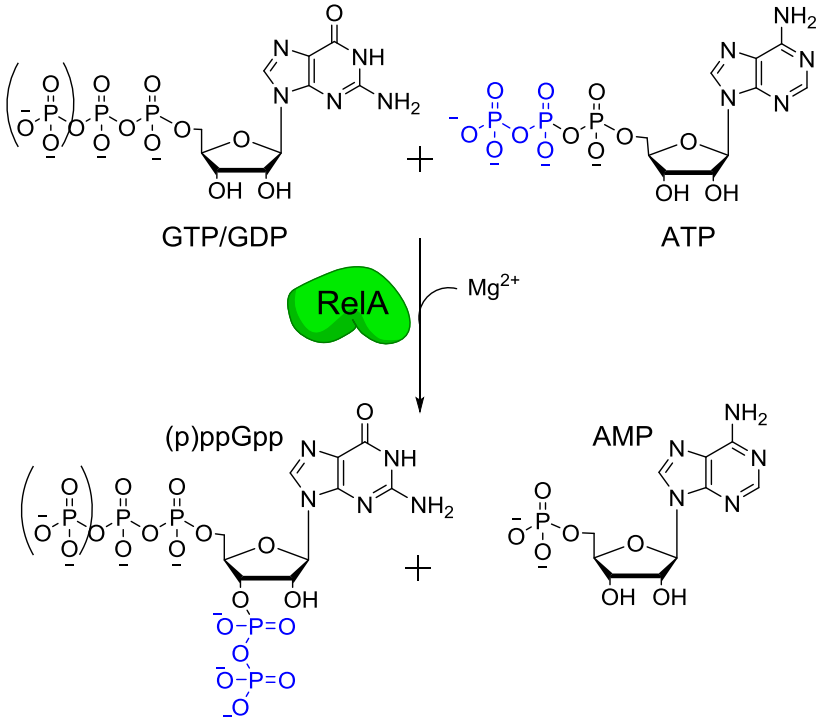

Figure 1.6.1. Chemical schematic detailing the RelA-mediated transfer of the terminal pyrophosphate from the 5' position in ATP to the 3' position of either GTP or GDP.

1.6.1 Proposed Structural and Functional Features of RelA

As described previously for other long RSH enzymes (1.5), RelA consists of a catalytic N-terminal region and a regulatory C-terminal region joined by a flexible linker region [189] (Figure 1.5.2). The majority of detailed studies have focused on the RelA enzyme from *E. coli* and unless stated otherwise any RelA mentioned in this section is that from *E. coli*. The importance of C-terminal regulation of *E. coli* RelA activity has been more extensively studied than its regulatory role within other long RSH enzymes (Figure 1.6.2) [282, 283]. Research by Gropp *et al.* showed that the overexpression of *E. coli* RelA C-terminal region (residues 455 to 744) has a negative effect on (p)ppGpp synthesis under amino acid starvation [283]. Interestingly the overexpression of the RelA N-terminal region resulted in constitutive (p)ppGpp synthetase activity [282], strongly supporting the suggestion that the C-terminal region is involved in downregulating (p)ppGpp synthetase activity. Residues Cys-612, Asp-637 and Cys-638 were shown to have key roles in co-ordinating this negative regulation [283]. Mutational analysis of Cys-612, Asp-637, and Cys-638 highlighted the importance of these residues in the regulation of RelA activity, but showed no interference with ribosome binding [283]. The residues were proposed to co-ordinate regulation by the formation of disulphide bonds between the cysteine residues. No structural data is currently available for the enzyme RelA, though structural data is available for the N-terminal region of Rel_{Seq} [254] and a SAS enzyme from *B. subtilis* [284]. The absence of crystallographic information for the C-terminus region of RSH enzymes makes any structural rationalisation of regulation difficult. The C-terminal region was suggested to potentially further mediate negative regulation of synthetase activity via dimerization [282]. Further analysis of the C-terminal region demonstrated the requirement of residues 550-682 for homo-dimerisation, ribosomal association and interference with RelA activation [282].

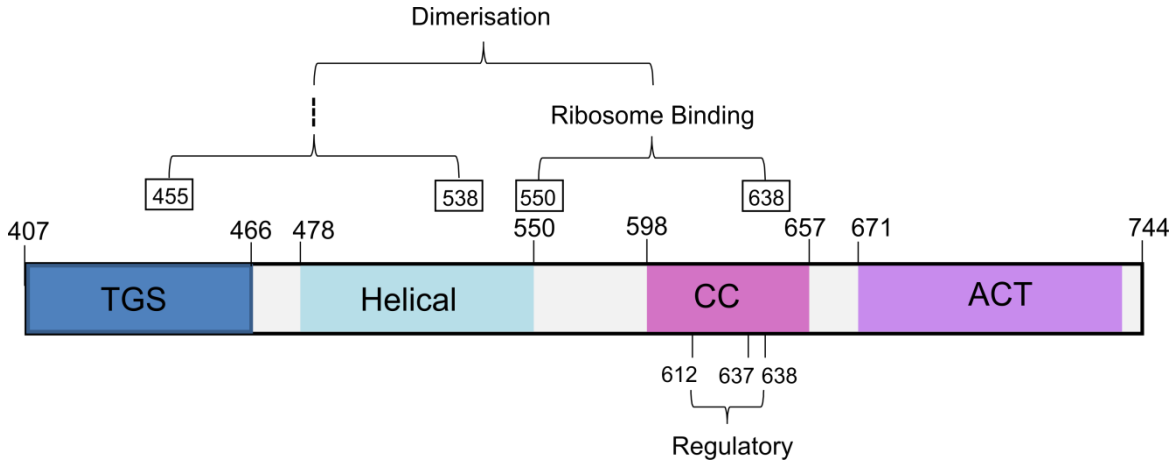

Figure 1.6.2. Identified residues and sections of the C-terminal domain of *E. coli* RelA involved in RelA dimerization, ribosomal binding and regulation of (p)ppGpp synthetase activity [282, 283].

1.6.1.1 **Inactive Hydrolase Domain**

RelA enzymes are mono-functional long RSH enzymes, which are incapable of hydrolysing the 3' pyrophosphate in guanosine penta-/tetra-phosphate. In 1998 the classification of a new superfamily of metal-dependent phosphohydrolases (1.5.1.2) detailed the requirement of a hydrolase domain (HD) motif for the hydrolytic activity of RSH enzymes [274]. Analysis of the RelA sequence from *E. coli* and *H. influenzae* demonstrated that this HD motif was absent within these sequences [274] (Figure 1.6.3). The amino acid substitutions within this motif in the hydrolase active site prevents the Mn^{2+} dependent mechanism of (p)ppGpp hydrolysis as these ligands are important in co-ordinating the manganese ion (Figure 1.5.6, H53 and H77) [274]. These mutations were not however suggested to alter the domain structure.

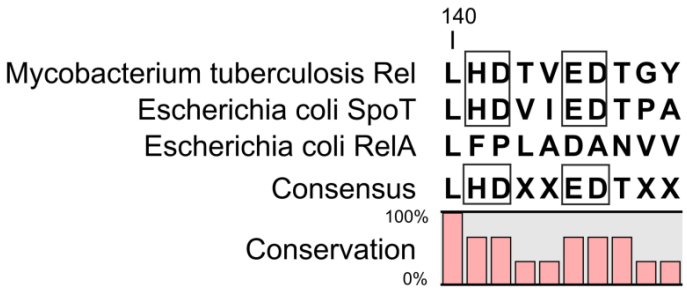

Figure 1.6.3. Amino acid alignment of HD domain motif across long RSH proteins; Rel_{Mtb}, *E. coli* SpoT and *E. coli* RelA.

1.6.1.2 **Synthetase Domain and regulation of (p)ppGpp synthesis**

RelA enzymes, like all RSH enzymes, contain a distinct synthetase domain (aa 251-359 in *E. coli* RelA) in their N-terminal region. A synthetase domain motif has been identified and furthermore shows differentiation between monofunctional RelA enzymes (EXDD) and bi-functional RSH enzymes (R/KXKD) [285] (Figure 1.6.4). Identification of the motif was achieved by comparison of the Rel_{Seq} synthetase domain and the structure of DNA polymerase, which is known to contain three conserved aspartate (D) residues involved in the co-ordination of two magnesium ions [286]. Both the RXKD and EXDD motifs are suggested to accommodate the co-ordination of one magnesium ion. The EXDD motif in RelA is thought to also be important in the co-ordination of a second magnesium ion (Mg^{2+}), which is possible because of the switch from a positively charged lysine to a negatively charged aspartate residue [285].

The residues G251 and H354 within the synthetase active site are also important in determining synthetase activity. Analysis of a spontaneous relaxed *B. subtilis* mutant previously highlighted a mutation in the glycine at the equivalent position to G251 in *E. coli* RelA [287]. Mutational analysis of G251E and H354Y in the RelA enzyme N-terminal domain demonstrated reduced (p)ppGpp synthetase activity [283]. This lessened activity was more exaggerated for the G251E mutant than the H354Y and related to an impaired ability to bind both ATP and GTP or ATP respectively [283]. These data suggested that residues at 251 and 354 might also prove important in substrate binding and subsequent synthetase activity.

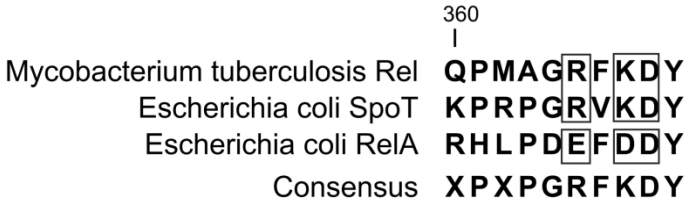

Figure 1.6.4. Amino acid alignment of synthetase motif across long RSH proteins; Rel_{Mtb}, *E. coli* SpoT and *E. coli* RelA.

These synthetase motifs have been further implicated as pivotal in the substrate preference of these enzymes [285]. The mono-functional RelA enzyme from *E. coli*, with

its EXDD synthetase motif, is reported to utilise GDP as its primary pyrophosphate acceptor [285]. Conversely, the bi-functional Rel enzyme from *M. tuberculosis*, with its RXKD synthetase motif, is reported to have a preference for GTP as a pyrophosphate acceptor [285]. When these motifs are interchanged between the two aforementioned RSH enzymes, the substrate preference is respectively reversed [285]. The substitution of the EXDD motif with the RXKD motif increased the (p)ppGpp synthetase activity observed in the resultant mutant, with the converse true when the motifs were alternately substituted. Importantly, none of these observations were noticeable when motifs were altered in the N-terminal mutants of these two proteins [256], which led to the conclusion that this motif co-ordinates with the C-terminal region in the regulation of RSH enzyme synthetase activity.

1.6.2 **Activation of RelA by Stalled Ribosomal Complexes**

During the stringent response, biosynthesis of stable RNA molecules (tRNA and rRNA) are reduced and are described as being under stringent control [288]. From the preliminary data showing that RelA was associated with the ribosomal fractions after centrifugation [289], specific components involved in the interaction have since been identified. Early *in vitro* work highlighted a localisation of RelA to the ribosome [182] which could be purified using high salt concentrations [290]. The enzyme RelA was found to only be activated by ribosomes of bacterial origin; those from yeast, reticulocyte (immature red blood cells), or calf brain showed no measurable (p)ppGpp synthesis [291]. Furthermore hybrid ribosomes with a mixture of prokaryotic (*E. coli*) and eukaryotic (brain) ribosomal subunits showed no greater activation than that seen for the individual bacterial ribosomal subunit [291]. Across bacterial species there appears to be greater flexibility in ribosome activation of RelA, as seen for heterologous assays containing RelA/Rel enzymes from one organism and ribosomes from another [290, 292].

1.6.2.1 **Identifying Key Components for RelA Activation**

From the earliest studies elucidating the identity of RelA and subsequently its association with ribosomes, interest has focused on the mechanism by which RelA is activated by these stalled ribosomes and required cofactors. Activation of the enzyme RelA has now been well studied [168, 182, 293-297] and many aspects are becoming clearer.

1.6.2.1.1 **The Ribosomal Protein L11**

Friesen *et al.* identified an *E. coli* mutant strain displaying a relaxed phenotype, which was shown to contain a defective 50S ribosomal protein [298]. The mutation was within the *relC* gene, now referred to as *rplK*, and the resultant mutant was incapable of accumulating (p)ppGpp upon amino acid starvation [298]. The *rplK* gene encodes ribosomal protein L11, a key component of the 50S subunit of the ribosome [299]. The L11 ribosomal protein is part of the ribosomal GTPase-associated region (GAR) which is located within the 50S subunit [300]. This region of the ribosome is important in facilitating GTPase activity of initiation, elongation and termination factors [300]. The L11 protein is composed of an N-terminal domain, a C-terminal domain and a flexible linker region. The C-terminal domain has been shown to interact with nucleotides 1051 to 1108 in domain II of 23S ribosomal RNA [301]. The N-terminal domain of L11 is however more flexible with respect to its position and proximity to the ribosome [302]. Interactions have been observed between the N-terminal domain of L11 and EF-G [302], RF1 [303], thiostrepton and micrococcin [304].

No ppGpp synthesis was observed with *in vitro* RelA activity assays using purified ribosomes lacking the L11 protein [168] or with a mutated L11 protein [305]. The subsequent addition of purified L11 however showed recovery of ppGpp synthesis in these assays [168]. In 2007 Jenvert and Schiavone showed that the N-terminal domain (NTD) of L11 alone was able to stimulate (p)ppGpp synthesis by 20% or 62% in the presence of unacylated tRNA [306]. Mutational analysis showed that activation of RelA was reliant on the flexibility of the L11 NTD and specifically the presence of the proline-rich helix in the NTD [306]. The importance of the flexibility in L11 was suggested to relate to the allowed movement of the proline rich helix of the NTD and its subsequent ability to interact with RelA. Proline rich helices have been shown to be important in allowing protein: protein interactions The N-terminal domain of L11 has a highly conserved proline-rich helix which structural data suggests is on the surface of L11 facing away from the ribosome [307]. The ribosomal protein L11 has also been implicated in the activation of EF-G GTPase activity [308].

1.6.2.1.2 **RNA species**

In vitro assays for RelA have shown stimulation to be dependent on ribosome-associated factors such as tRNA and mRNA in addition to purified ribosomes. It was suggested by

Wendrich *et al*. (2002) that RelA relies on the presence of a long strand of mRNA in complex with a ribosome as a means of recognising stalled ribosomes [168]. Incubation of RelA with mRNA alone however is not sufficient to substantially increase (p)ppGpp synthetase activity [168, 296], implying that the recognition of mRNA is not sufficient for activation of the enzyme but instead is important for RelA stability.

In 1973 Haseltine and Block detailed the dependence of (p)ppGpp synthesis on the presence of both the 30S and 50S ribosomal subunits, mRNA template and uncharged tRNA capable of recognising the mRNA template [180]. Their work further identified the requirement of the uncharged tRNA to recognise the corresponding codon adjacent to the codon for $tRNA^{fmet}$ (at the A-site) [180]. Despite an early hypothesis that RelA turnover led to the dissociation of unacylated-tRNA from the ribosomal A-site [168], a two layer filter binding assay showed the tRNA dissociates independently of RelA [295]. Knutsson Jenvert *et al*. showed a higher level of RelA activity upon pre-incubation with tRNA, supporting the premise that these two components interact [296]. They were unable to validate this hypothesis however as filter binding assays showed the level of binding between RelA and tRNA was not strong, with binding not matching the level of either tRNA or RelA in the experiment [296]. Furthermore alteration to the RelA: ribosome ratios showed no alteration in tRNA titration curves, with maximal activity still observed at all ratios tested [296]. In 2011 Payoe *et al*. were able to show that tRNA molecules known to dissociate slowly from ribosomes such as $tRNA^{val}$ are able to stimulate (p)ppGpp synthetase activity at much lower concentrations. This supports previous theories that RelA stimulation is dependent on the presence of unacylated-tRNA in the ribosomal A-site [296]. It further suggests that recovery of the cell from amino acid starvation induced stringent response may be dependent on the identity of the amino acid which was originally limited [295].

1.6.2.2 **Development of RelA Activation Models**

In 2002 Wendrich *et al*. proposed a 'hopping' model for RelA activation whereby RelA is stimulated by stalled ribosomes (1.3.1.3) and is then activated and simultaneously released from the ribosome [168] (Figure 1.6.5). This model was backed primarily by binding assays demonstrating that RelA binds to ribosomes in a 0.95:1 ratio in the presence of long mRNAs [168]. This binding is reduced 2-fold however in the presence of

substrates (ATP and GTP), so suggesting that the activity of RelA occurs when it is unbound. The 'hopping' model suggests that RelA is initially bound to the ribosome, where it is activated by the binding of unacylated tRNA at the ribosomal A-site before being released in an active conformation. The RelA enzyme is then thought to 'hop' from one stalled ribosome to another following one turnover of RelA (Figure 1.6.5).

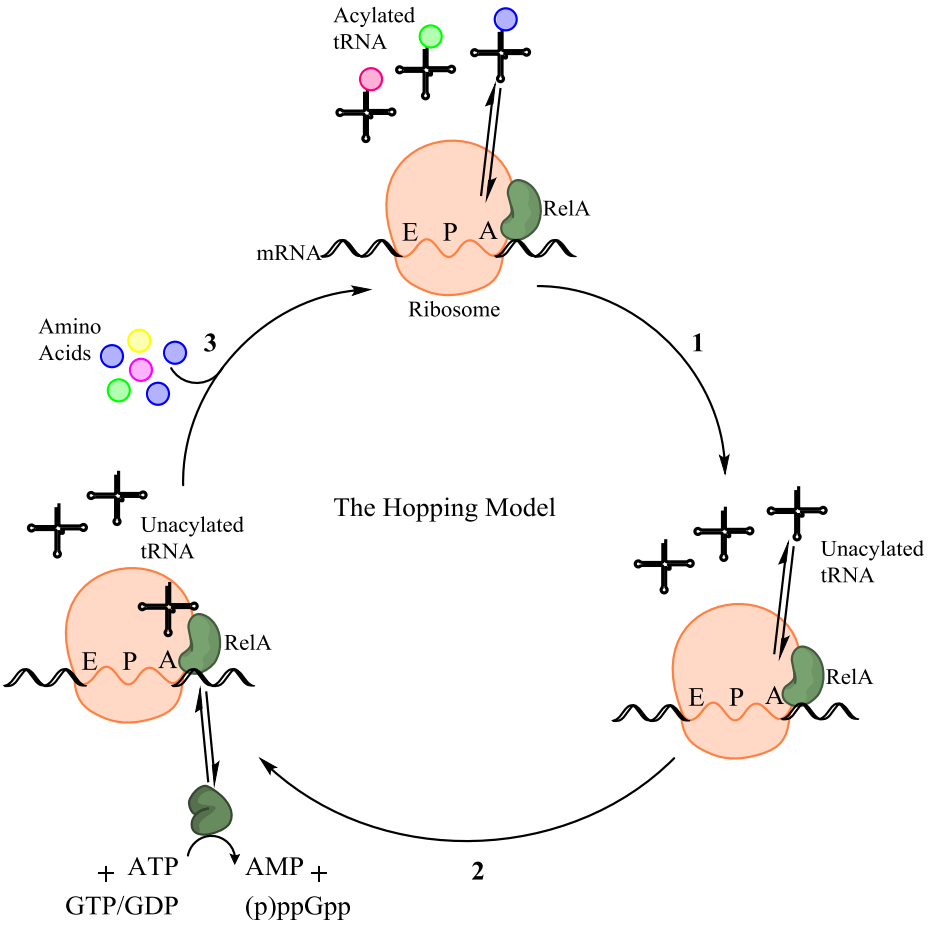

Figure 1.6.5. Schematic illustration of the hopping model for RelA proposed by Wendrich *et al.* [168] (1) Transition of nutrient rich conditions to amino acid deprivation with correspondent increase in unacylated tRNA. (2) Level of unacylated tRNA increases to a point where it can bind to the ribosomal A site and then cycles of RelA being released, turning over once and rebinding to the ribosome. (3) Amino acid levels increase, the concentration of unacylated tRNA decreases and RelA remains bound to the ribosome.

This model was built on by English *et al.* (2011) who proposed an 'extended hopping model' based on single-molecule investigations, which identified two *in vivo* states of RelA: a slow state when inactive in the ribosome-bound form, and a fast state under

amino acid starvation in its free form [297] (Figure 1.6.6). Their model is largely based on that of Wendrich *et al*. but suggests that RelA is capable of sustaining activity for an extended time upon dissociation from the ribosome, without the need for rebinding to a ribosome. This theory is supported by various experiments including the dissociation of RelA from ribosomes for hundreds of milliseconds [297], and the *in vitro* turnover rate of RelA being relatively high (4500 pmol pppGpp pmol RelA^{-1} min^{-1}) [296], a value supported by *in vivo* data [309, 310].

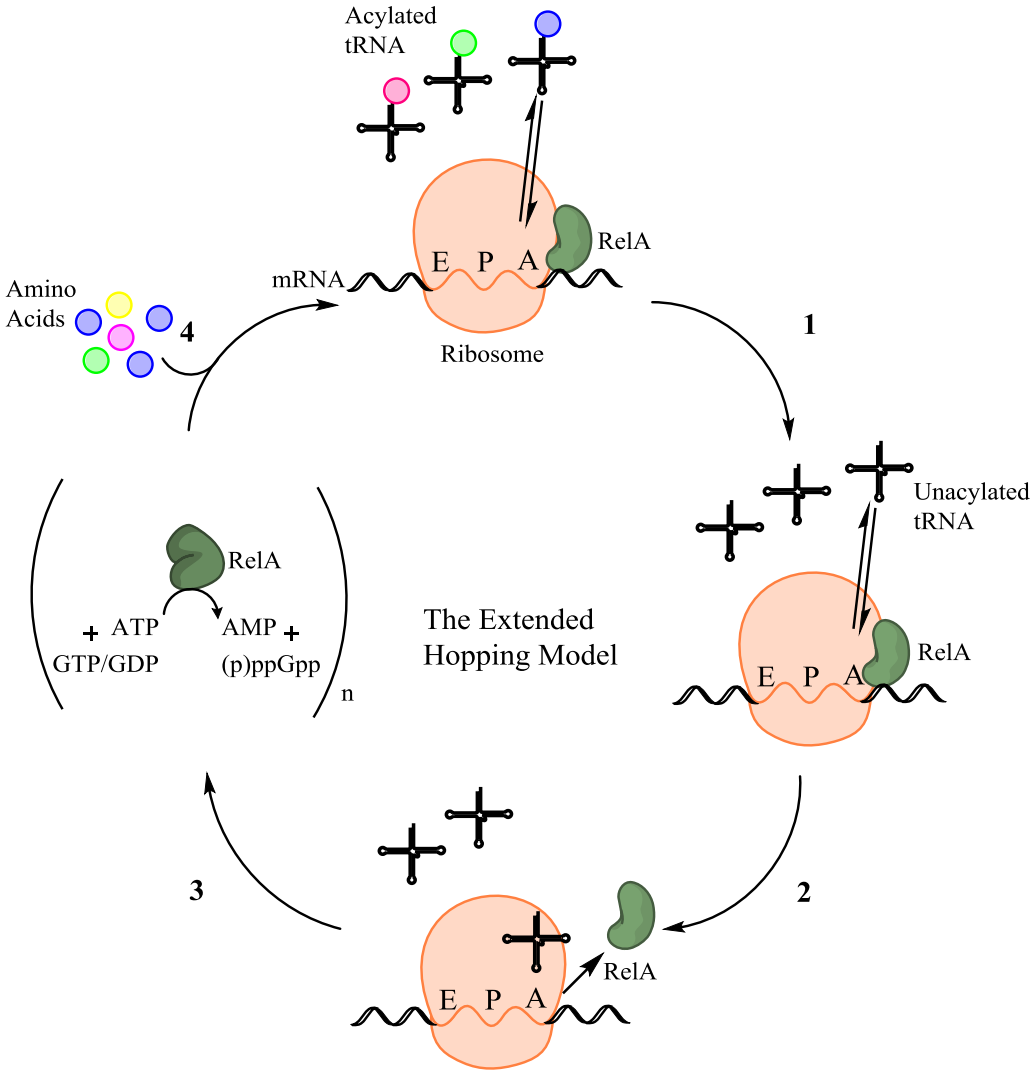

Figure 1.6.6. Schematic illustration of the extended hopping model for RelA proposed by English *et al*.[297] (1) Transition of nutrient rich conditions to amino acid deprivation with correspondent increase in unacylated tRNA. (2) Level of unacylated tRNA increases to a point where it can bind to the ribosomal A site and RelA is released in a constitutively active conformation. (3) Amino acid levels increase, the concentration of unacylated tRNA decreases and RelA rebinds to the ribosome.

This model however highlights the lack of understanding as to how the enzyme RelA is switched off, and what causes it to re-associate with the ribosome.

1.6.2.3 **RelA and Ribosomal Binding**

In 2001 Yang *et al*. determined that the amino acid residues 550 to 682 were required for the binding of RelA to the ribosome [305]. Mutational studies of the ribosomal protein L11 were initially used to determine its importance in regulating RelA activity, by demonstrating the interaction between L11 N-terminal region and RelA [305]. These observations strongly suggested that RelA was binding at least in part to the ribosome via the N-terminus of the ribosomal protein L11, and that this interaction was likely facilitated by the C-terminal region of RelA.

In 2013 cryo-electron microscopy (Cryo-EM) was used to study RelA complexed with the ribosome [311]. In the interest of forming the simplest of stable RelA ribosome complexes, binding studies for various cofactors were used. These studies further demonstrated the importance of the RelA C-terminal region for ribosomal binding as a C-terminal deletion mutant showed an inability to bind to ribosomes under any conditions tested [311]. In addition to this, binding studies confirmed the requirement of uncharged tRNA for ribosomal binding of the full length RelA enzyme [311]. The presence of mRNA or nucleotides did not alter binding efficiencies. A 10.8 Å resolution cryo-EM structure of full length RelA (~80% of protein mass identified) complexed with ribosomes and uncharged tRNA allowed greater understanding of this interaction [311]. RelA was found to bind in a similar site to that for EF-Tu, EF-G or other GTPases. The density attributed to RelA divided into two separate regions (N-terminal and C-terminal) connected by a linker region [311]. The first region (presumably C-terminal) was observed to bind to the 50S subunit via the ribosomal protein L11 (N-terminal region) and the nucleotides 1051-1108 of the 23S rRNA [311]. The second region (presumably N-terminal) is seen to rest in the cavity formed by helices h5 (nucleotides 358-359, 55-56) and h14 (nucleotides 340-342) of the 16S rRNA [311].

The position of RelA was in close proximity to the unacylated tRNA, however the low resolution prevents the precise determination of interacting amino acid residues and

nucleotides. The unacylated tRNA is in a distorted conformation akin to that previously observed for the A/T state of aminoacyl tRNA in complex with EF-Tu when bound to the ribosome [312]. The conformation of the unacylated tRNA however differs to that of the A/T state of the aminoacyl tRNA in complex with EF-Tu, by more acute bending of nucleotides in the D-loop [311]. This coupled with further alteration in the T-loop conformation moves the unacylated tRNA closer to the L11 region (Figure 1.6.7) [311]. These data led to the proposal that the initial binding of RelA to the stalled ribosome is mediated by its C-terminus to the shoulder region of the smaller ribosomal unit. Once bound it is thought to interact with the distorted tRNA, subsequent to its transition from the A/A state to the A/T state that stabilises the interaction of both of these molecules with the ribosome. Interactions between the distorted tRNA and the 50S subunit via L11 are thought to bring structural order to this area and subsequently aid the activation of RelA activity by interaction with the L11 protein. Further structural information, perhaps to a higher resolution, is required to get a complete picture of exactly how RelA is activated by stalled ribosomal complexes.

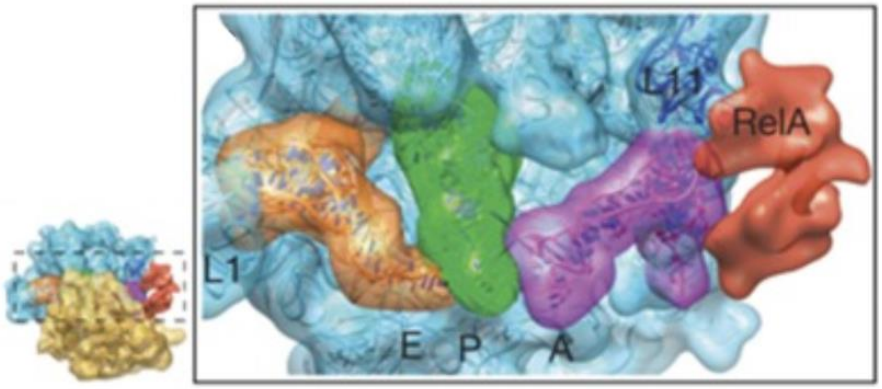

Figure 1.6.7. Cryo-EM image of RelA associated with the ribosome. The close up displays the enzyme RelA interacting with the ribosomal protein L11 and a distorted tRNA molecule situated in the ribosomal A site. Copyright John Wiley and Sons. Reproduced with permission from [311].

1.6.3 **Activation of RelA by Small Molecules**

Activation of RelA by its product ppGpp was demonstrated in 2012 by Shyp *et al*. [313]. Supplementation of *in vitro* ribosome activated RelA assays with ppGpp (100 µM) showed

increased activation of the enzyme (~250 ppGpp per RelA per min) when compared to standard ribosome activated assays (~25 ppGpp per RelA per min) [313]. Activation of RelA by ppGpp could also be seen in conjunction with L11 only (~60 ppGpp per RelA per min), albeit to a lesser extent [313]. This activation is thought to occur in a synergistic manner and is suggested to relate to an allosteric mechanism of positive regulation for RelA. This method of activation is beneficial compared to regulation at the transcriptional level as it does not require *de novo* synthesis of proteins and mRNA. Nonetheless, it is rarely seen and only a few other examples are known [314, 315].

1.6.4 **Activation of RelA by Methanol**

Kinetic characterisation of the ribosomal wash from *E. coli* in the absence of additional stalled ribosomal complexes, detailed a basal level of synthetase activity which could be amplified tenfold by the addition of 20% (v/v) methanol [293]. Further analysis showed that the (p)ppGpp synthesis was optimal at 15-20% methanol when incubated at 25-30 °C [293]. At the temperatures 30-33 °C however incubation with 20% methanol saw a 60% decrease in (p)ppGpp synthesis. In 1974 Block and Haseltine described the purification of RelA from ribosomal wash fractions [294]. Amplification of the pppGpp synthetase activity of the purified enzyme in the presence of 20% methanol was also observed. The methanol was suggested to provide a semi-hydrophobic environment, which could mimic the micro-environment created by the stalled ribosomes. Despite no further work elucidating evidence for the mechanism by which methanol stimulates RelA activity, it has been frequently exploited as a means of biosynthesising the nucleotide guanosine tetraphosphate [316, 317].

1.6.5 **RelA and Bacterial Virulence**

Research has shown RSH proteins and their role in the stringent response are important to the virulence and survival of many pathogens including *Streptococcus mutans* [220], *Pseudomonas aeruginosa* [318], and *Mycobacterium tuberculosis* (*M. tuberculosis*) [319]. Research detailing the potential use of double *relA*/ *spoT* deletion mutants (Δ*relA*Δ*spoT*) of both *B. pseudomallei* and *Y. pestis* as potential live vaccine candidates is detailed below

[250, 320]. The *B. pseudomallei* Δ*relA*Δ*spoT* mutant was observed to be defective in intracellular replication in murine macrophages and attenuated in acute and chronic mouse models of melioidosis [320]. The *Y. pestis* Δ*relA*Δ*spoT* mutant was also shown to be attenuated and further shown to confer full protection against a virulent strain of *Y. pestis* when delivered subcutaneously [250]. Only partial protection (60%) was observed however against pulmonary challenge with the virulent strain [250]. Single *relA* deletion mutants (Δ*relA*) displayed no effect on growth in comparison to the wild-type strain. The role of RelA is thought to be reduced in *Y. pestis* because of the presence of an analogous stress response system which responds to calcium depletion [250].

In 2009 Dean *et al*. showed that *Francisella novicida* contained a gene (FTN_1518) encoding a RelA protein [321]. Null mutants of this gene were unable to synthesise (p)ppGpp under amino acid starvation conditions and displayed similar phenotypic changes from wild type as observed for *E. coli relA* mutants [321]. One of the key observations made with this mutant strain was its reduced virulence in a murine model, with the mutant strain estimated to be attenuated >100 fold in comparison with wild type [321]. Although *Francisella novicida* is not considered a potential biological warfare agent, it is often used as a model system for *Francisella tularensis*.

1.6.6 Current Attempts to Develop RelA Inhibitors

The importance of the global regulator ppGpp to bacterial survival, virulence, biofilm formation, and antibacterial tolerance has sparked interest in the enzymes capable of synthesising this molecule as potential antibacterial targets.

1.6.6.1 Inhibition by Current Antibiotics or ATP Analogues

RelA has been shown to be inhibited by a variety of known antibacterial compounds and various ATP analogues [259, 260, 291, 296]. Several groups have demonstrated inhibition of ppGpp synthesis upon the addition of antibiotics known to act against the ribosome [260, 296]. In 1974 Cochran and Byrne showed inhibition of RelA activity by the ribosomal antibiotics oxytetracycline (500 μg/μL reduces activity to 6%) and fusidic acid (1000 μg/μL reduces activity to 10%) [260]. Oxytetracycline (Figure 1.6.7) is known to prevent the binding of tRNA to the ribosomal A-site [322], and therefore in this context is preventing formation of the stalled ribosomal complex and leading to the strong inhibition of (p)ppGpp synthesis. Tetracycline was also shown to inhibit the activity of *E. coli* RelA both

in the presence and interestingly absence of ribosomes [296]. This latter finding suggests that perhaps there is a direct interaction between this antibiotic and the enzyme RelA. Fusidic acid (Figure 1.6.7) inhibits the translocation of tRNA within the ribosomal peptidyl transferase centre [323]. In the context of RelA activity this would interfere with the association of the unacylated tRNA into the A site of the ribosome, but would not completely prevent it, thus explaining the weaker inhibition observed. Inhibition has also been observed for the *E. coli* RelA by the peptide antibiotics micrococcin, thiostrepton, and viomycin [296]. Thiostrepton requires the ribosomal protein L11 to bind to the ribosome [324], and it is therefore likely competitively binding to L11 and so reducing RelA activation.

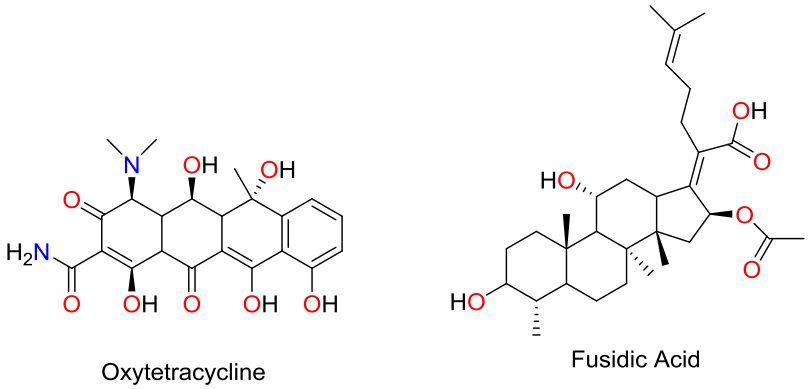

Figure 1.6.8. Structure of antibiotics which inhibit *E. coli* RelA: Oxytetracycline (left) and Fusidic acid (right).

Nucleotide analogues have also been demonstrated to inhibit RelA activity [259, 291]. In 1973 Richter *et al.* described the weak inhibition of ppGpp synthesis by *E. coli* RelA in the presence of the ATP analogue AMPPNP (Figure 1.6.9), with 10 mM AMPPNP required to reduce the synthesis to 2.9% [291]. Another paper by Richter *et al*. in 1979 found that another ATP analogue, ppApp (Figure 1.6.9), inhibited the synthesis of ppGpp *in vitro* [259]. In the ribosome free assay ppApp inhibited ppGpp synthesis 100% at 400 µM, upon the addition of ribosomes however inhibition reduced to 50% at 2 mM ppApp [259].

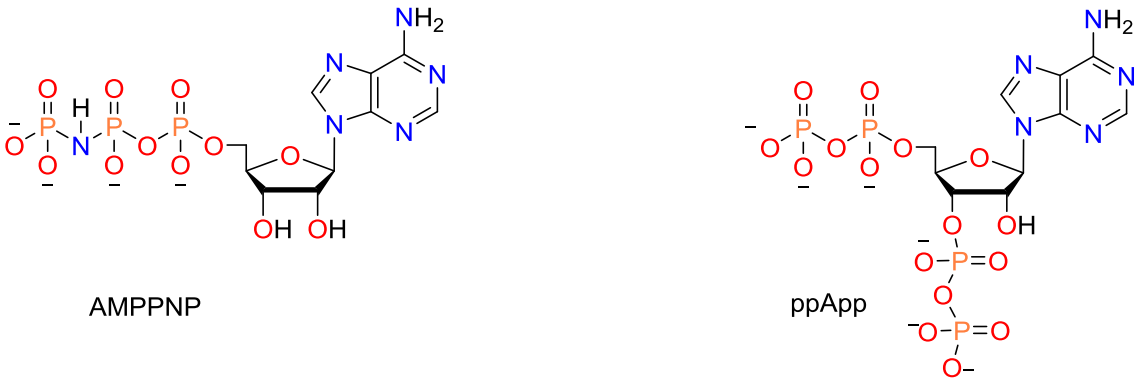

Figure 1.6.9. Structure of nucleotide analogues which inhibit *E. coli* RelA: AMPPNP (left) and ppApp (right).

1.6.6.2 **Inhibition by Designed ppGpp Analogues**

Synthesis of a library of guanosine tetraphosphate (ppGpp) analogues in 2008 led to the identification of 'compound 10', and subsequently Relacin as RSH inhibitors [325-327]. Guanosine tetraphosphate analogues were designed to incorporate two main features: the presence of non-hydrolysable methylene-bisphosphonate groups in the stead of pyrophosphates at 5' and 3' positions of the sugar ring, and the presence of either ribose or 2'deoxyribose as the sugar moiety [327]. All of the ppGpp analogues were reported to display an inhibitory effect; however, 'compound 10' (Figure 1.6.10) showed the greatest promise, with 100% inhibition of *S. equisimilis* Rel at 5 and 10 mM and 100% inhibition of *E. coli* RelA at 10 mM [327]. Docking of the compound into the crystal structure of *S. equisimilis* Rel NTD [254] suggested that it was competitively binding with the GTP binding site of the synthetase domain.

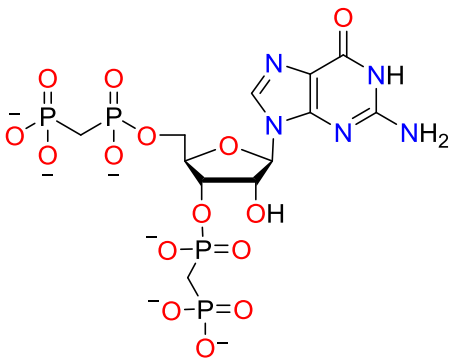

Figure 1.6.10. Structure of Compound 10.

In 2012 Wexselblatt *et al.* published the inhibitory effects of another ppGpp analogue termed Relacin [325]. Relacin is a 2'-deoxyguanosine-based analogue of ppGpp, with the pyrophosphate moieties at the 5' and 3' positions of the ribose replaced with glycyl-glycine dipeptides linked to the sugar by a carbamate bridge (Figure 1.6.11) [325]. The guanine base in Relacin also contains an additional isobutanal group (Figure 1.6.11).

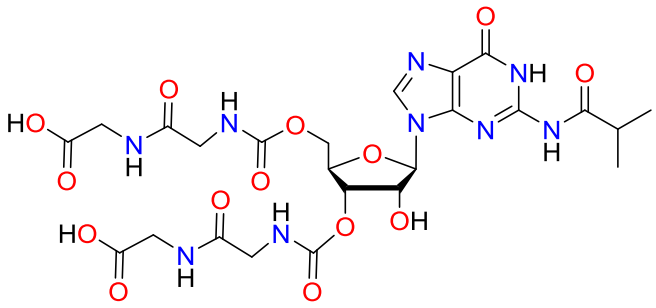

Figure 1.6.11. Structure of the ppGpp analogue Relacin.

In vitro activity of *E. coli* RelA and *D. radiodurans* Rel were shown to be inhibited by this molecule in a dose-dependent manner, with 100% and 80% inhibition of (p)ppGpp synthesis observed respectively at 5 mM Relacin [325]. Inhibition was observed for the RelA mutant protein (RelAC638F) which displays activity in a ribosome-independent fashion [283], implying a direct interaction between RelA and Relacin. *In vivo* analysis using serine hydroxamate to induce amino acid starvation in *Bacillus subtilis* (*B. subtilis*) culture demonstrated similar dose-dependent inhibition, though with reduced efficiency than that observed *in vitro* (~30% inhibition at 5 mM) [325].

1.6.7 Development of New RelA Inhibitors as Antibacterial Agents

Given the aforementioned inhibitors, it is perhaps surprising that no potential antibiotics have yet progressed to clinical trials for this potential antibacterial target. Identified inhibitors only demonstrate inhibition at high concentrations currently, with perhaps the most successful inhibitor to date, Relacin, demonstrating inhibition at the high concentration of 5 mM [325]. An ideal compound for drug development would instead have very high inhibitory activity at low concentrations, potentially in the nano or micromolar range [328]. Inhibitors with a high IC_{50} value require a higher dose regime for treatment which typically results in a higher level of associated toxicity. Known antibiotics

which have been shown to inhibit ribosome-mediated RelA activity also carry the problem of existing resistance within microbial communities.

Further elucidation of promising inhibitory compounds against the RelA enzyme, which can be developed as antibacterial agents, relies on two key areas. The first is the attainment of a RelA crystal structure. Key structural differences within the synthetase active site suggest a possible distinct mechanism of reaction for those catalysed by mono-functional or bi-functional RSH proteins [256]. The crystallisation of a RelA enzyme active site would provide further insight into the importance of the identified differences between these two proteins. In addition to this it would allow the development or design of potential inhibitors using *in silico* screening (1.1.4). The second area is the development of a high throughput means of screening for inhibitory compounds (1.1.4). High throughput screens can allow for the simultaneous testing of vast quantities of potential inhibitory compounds, often yielding nanomolar or micromolar inhibitors [43]. Designing such a method has been made substantially easier in recent years by the development of various novel methods of (p)ppGpp detection, since neither HPLC nor TLC analysis lends itself to a high throughput application. In 2008 Rhee *et al*. described the use of a fluorescent chemosensor which they name PyDPA as a means of detecting ppGpp both *in vitro* and within cells [329]. The PyDPA was capable of binding the pyrophosphate moieties at either the 3' or 5' position of the ribose ring within ppGpp [329]. The binding of two PyDPA molecules to one ppGpp molecule causes the stacking of the pyrene groups, and a resultant pyrene-excimer fluorescence observable at 470 nm [329]. Despite displaying selectivity for (p)ppGpp, synthesis of PyDPA could be lengthy and would require a secondary coupling to zinc ions prior to use.

In 2013 Zhang *et al.* described the use of an on-off-on fluorescent sensor for the detection of ppGpp [330]. This method utilises the ability of copper ions (Cu^{2+}) to quench the fluorescence emission of deoxyribose nucleic acid silver (DNA-Ag) nanoclusters (Figure 1.6.12). The ability of ppGpp, via its rich electrons within its phosphate groups, to co-ordinate the Cu^{2+} is strong and consequently restores the fluorescence of DNA-Ag nanoclusters by binding the copper within the system [330]. This detection method was found to work at ppGpp concentrations between 2 and 200 µM and was specific to the nucleotide ppGpp [330].

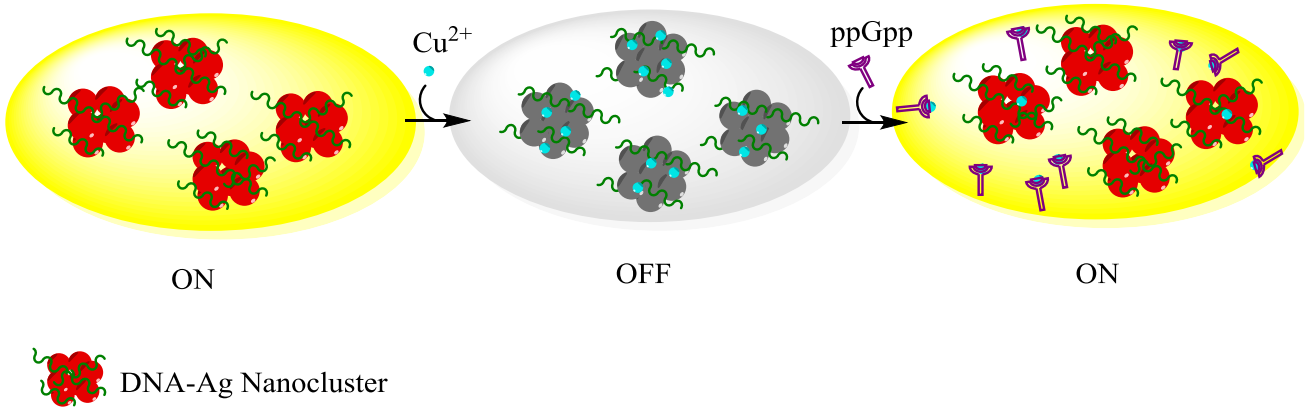

Figure 1.6.12. Schematic illustration of the on-off-on fluorescence detection of ppGpp. Fluorescence is denoted by background colour, fluorescent condition (yellow) and no fluorescence (grey) [330].

Finally, in 2014 a method was published for the detection of ppGpp using its ability to inhibit the redox reaction between Fenton-like reagent (Fe^{3+} and H_2O_2) and 2,2'-azino-bis(3-ethylbenzthiazoline-6-sulfonic acid) (ABTS) [331]. The ability of ppGpp to co-ordinate the iron ion (Fe^{3+}) results in the prevention of the chromogenic reaction between the ABTS and Fenton-like reagent [331]. This detection method was also shown to be selective for ppGpp over other nucleotides and was determined to have a detection limit of 0.19 µM ppGpp [331]. The maximal concentration of ppGpp tested by this method however was 11 µM, with a linear range between 2 and 7 µM [331]. Such a narrow linear range could have negative implications on the development of a sufficient screening window for a high throughput screen (1.1.4, 4.3.5).

1.7 Project Aims

Many bacterial species contain or obtain mechanisms of resistance to one or several clinically available antibiotics. The emergence of bacterial species resistant to these antibiotics is said to be increasing, largely due to the misuse of antibiotics [1, 2]. Furthermore, recent years have seen a decline in new antibiotics licensed for clinical use [3].

Potential biowarfare agents such as *F. tularensis*, *Y. pestis*, and *B. pseudomallei* may also contain engineered antibacterial resistance in addition to their native resistance mechanisms. A result of this is the heightened requirement for novel antibiotics which work against these organisms. *F. tularensis*, *Y. pestis*, and *B. pseudomallei* are all facultative intracellular pathogens. Each organism has a unique method of intracellular survival [4-6], and consequently a common target is required for the identification of a broad spectrum antibiotic.

The stringent response co-ordinates several metabolic pathways required for bacterial survival under various stress conditions (i.e.: phosphate, carbon, amino acid or fatty acid starvation) [7-9]. During the stringent response the bacteria enter a dormant state required for survival whilst in unfavourable conditions. The stringent response is co-ordinated by the signalling molecules guanosine penta-/tetra-phosphate ((p)ppGpp) [9, 10], which exert many direct and indirect effects throughout the cell [9, 11]. In β- and γ-Proteobacteria the enzyme principally responsible for (p)ppGpp synthesis is RelA [12]. Reduced virulence of *F. novicida* [13], *B. pseudomallei* [14] and *Y. pestis* [15] *in vivo* is observed in *relA* gene knockouts. Current knowledge on the enzyme RelA is almost exclusively based on data recorded for *E. coli* RelA [16-19]. Furthermore, the majority of analysis involves a radiolabelled assay [16, 18]. Such a method is ill-suited for the development of a high throughput screen, a common method used for the identification of small molecule inhibitors of enzymes.

There were several aims of this project. The primary aim was to express, purify, and characterise the RelA enzyme from *F. tularensis*. Given the complex regulation of *E. coli* RelA [16, 20], the regulation of *F. tularensis* RelA by a range of potential activators including: stalled ribosomal complexes, RNA species, methanol, and ppGpp, were also of interest. The second aim of this project was the design and development of a high

throughput screening method for the identification of small molecule inhibitors of RelA enzymes, primarily *F. tularensis* RelA. Research into the expression, purification and preliminary characterisation of RelA enzymes from *Y. pestis* and *B. pseudomallei* was also of interest.

Chapter 2: **Characterisation of *F. tularensis* RelA**

The biochemical characterisation of the enzyme *F. tularensis* RelA was deemed important for two key reasons. An improved understanding of how *F. tularensis* RelA works would potentially elucidate the significance of the identified sequence anomalies as described below within this enzyme. Secondly, the identification of key kinetic parameters (i.e., V_{max} and K_M) is an essential pre-requisite for the development of a robust high throughput screening method for inhibitors of this enzyme.

The enzyme RelA catalyses the transfer of the β, γ-pyrophosphate group from the 5' position of the ribose ring in ATP to the 3' position of the ribose ring in GTP or GDP. The products of this reaction are adenosine monophosphate (AMP) resulting from the ATP and guanosine penta/tetraphosphate (pppGpp/ppGpp) depending on whether GTP or GDP respectively was used as the substrate.

A recent paper detailed the crystal structure of a SAS protein from *B. subtilis* in the presence of the ATP analogue AMPCPP [284]. Superimposition of this structure's AMPCPP occupied synthetase active site with that of the GDP occupied Rel_{Seq} synthetase active site allowed the authors to suggest a mechanism for (p)ppGpp synthesis [284]. The predicted mechanism for this reaction is thought to involve an SN2-like reaction in which the 3' hydroxyl group of GTP is partially deprotonated by nearby glutamic acid residue within the enzyme's active site. The consequent nucleophilic attack at the β-phosphate results in the cleavage of the pyrophosphate moiety from the ATP and its subsequent addition to the GDP/GTP molecule, Figure 2.1. During this mechanism the phosphate groups are co-ordinated by an essential magnesium ion.

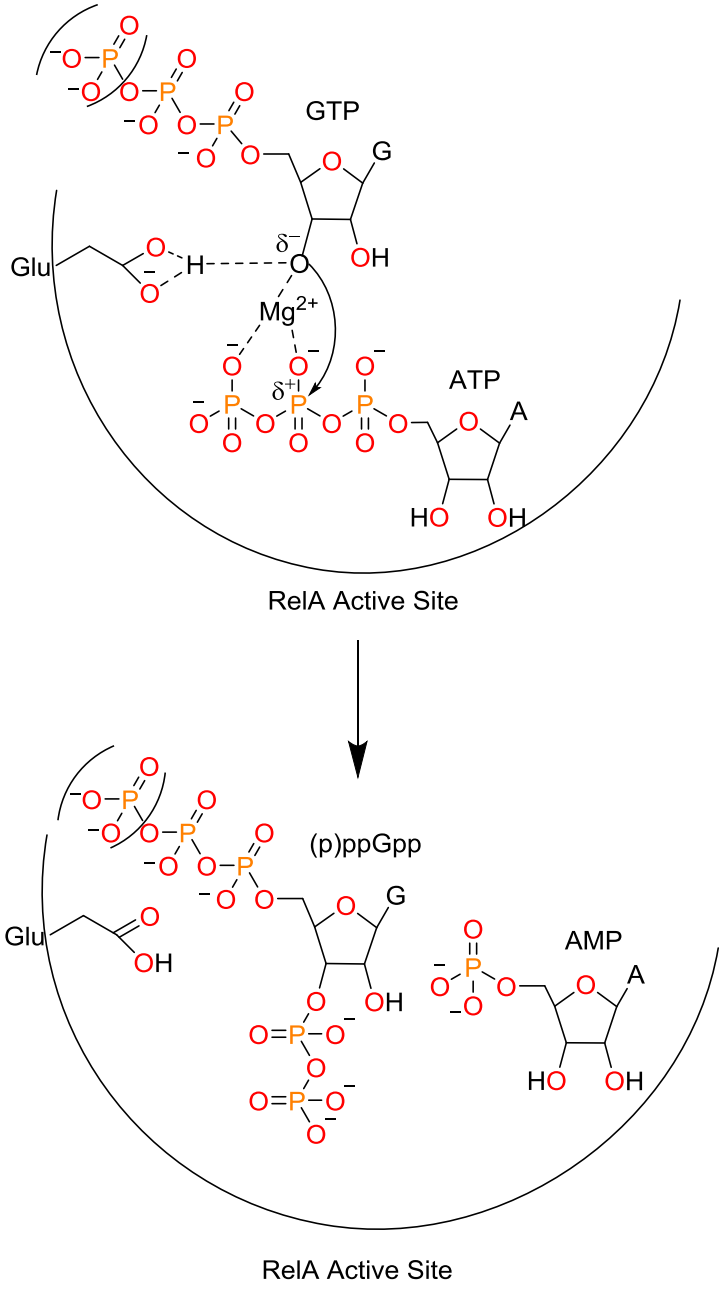

Figure 2.1. Scheme of the proposed catalytic mechanism of (p)ppGpp synthesis by small alarmone synthetase (SAS) from *B. subtilis*. Adapted from [284].

As discussed previously the structure of RelA enzymes can be broadly divided into a catalytic N-terminal region and a regulatory C-terminal region (1.5.1). Within the C-terminal region the following 4 domains have been identified; TGS, Helical, CC and ACT domains [189]. The precise function of most of these domains is still unclear for RelA enzymes. The C-terminal region has however been strongly linked to both the regulation and dimerization of *E. coli* RelA activity [282, 283], suggesting that alterations within this region could have profound consequences on the enzymes activity and multimeric state.

The RelA enzyme from *F. tularensis* contains a truncated C-terminal region, around 100 amino acids shorter than the average RelA enzyme, and is one of only three RelA enzymes known to not contain an ACT domain [189] (Figure 2.2).

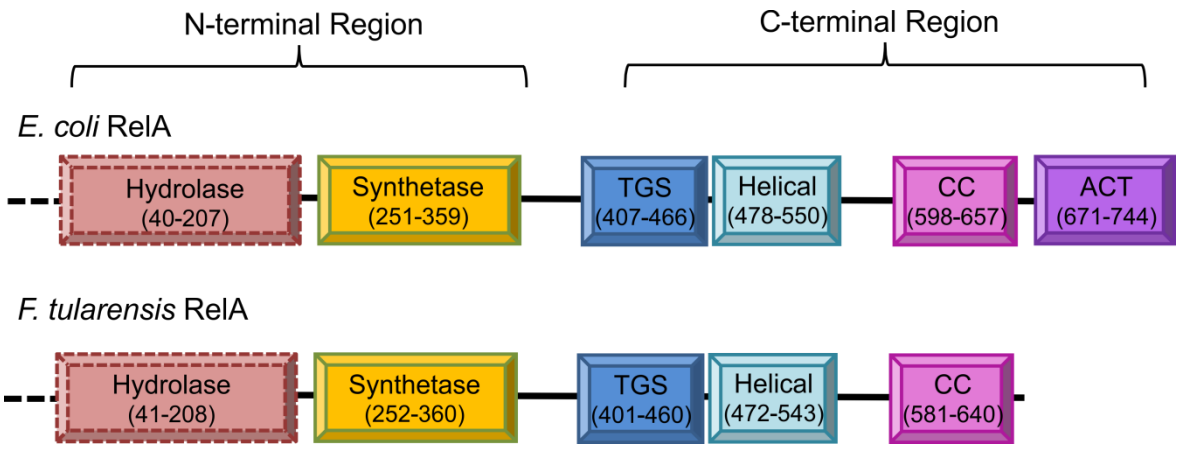

Figure 2.2. Comparison of *F. tularensis* RelA domain structure with that of *E. coli* RelA enzymes. Dashed outline for hydrolase domain indicate lack of activity in this domain.

Besides it significantly shortened C-terminal region *F. tularensis* RelA differs from the majority of other RelA enzymes in its synthetase structural motif. The identification of a potential catalytic loop (α13/ β4) observed within the Rel_{Seq} crystal structure with a proposed key aspartic acid residue [254] led to the proposal of the EXDD and RXKD active site motifs [256]. Further work suggested that the type of motif the RSH proteins contained dictated the preferential binding of the pyrophosphate acceptor (i.e.; GDP or GTP) [285] (1.6). The synthetase domain in *F. tularensis* RelA however contains the alternative motif EXSD (Figure 2.3), which can be found in a range of other *Francisella* species (A.1).

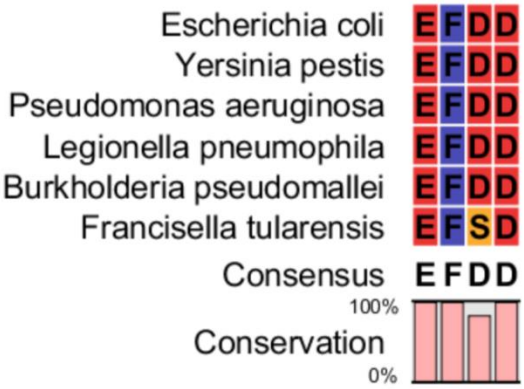

Figure 2.3. Alignment of RelA synthetase domain motifs from *E. coli* (A1Z90180), *Y. pestis* (AJJ30322), *P. aeruginosa* (KGB87144), *L. pneumophila* (GAN26584), *B. pseudomallei* (CPG90944) and *F. tularensis* (CAG466141) made in CLC Sequence Viewer).

This alternative motif shows the replacement of the primary aspartate with a serine (Figure 2.4). The primary aspartate has been proposed to allow the co-ordination of a second magnesium ion [256]. In fact the charge reversal between the positive amine side group of lysine and the negative carboxylate group of aspartate was suggested as the key defining feature for the interaction between the additional magnesium ion and the active site [256]. Interestingly, despite carrying no charge, serine has been shown to co-ordinate magnesium ions in other enzymes. One example of this can be found within the DNA mismatch repair protein MutS, which co-ordinates magnesium directly with serine at position 621 and also via a water molecule co-ordinated between Asp-693 and Glu-694 [332].

Alterations to the active site motif in *F. tularensis* RelA however do raise questions about whether the (p)ppGpp synthetase activity in the presence of an EXSD motif is more closely aligned to that with RXKD or EXDD motifs.

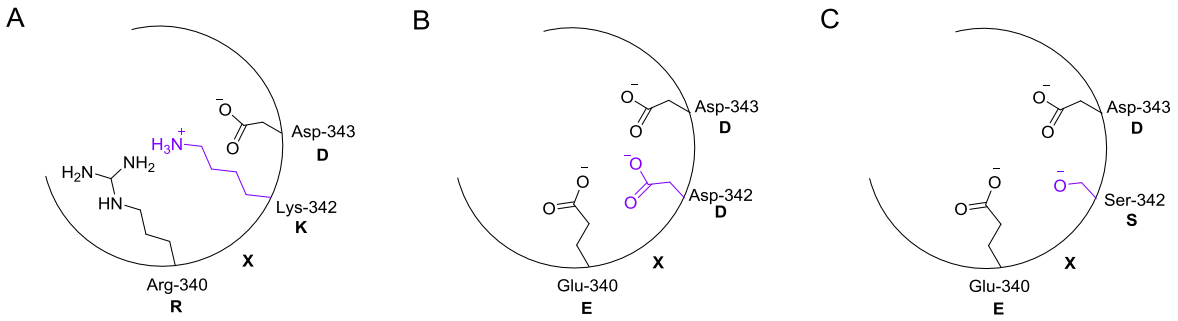

Figure 2.4. Active site motifs for Long RSH enzymes. (A) RXKD motif for Rel proteins (B) EXDD motif for RelA proteins. (C) EXSD motif for *F. tularensis* RelA. Residues implicated in the ability of the enzyme to co-ordinate a second magnesium ion are highlighted in purple.

2.1 Expression and Purification of *F. tularensis* RelA

2.1.1 Expression of *F. tularensis* RelA

An expression plasmid containing the *F. tularensis relA* gene (FTT_1508c) was previously prepared by Dr. L. Batten [333] to facilitate heterologous expression in *E. coli*. The RelA encoding gene, FTT_1508c, was amplified from *F. tularensis* subspecies *tularensis* SCHU S4 genomic DNA by PCR [333]. For the PCR amplification, the primers were designed to encode an N-terminal hexahistidine (His_6) tag to facilitate subsequent protein purification. After restriction, the PCR product was ligated between the NcoI and XhoI sites of pET16b vector [333]. A restriction digest (7.3.7) of the resultant plasmid with restriction enzymes NcoI and XhoI confirmed the presence of the *F. tularensis relA* gene (Figure 2.5).

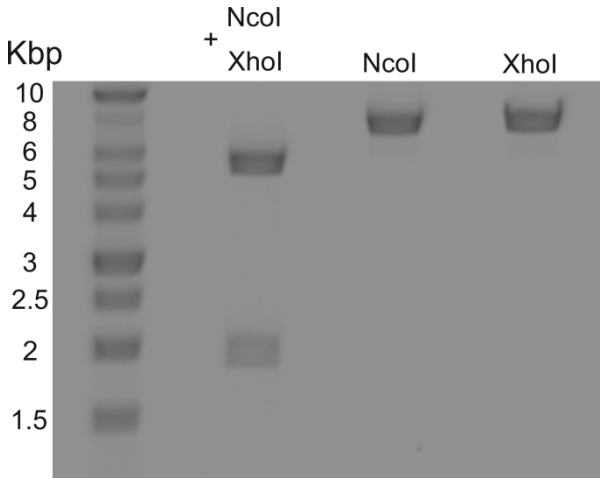

Figure 2.5. Restriction digests (7.3.7) of pET16b::*Ft*relA with the restriction enzymes NcoI and XhoI to confirm the presence of the *Ft*relA gene (1.94 Kbp).

To achieve maximal yield of *F. tularensis* RelA, the pET16b::*Ft*relA plasmid was transformed into the *E. coli* BL21 (DE3) Rosetta strain for heterologous expression. Optimal expression of *F. tularensis* RelA was assessed by small scale expression studies with varying temperatures, IPTG concentrations and length of induction [333]. Work by Dr L. Batten described the optimum conditions to be overnight expression at 16 °C with the addition of 0.4 mM IPTG to initiate expression [333], although further work with addition of 1 mM IPTG yielded similar results. *F. tularensis* RelA was expressed on a large scale (5 L of *E. coli* BL21 (DE3) Rosetta pET16b::*Ft*relA) and these cultures yielded 15.32 ± 1.1 g cell pellet.

2.1.2 **Purification of *F. tularensis* RelA**

The difficulty in purifying *E. coli* RelA is well documented [168, 296] and is attributable to its high molecular weight, and its ability to non-specifically bind to laboratory materials as well as host cell proteins [309]. Further to this, the activity of this enzyme rapidly decreases across freeze-thaw cycles [313]. For this reason *F. tularensis* RelA was purified by both nickel imidoacetic acid (Ni-IDA) affinity chromatography (7.4.2) and size exclusion chromatography (7.4.5). Purifications were carried out over two consecutive days, and frozen in aliquots. These were limited to single use only and all aliquots were used within 8 weeks of purification.

F. tularensis RelA was initially purified by Ni-IDA affinity chromatography, utilising an imidazole gradient of 20 to 500 mM over 8 column volumes. Imidazole was removed by dialysis (7.3.3) in order to prevent protein precipitation. From a 15.32 ± 1.1 g cell pellet the purification method resulted in the recovery of 150-200 mg of RelA, however RelA was observed to co-purify with a large number of host cell proteins (Figure 2.6). Routinely Ni-IDA purified RelA could be concentrated to ~20 mg/mL.

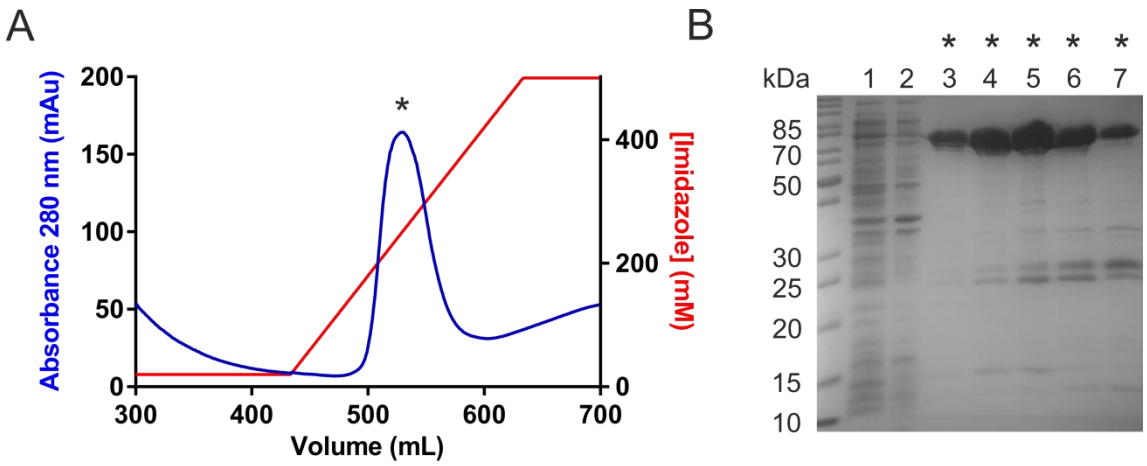

Figure 2.6. Purification of *F. tularensis* RelA (74 kDa) by nickel affinity chromatography (7.4.2). (A) Absorbance 260 nm trace (B) SDS-PAGE analysis of fractions from nickel affinity chromatography. Lanes: 1, cleared lysate; 2, flow through; 3-7, eluate fractions from Ni-IDA chromatography. Lanes marked with an asterisk (*) correspond to the peak similarly marked in (A).

F. tularensis RelA was further purified by size exclusion chromatography on a Superdex 200 (HiLoad 26/60, prep grade). Purification reproducibly yielded three main peaks (Figure 2.6a), with the most intense peak attributable to *F. tularensis* RelA as judged by SDS-PAGE (7.2.1) (Figure 2.7b). RelA eluted from this size exclusion chromatography (yielding 75-100 mg, from 150-200 mg applied in 3 mL injections) could be concentrated to ~10 mg/mL prior to observation of any protein precipitation. Aliquots (200-500 µL, ~4-10 mg/mL) were stored at -80 °C prior to use.

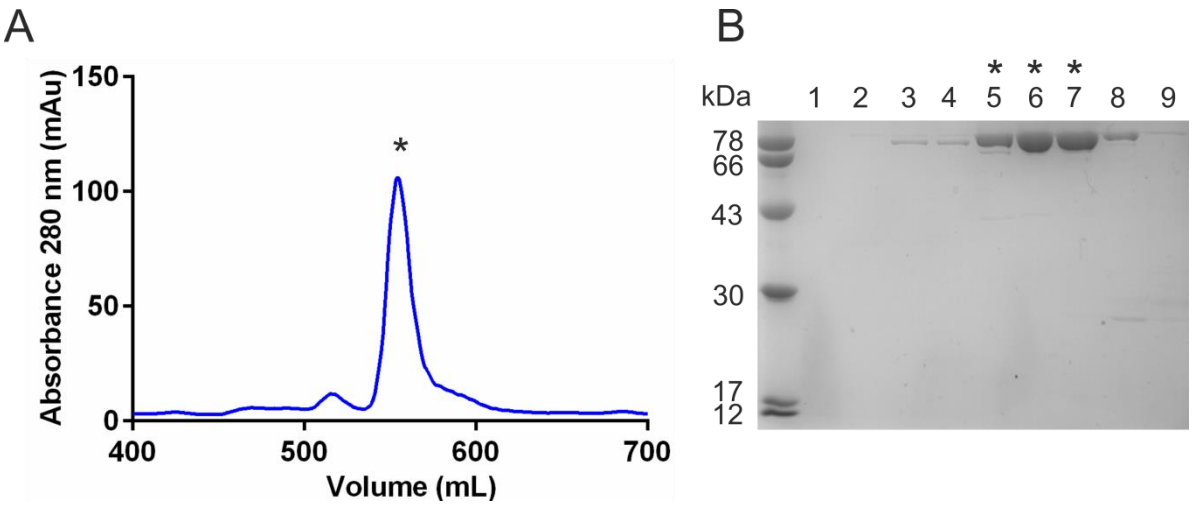

Figure 2.7. Purification of *F. tularensis* RelA (74 kDa) by size exclusion chromatography (7.4.5). (A) Absorbance 280 nm trace (B) SDS-PAGE analysis of fractions from size exclusion chromatography. Lanes: 1-8, eluate fractions from size exclusion chromatography; those marked with * correspond to those containing *F. tularensis* RelA and to the peak similarly marked in (A).

Previous studies of RelA activity have involved the use of HEPES as a buffering agent [168, 295, 296]. Purification of *F. tularensis* RelA with HEPES as the buffer for dialysis and gel filtration yielded around 100 mg *F. tularensis* RelA after dialysis and concentrations of only around 1.8-2 mg/ mL following size exclusion chromatography prior to observed protein precipitation. The recovery of *F. tularensis* RelA when Tris is used as the buffering agent increases to 180-250 mg following dialysis and concentrations of up to 10 mg/ mL prior to protein precipitation.

2.2 Multimeric State of *F. tularensis* RelA

Dimerization of *E. coli* RelA via its C-terminal domain has previously been noted [282]. Given its truncated C-terminal region, the ability of *F. tularensis* RelA to dimerise was therefore of interest. The multimeric state of purified *F. tularensis* RelA was established by analytical size exclusion chromatography (7.4.6). Elution volumes were monitored (by absorbance at 280 nm) for protein standards (Sigma Aldrich) on an analytical Superdex 200 column (10 mm x 300 mm) for the calculation of a calibration curve. The apparent molecular weight of *F. tularensis* RelA was then determined by measuring its elution volume. A single peak was observed for *F. tularensis* RelA (Figure 2.8a) and gave an

estimated molecular weight of 128 ± 1.57 kDa (Figure 2.8b), roughly corresponding to the dimeric state of *F. tularensis* RelA (calculated molecular weight 148 kDa).

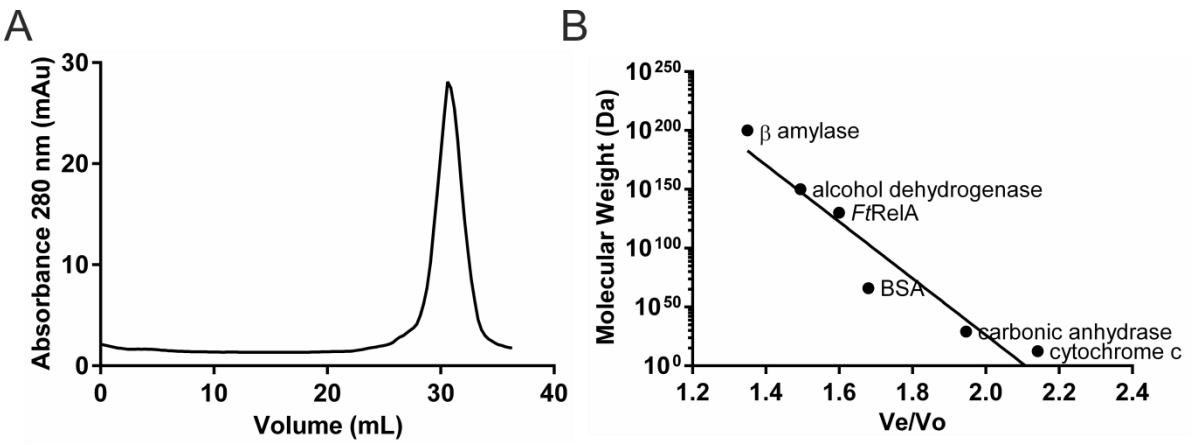

Figure 2.8. The multimeric state for *F. tularensis* RelA by analytical size exclusion chromatography (7.4.6). (A) Absorption trace (280 nm) for size exclusion chromatography (Superdex 200) yielding a single peak with an apparent molecular weight of 128 ± 1.57 kDa corresponding to the dimeric state of the enzyme (calculated molecular mass of dimer 148 kDa). (B) Calibration curve for apparent molecular weight determination.

Analysis of the multimeric state of *F. tularensis* RelA following incubation at 30 °C, a temperature at which it is enzymatically active, for 20 minutes yielded two peaks by size exclusion chromatography (Figure 2.9, red trace). The additional peak relates to either the formation of protein aggregation in a non-specific manner or the formation of a tetramer (estimated molecular weight of 284.87 kDa) of unknown functional significance. The additional peak however only corresponds to a very low proportion (<10% of the total integrated area) of the total protein.

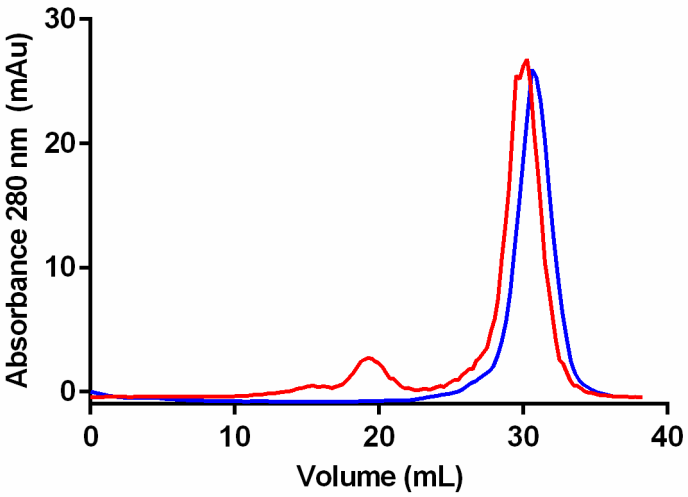

Figure 2.9. The temperature-related multimeric state for *F. tularensis* RelA by analytical size exclusion chromatography (7.4.6). Absorption traces (280 nm) yielding a single peak and two peaks for *F. tularensis* RelA when incubated at 4 °C (blue) or 30 °C (red) respectively.

2.3 Substrate Specificity of *F. tularensis* RelA

Substrate preferences for *E. coli* RelA [260] and *M. tuberculosis* [192] and *B. subtilis* [259] Rel synthetase activity have already been published. The reported preferences for pyrophosphate acceptor (GTP/GDP) have been associated with the synthetase active site motif of the enzyme [285]. The unusual motif of EXSD observed in *Francisella* species suggested substrate specificity of *F. tularensis* RelA might therefore be of interest. End-point *F. tularensis* RelA activity assays were prepared with *F. tularensis* RelA, ATP (2 mM) and either GDP, GTP or, as a negative control CTP (A.2) at 2 mM (7.4.9). Analysis by ion pair reverse phase HPLC (7.4.7) showed that efficient formation of AMP and the 3'-pyrophosphorylated product were only observed in the presence of GTP as a co-substrate (Figure 2.10). The nucleotides GDP and CTP were not accepted as substrates. For other reported RSH enzymes the differentiation between GTP and GDP is not absolute, but instead a preference relating to alterations in measured V_{max} and K_M values [285]. This is in contrast with *F. tularensis* RelA that shows no measurable formation of ppGpp from GDP, but will turn over GTP in a highly specific manner.

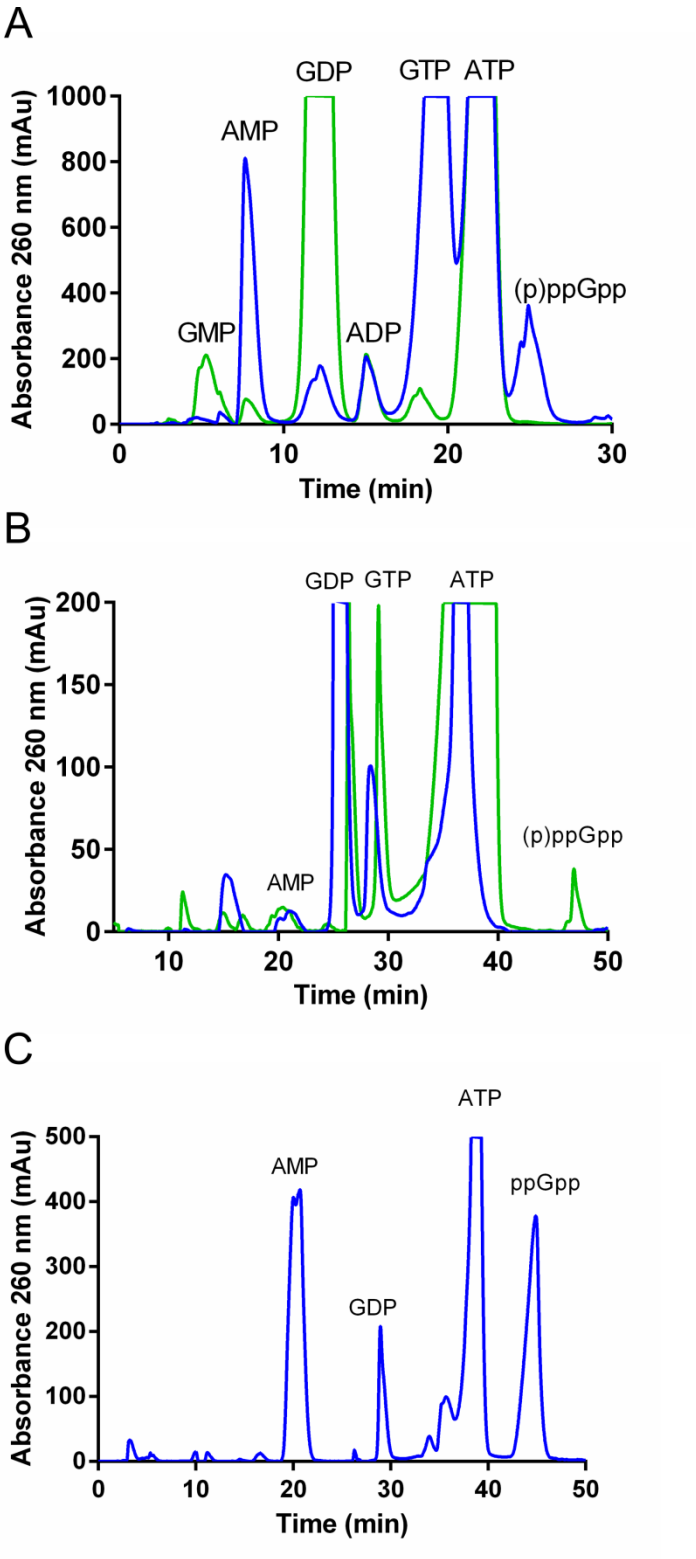

Figure 2.10. IP RP HPLC analysis of *F. tularensis* RelA specificity for either GDP (blue) or GTP (green) as the pyrophosphate acceptor. (A) *F. tularensis* RelA basal activity (no activating factors) (7.4.9, 7.4.8.4). (B) *F. tularensis* RelA ribosome-mediated activity (7.5.9, 7.4.8.3). (C) *F. tularensis* RelA methanol-stimulated activity (7.5.20, 7.4.8.2).

This specificity was still observed when *F. tularensis* RelA was activated by stalled ribosomal complexes (7.4.9.2) (Figure 2.10b), but interestingly not observed in the presence of methanol (7.4.9.3) (Figure 2.10c). In the presence of a methanol-containing buffer (30% v/v) a distinct peak can be observed for ppGpp (Figure 2.10c).

2.4 Kinetic Characterisation of *F. tularensis* RelA by Ion Pair Reverse Phase HPLC

2.4.1 Assay Optimisation

2.4.1.1 Temperature Optimisation

End point assays (1 hour) with 2 mM of each substrate (GTP and ATP) were set up over a range of temperatures from 22- 37 °C, to ascertain the optimal temperature for *F. tularensis* RelA activity (7.4.10). However, optimal activity for *F. tularensis* RelA was observed at ~30 °C (Figure 2.11). *F. tularensis* is typically incubated at 37 °C [118, 334] or at 30 °C [335, 336] dependent on the host cell conditions. Previous literature for *E. coli* RelA has also suggested that lower temperatures between 25-30 °C are required for RelA synthetase activity in the absence of stalled ribosomes [309]. Thus, further biochemical experiments for *F. tularensis* RelA were incubated at 30 °C.

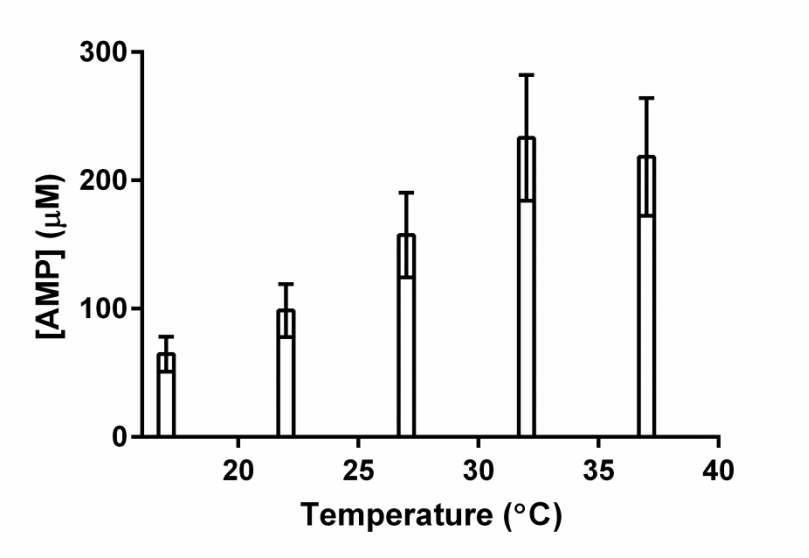

Figure 2.11. IP RP HPLC analysis (7.3.8.2) of the optimal temperature for *F. tularensis* RelA synthetase activity in the absence of activating factors.

2.4.1.2 **Buffer Optimisation**

To ensure optimal conditions for the measurement of *F. tularensis* RelA kinetic parameters the effect of buffering agent, reducing agent and divalent cation concentration were investigated. Previous studies of RelA activity have involved the use of HEPES as a buffering agent [168, 295, 296]. Following the observed increase in *F. tularensis* RelA stability with Tris as a buffering agent during purification (2.1.2), analysis of *F. tularensis* RelA activity was also measured with Tris as the buffering agent.

Concentrations of the potassium and magnesium metal ions routinely used for RelA activity assays are in the range of 5-20 mM [168, 260, 295, 296], therefore the assay buffer for *F. tularensis* RelA contained 15 mM of each metal ion. The presence of the reducing agent β-mercaptoethanol is also common in RelA assay buffers [168, 295]. During the studies described herein, experiments by 4th year MChem project student C. Frankling demonstrated that *F. tularensis* RelA showed poor stability at higher concentrations of β-mercaptoethanol [337]. The activity assay buffer described by Payoe *et al.* [295], upon which the assay buffer for *F. tularensis* RelA was largely based, however used a low concentration of 1 mM β-mercaptoethanol. This concentration was within the range in which *F. tularensis* RelA is stable [337].

2.4.2 Ion Pair Reverse Phase HPLC Analysis

The most common method for measuring RelA activity currently is the analysis of radiolabelled assays by thin layer chromatography on a polyimine substrate [168, 295, 296]. Reactions are usually monitored using α[^{32}P]-GTP [295, 296] or γ[^{32}P]-ATP [168] as labelled substrates. One disadvantage of this analysis method is the inability to observe both the nucleotide products AMP and (p)ppGpp. In addition to this, the safety precautions associated with the use of such a method did not best suit the long term objective of this project to identify inhibitors of *F. tularensis* RelA. For these reasons an alternative method of analysis was investigated. Previous research had demonstrated the analysis of (p)ppGpp synthetase assays by high performance liquid chromatography (HPLC) [168] and subsequently the suitability of this method was tested. Cordell *et al.* (2008) published an ion pair reverse phase method of nucleotide separation by HPLC, utilising dimethylhexylamine (DMHA) as the ion pair reagent [338]. Analysis of many nucleotides was shown using this method, however it did not demonstrate the separation or analysis of (p)ppGpp. Initial work therefore involved the adaptation and optimisation of the HPLC method (Figure 2.12, 7.4.8.1 [333]) to ensure good separation of mono-, di-, tri-, tetra- and pentaphosphates.

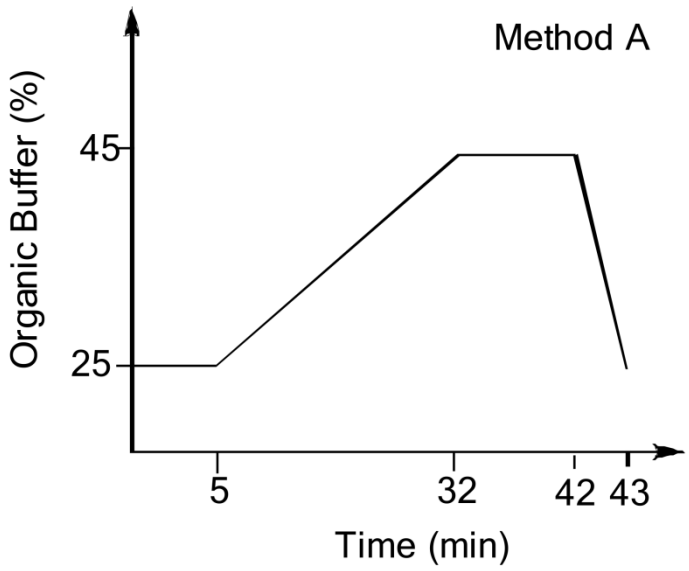

Figure 2.12. Graphic presentation of IP RP-HPLC analytical Method A for the separation of nucleotides (7.4.8.1.)

Early method development strived to achieve the separation of all the nucleotides (substrates and products) within the reaction, alongside potential diphosphate contaminants (GDP and ADP). For all the IP RP-HPLC methods described herein the aqueous (5% methanol: 95% water v/v) and organic (80% methanol: 20% water v/v) phases contained 15 mM DMHA and were made to pH 7.0 with acetic acid. The optimal separation of AMP from the observed injection peak was determined by varying the starting percentage of organic phase from 5 to 14%. The incline of the gradient was maintained by extending the time of the gradient to accommodate the lower starting percentage (Figure 2.13a). Analysis of the HPLC traces (absorbance trace at 260 nm) for individual gradients showed that the optimal initial organic phase percentage was 9% (green trace) (Figure 2.13b).

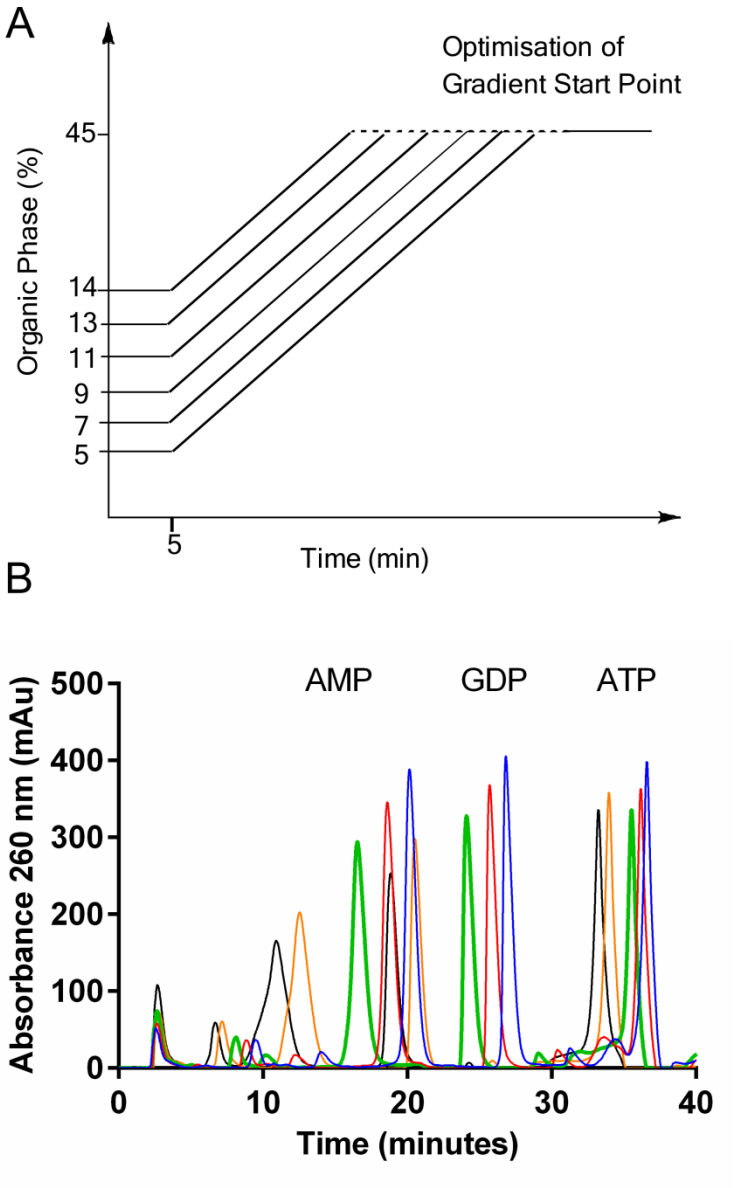

Figure 2.13. IP RP HPLC analysis (7.4.8) of nucleotide standards (2 mM GTP, ATP, and AMP) with varying starting percentage of organic phase. (A) Graphical representation of methods used at different starting percentages. (B) HPLC traces for nucleotides analysed with a method starting at 5% (blue), 7% (red), 9% (green), 11% (purple), 13% (orange), or 14% (black) organic buffer.

To determine the optimal distribution of mono-, di- and triphosphates across the gradient, the end point of the gradient was varied between 45 and 55% organic phase (7.4.8). Higher percentage end points for organic phase shifted all the peaks to the left (Figure 2.14). The guanosine penta- and tetraphosphate should elute after the triphosphates, to allow optimal separation of all phosphate species the optimal gradient end point was determined to be 51% (green trace) (Figure 2.14).

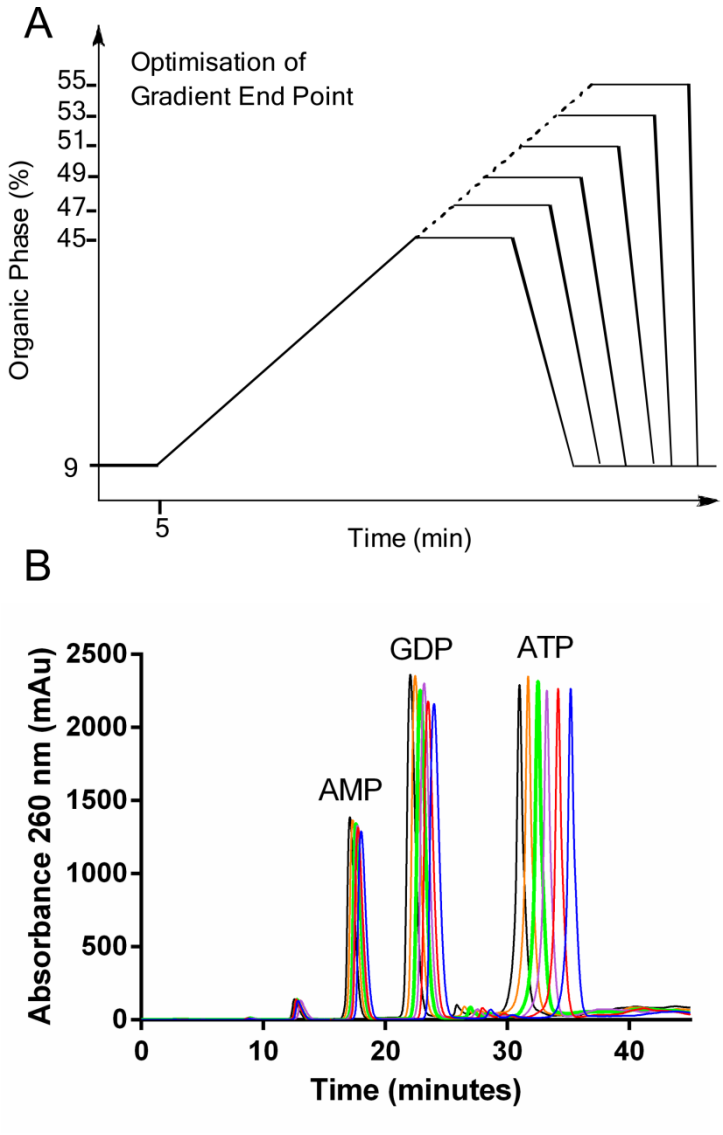

Figure 2.14 IP RP HPLC analysis (7.3.8) of nucleotide standards (2 mM GTP, ATP, and AMP) with varying end percentage of organic phase. (A) Graphical representation of methods used at different starting percentages. HPLC traces for nucleotides analysed with a gradient ending at 45% (blue), 47 (red), 49 (purple), 51 (green), 53 (orange), and 55% (black).

The optimal gradient for analysis of (p)ppGpp synthetase activity was determined to be 9-51% organic phase (full method described in 7.4.8.2). Analysis of a ppGpp synthesis assay (7.5.20) confirmed elution of ppGpp as a single peak after ATP (Figure 2.15).

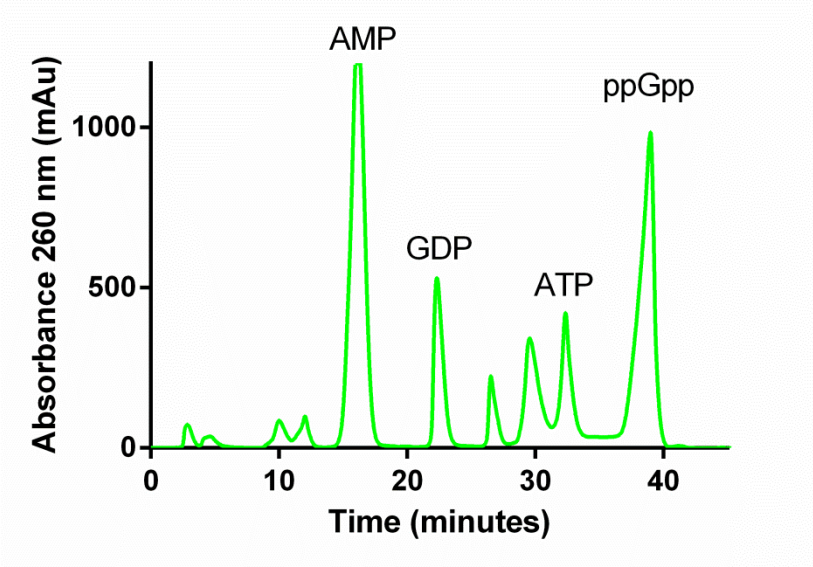

Figure 2.15. IP RP HPLC analysis (7.4.8.2) of a methanol activated *F. tularensis* RelA synthetase activity assay. Peaks corresponding to AMP, GDP, ADP, and ATP were identified by analysis of commercially sourced standards. The peak labelled ppGpp was identified by LCMS analysis.

LCMS analysis (7.4.11) of *F. tularensis* RelA activity was used to validate the identity of the observed (p)ppGpp peaks from HPLC analysis (7.4.7). Aqueous and organic phases were modified to accommodate electrospray ionisation (ESI) negative mass spectrometry. The modified phases contained hexafluoroisopropanol (HFIP) as this compound has been shown to be good for efficient electrospray ionisation of oligonucleotides following separation using an ion pairing reagent [339]. LCMS analysis identified the terminal two peaks as ppGpp and pppGpp at retention times 24.8 and 26.0 min respectively (Figure 2.16).

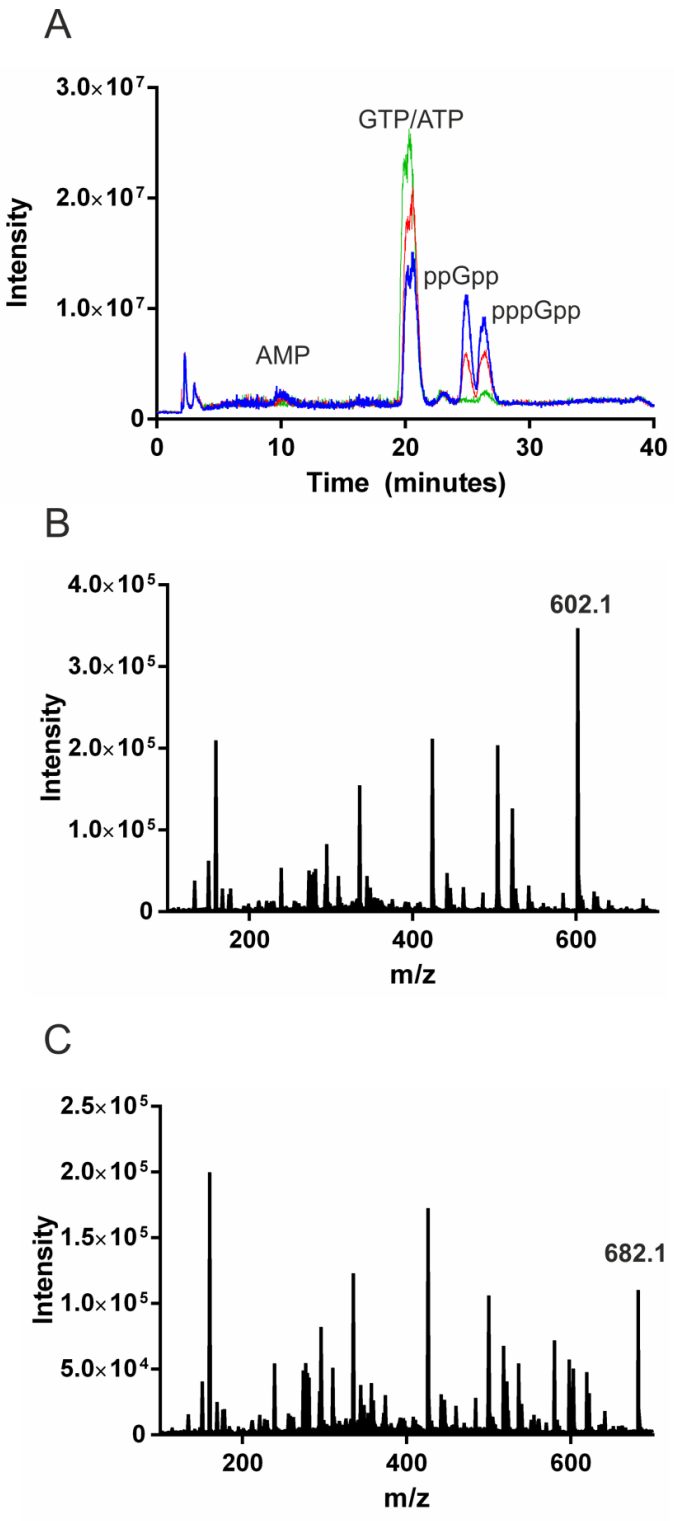

Figure 2.16. LCMS analysis (7.4.11) of *F. tularensis* RelA synthetase activity. (A) Total Ion Current (TIC) chromatogram for *F. tularensis* activity over time; 0 min (blue), 30 min (red) and 60 min (green). Identification of key peaks for (B) ppGpp (m/z 602.1, calculated [M-H]- 602.1) and (C) pppGpp (m/z 682.1, calculated [M-H]- 682.2) for absorbance peaks at 24.8 min and 26.0 min respectively.

Extension of the gradient to an end point of 80% organic phase (7.4.8.3) was used to increase the separation of the guanosine penta- and tetra-phosphate peaks. Time course analysis of *F. tularensis* RelA activity using this method however showed a marked decrease in measured concentrations of (p)ppGpp compared to AMP (Figure 2.17). This was unexpected as these nucleotides would be predicted to form in a 1:1 stoichiometry.

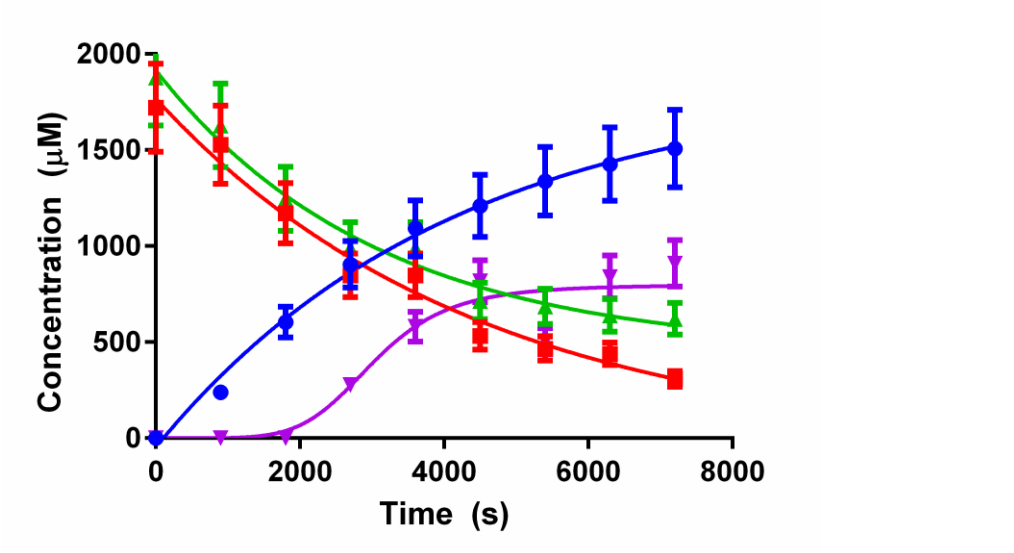

Figure 2.17. IP RP HPLC analysis (7.4.8.3) of *F. tularensis* RelA activity over time. The analysis shows the concentrations of AMP (blue), (p)ppGpp (purple), GTP (green), ATP (red) over time.

Two reasons for the underestimation of (p)ppGpp concentrations were identified. The elution of guanosine tetraphosphate (ppGpp) and pentaphosphate (pppGpp) gave broad peaks with only partial resolution (A.3). This resulted in poor integration of peaks and resultant underestimation of (p)ppGpp concentration, particularly at low concentrations. Further investigation into the method of assay quenching at selected time points showed that the addition of formic acid resulted in degradation of guanosine penta- and tetra-phosphates (Figure 2.18). An alternative method of assay quenching (heating at 80 °C for 2 minutes) demonstrated much less degradation of guanosine penta- and tetra-phosphates (Figure 2.18). All subsequent experiments were therefore quenched by heating.

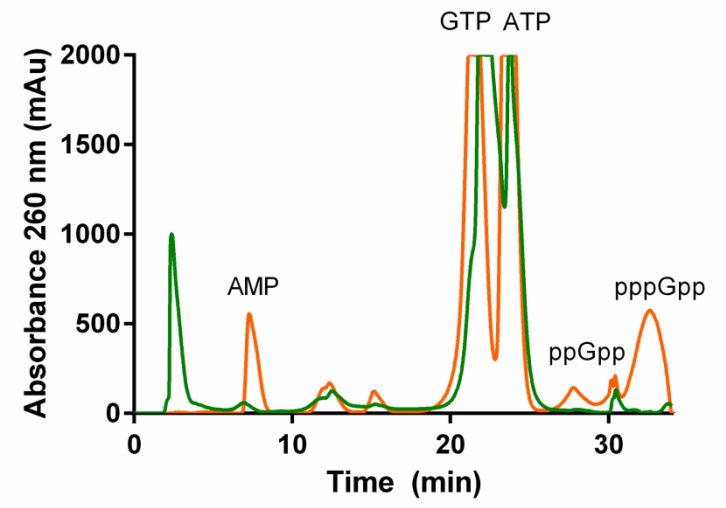

Figure 2.18. IP RP HPLC analysis (7.3.8.4) of *F. tularensis* RelA synthetase assays (2 mM GTP and ATP) when quenched by either 1M (final concentration) formic acid (green) or by heating to 80 °C for 2 minutes (orange).

In order to observe the combined guanosine nucleotide products a further modification of the HPLC method was introduced with a gradient of 25- 60% organic phase (7.4.8.4). This resulted in the co-elution of ppGpp with pppGpp, which resulted in single well defined peak for both products (Figure 2.19).

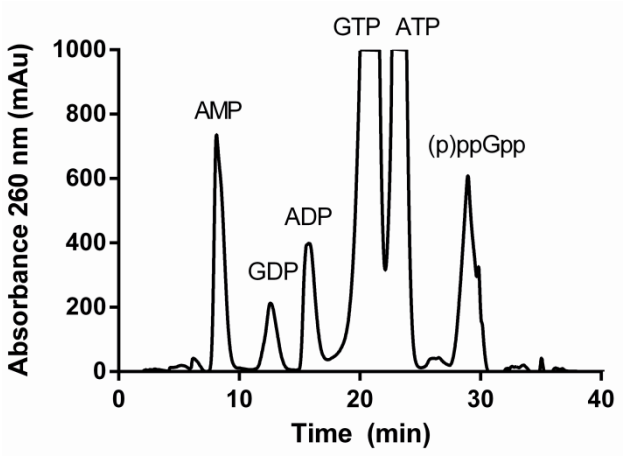

Figure 2.19 IP RP HPLC analysis (7.4.8.4) of a methanol activated *F. tularensis* RelA synthetase activity assay. Peaks corresponding to AMP, GDP, ADP, and ATP were identified by analysis of commercially sourced standards.

This allowed accurate quantification of both hyperphosphorylated guanosine products at lower concentrations. Analysis of *F. tularensis* RelA activity with this method demonstrated a virtually stoichiometric increase in AMP and (p)ppGpp over time (Figure 2.20).

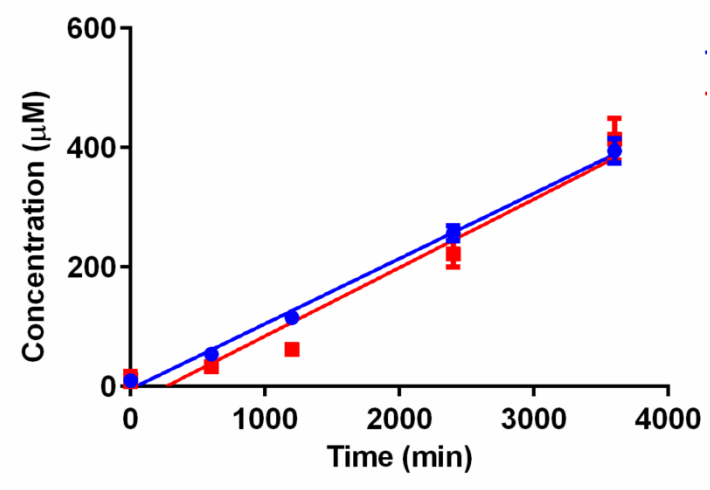

Figure 2.20. Analysis of AMP (blue) and (p)ppGpp (red) production over time (0.8 mM ATP, 2 mM GTP) by *F. tularensis* RelA when analysed by IP RP HPLC (7.4.8.4).

2.4.3 Kinetic Characterisation of *F. tularensis* RelA

Steady state kinetic parameters for *F. tularensis* RelA were obtained by analysing a series of reaction time course experiments over a range of substrate concentrations (7.4.12). HPLC analysis of time course experiments measured product concentration in aliquots withdrawn at 0, 10, 20 and 40 min (Figure 2.21 and Table 2.1). Time course experiments were then used to determine initial rates resulting in less than 15% turnover of substrate. Initial rates were calculated using Equation 2.1. Here Y and X represent values from their respective axis and Y_0 denotes the intersection of the Y axis. Initial rates calculated from AMP production are detailed in Table 2.1, those calculated from (p)ppGpp production are detailed in Table A.1 (A.4).

Equation 2.1.

$$Initial\ rate = \frac{(Y - Y_0)}{X}$$

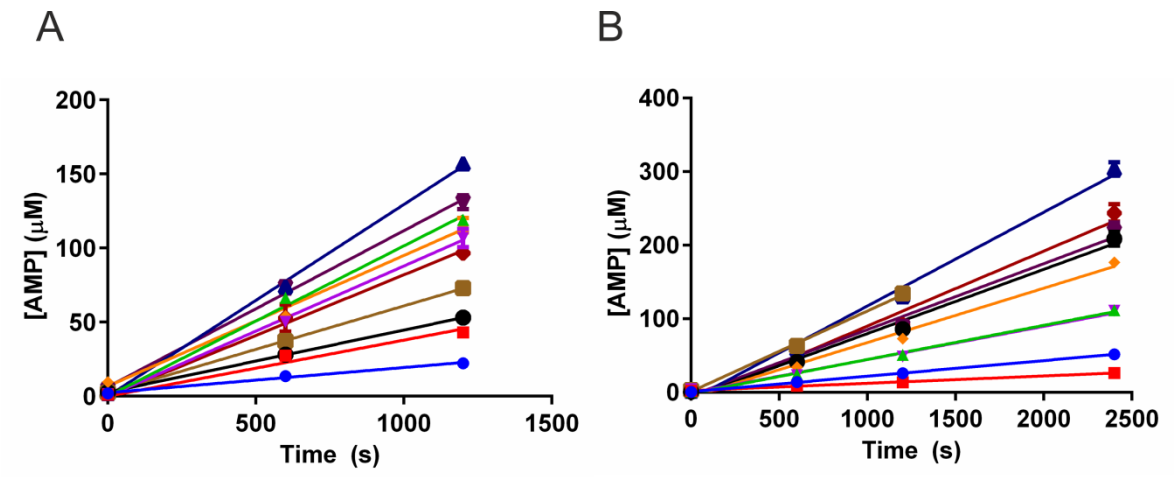

Figure 2.21. IP RP HPLC analysis (7.4.8.4) of *F. tularensis* RelA activity over time. (A) At 2 mM GTP and varying concentrations of ATP; 100 µM (blue), 200 µM (red), 250 µM (black), 350 µM (brown),400 µM (green), 600 µM (purple), 800 µM (orange), 1000 µM (navy), 1500 µM (maroon), 2000 µM (burgundy). (B) At 2 mM ATP with varying concentrations of GTP; 250 µM (red), 400 µM (blue), 750 µM (green), 1000 µM (purple), 1250 µM (orange), 1750 µM (black), 2000 µM (brown), 2250 µM (navy), 2750 µM (maroon), and 3750 µM (burgundy). These correspond to the data presented in Table 2.1.

Table 2.1. Initial rates calculated by IP RP HPLC analysis of AMP production in *F. tularensis* RelA activity assays with varying concentration of substrates.

[GTP] /μM	Initial rate/ nM s^{-1}	R^2	[ATP]/ μM	Initial rate/ nM s^{-1}	R^2
3750	102 ± 5.1	0.98	2000	77.1 ± 4.0	0.97
2750	89.6 ± 3.6	0.98	1500	105 ± 3.1	0.98
2250	127 ± 4.1	0.99	1000	129 ± 5.4	1.00
2000	110 ± 2.8	0.99	800	88.3 ± 3.6	1.00
1750	87.3 ± 3.2	0.99	600	87.8 ± 2.9	1.00
1250	73.9 ± 2.7	0.99	400	98.3 ± 6.0	0.99
1000	45.2 ± 1.6	0.96	350	58.7 ± 1.0	0.99
750	46.4 ± 1.1	0.99	250	41.9 ± 0.7	1.00
400	21.2 ± 0.4	1.00	200	34.9 ± 2.1	0.99
250	9.96 ± 0.3	0.99	100	17.0 ± 1.1	0.99
0	00.00	-	0	00.00	-

Fitting the velocity curves (plotting initial rates of reaction against concentration of substrate) suggested a better fit for a sigmoidal (R^2 = ~0.947) than a hyperbolic function (R^2 = ~0.899) (Figure 2.22). Kinetic parameters were therefore calculated from velocity curves fitted to a sigmoidal function, Equation 2.2. Here *v* denotes the initial rates, V_{max} denotes the rate of reaction at substrate saturation, $K_{1/2}$ denotes the concentration of substrate required to give half the V_{max}, S is the substrate concentration and h is the apparent Hill coefficient.

Equation 2.2.

$$v = \frac{V_{max} S^h}{\left(K_{1/2}^h + S^h\right)}$$

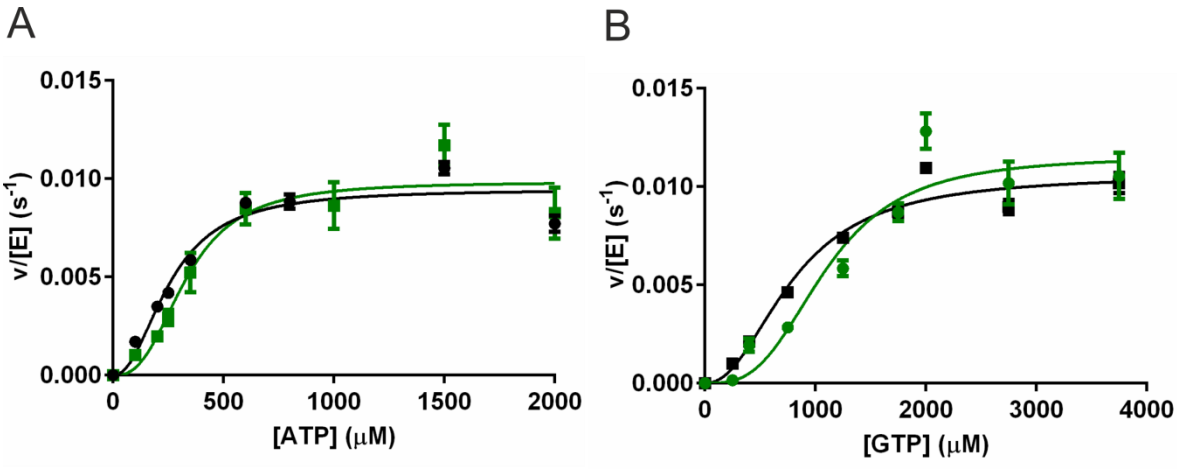

Figure 2.22. Saturation curves of *F. tularensis* RelA for GTP (A) and ATP (B) with initial rates calculated by IP PR HPLC analysis (7.4.8.4) from AMP production (black) and pppGpp production (green).

There are several kinetic models that explain sigmoidal velocity curves [340], one of which is an enzyme that is allosterically regulated [341]. The Lineweaver-Burk plot for *F. tularensis* RelA steady state data curves in a manner consistent with positive co-operativity of nucleotide binding [342] (Figure 2.23). This is when the binding of one nucleotide to the enzyme encourages the binding of second nucleotide. For allosteric enzymes this can relate to a conformational change within the enzyme, which corresponds to a resultant state with a higher affinity for the second nucleotide.

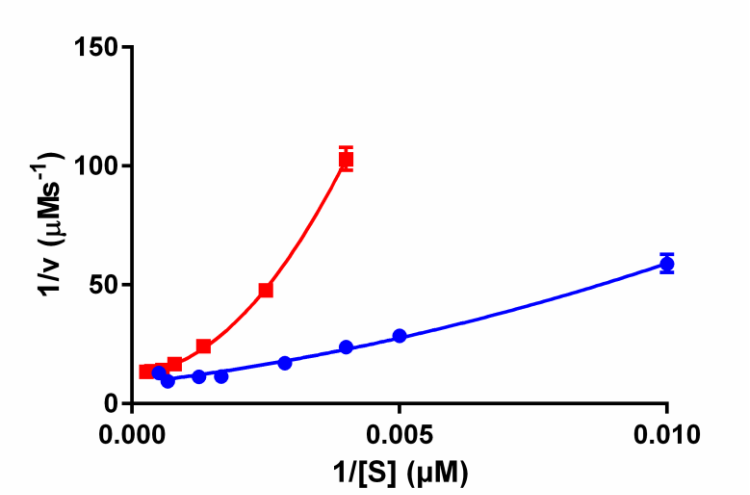

Figure 2.23 Lineweaver-Burk double reciprocal plot for *F. tularensis* RelA over a range of GTP (red) and ATP (blue) concentrations, as determined by IP RP HPLC analysis (7.3.8.4). Data was fitted to a second order polynomial (quadratic) function in GraphPad Prism.

The $K_{1/2}$ values for ATP as a substrate are within error whether calculated from rate of formation of AMP or (p)ppGpp, with the values of 259 ± 37.2 µM and 332 ± 47.8 µM respectively. The $K_{1/2}$ values for GTP as a substrate when calculated from either AMP or pppGpp formation are 800.7 ± 115.6 µM and 1095 ± 183.8 µM. These values are also within error. The Hill coefficient (h) relates to the number of binding sites on the enzyme and the degree of cooperativity between them [342]. An exact interpretation of Hill coefficient is difficult; however the calculated value cannot exceed the number of interacting sites [342]. This suggests that an average Hill coefficient of 2.53 ± 0.22 calculated for *F. tularensis* RelA could relate to 2 or 3 interacting sites.

Table 2.2. Kinetic parameters derived from HPLC analysis of *F. tularensis* RelA activity assays for GTP and ATP substrates.

Substrate	ATP		GTP	
Product Measured	AMP	(p)ppGpp	AMP	(p)ppGpp
V_{max}/ x10^{-3} s^{-1}	09.46 ± 0.8	09.83 ± 0.8	10.59 ± 0.9	11.54 ± 1.5
$K_{1/2}$/ μM	259.0 ± 37	332.0 ± 48	800.7 ± 116	1095 ± 184
h	02.17 ± 0.7	02.71 ± 1.0	02.18 ± 0.5	03.07 ± 1.29
R^2	0.95	0.94	0.97	0.93

2.5 Kinetic Characterisation of *F. tularensis* RelA by ^{31}P NMR

A sigmoidal fit for saturation kinetics has not been previously observed for a RelA enzyme, but has conversely been observed for Rel proteins when unstimulated [285]. It was therefore important to verify the observations by HPLC analysis with another analysis method. NMR analysis for monitoring enzymatic reactions is uncommon, due to its intrinsic low sensitivity and subsequent long acquisition times. The relatively slow turnover of *F. tularensis* RelA in the absence of activators (as judged by HPLC analysis), however suggested that ^{31}P NMR (7.4.13) might prove to be a suitable alternative method for this enzyme.

Signals for each phosphorus atom in the substrates and products were identified (Figure 2.24 and Table 2.3). Clearly defined peaks could be observed for the phosphorus atoms relating to the products AMP-α (3.32 ppm) and pppGpp-β (-19.88 ppm).

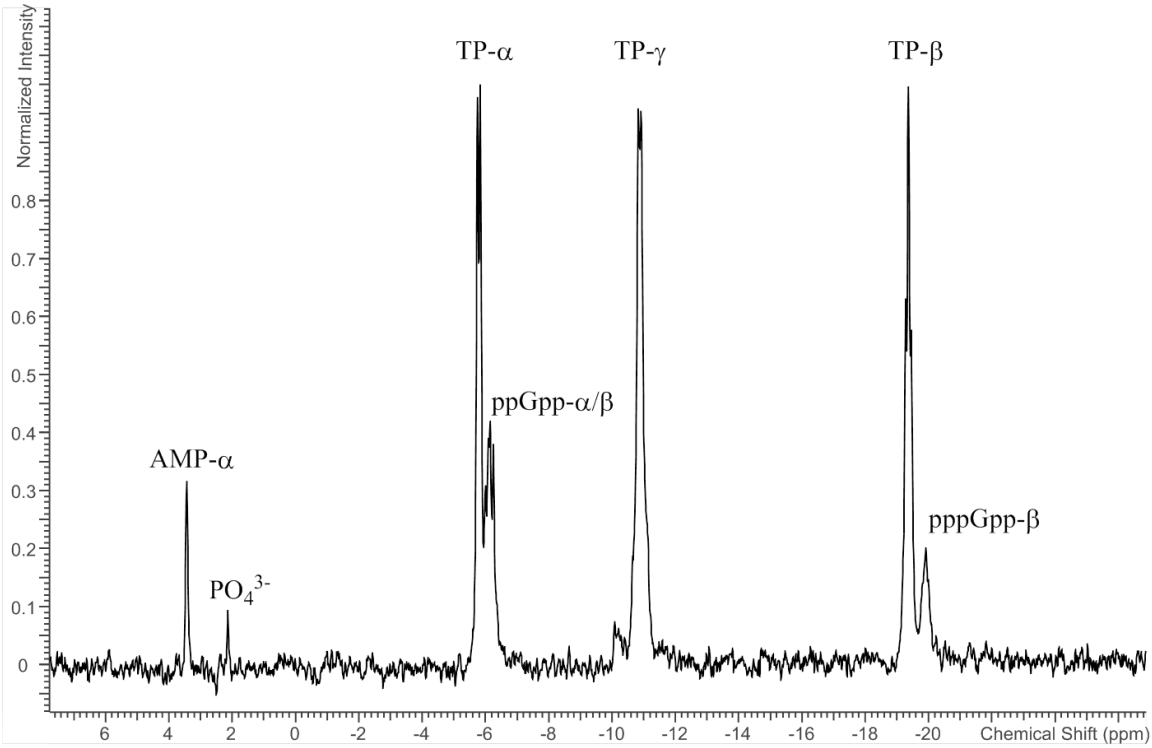

Figure 2.24. ^{31}P NMR analysis (7.4.13) of nucleotides from *F. tularensis* RelA synthetase activity assay.

Table 2.3. Chemical shifts for all phosphorus containing species in *F. tularensis* RelA activity assays analyzed by ^{31}P NMR.

Phosphorus Atom	Chemical Shift/ ppm
AMP-5'α	3.32
PO_4^{3-}	1.94
Triphosphate-5'α	-5.71
Diphosphate-5'α / Pentaphosphate 3'α and β	-6.13
Diphosphate- 5'β/ Triphosphate- 5'γ	-10.85
Triphosphate-5'β	-19.28
pppGpp- 5'β	-19.88

Analysis over time was possible, however due to the inherent low sensitivity of the technique time points were spaced every 22 minutes. Increase in time point spacing led to a requirement of increased substrate turnover for determining initial rates (Figure 2.26 and Table 2.4). However, extended time course analysis by ^{31}P NMR demonstrated approximate linearity (R^2 ~0.99) up to 60 minutes (Figure 2.25).

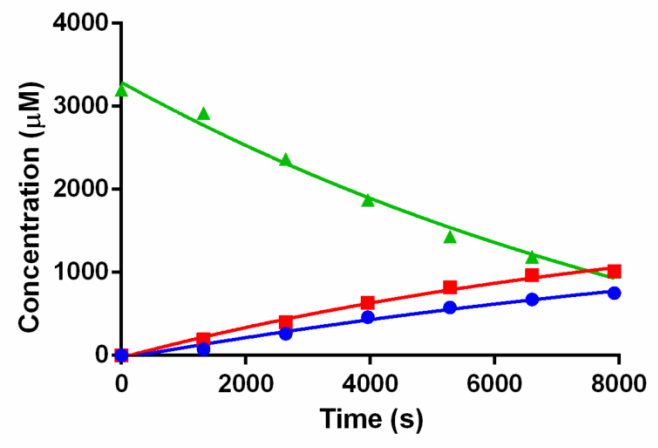

Figure 2.25. ^{31}P NMR analysis of *F. tularensis* synthetase activity, with a starting concentration of 2 mM ATP and 1.75 mM GTP, as monitored by calculated concentration of AMP (blue), GTP/ATP (green) and pppGpp (red) over time.

Using integrals of the signals for ATP and GTP in the initial reaction condition (t = 0 s) as a calibration of concentrations, signals from subsequent time points could be integrated to measure the concentrations of nucleotides. The conversion of GTP to pppGpp was observed to occur in a specific manner. Only one minor by-product was observed, inorganic phosphate (Figure 2.24, peak 2, 1.94 ppm), which accumulates slowly during the activity assays. This observation is consistent with the instability of pppGpp under assay conditions. Alternatively it could relate to the presence of a very low level of contaminating GppA/PPX phosphatase, which are enzymes known to accept guanosine pentaphosphate (pppGpp) as a substrate [187].

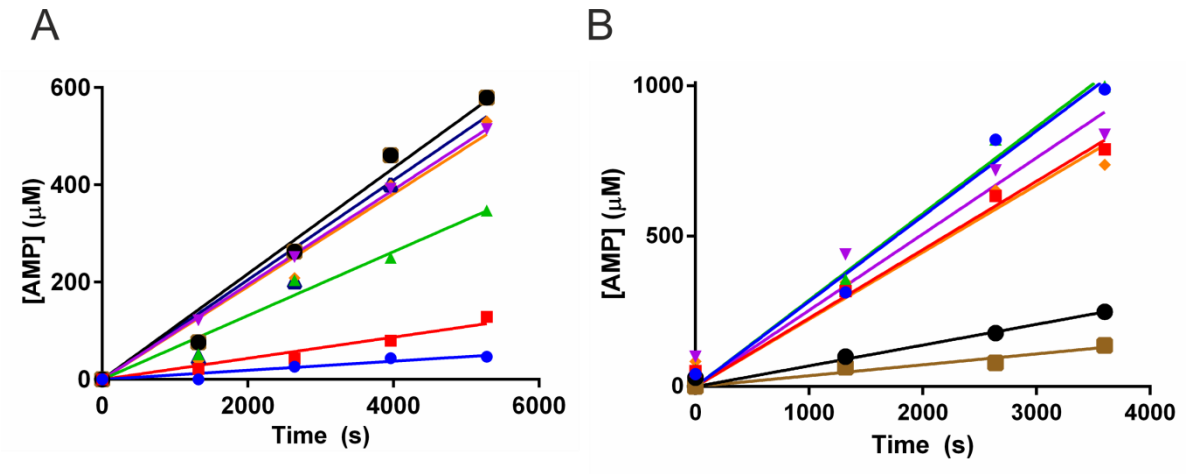

Figure 2.26. ^{31}P NMR IP RP HPLC analysis (7.3.8.4) of *F. tularensis* RelA activity over time. (A) At 2 mM GTP and varying concentrations of ATP; 0.125 mM (blue), 0.25 mM (red), 0.5 mM (green), 0.75 mM (orange), 1 mM (purple), 1.25 mM (navy) or 1.5 mM (black). (B) At 2 mM ATP with varying concentrations of GTP; 0.5 mM (brown), 1 mM (black), 1.5 mM (orange), 2 mM (purple), 3 mM (green), 4 mM (red) or 5 mM (blue). These correspond to the data presented in Table 2.4.

Table 2.4. Initial rates calculated by ^{31}P NMR analysis of AMP production in *F. tularensis* RelA activity assays with varying concentration of substrates.

[GTP] /μM	Initial rate/ nM s^{-1}	R^2	[ATP]/ μM	Initial rate/ nM s^{-1}	R^2
4000	143 ± 15	0.97	1750	122 ± 12	0.97
3000	134 ± 10	0.98	1500	117 ± 9.0	0.99
2000	169 ± 25	0.96	1250	117 ± 9.0	0.98
1500	93.8 ± 9.4	0.97	1000	108 ± 11.4	0.97
1000	60.3 ± 4.1	0.98	750	98.5 ± 1.3	1.00
750	41.1 ± 5.9	0.94	500	67.6 ± 6.5	1.00
500	14.4 ± 1.2	0.93	250	23.9 ± 2.6	0.97
250	9.01 ± 1.1	0.86	125	10.7 ± 1.2	0.95
0	0.000	-	0	0.000	-

Plots of time courses for product formation were fitted to determine linear rates of reaction (Figure 2.26 and Table 2.4). Initial rates calculated from AMP production are detailed in Table 2.4, those calculated from (p)ppGpp production are detailed in Table A.2 (A.5). Initial rates determined over a range of substrate concentrations were plotted to yield velocity curves (Figure 2.27).

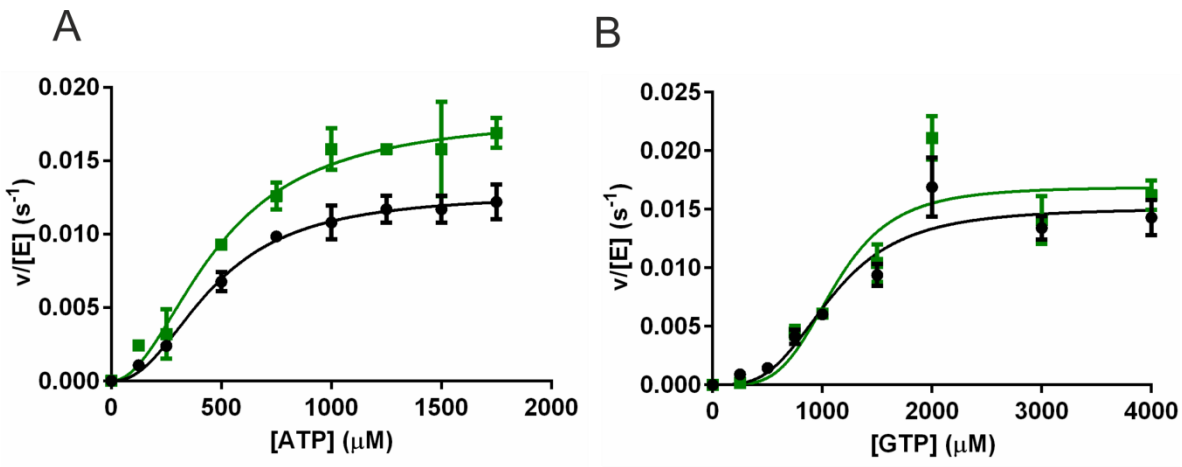

Figure 2.27. Saturation curves of *F. tularensis* RelA for GTP (A) and ATP (B) with initial rates calculated by ^{31}P NMR analysis from AMP production (black) and pppGpp production (green).

As observed previously by IP RP HPLC analysis, these velocity curves also fitted to a sigmoidal function and gave comparable calculated values for $K_{1/2}$ and V_{max} for GTP and ATP (Table 2.5 and Table 2.1). Data obtained by ^{31}P NMR should however be considered as an estimate only, as the concentrations were determined over an extended time period (up to 1 hour). This had the advantage of more accurate determination of the product nucleotide concentrations (following accumulation to higher concentrations). This is associated however with the caveat that these rates cannot be regarded as 'initial' rates of reaction, as typically required for classical enzyme kinetics, with an average of 34.4 ± 2.8% turnover of substrate measured. Bearing these caveats in mind, the correlation of the values for apparent V_{max} and apparent $K_{1/2}$ from the NMR experiments show a good internal correlation and compare well with the values determined by HPLC (Tables 2.2).

Table 2.5. Kinetic parameters derived from NMR analysis of *F. tularensis* RelA activity assays for GTP and ATP substrates. R^2 is a measure of goodness of fit.

Substrate	ATP		GTP	
Product Measured	AMP	(p)ppGpp	AMP	(p)ppGpp
V_{max}/ x10^{-3} s^{-1}	12.76 ± 0.3	18.13 ± 1.2	15.10 ± 1.6	16.92 ± 2.2
$K_{1/2}$/ μM	463 ± 18	482 ± 49	1087 ± 146	1114 ± 175
h	2.27 ± 0.17	2.01 ± 0.32	3.31 ± 1.22	4.11 ± 2.13
R^2	0.99	0.99	0.94	0.90

2.6 **Global Fits and Final Kinetic Values**

A global fit for initial rate data calculated from HPLC analysis (for both products AMP and (p)ppGpp) and ^{31}P NMR analysis (for AMP), showed an overall fit to a sigmoidal curve (Figure 2.28). The pppGpp data from ^{31}P NMR was excluded from the global fit as the overlapping peak between the pppGpp-β (-19.88 ppm) and the triphosphate-β (19.28 ppm) (Figure 2.24) led to inaccuracy in the calculated quantity of pppGpp. Fitting this combined data and allowing the V_{max} and $K_{1/2}$ to be shared constants (i.e.; a global fit across the data) yielded a sigmoidal curve with R^2 values of 0.93 and 0.88 for ATP and GTP respectively (Figure 2.28). $K_{1/2}$ and V_{max} values were also calculated (Table 2.6).

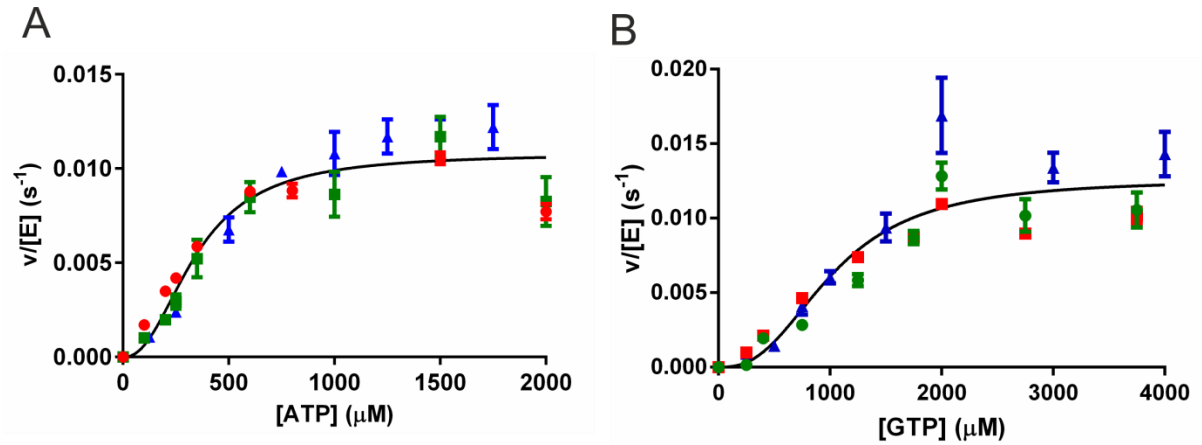

Figure 2.28. Saturation curves of *F. tularensis* RelA for GTP (A) and ATP (B) with initial rates calculated by both IP RP HPLC (AMP and (p)ppGpp) and ^{31}P NMR analysis (AMP) fitted to Equation 1 with the shared kinetic parameters for V_{max} and $K_{1/2}$.

Kinetic parameters calculated by IP RP HPLC analysis were used for all future characterisation and applications for *F. tularensis* RelA, to avoid the introduction of error from the ^{31}P NMR analysis.

Table 2.6. Calculated Kinetic Parameters for *F. tularensis* RelA when a global fit is applied to both ^{31}P NMR (AMP) and IP RP HPLC (AMP and pppGpp) data sets. R^2 is a measure of goodness of fit.

Substrate	ATP	GTP
V_{max}/ x10^{-3} s^{-1}	10.79 ± 0.59	12.6 ± 1.19
$K_{1/2}$/ μM	344.3 ± 33.95	1026 ± 134.5
h	2.26 ± 0.44	2.58 ± 0.70
R^2	0.932	0.881

2.7 Discussion of *F. tularensis* RelA Characterisation

F. tularensis RelA contains several structural irregularities compared to that of other RelA enzymes. An unusual active site motif and truncated C-terminal region, around 100 amino acids shorter than other RelA enzymes, could have many implications on the activity of the RelA from *F. tularensis*. Here the expression, purification, multimeric state and kinetic properties of the enzyme reported in this chapter are discussed.

Small scale expression studies showed that the optimal recovery of *F. tularensis* RelA was achieved from overnight expression in BL21 (DE3) Rosetta at 16 °C, when induced with 0.4 mM IPTG [333]. The strain *E. coli* BL21 (DE3) Rosetta is primarily used for the expression of eukaryotic proteins as it contains a plasmid encoding tRNAs with codons rarely used for *E. coli* [343]. Although *F. tularensis* RelA is not a eukaryotic protein the increased diversity of tRNA molecules within the cell could result in a reduced rate of translation, which in turn could limit protein misfolding. Reducing protein misfolding is of particular importance as misfolded proteins can form highly aggregated protein masses referred to as inclusion bodies [344], from which protein purification is difficult. Large scale expression showed low cell pellet yields (3-5 g/L) corresponding to the lower yield observed with cultures grown at temperatures ≤ 18 °C [345], 16 °C in this case. This reduced growth rate can also be beneficial in the overexpression of larger proteins as it further reduces protein misfolding [346].

The purification of proteins using nickel affinity chromatography via the presence of a hexahistidine tag [347] is common practise in the area of biochemistry. A hexahistidine tag was introduced at the N-terminal region of *F. tularensis* RelA to prevent later interruption of the expected C-terminal interaction with ribosomes, as has been observed for *E. coli* RelA [305]. Purification of *F. tularensis* RelA by nickel affinity chromatography required a starting concentration of 10-20 mM imidazole to achieve maximal binding of the enzyme to the column. As a consequence of this, coupled with the innate propensity of the enzyme to bind other proteins [309], it was observed that high levels of contaminating proteins co-purified with *F. tularensis* RelA (Figure 2.6). A second purification step, size exclusion chromatography, was introduced to remove most of the co-purifying *E. coli* proteins. Following size exclusion chromatography the purity of *F. tularensis* RelA was substantially improved (Figure 2.7), however the total *F. tularensis* RelA yield from 5 L of culture was reduced from 150-200 mg (with contaminants) to 75 –

120 mg (pure). Perhaps the first noteworthy difference between the properties of *F. tularensis* RelA and that of other RelA enzymes is the stability of purified *F. tularensis* RelA to concentrations of ~10 mg/mL compared to ~1 mg/ mL reported for *E. coli* RelA [296]. The probability of recovering soluble protein from heterologous expression of recombinant proteins is reported to decrease for proteins with a higher molecular weight (>60 kDa) [348]. *F. tularensis* RelA, with a molecular weight around 10 kDa lower than other RelA enzymes, may therefore have a greater degree of solubility so allowing it to reach higher concentrations. Alternatively it could relate to the further purification of *F. tularensis* RelA with size exclusion chromatography. It is common practise for *E. coli* RelA purification to involve a precipitation step for the separation of nickel purified RelA from impurities [295, 296, 309]. Further purification of *E. coli* RelA by size exclusion chromatography showed only a mild increase in the maximal concentration achieved before observable protein precipitation (3.2.2). This supports the hypothesis that the main contributing factor for the high concentration achievable with *F. tularensis* RelA is its truncated C-terminal region and subsequent lower molecular weight (74 kDa).

Previous work with *E. coli* RelA has demonstrated the enzymes ability to dimerise via its C-terminal region [282, 283] (1.6.1). The key residues for this dimerization were localised to two regions within the C-terminus; amino acids 455-538 and amino acids 550-682 [282]. Further work by Gropp *et al*. elucidated that the following amino acids were essential for dimerization Cys-612, Asp-637 and Cys-638 [283]. These amino acids are all present in *F. tularensis* RelA (A.6); however at only 647 amino acids in length these residues share close proximity to the end of the C-terminus of the protein. The affinity for dimerization of *F. tularensis* RelA might be reduced should this proximity to the end of the protein reduce the contribution of these key residues. Dimerization could further be disrupted if there were important residues downstream from those identified by Gropp *et al*. [283]. Size exclusion chromatography demonstrated that *F. tularensis* RelA purifies as an apparent dimer (Figure 2.8), consistent with residues in the truncated C-terminal region being sufficient to maintain a stable dimeric interaction.

The second noteworthy difference between the properties of *F. tularensis* RelA and that of other RelA enzymes is the specificity of the enzyme for the substrate GTP as a pyrophosphate acceptor. Previous work on synthetase activity in long RSH enzymes from *E. coli* [260], *M. tuberculosis* [192] and *B. subtilis* [259] has demonstrated a preference for either GDP or GTP as a substrate but invariably the acceptance of both. Data presented in

this chapter details the first example of a RelA enzyme which has an explicit specificity for one of these two main pyrophosphate acceptors. This very high degree of GTP substrate selectivity was also observed under activating conditions with stalled ribosomal complexes (Figure 2.10b). Interestingly *F. tularensis* RelA demonstrated an acceptance of GDP as a pyrophosphate acceptor when 'activated' by the addition of the primary alcohol methanol to the buffer (Figure 2.10c). The effect of methanol on protein conformation has been previously demonstrated to strengthen hydrogen bonds and weaken hydrophobic interactions [349]. Analysis of the Rel_{Seq} N-terminal region crystal structure [254], demonstrated numerous hydrophobic residues around the active site. It is possible that the methanol is able to alter the synthetase active site structure and therefore facilitate the binding of GDP. The overexpression of *E. coli* RelA C-terminal region within *E. coli* cells demonstrated a negative effect on the accumulation of ppGpp [283]. The observed activation of RelA in the presence of methanol containing buffers could therefore relate to the associated disruption of the regulatory interactions between the N- and C-termini. Furthermore, the disruption of these interactions could accommodate the acceptance of the alternative pyrophosphate acceptor GDP.

The benefits of selecting GTP as the only pyrophosphate acceptor are many fold, but largely relate to the greater abundance of GTP within the cell [350], and the observed transcriptional regulation determined by the levels of GTP within the cell [207, 351]. A recent review on the signalling molecules (p)ppGpp emphasised the importance of GTP metabolism with the full activation of the stringent response within several Gram-positive bacteria [206]. The interplay between GTP and the global stringent response strongly relies on the regulation of GTP biosynthesis by (p)ppGpp [352], the direct correlation of lower GTP concentrations and the reduced transcription from promoters with GTP as the initiating nucleotide (iNTP) [353], and the GTP dependent CodY-mediated repression of target promoters [351]. The use of GTP as the exclusive pyrophosphate acceptor further drives down the intracellular GTP concentration. For *B. subtilis* the decrease in GTP concentrations is matched with a concomitant increase in ATP concentration, which can support the transcription from promoters using ATP as the iNTP [207]. Such a selectivity for GTP as the pyrophosphate acceptor guarantees a tight coupling between the stringent response and GTP metabolism. For organisms containing smaller genomes, such as *F. tularensis* [102], efficiency is pivotal and therefore the resultant effective switch from normal to starved physiology associated with this tight coupling is likely to be highly

advantageous. The stringent response in *E. coli* appears to be predominantly co-ordinated by ppGpp, with this molecule showing a ~10 fold increase in potency over pppGpp in growth inhibition [187]. A preference for pppGpp or ppGpp has not been established yet for *F. tularensis*, but could have interesting consequences on the interpretation of this observation with respect to its importance for the organism.

Steady state kinetic analysis of *F. tularensis* RelA also highlighted further aspects in which RelA behaves in a manner independent to that of other RelAs. Kinetic analysis of the *E. coli* RelA enzyme in the absence of full activation has shown typical Michaelis-Menten kinetics [260, 285]. Here however the kinetic profile for the *F. tularensis* RelA in the absence of activating factors fits a sigmoidal curve, and as a consequence V_{max} and $K_{1/2}$ are the calculated kinetic parameters. The value for $K_{1/2}$ denotes the concentration of substrate required to reach half the maximal velocity. Measurement of both the nucleotide products AMP and (p)ppGpp by HPLC analysis gave comparable sigmoidal fits and calculated kinetic parameters (Table 2.2). The observed sigmoidal curve was verified by the alternative technique of ^{31}P NMR spectroscopy, with further comparable kinetic parameters calculated using AMP production for rate determination (Table 2.5). Partial overlap of chemical shifts for the β-phosphate peaks for pppGpp and triphosphates made the accurate interpretation of pppGpp concentration by this method more difficult. This coupled with the observed hydrolysis of the terminal 5'-phosphate of pppGpp to form inorganic phosphate (Figure 2.24) led to the exclusion of this data from a global fit of all obtained data. The global fit of data gave a sigmoidal curve with an R^2 value of 0.93 and 0.88 for ATP and GTP respectively, with both fitting a hyperbolic curve with an R^2 value of 0.85, thereby confirming that the data better fitted a sigmoidal curve. A sigmoidal curve has been observed for the bifunctional long RSH enzyme, Rel_{Mtb}, synthetase activity in the absence of activating factors [285]. Sajish *et al.* suggest that this kinetic profile is linked to the RXKD motif found in the synthetase active site [285]. As discussed previously *F. tularensis* RelA contains an unusual active site motif of EXSD, it is therefore possible that this unusual motif acts in a function more akin to that of the RXKD motif compared to that of EXDD. This is further supported by the observation of GTP selectivity, as RXKD motifs are proposed to encode a preference for GTP as the pyrophosphate acceptor. Several mechanisms can account for a sigmoidal velocity curve, including the interesting possibility of allosteric regulation [341]. For a full understanding of the kinetic profile of *F.*

tularensis RelA the addition of binding data by methods such as isothermal titration calorimetry is required.

Chapter 3: **Regulation of *F. tularensis* RelA Activity**

3.1 **Background**

As overviewed in Chapter 1.6, the activation of RelA by stalled ribosomal complexes is an important mechanism that allows a bacterial cell to sense amino acid deprivation within the environment from a hiatus in protein synthesis. Much is still unknown about the specific mechanism by which RelA is activated by these stalled ribosomes but years of research [168, 280, 297, 354-356] have allowed a model of activation to be developed [297]. Research with *E. coli* RelA has demonstrated a requirement for unacylated tRNA, mRNA, and 70S ribosomes containing the ribosomal protein L11 (1.6.2). Further understanding of this activation process in pathogenic bacterial species could elucidate novel targets for antibacterial drug discovery.

The isolation of ribosomes from pathogenic species however is potentially problematic, with many biosafety considerations. Work with *M. tuberculosis* Rel enzyme has overcome this via the use of a heterologous *in vitro* RelA activating system with ribosomes from *E. coli* used in the stead of those from *M. tuberculosis* [192]. Further research into the acceptability of stalled ribosomes from heterologous species has been examined with *E. coli* RelA, with similar results obtained [290]. Interestingly, the activation of *E. coli* RelA varied dependent on the source of ribosome [290] suggesting certain ribosome-to-RelA matches are better for activation than others. The N-terminal of L11 can activate RelA, with even further activation seen in the presence of unacylated tRNA [306]. Interactions between the N-terminal of L11 and C-terminus of RelA could be co-ordinating this observed variation of activation. Activity of RelA in the presence of certain RNA species, namely transfer RNA and messenger RNA, has also been shown for *E. coli* RelA [168, 296]. In this chapter the activation of *F. tularensis* RelA by stalled ribosomal complexes from two alternative species; *E. coli* MRE600 and *F. philomiragia* is described.

In addition to the activation of RelA observed in the presence of stalled ribosomal complexes, further activation has been observed in the presence of ppGpp. Given the nature of the stringent response, such a positive feedback mechanism offers an efficient way to amplify the global response with minimal cost to the cell. The molecular basis for the mechanism of positive regulation of RelA by ppGpp has yet to be elucidated and the

binding site for the nucleotide ppGpp is unknown. The presence of an ACT domain in RelA enzymes [189], offers potential for a regulatory ligand binding site. With the absence of an identified ligand for the ACT domain in this protein family [357], and the observation that ppGpp is capable of positively regulating these enzymes, it is tempting to postulate that ppGpp is eliciting its effect in an ACT domain-dependent manner. The absence of an ACT domain within *F. tularensis* RelA allows us to address this hypothesis and is described within this chapter.

3.2 Activation of *F. tularensis* RelA by Stalled Ribosomal Complexes

3.2.1 Expression and Purification of Ribosomes

Bio-safety considerations required the isolation of ribosomes from an alternative species to *F. tularensis*, with two alternative ribosome sources therefore investigated. Firstly, the well characterized *E. coli* MRE600 strain which lacks ribonuclease I [358] and has consequently been widely used for ribosome purification [359-361]. Secondly, another member of the *Francisella* genus, *F. philomiragia*, which is of low virulence [106] and also encodes within its genome a RelA enzyme lacking the ACT domain in its C-terminus [189].

3.2.1.1 SulfoLink-Cysteine Chromatography

The traditional method of ultracentrifugation for purifying ribosomes is long and laborious [362] and is therefore not always an efficient method to use. Maguire *et al*. have developed an affinity chromatography method for ribosome purification using SulfoLink resin (Pierce) reacted with L-cysteine [359] (Figure 3.1). They used this method for ribosome purification from *Dienococcus radiodurans* and clinical isolates of pathogenic bacteria [359] and it therefore seemed a promising method for the isolation of ribosomes from *F. philomiragia*.

SulfoLink-Cysteine chromatography utilises agarose beads with an 18 atom alkyl chain containing a terminal iodoacetyl group which is then reacted with L-cysteine (7.5.3) (Figure 3.1). The ribosomes are suggested to interact with the alkyl linker itself not the terminal group, as alterations of the reacting nucleophile did not alter the binding [359].

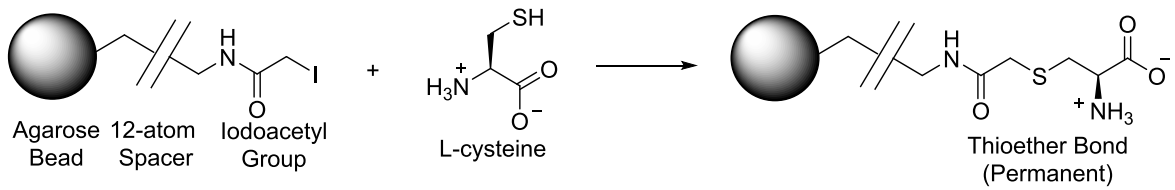

Figure 3.1. Schematic detailing the reaction of L-cysteine with SulfoLink resin (Pierce).

Later work by Meskauskas *et al.* demonstrated the use of this method for the purification of active ribosomes from yeast, but detailed the co-purification of tRNA with ribosomes [363]. Meskauskas *et al*. removed contaminating tRNA by treatment with puromycin, in the experiments detailed within this thesis an ultrafiltration step was utilised for the removal of co-purifying tRNA (7.4.4).

3.2.1.2 **Purification of *E. coli* Ribosomes**

Ribosomes were isolated from early to mid-logarithmic growth of *E. coli* MRE600 cultures (optical density of 0.4-0.6), as calculated from growth curves (7.5.1) (Figure 3.2). Ribosome concentrations have been shown to be at their highest during this period of bacterial growth [364]. A 5 L growth typically yielded 6.6 ± 0.4 g of cells.

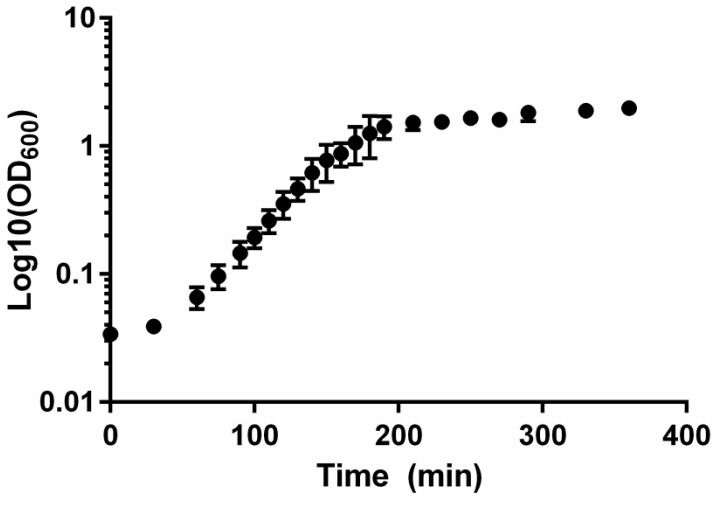

Figure 3.2. Growth cure of *E. coli* MRE600 in LB media supplemented with magnesium sulfate (10 mM). Growth was measured from the optical density of the culture at 600 nm.

Following cell lysis and centrifugation to yield a cleared cell lysate, ribosomes were purified using a gradient of 100-300 mM NH_4Cl on a SulfoLink-cysteine column (XK26/20 column) (7.5.3). Chromatographic analysis of purifications consistently yielded a single peak at 280 nm (Figure 3.3a). Fractions containing ribosomes, as judged by SDS-PAGE (7.3.1) analysis (Figure 3.3b), were pooled and concentrated using an Amicon pressure cell (7.4.4).

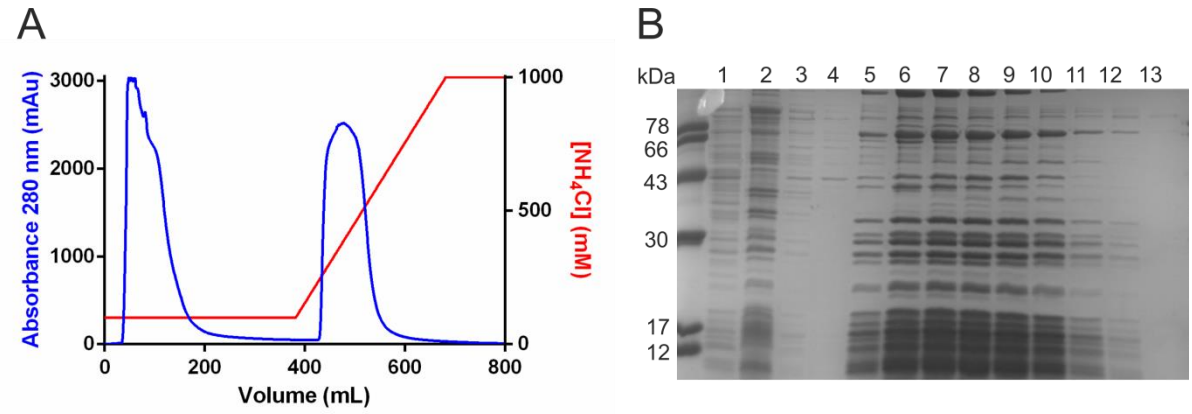

Figure 3.3. Purification of ribosomes from *E. coli* MRE600 cellular extracts using SulfoLink-cysteine chromatography. (A) Absorbance trace at 280 nm (blue) over a gradient of NH_4Cl (red). (B) SDS-PAGE analysis of ribosome purification. Lane 1; cleared lysate, lane 2; flowthrough, lanes 3-13; fractions correlating to the eluate during NH_4Cl gradient.

The concentration of the purified ribosomes was established using Beer's Law and the absorbance at 260 nm with the mass extinction coefficient for the RNA species (4.81×10^7 $M^{-1}cm^{-1}$). Concentrated ribosomes (8.93 µM) were stored at -80 °C prior to use. The ribosomal RNA from *E. coli* ribosomes were further analysed using bleach agarose gel electrophoresis (7.4.5), which showed separation of 23S (2.90 kb), 16S (1.54 kb), and 5S rRNA species (0.12 kb) (Figure 3.4).

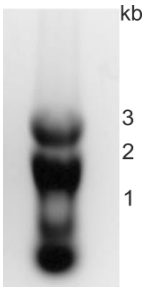

Figure 3.4 Analysis of the *E. coli* MRE600 ribosomal RNA (rRNA) species by bleach agarose gel electrophoresis (7.5.5). Observed separation for the 23S rRNA (2.90 kb), 16S rRNA (1.54 kb) and 5S rRNA (0.12 kb), residual band corresponds to other purified RNA species (tRNA and mRNA).

3.2.1.3 **Purification of *F. philomiragia* Ribosomes**

F. philomiragia were cultured in Trypticase Soy broth (TSB) supplemented with L-cysteine (7.9.24). Ribosomes were isolated from early to mid-logarithmic growth of *F. philomiragia* cultures (7.5.2) (optical density of 0.8-1.0), as calculated from growth curves (7.5.1) (Figure 3.5). A 1 L growth typically yielded 6.86 ± 1.02 g of cells.

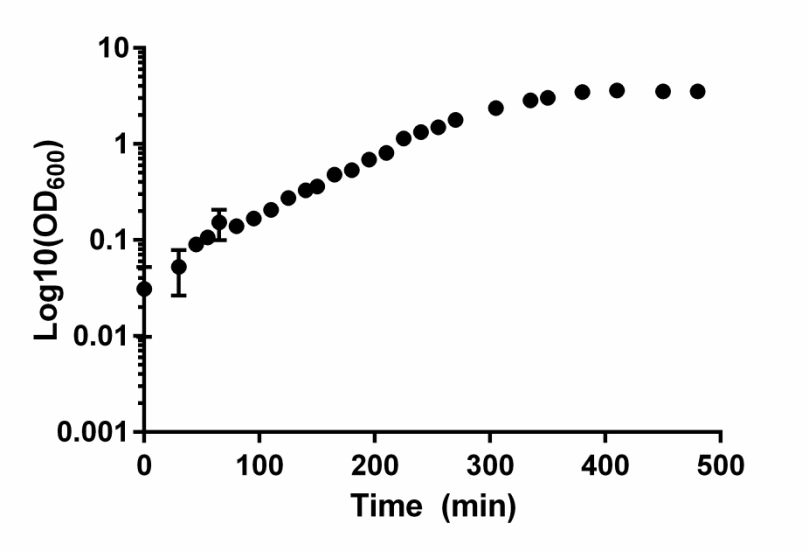

Figure 3.5. Growth cure of *F. philomiragia* in trypticase soy broth (TSB) supplemented with L-cysteine (8 mM). Growth was measured from the optical density of the culture at 600 nm.

Ribosomes were purified using a gradient of 100-300 mM NH_4Cl on a SulfoLink-cysteine column (7.5.4) (XK16/20 column), with a single peak observed at 280 nm (Figure 3.6). Fractions containing ribosomes, as judged by SDS-PAGE analysis (7.3.1), were pooled and concentrated using an Amicon pressure cell (7.4.4).

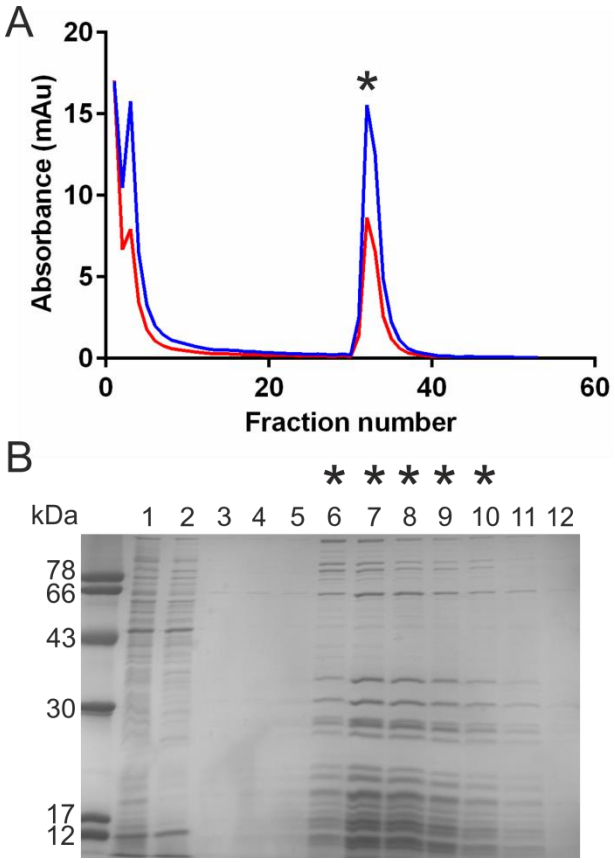

Figure 3.6. Purification of ribosomes from *E. coli* MRE600 cellular extracts using SulfoLink-cysteine chromatography. (A) Absorbance at 260 nm (blue) and 280 nm (red) for fractions collected throughout the purification. (B) SDS-PAGE analysis of ribosome purification. Lane 1; cleared lysate, lane 2; flowthrough, lanes 3-12; fractions correlating to the eluate during NH_4Cl gradient. Lanes marked with an asterisk (*) correspond to the peak similarly marked in (A).

The concentration of the purified ribosomes was established as previously described for *E. coli* MRE600 ribosomes (3.2.1.2). Concentrated ribosomes (4.96 µM) were stored at -80 °C prior to use. The ribosomal RNA from *F. philomiragia* ribosomes was too unstable for further analysis by bleach agarose gel electrophoresis.

3.2.2 Expression and Purification of *E. coli* W3110 RelA

The gene encoding *E. coli* RelA, including a sequence encoding an N-terminal hexahistidine tag, was purchased within the pCA24N plasmid as part of the ASKA Clone library (NBRP, Japan). The pCA24N::*Ec*relA plasmid was chemically transformed (7.3.4) into the *E. coli* BL21 (DE3) strain for protein expression. Large scale (5 L) expression (7.5.6) typically yielded 22 ± 3 g cell pellet. *E. coli* RelA was purified by nickel affinity chromatography (7.5.7), over a gradient of 0 to 500 mM imidazole (7.4.7) (Figure 3.7). SDS-PAGE analysis (7.3.1) of fractions detailed the presence of *E. coli* RelA alongside a number of contaminants (Figure 3.7b).

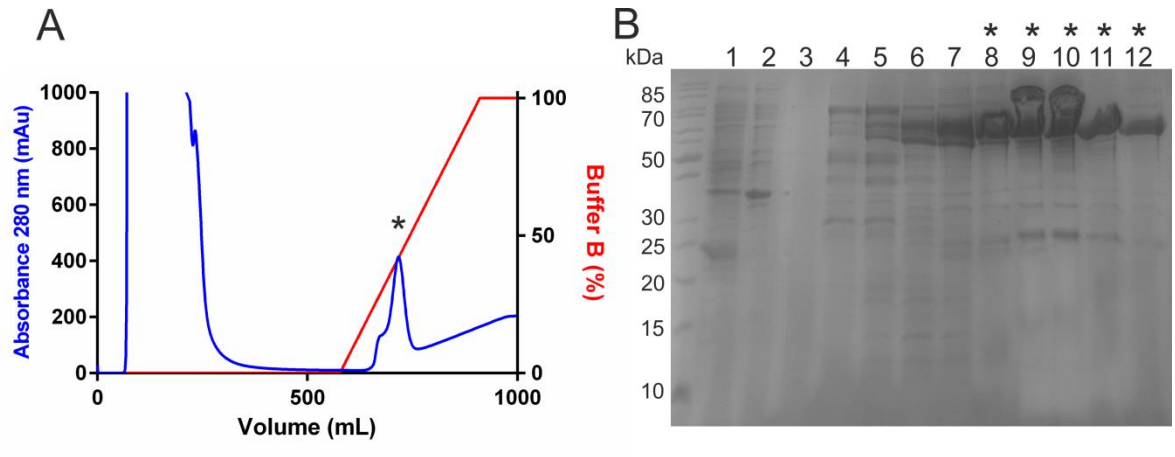

Figure 3.7. Purification of *E. coli* RelA (82 kDa) by nickel affinity chromatography (A) Absorbance 260 nm trace (B) SDS-PAGE analysis of fractions from nickel affinity chromatography. Lanes: 1, cleared lysate; 2, flow through; 3-12, eluate fractions from Ni-IDA chromatography. Lanes marked with * correspond to the similarly marked peak in (A).

The purity of *E. coli* RelA was improved by a size exclusion chromatography step (7.5.8). The largest peak observed from the absorbance (280 nm) trace was shown to correspond to *E. coli* RelA by SDS-PAGE analysis (Figure 3.8). Purified *E. coli* RelA was concentrated to ~0.4 -2 mg/mL and stored at -80 °C.

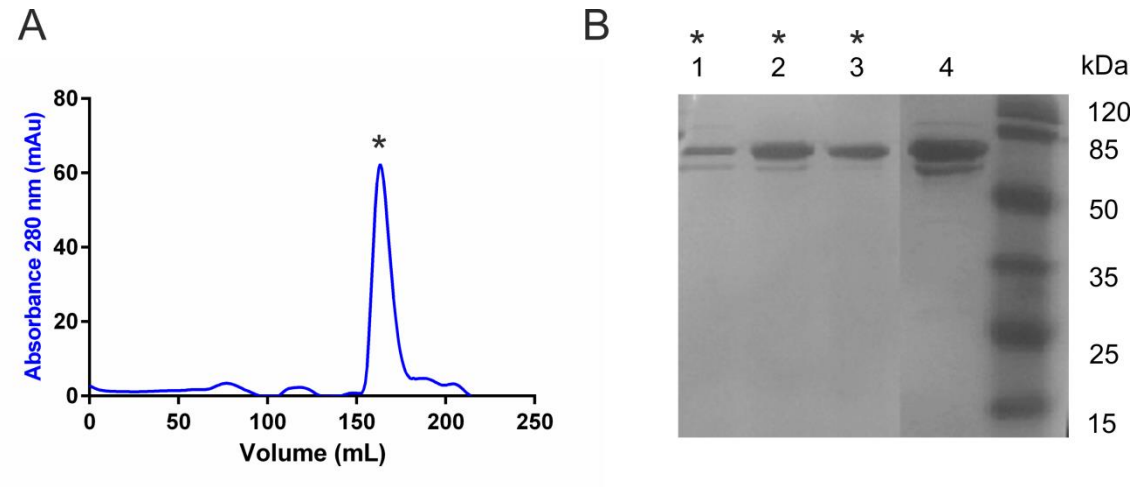

Figure 3.8. Purification of *E. coli* RelA (82 kDa) by size exclusion chromatography (A) Absorbance 260 nm trace (B) SDS-PAGE analysis of fractions from size exclusion chromatography. Lanes: 1-3, eluate fractions from peak similarly marked in (A); lane 4: Concentrated *E. coli* RelA following size exclusion chromatography.

3.2.3 Activation of *F. tularensis* RelA by *In vitro* Ribosome Stalling

Across the literature there is a great disparity amongst the methods used for *in vitro* stalling of ribosomes [168, 295, 296]. One method for stalling ribosomes involves the initial breakdown of the ribosomal 70S complex to individual constituents by heating, followed then by reforming in the presence of unacylated tRNA and mRNA [295]. Within the published methods for ribosome-activated (p)ppGpp synthetase activity, the reported concentrations for assay components including ribosomes, RNA species, substrates or even RSH enzyme also show a high degree of variation [168, 295, 296].

Initial experiments for the ribosome-mediated activation of *F. tularensis* RelA were modelled on the comprehensive method detailed by Payoe *et al.* for ribosome activation of the *E. coli* RelA (7.5.9.1) [295]. IP RP HPLC analysis showed *F. tularensis* RelA (p)ppGpp synthetase activity with GTP as the pyrophosphate acceptor (Figure 2.9b). This method of ribosome-mediated RelA activation did not result in high levels of (p)ppGpp (≤40 µM). Analysis of (p)ppGpp synthetase activity over a range of RelA concentrations, showed maximal activity was observed with a RelA concentration above 3 µM. Maximal turnover of RelA (154 AMP per hour per RelA) is observed however at 1.44 µM (Figure 3.9).

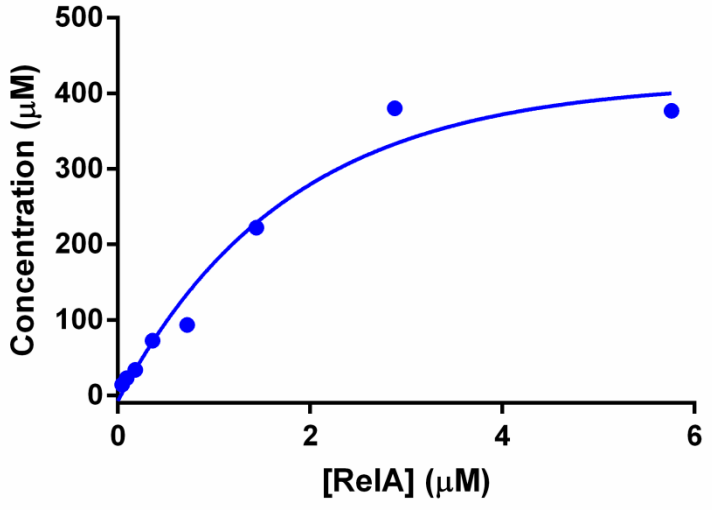

Figure 3.9. IP RP HPLC analysis (7.4.8.3) of ppGpp synthetase activity at varying concentrations of *F. tularensis* RelA in the presence of ~1 μM stalled *E. coli* MRE600 ribosomes.

The levels of activity detailed above for *F. tularensis* RelA were substantially lower than those previously observed for *E. coli* RelA using this method [295]. The observed low sensitivity of Method C IP RP HPLC for the detection of (p)ppGpp (2.4.2) coupled with the observation that greater activity was observed at higher RelA concentrations therefore led to the modification of the assay set up.

The modified protocol included RelA associated stalled ribosomal complexes that were formed by incubation at 30 °C for 5 minutes prior to the initiation of the assay (7.5.9.2). End-point assays were initiated by the addition of GTP and quenched following 1 hour incubation at 30 °C instead of 22 °C as described by Payoe *et al.* [295]. The (p)ppGpp synthetase activity in a range of different RelA and ribosome combinations (Table 3.1) were analysed by IP RP HPLC (7.4.8.4).

Table 3.1. Different ribosome associated RelA (p)ppGpp synthetase activity assays.

***E. coli* RelA Assays**	***F. tularensis* RelA Assays**
E. coli RelA and *E. coli* Ribosomes	*F. tularensis* RelA and *E. coli* Ribosomes
E. coli RelA and *F. philomiragia* Ribosomes	*F. tularensis* RelA and *F. philomiragia* Ribosomes
E. coli RelA only	*F. tularensis* RelA only
E. coli Ribosomes only	*F. philomiragia* Ribosomes only

IP RP HPLC analysis (7.4.8.4) of 1 hour end point measurements of *F. tularensis* RelA activity (7.5.9.2) demonstrated individual peaks with strong absorbance values for all substrates and products (Figure 3.10).

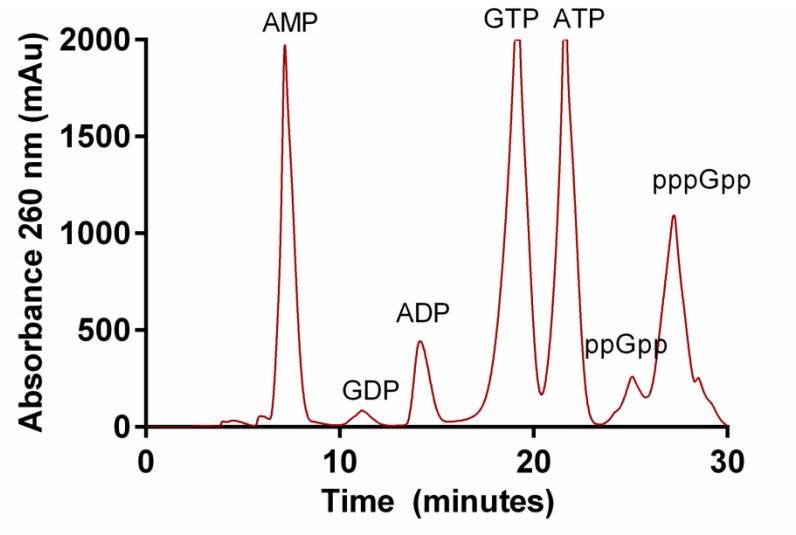

Figure 3.10. Absorbance at 260 nm trace for IP RP HPLC analysis (7.3.8.4) of *F. tularensis* RelA activity in the presence of *E. coli* MRE600 stalled ribosomal complexes.

E. coli RelA showed comparable, although not optimal, levels of (p)ppGpp activity to the range previously observed by Jenvert *et al*. [296]. This demonstrated that this method for stalling ribosomes was capable of activating RelA. The activation of *E. coli* RelA compared to basal activity (in the presence of RelA alone) by stalled *F. philomiragia* ribosomes was observed (Figure 3.11), demonstrating the ability of these stalled complexes to increase (p)ppGpp synthesis. *E. coli* RelA showed greater activity in the presence of either *E. coli* or *F. philomiragia* ribosomes than in the absence of any ribosomal complex, with a 16 fold

and 11 fold increase respectively (Figure 3.11). These data demonstrate that activation of *E. coli* RelA by stalled ribosomal complexes using the method described above gave comparable results to those previously published for the enzyme.

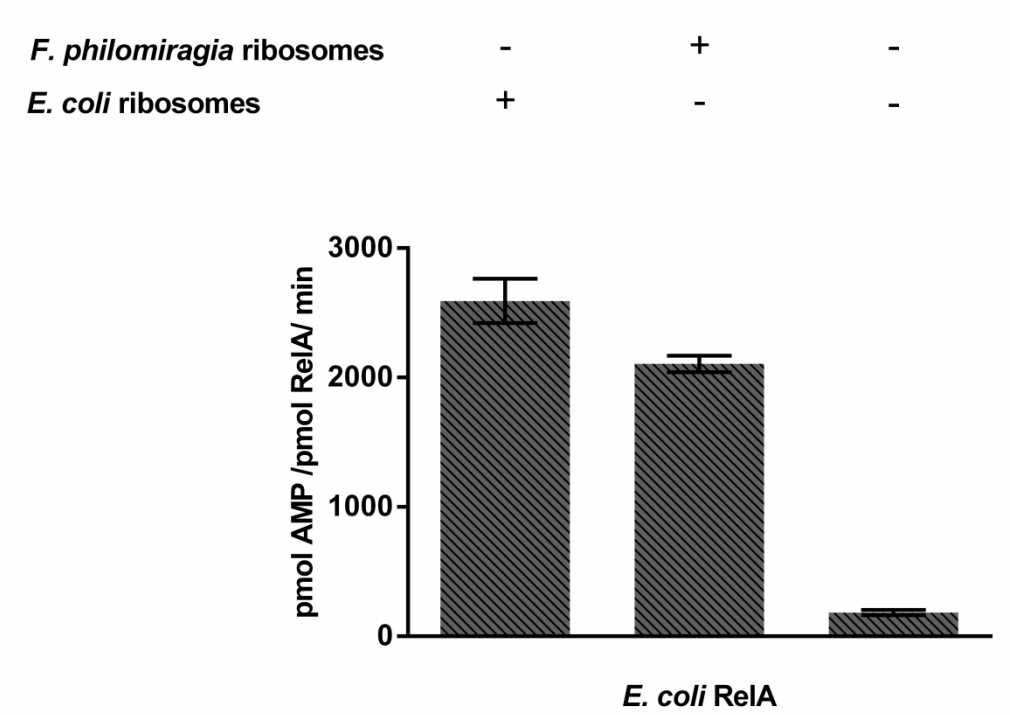

Figure 3.11. Comparison of *E. coli* RelA activity in the presence of stalled ribosomal complexes formed with ribosomes from *F. philomiragia* or *E. coli* with basal activity (no stalled ribosomes) as measured by IP RP HPLC (7.4.8.4). For comparison with data by Jenvert *et al.* [296] observed at rate of pmol AMP per pmol RelA per min.

F. tularensis RelA also demonstrated (p)ppGpp synthetase activity in the presence of *E. coli* stalled ribosomes, with an 11 fold increase upon basal activity observed (Figure 3.12). Conversely only a 1.39 fold increase in *F. tularensis* RelA activity was observed in the presence of *F. philomiragia* stalled ribosomal complexes. Maximal *F. tularensis* RelA activity (701.5 ± 30.5 pmol AMP per pmol RelA per min) did not reach that of *E. coli* RelA (2952 ± 99.14 pmol AMP per pmol RelA per min) under any conditions tested.

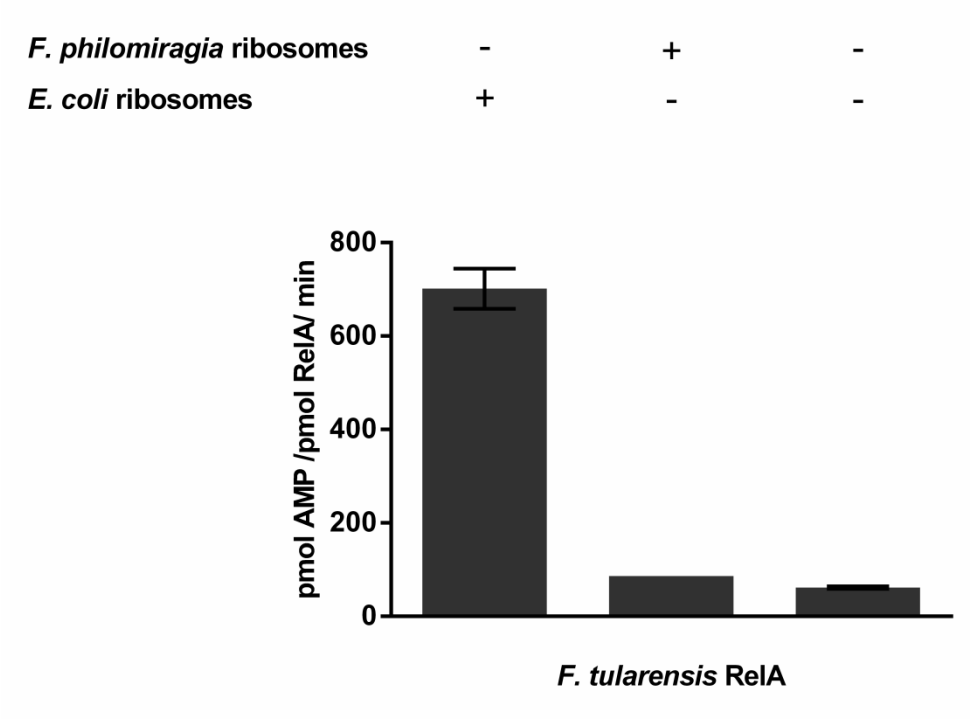

Figure 3.12. Comparison of *F. tularensis* RelA activity in the presence of stalled ribosomal complexes formed with ribosomes from *F. philomiragia* or *E. coli* with basal activity (no stalled ribosomes) as measured by IP RP HPLC (7.4.8.4).

3.2.4 Importance of *F. tularensis* L11 for *F. tularensis* RelA Activity

The importance of the ribosomal protein L11 in RelA activation has been well documented [299, 305, 306]. *E. coli* RelA has also shown mild activation in the presence of L11 and ppGpp alone [313]. The activation of *F. tularensis* RelA by *F. tularensis* L11 was therefore of interest.

Initial work involved the subcloning of a synthetic *F. tularensis rplK* gene codon-optimised for *E. coli* (MWG, Eurofins) into a pET16b vector (7.5.10), by restriction digest of the pEX::*Ft*rplK with NcoI and XhoI followed by ligation into a similarly digested pET16b vector (Figure 3.13, B.1). Plasmids were purified from colonies that grew following the transformation of ligation reactions into *E. coli* JM109/ XL-10 Gold cells. Restriction digestion of purified plasmids identified two that contained the pET16b vector (2.45 kb) and the *FtrplK* gene (0.46 kb) (Figure 3.13; lanes 6 and 8). The *F. tularensis* L11 was engineered to contain a C-terminal strep tag, to allow for purification by streptavidin binding affinity chromatography.

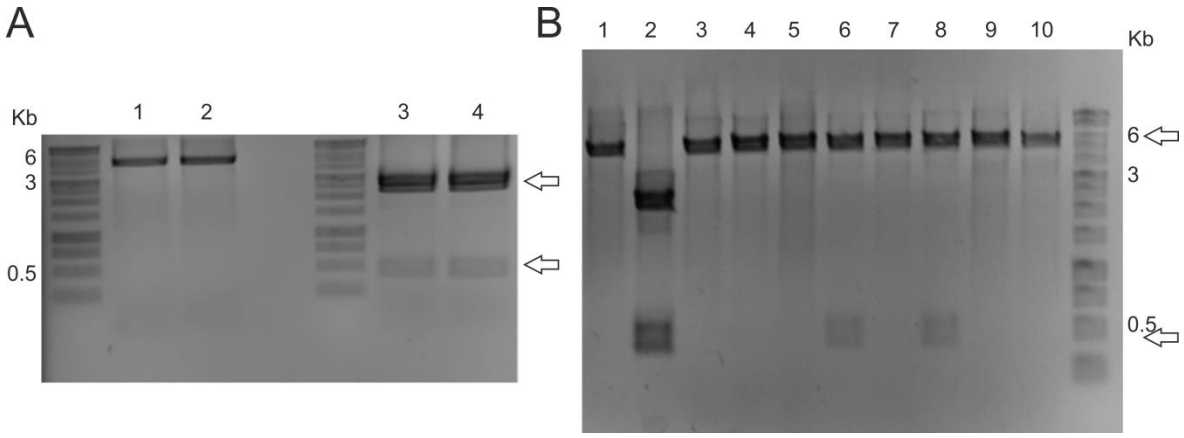

Figure 3.13. Subcloning of *F. tularensis rplK* gene (0.461 Kb) from pEX vector (2.45 Kb) into pET16b (5.643 Kb). (A) Gel electrophoresis extraction of purified pET16b (lanes 1 and 2) and purified pEX::*Ft*rplK (lanes 3 and 4). (B) DNA agarose gel electrophoresis analysis of restriction digests of plasmids from positive transformants following ligation (lanes 3-10), compared to comparably digested pET16b (lane 1) and pEX::*Ft*rplK (lane 2).

Optimal expression of *F. tularensis* L11 was assessed by small scale expression studies with varying temperatures and length of expression (7.5.11). Analysis by SDS-PAGE analysis revealed the optimal conditions for *F. tularensis* L11 (15 kDa) expression as 27 °C for 4 hours (Figure 3.14).

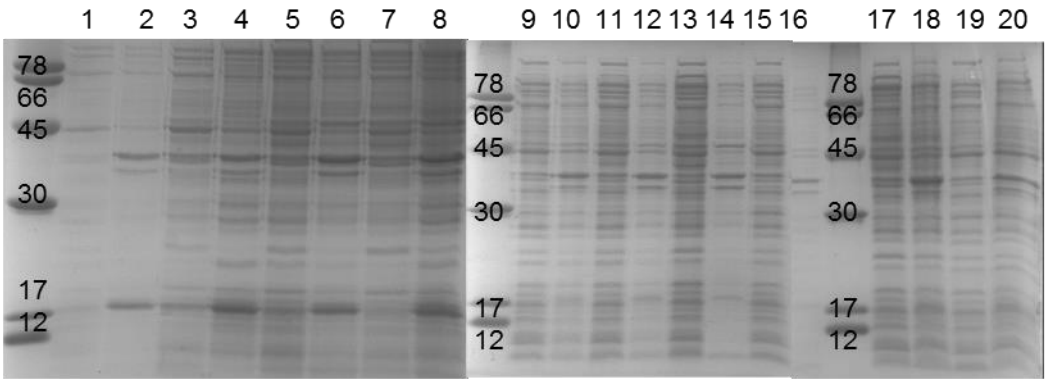

Figure 3.14. SDS-PAGE analysis of small scale expression studies for *F. tularensis* L11. Lanes 1-8; expression at 27 °C for 0 hours (1 and 2), 2 hours (3 and 4), 4 hours (5 and 6), and 16 hours (7 and 8). Lanes 11-16; expression at 16 °C for 0 hours (11 and 12), 4 hours (13 and 14), and 16 hours (15 and 16). Lanes 17-18; expression at 37 °C for 4 hours (17 and 18). Lanes 9-10 and 19-20; *E. coli* BL21 pET16b empty vectors at 27 and 37 °C respectively. Odd numbered lanes correspond to soluble protein fractions and even numbered lanes correspond to insoluble protein fractions. Arrow indicates L11 (15 kDa).

F. tularensis L11 was expressed on a larger scale (7.5.12) (1 L of *E. coli* BL21 (DE3) pET16b::*Ft*rplK) and yielded a 4.94 g cell pellet. *F. tularensis* L11 was purified by streptavidin binding affinity chromatography (7.5.13), utilising a gradient of 0 to 2.5 mM desthiobiotin. SDS-PAGE analysis (7.3.1) showed fractions containing pure *F. tularensis* L11 (Figure 3.15). *F. tularensis* L11 (10 mg) was concentrated (7.4.4) to ~1 mg/mL (66.7 µM) and stored as aliquots at -80 °C.

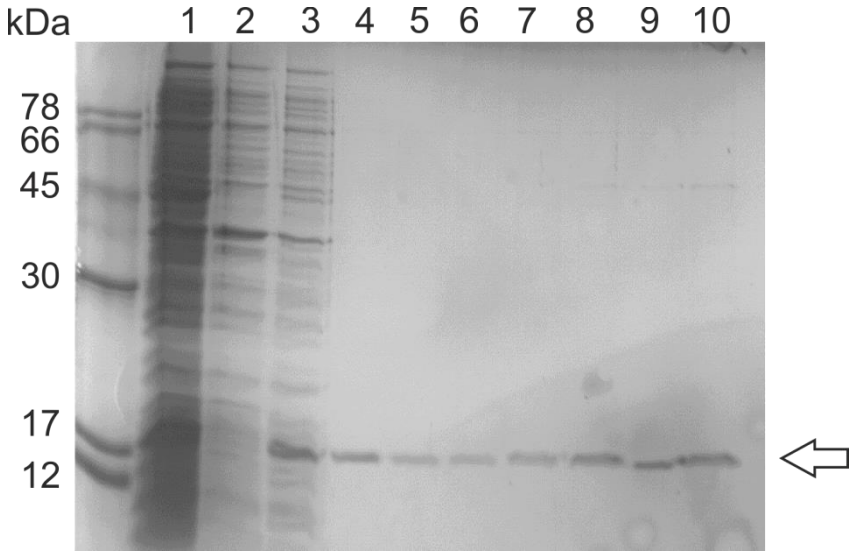

Figure 3.15. SDS-PAGE analysis of fractions from *F. tularensis* L11 (15 kDa) purification by streptavidin binding affinity chromatography. Lane 1; cleared lysate, lane 2; flowthrough, lanes 3-10; fractions correlating to the eluate. Arrow indicates L11 (15 kDa).

Initial (p)ppGpp synthetase activity assays with *F. tularensis* RelA supplemented with *F. tularensis* L11 (7.5.14) demonstrated no significant increase in (p)ppGpp synthesis. Interestingly higher guanosine diphosphate concentrations of 217.1 ± 31 µM and 388.3 ± 55 µM for 5 and 10 µM *F. tularensis* L11 respectively were observed when in the presence of *F. tularensis* RelA (Figure 3.16). *F. tularensis* L11 alone was not able to produce as high levels of GDP (35.04 ± 0.9 µM) (Figure 3.16).

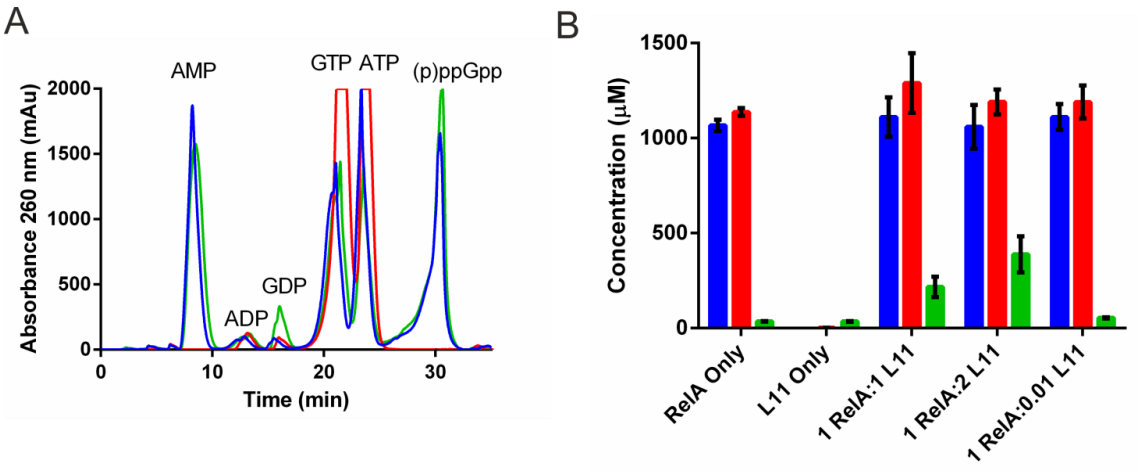

Figure 3.16. *F. tularensis* RelA (p)ppGpp synthetase activity in the presence of *F. tularensis* L11. HPLC analysis of AMP (blue), (p)ppGpp (red) and GDP (green) produced from end-point measurements (1 hour) of *F. tularensis* RelA and *F. tularensis* L11 coupled assays and controls.

3.2.5 Importance of Ribonucleic Acids for *F. tularensis* RelA Activity

Previous analysis of *E. coli* RelA has demonstrated mild activation in the presence of individual ribonucleic acids including mRNA and tRNA molecules [168, 296]. The ability of *F. tularensis* RelA, with its truncated C-terminus, to be activated by the presence of these compounds was therefore of interest (7.5.15). Incubation of *F. tularensis* RelA (5 µM) with 2.5 µM mRNA (5'-CAAGGAGGUAAAAAUGGUCGUCGCACGU3') demonstrated a mild but distinct activation (~1.21 fold increase at 60 min) of (p)ppGpp synthesis (Figure 3.17). Incubation of *F. tularensis* RelA (5 µM) with 2.5 µM unacylated tRNA (formyl-methionine) demonstrated a similarly mild but distinct activation (~1.27 fold increase at 60 min) (Figure 3.17).

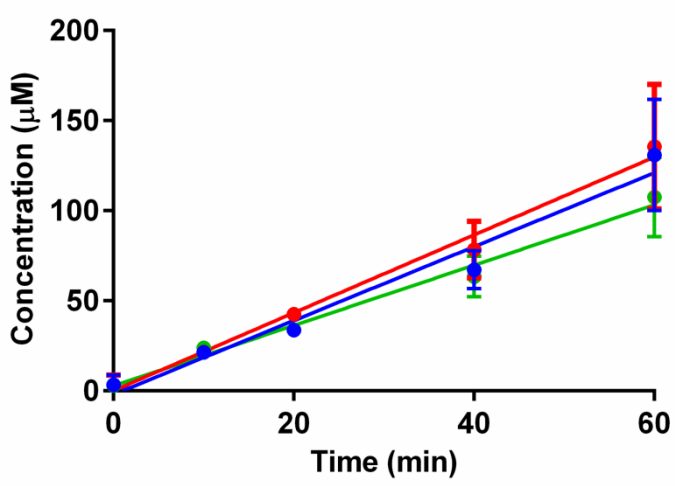

Figure 3.17. IP RP HPLC analysis (7.3.8.4) of *F. tularensis* RelA activity over time in the presence of mRNA (blue) or tRNA (red) in comparison of activity in the absence of any RNA species (green).

IP RP HPLC analysis showed linear product formation over time ($R^2 \geq 0.89$) under all conditions tested (Figure 3.17). The calculated rates for these linear fits demonstrated an increased rate of product formation in the presence of tRNA, from 1.67 ± 0.12 μM min^{-1} to 2.16 ± 0.17 μM min^{-1}. A slightly milder increase in rate was observed in the presence of mRNA, from 1.67 ± 0.12 μM min^{-1} to 2.05 ± 0.17 μM min^{-1}.

3.3 Small Molecule Activation of *F. tularensis* RelA

F. tularensis RelA demonstrated an unusual sigmoidal fit for substrate saturation curves (2.4.3). One explanation for the observation of a sigmoidal saturation curve is the allosteric regulation of an enzyme, and a double reciprocal Lineweaver-Burk plot for *F. tularensis* RelA suggested positive cooperativity (Figure 2.21). Positive cooperativity can be induced by conformational changes caused by the binding of a ligand [365]. The absence of any known activating factors such as stalled ribosomes or methanol in these assays suggested that the observed activation related to a product or by-product of the enzymatic reaction. The nucleotide product AMP and by-product ppGpp as well as inorganic phosphate, shown to be a by-product of this reaction by ^{31}P NMR analysis (2.5), were therefore of interest for more detailed investigation. The nucleotide product pppGpp proved unstable by the methods used and could not be purified to homogeneity, due to the loss of the labile 5' terminal phosphate.

3.3.1 Biosynthesis and Purification of Guanosine Tetraphosphate (ppGpp)

To determine the possible activation of *F. tularensis* RelA by guanosine tetraphosphate (ppGpp), the nucleotide needed to first be synthesised. Previous work with *E. coli* RelA had shown increased synthesis of ppGpp from GDP in the presence of methanol [309]. The ppGpp was therefore biosynthesised using purified *E. coli* RelA (3.2.2, 7.5.17) as a catalyst in the presence of a buffer containing 30% methanol at 25 °C overnight. Separation of ppGpp from the other nucleotides remaining in the biosynthetic reaction was achieved using ion exchange chromatography (7.5.17). Nucleotides were eluted over a gradient of 100 to 500 mM LiCl. Fractions shown to contain purified ppGpp, as judged by TLC analysis (Figure 3.18, Table 3.3), were pooled and lyophilised.

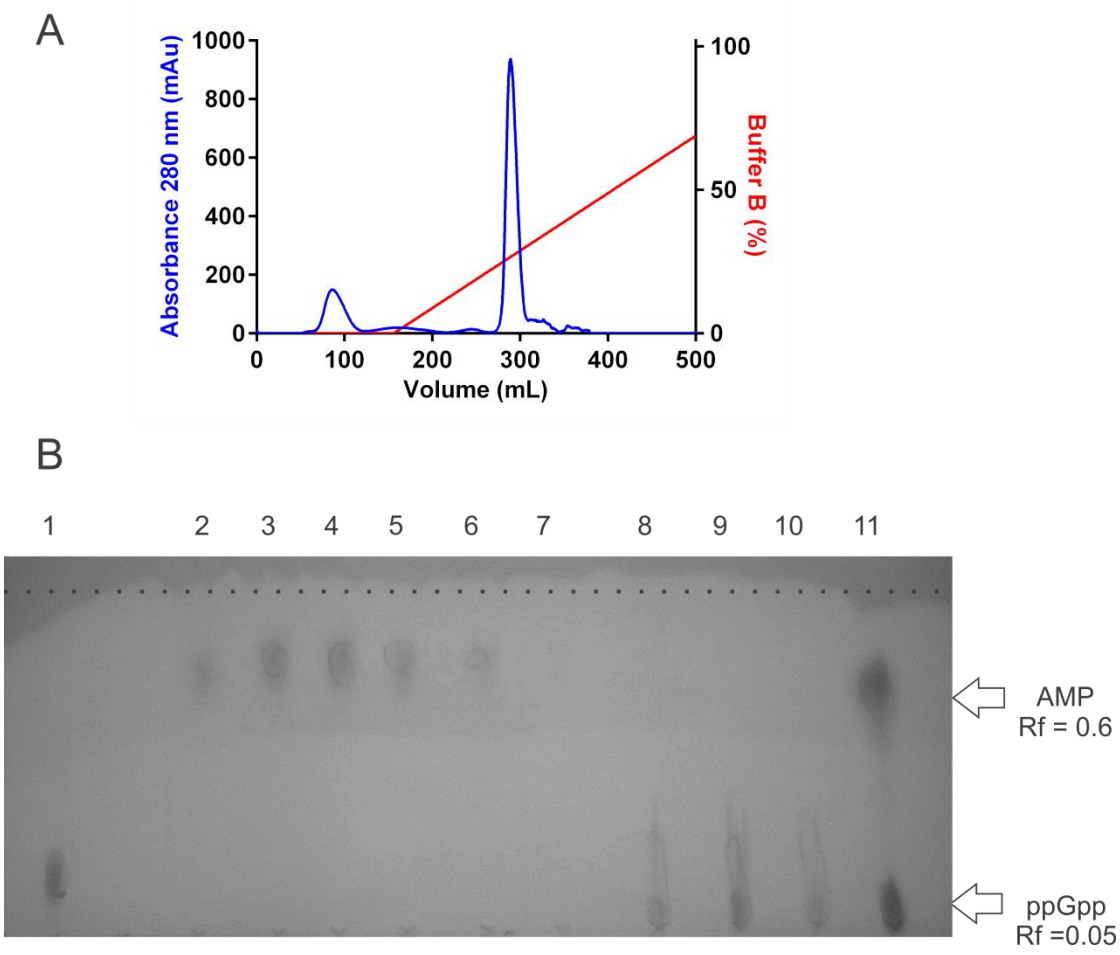

Figure 3.18. Purification of guanosine tetraphosphate (ppGpp) by ion exchange chromatography (7.5.17). (A) Absorbance trace at 280 nm (blue) over a gradient of LiCl (red). (B) TLC analysis of ppGpp purification. Lane 1; commercial GTP standard, lane 2-10; eluate fractions collected during the LiCl gradient, Lane 11; ppGpp synthesis assay prior to loading onto DEAE sepharose column. Solvent front is denoted by dotted line.

High levels of LiCl could have profound effects on *F. tularensis* RelA activity, especially given its requirement for a high salt concentration, therefore the LiCl was removed from the purified ppGpp by size exclusion chromatography (7.5.17). The separation of LiCl from ppGpp was achieved using a G10 sephadex column (10 mm x 600 mm), with distinct peaks observed for ppGpp (absorbance at 280 nm) and for LiCl (conductivity mS/cm) (Figure 3.19). Fractions containing desalted ppGpp, as judged by chromatograph (Figure 3.19), were pooled and lyophilised. Lyophilised ppGpp was dissolved in water and the concentration determined by absorbance at 260 nm using the mass extinction coefficient 13, 600 $M^{-1}cm^{-1}$ and aliquots lyophilised prior to storage at -80 °C.

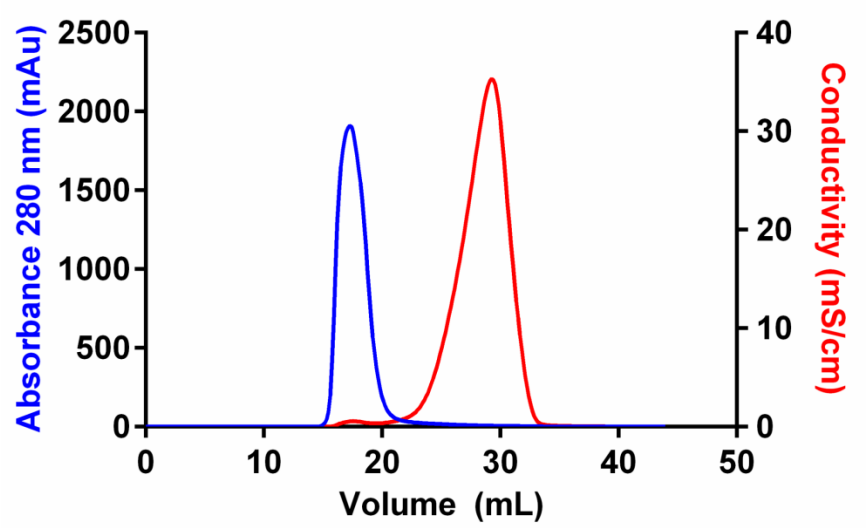

Figure 3.19. Separation of guanosine tetraphosphate (ppGpp) from LiCl by size exclusion chromatography (G10 sephadex).

Purified guanosine tetraphosphate was analysed by nuclear magnetic resonance (NMR) spectroscopy (7.5.18), in 1× RelA assay buffer (7.9.19) to allow comparison with further experiments. Phosphorus-31 (^{31}P) NMR spectroscopy gave four doublet peaks at -10.70, – 10.40, -6.43 and -6.22 ppm (B.2). ^{31}P -^{31}P correlation spectroscopy (COSY) analysis revealed the predicted coupling between peaks at – 10.70 and - 6.22 ppm and between those at – 10.40 and – 6.43 ppm (B.3). High similarity between the environments of either the α or α' phosphates and the β or β' phosphates has prevented assignment of these individual peaks. A small amount of contaminating inorganic phosphate, which might arise from ppGpp degradation during the course of the experiment, was also observed

(B.2). ^{1}H NMR spectroscopy confirmed that the product was a guanosine derivative and not an adenosine derivative by the presence of only a single proton peak (at the 8 position) for the base consistent with that of guanine (B.4).

3.3.2 Activation of *F. tularensis* RelA by Small Molecules

Synthetase activity of *F. tularensis* RelA was measured in the presence of low (10 µM), medium (100 µM) or high (1000 µM) concentrations of potential small molecule activators (AMP, ppGpp, or PO_4^{3-}) (7.5.19). The background concentration of additional ppGpp or AMP was subtracted to give the concentration of each product newly formed during the experiment. No alteration in synthetase activity was observed in the presence of phosphate at any concentration tested (Figure 3.20). No significant activation of *F. tularensis* RelA was observed in the presence of AMP at any concentration either. As discussed previously (2.4.2) a greater variation in the measurement of (p)ppGpp concentrations occurs from the breakdown of the penta- into the tetraphosphate. Here the small increases in the average activity seen in the presence of AMP are most likely a result of the greater variability in (p)ppGpp quantification, as indicated by the increased standard deviation (Figure 3.20). Most interestingly there is a clear increase in *F. tularensis* RelA synthetase activity in the presence of ppGpp at medium (1.82 fold increase) and high concentrations (2.86 fold increase) (Figure 3.21).

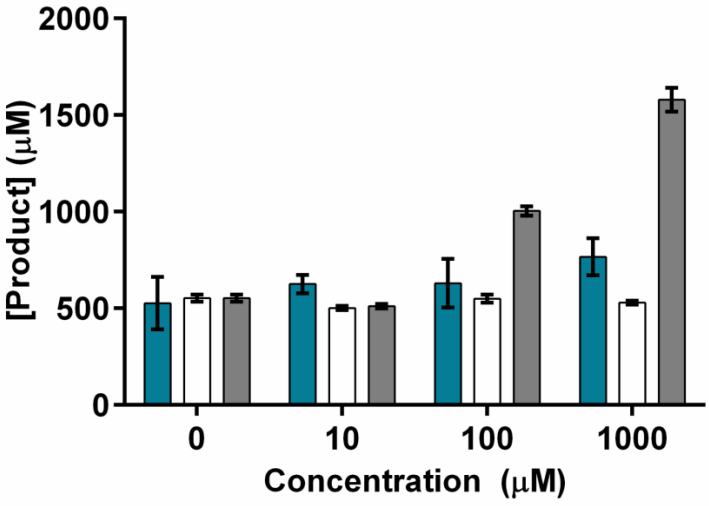

Figure 3.20. IP RP HPLC analysis (7.3.8.4) of *F. tularensis* RelA activity (1 hour end point) in the presence of AMP (blue), PO_4^{3-} (white), or ppGpp (grey) as additive factors.

Repeating this activation measurement over a wider range of ppGpp concentrations (0-1000 µM) (7.5.20) allowed determination of an EC_{50} for ppGpp of 60 ± 1.9 µM (Figure 3.21) and a maximal 1.5 fold activation, similar to the 2 fold activation observed for *E. coli* RelA [313].

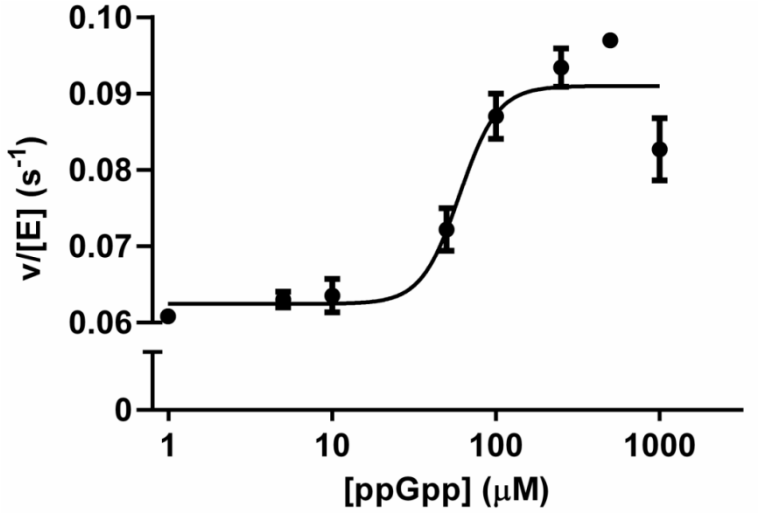

Figure 3.21. IP RP HPLC analysis (7.3.8.4) of *F. tularensis* RelA activity (1 hour end point measurements) in the presence of varying ppGpp concentrations.

The EC_{50} was calculated from a rearrangement of Equation 3.1. Here Y refers to rate, with Y_{min} denoting the minimum rate and Y_{max} denoting the maximum rate. EC_{50} represents the concentration of ligand required to give 50% of full activation and h is the apparent Hill slope.

Equation 3.1

$$Y = Y_{min} + \left(\frac{Y_{max} - Y_{min}}{1 + 10^{(LogEC_{50} - x) - h}}\right)$$

3.4 Activation of *F. tularensis* RelA by Methanol

Previous work with *E. coli* RelA has demonstrated activation of the enzyme by primary alcohols such as methanol [309]. *F. tularensis* RelA is also activated in the presence of methanol (7.5.21), interestingly with the presence of GDP as a pyrophosphate acceptor. Activity of *F. tularensis* RelA was tested over a range of buffers with varying methanol

concentrations (15-75%), and demonstrated an increase in activity in buffers containing up to 45% methanol (Figure 3.22). At higher methanol concentrations (60 or 75%) no activity was observed.

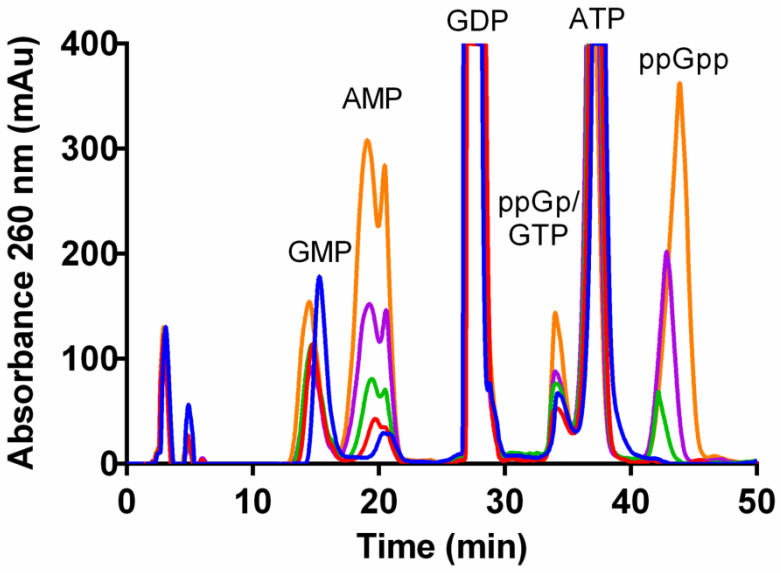

Figure 3.22. IP RP HPLC analysis (7.4.8.2) of *F. tularensis* RelA using GDP as pyrophosphate acceptor in a 5% (blue), 15% (red), 25% (green), 35% (purple) or 45% (orange) methanol containing buffer (v/v).

Previous measurements of *E. coli* RelA activity in the presence of methanol are reported at 25 °C [309], the activity of *F. tularensis* RelA at 25, 30 and 37 °C was therefore tested (7.5.21.2). The enzyme demonstrates similar levels of activity after 1 hour at 25 °C (Figure 3.23) to that observed at 30 °C (Figure 3.22) but no activity was observed at 37 °C (Figure 3.23).

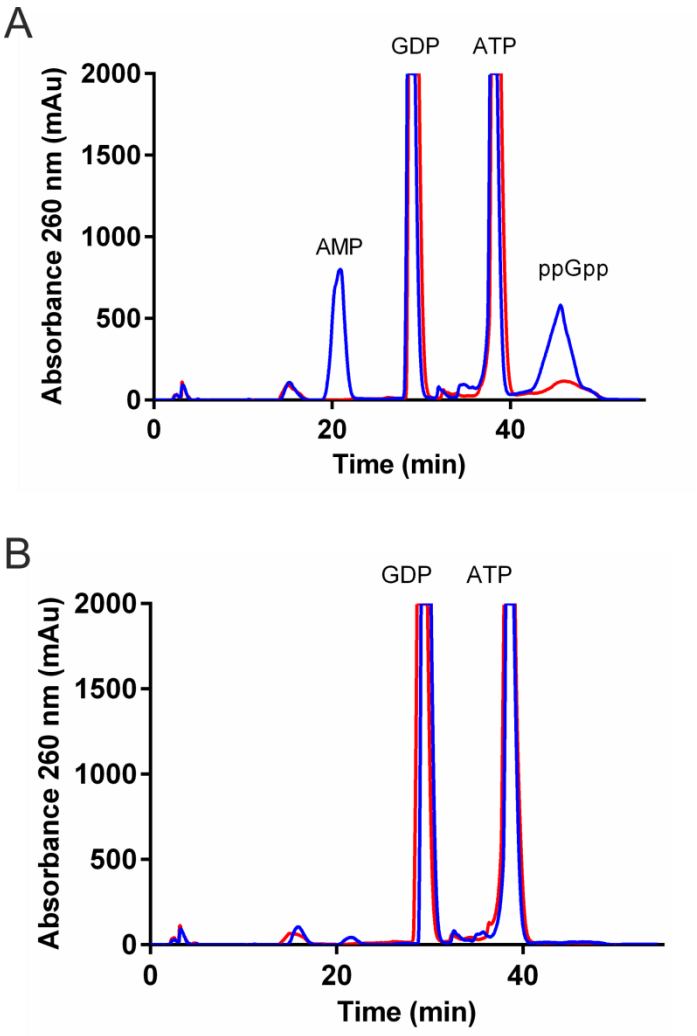

Figure 3.23. IP RP HPLC analysis (7.3.8.2) of 1 hour end point measurements of *F. tularensis* RelA activity with GDP as the pyrophosphate acceptor (blue) compared to inactivated RelA (red) at either 25 °C (A) or 37 °C (B) when incubated in a buffer containing 45% methanol (v/v).

3.5 Discussion of *F. tularensis* RelA Regulation

Activation of *E. coli* RelA by stalled ribosomes from alternative species has been previously reported [192, 290]. Within this chapter the (p)ppGpp synthetase activity of *F. tularensis* RelA in the presence of either *E. coli* MRE600 or *F. philomiragia* stalled ribosomal complexes is demonstrated. Interestingly relatively strong activation of *F. tularensis* RelA was observed in the presence of *E. coli* MRE600 stalled ribosomes (11 fold increase), but much weaker activation was observed with *F. philomiragia* stalled ribosomes (1.39 fold activation). These data demonstrate that at least one aspect of ribosomal activation of RelA is not species specific, as suggested by previously published data [192, 290]. The precise molecular determinant for this heterologous ribosome-mediated activation remains to be determined.

Under optimal conditions *F. tularensis* RelA demonstrated a 4 fold reduction in synthetase activity compared to *E. coli* RelA. It is possible that this overall weaker activity relates to the differences within the sequence for *F. tularensis* RelA and that of other RelA enzymes (2). An alternative explanation for the specific decrease in activity for *F. tularensis* RelA with *F. philomiragia* ribosomes may be the requirement for an unknown additional cofactor, which co-purifies with *E. coli* MRE600 ribosomes but not *F. philomiragia* ribosomes. It is possible to postulate that given the absence of ribonuclease I from *E. coli* MRE600 [358] this additional factor could be a RNA moiety.

Here we describe significantly weaker activation of *F. tularensis* RelA by the ribosomes purified from *F. philomiragia*. *F. philomiragia* is not only another *Francisella* species, but also encodes one of the three RelA enzymes identified to be missing an ACT domain [189]. In spite of this the stalled ribosomal complexes from this species were virtually unable to activate the *F. tularensis* RelA synthetase activity. Further to the possibility of an additional cofactor requirement, it is possible to speculate that within *F. tularensis* the enzyme RelA is not the principle enzyme responsible for triggering the stringent response under amino acid starvation. Within *F. tularensis* there is another putative (p)ppGpp synthetase (SpoT, gene FTT_0808). Sequence analysis of SpoT shows the presence of an extended C-terminal region, compared to that of *F. tularensis* RelA, containing an ACT domain. It is possible to postulate that the SpoT enzyme in *F. tularensis* is the primary enzyme for the amino acid starvation induced stringent response. *In vitro* analysis of

ribosome-mediated activation of SpoT-mediated (p)ppGpp synthesis would be required to provide support for such a hypothesis.

F. tularensis RelA contains no ACT domain and this offers a unique position to study the binding partner for this domain, as it provides a naturally occurring control. The binding of an amino acid to the ACT domain in several enzymes has been shown to downregulate that enzyme's activity [357, 366]. Furthermore, the activation of RelA synthetase activity has been strongly linked to the depletion of amino acids [168, 178]. Given these observations, one potential hypothesis for the function of the ACT domain in RelA is that it functions to downregulate the enzyme's activity following recovery from amino acid starvation. In this hypothesis the increase in amino acid concentrations following recovery from starvation conditions would result in increased binding of amino acids to the RelA ACT domain. The binding of this amino acid would then function to negatively regulate the RelA synthetase activity and metabolically return the cell to a pre-stress phenotype. Preliminary experiments were set up to investigate the effects of the amino acids serine and N-formylmethionine on the synthetase activity of *F. tularensis* RelA compared to ACT domain containing *E. coli* and *Y. pestis* RelAs (7.5.16, B.5). Neither amino acid demonstrated an inhibitory action on any of the RelA enzymes tested. Further research encompassing a wider range of amino acids at recorded cellular concentration could provide greater insights into the validity of this hypothesis.

The *F. tularensis* L11 gene (*FtrplK*) was subcloned into a pET16b vector to allow induction of protein expression by the addition of IPTG. The heterologous expression of soluble *F. tularensis* L11 in *E. coli* BL21 (DE3) cells was shown to be optimal at 27 °C for 4 hours (Figure 3.14). Large scale expression (1 L) yielded approximately 5 g cell pellet and streptavidin binding affinity chromatography demonstrated recovery of 10 mg purified *F. tularensis* L11. Initial activation assays coupling *F. tularensis* RelA with *F. tularensis* L11 demonstrated no significant increase in (p)ppGpp synthetase activity compared to the *F. tularensis* RelA control (Figure 3.16). As only mild activation was observed for *E. coli* RelA in the presence of N-terminal L11, with an increase of 6 to 20%, the absence of activation for *F. tularensis* RelA is perhaps not surprising. It could however allude to the reason behind the observed reduced ribosomal activation, as L11 has repeatedly been linked to RelA activity [299, 305, 306]. Further studies assessing the physical interaction between *F. tularensis* L11 and *F. tularensis* RelA complex and any resultant alteration in activity are therefore required.

To improve the understanding of the reduced activation of *F. tularensis* RelA by stalled ribosomal complexes, activation by the transfer and messenger RNA species were investigated. Preliminary work detailed the mild activation of RelA synthetase activity by mRNA and tRNA, by a 1.21 and 1.27 fold increase respectively. A similar weak increase in activity could be observed by comparing rate of product formation over time. Activation albeit mild by these RNA species suggests that *F. tularensis* RelA is still capable of binding to and responding to the level of RNA species linked to the deprivation of amino acids. Further analysis of RelA (p)ppGpp synthetase activity over a range of mRNA and tRNA concentrations would elucidate in detail the absolute extent of activation by these molecules.

In vitro activation of *E. coli* RelA by the signalling molecule ppGpp has previously been reported [313], but the means of activation by this molecule are still elusive. The presence of an ACT domain in long RSH proteins [189], known for their regulatory properties in other enzymes [357], suggested a possible binding site for ppGpp from which it could exert its effects. The unusual absence of an ACT domain in the *F. tularensis* RelA sequence provided a unique opportunity to test the hypothesis of ppGpp regulation via this domain. Experiments to test this hypothesis (Figures 3.20 and 3.21) demonstrated the specific activation of RelA synthetase activity upon the addition of ppGpp. Neither AMP nor KH_2PO_4 displayed a similar effect on the synthetase activity. Low levels (10 µM) of ppGpp were unable to stimulate *F. tularensis* RelA synthetase activity (Figure 3.20). A threshold value of ppGpp is a logical requirement of bacterial cells to prevent the constant activation of the stringent response. Analysis over a wider range of ppGpp concentrations likely to be found within the cell (0 to 1000 µM), suggested an EC_{50} value of 60 ± 1.9 µM. This value is delicately poised at the lower end of intracellular ppGpp concentrations [350], with the benefit of exerting greatest activation at the beginning of a stringent response. At the start of this global response the signal requires maximal amplification, so as to facilitate a rapid reaction to environmental stimuli. This is supported by *in vivo* data which suggests that the concentration of ppGpp can rise to ~900 µM upon growth of *E. coli* on isoleucine deficient media [157].

As demonstrated previously for *E. coli* RelA methanol is able to activate *F. tularensis* RelA (p)ppGpp synthetase activity. Buffers containing 30% methanol (approximate final concentration of 15% methanol) yielded optimal synthetase activity (Figure 3.22). Buffers containing greater than 45% methanol (≥22.5% methanol final concentration) resulted in

a rapid decrease in (p)ppGpp synthetase activity. This reduction in activity is likely to relate to protein denaturation and/or precipitation. Similar to previous observations for *E. coli* RelA in the presence of methanol (p)ppGpp synthetase activity was only stable below 30 °C (Figure 3.23). Increased conformational flexibility in the presence of methanol coupled with that observed from an increase in temperature is likely to result in the formation of protein aggregates. This is supported by the observed formation of a white precipitate when RelA within a methanol containing buffer is incubated at 37 °C. Perhaps one of the most unexpected observations with the methanol stimulated *F. tularensis* RelA assays was the removal of the selectivity for GTP as the pyrophosphate acceptor previously described (2.3). The effect of methanol on protein conformation has been previously demonstrated to strengthen hydrogen bonds and weaken hydrophobic interactions [349]. Structural alterations to the synthetase active site by methanol could account for the acceptance of GDP as a pyrophosphate acceptor under these conditions.

Chapter 4: **Development of a High Throughput Screen for RelA**

Current methods of analysis for RelA and RSH enzyme synthetase activity in general are not well adapted to a high throughput approach (1.6). High throughput experimental screening, described in Chapter 1.1.4, is an important method of discovering small molecule inhibitors of known or potential antibacterial targets. The importance of the stringent response and ppGpp concentration for bacterial virulence has been repeatedly demonstrated across a range of bacterial species [150, 250, 321]. With current methods of RelA inhibitor discovery dependent primarily on rationalised chemical design and synthesis [325, 327], very few inhibitors have been discovered to date. The ability to screen larger libraries of compounds against the enzyme with a greater variety of chemical scaffolds would increase the likelihood of finding a high potency enzyme inhibitor. The discovery of a highly potent inhibitor is a pre-requisite for drug development.

Enzyme inhibitors can be either reversible or irreversible in nature [367]. Reversible inhibitors will often dissociate rapidly following the formation of the enzyme inhibitor complex (EI). Competitive inhibitors bind to the enzymes active site and are often structural analogues of the enzymes substrate [368]. Furthermore in competitive inhibition, the inhibitor and the substrate compete for the same site on the enzyme, so that the enzyme can bind either the inhibitor (EI) or the substrate (ES) but never both (ESI) (Figure 4.1) [368]. As a consequence of this competitive inhibition can be overcome by increasing the substrate concentration [369].

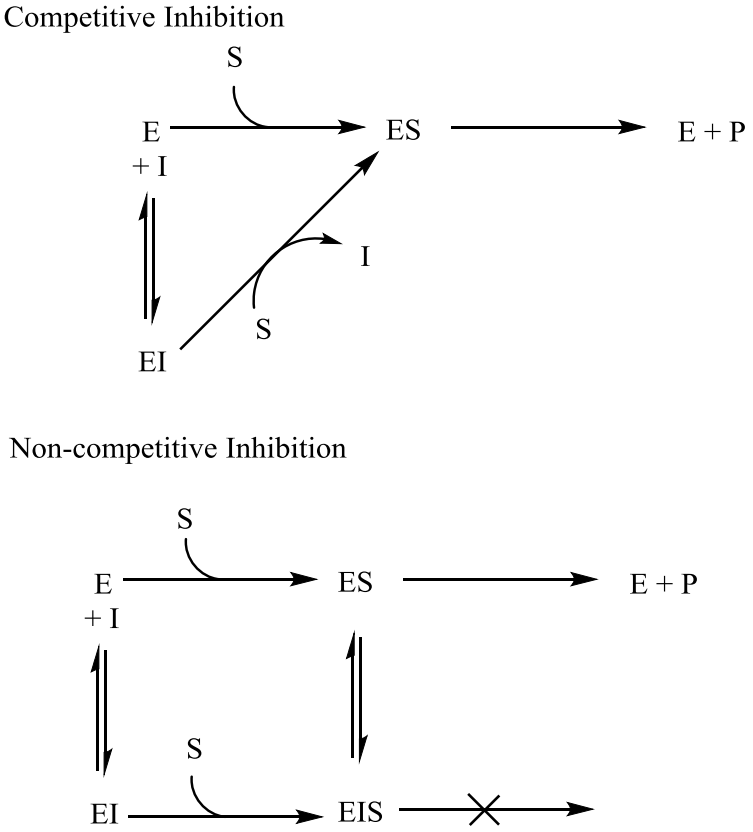

Figure 4.1. Reversible inhibition of enzymes by either competitive (top) or non-competitive (bottom) means [368]; where E denotes enzyme, S denotes substrate, P denotes product and I denotes inhibitor.

As an example, the current RSH enzyme inhibitor Relacin (Figure 1.6.11) is a designed structural analogue of guanosine tetraphosphate (ppGpp) (Figure 1.4.1) which is a substrate mimic for the hydrolase domain of RSH enzymes. Relacin is also reported to display inhibitory properties against the ppGpp synthetase *E. coli* RelA [325]. With an inactive hydrolase domain in RelA [189], the compound Relacin is a structural mimic of the product for this enzymes reaction rather than the substrate (1.5).

Alternatively enzyme inhibitors can be irreversible. In contrast to reversible inhibitors, irreversible inhibitors typically dissociate very slowly or not at all from the enzyme inhibitor complex (EI) [368]. The widely used antibiotic penicillin is an irreversible inhibitor which covalently modifies the enzyme transpeptidase [370]. Another example of an irreversible inhibitor is the inhibition of ornithine decarboxylase by the ornithine analogue α-difluoromethylornithine (DFMO) [371].

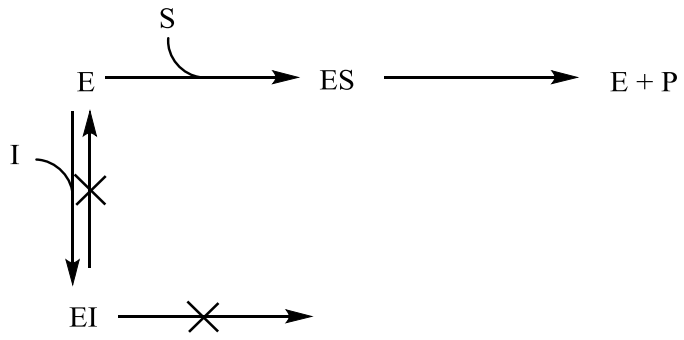

Figure 4.2. Irreversible inhibition of enzymes; where E denotes enzyme, S denotes substrate, P denotes product, and I denotes inhibitor.

4.1 Background to the RelA Coupled Enzyme Assay

Previous work with *F. tularensis* RelA has demonstrated the time-dependent release of inorganic phosphate (2.5). We hypothesised that the formation of this inorganic phosphate likely results from a secondary reaction in which the terminal 5' phosphate of the pppGpp is hydrolysed by low levels of a contaminating phosphohydrolases. This observation however prompted us to consider the potential for measuring RelA activity through the intentional coupling of the RelA enzyme with the known phosphohydrolase GppA from *E. coli*. Hara *et al*. showed that the *E. coli* GppA enzyme is capable of hydrolysing the terminal 5' phosphate from guanosine pentaphosphate in a specific manner [372]. Supposing that the catalytic efficiency (K_{cat}) and Michaelis-Menten constant (K_M) or equivalent for both enzymes were suitable, an excess of GppA should ensure the complete conversion of guanosine pentaphosphate (pppGpp) to inorganic phosphate (Pi) resulting in a 1:1 ratio (Figure 4.3). Such a system would allow quantification of the guanosine pentaphosphate formed and therefore RelA activity by the measured phosphate concentration. Inorganic phosphate can be measured by a variety of different methods, many of which are well suited to high throughput methods [45, 373, 374].

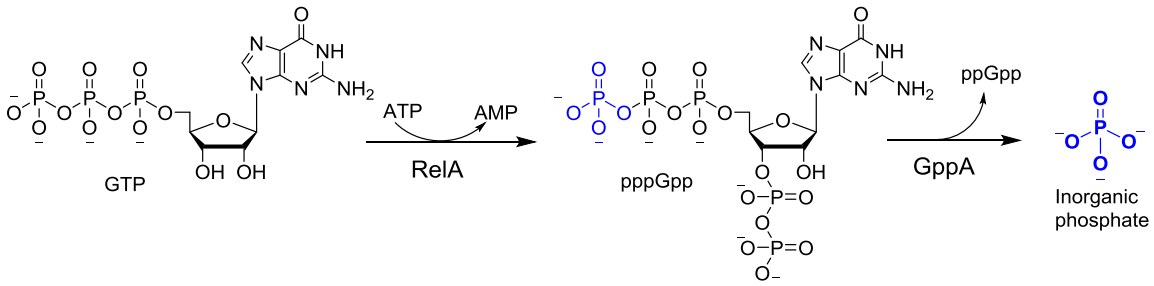

Figure 4.3. Chemical schematic outlining the RelA and GppA enzyme coupled assay. Resultant phosphate used to determine pentaphosphate concentration is highlighted in blue.

4.2 Validation of Enzyme Coupled Assay

4.2.1 Expression and Purification of *E. coli* GppA

The *E. coli* MG1655 *gpp* gene was purchased from NBRP (ASKA Clone library, SHIGEN, Japan) in the plasmid pCA24N, carrying chloramphenicol resistance [375]. Digestion of the plasmid with the restriction SfiI showed two bands corresponding to the pCA24N vector and gpp gene (1.48 Kb) (Figure 4.4).

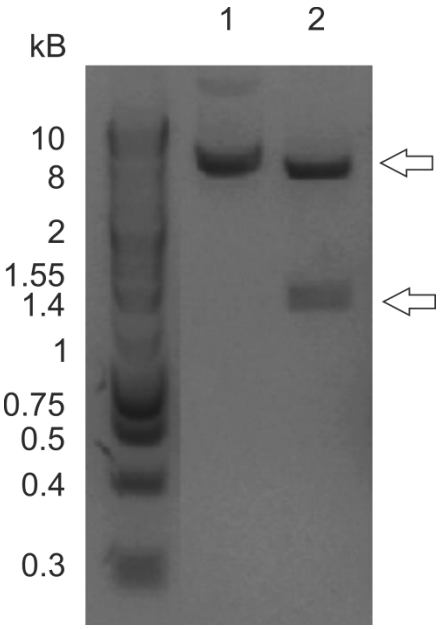

Figure 4.4. DNA gel electrophoresis of pCA24N::*Ec*gpp undigested (1) and following digestion with restriction enzyme SfiI (2). Arrows indicate the pCA24N vector (5.24 Kbp) and gpp insert (1.48 Kbp).

The *E. coli* his-tagged *gpp* gene was expressed at 27 °C for 4 hours as described by Kitagawa *et al*. [375] (7.6.1.2). Expression of GppA (5 L cell culture) typically yielded 14.6 ± 2.23 g cell paste. GppA was then purified initially by nickel affinity chromatography (7.6.1.3), and further impurities removed by size exclusion chromatography on a Superdex 200 (7.6.1.4).

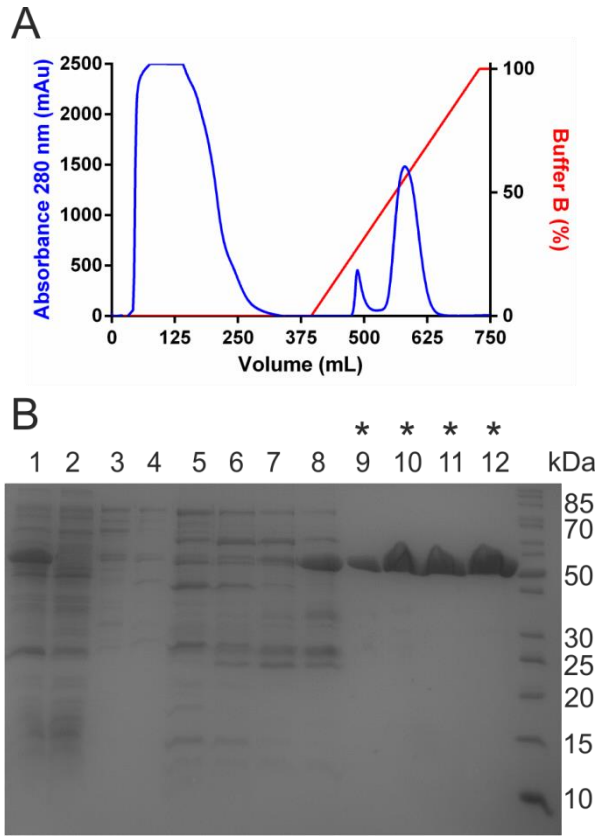

Figure 4.5. Purification of *E. coli* GppA by Nickel affinity chromatography. (A) Absorbance trace at 280 nm (blue) over a gradient of Buffer B (red). (B) SDS-PAGE analysis of ribosome purification. Lane 1; cleared lysate, lane 2; flowthrough, lanes 3-12; fractions correlating to the eluate during gradient. Lanes marked with an asterisk (*) contain *E. coli* GppA (55 kDa).

Both stages of purification yielded GppA at a high level of purity as judged by SDS-PAGE analysis (Figures 4.5 and 4.6). Initial purification of *E. coli* GppA was by nickel affinity chromatography on a Ni-IDA sepharose column (7.6.1.3). Host (*E. coli*) proteins demonstrating a high affinity for the Ni-IDA sepharose column were seen to elute early during the imidazole gradient (Figure 4.5a. ~490 mL, and 4.5b. lanes 5-8). Imidazole was removed from the purified *E. coli* GppA by dialysis (7.4.3). To ensure the purity of GppA, the enzyme was further purified using size exclusion chromatography (7.6.1.4). Purification on a Superdex 200 (HiLoad 26/60, prep grade) column yielded three main peaks, with the largest peak attributable to *E. coli* GppA as judged by SDS-PAGE analysis (Figure 4.6).

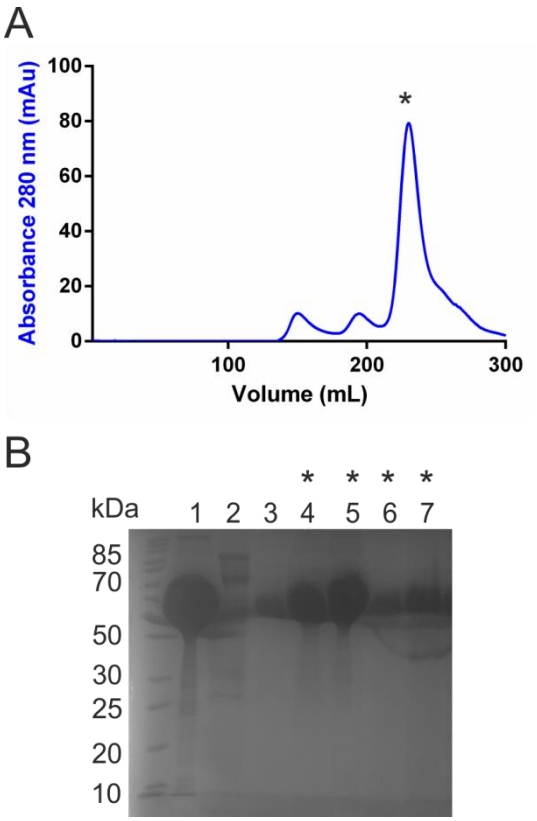

Figure 4.6. Purification of *E. coli* GppA (55 kDa) by size exclusion chromatography (A) Absorbance 280 nm trace (B) SDS-PAGE analysis of fractions from size exclusion chromatography. Lanes: 1, concentrated nickel purified GppA; lane 2, fraction corresponding to first peak; lanes 4-5, eluate fractions from third peak. Lanes marked with an asterisk (*) correspond to the peak similarly labelled in (A).

Purified *E. coli* GppA (~150-200 mg) could be concentrated to ~6 mg/mL prior to observation of any protein precipitation. Aliquots (100- 200 µL) were stored at -80°C prior to use.

4.2.2 ^{31}P NMR analysis of *F. tularensis* RelA and *E. coli* GppA Coupled Assay

^{31}P NMR analysis (7.6.1.5) was used to demonstrate the efficient conversion of guanosine pentaphosphate to guanosine tetraphosphate and phosphate by *E. coli* GppA when coupled to *F. tularensis* RelA. Experiments determined conversion over a range of *E. coli* GppA (0-5 µM) concentrations in the presence of a constant *F. tularensis* RelA concentration (5 µM). Enzyme concentrations were selected based on the low sensitivity of the analytical method.

To establish a baseline, control assays containing ATP (2 mM) and GTP (2 mM) with either *F. tularensis* RelA or *E. coli* GppA only were analysed by ^{31}P NMR. For *F. tularensis* RelA activity phosphate peaks corresponding to nucleotide triphosphates (NTP), AMP and pppGpp-β phosphate were monitored. Over time, a distinct increase in the signal at -19.88 ppm corresponding to the 5' β phosphate of pppGpp was observed, alongside the signal at 3.32 ppm for AMP (Figure 4.7). The increase in signal observed at -6.13 ppm is a multiplet peak which relates to the α-phosphates from nucleotide diphosphates (NDPs), guanosine tetraphosphate and potentially the guanosine pentaphosphate. As this peak could not be clearly resolved to differentiate between the individual α-phosphates, it was not monitored during reactions.

A

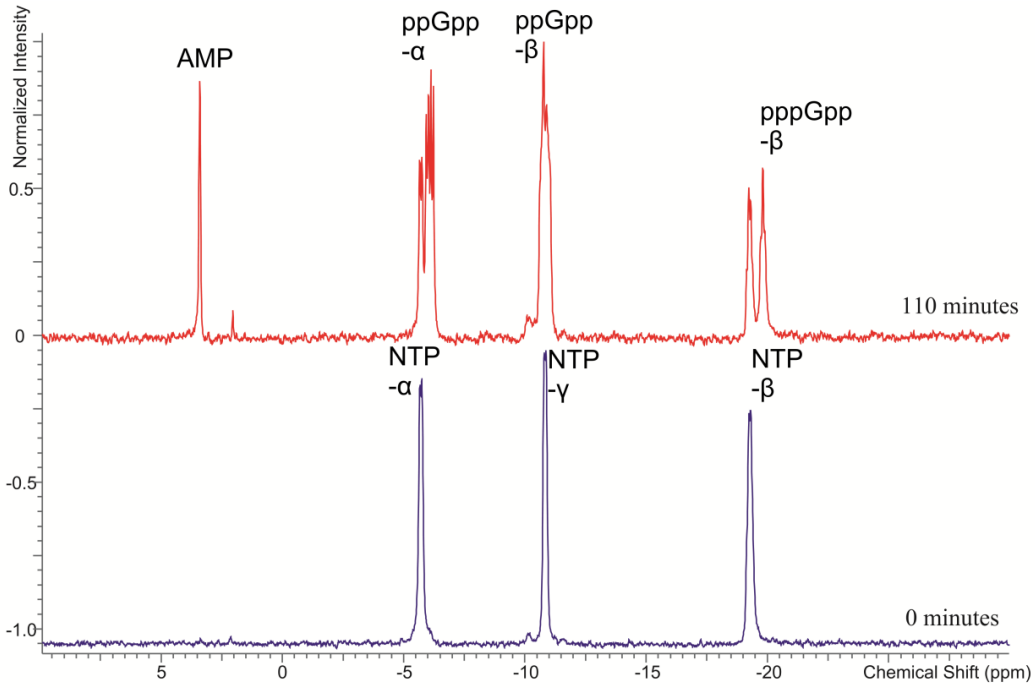

B

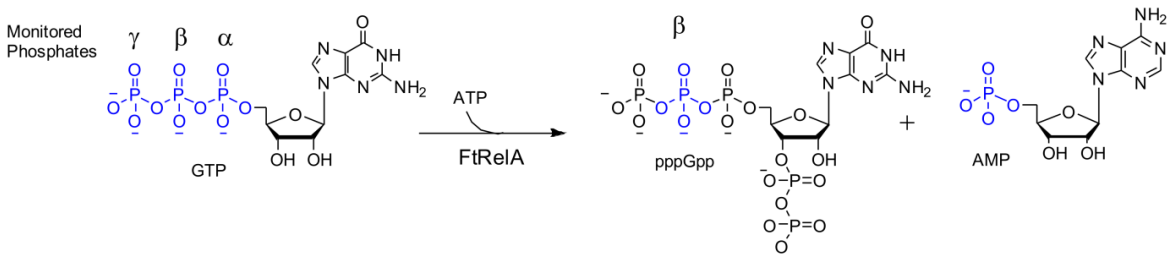

Figure 4.7. ^{31}P NMR *F. tularensis* RelA activity. (A) Chemical shifts observed at 0 and 110 minutes for *F. tularensis* RelA activity in the presence of ATP (2 mM) and GTP (2 mM). (B) Chemical schematic for the *F. tularensis* RelA activity, with phosphates of interest labelled and highlighted in blue.

Conversely analysis of the control experiment with *E. coli* GppA activity alone (i.e.; in the absence of RelA), detailed no signal for AMP (3.32 ppm) or 5′ β phosphate of pppGpp (-19.88 ppm) as expected (Figure 4.8). Signals corresponding to inorganic phosphate (1.94 ppm) and nucleotide diphosphates (-6.13 and -10.68 ppm) were however observed (Figure 4.8). The observed increase in these phosphate peaks relates to the phosphatase activity of *E. coli* GppA and this was investigated further (4.2.3).

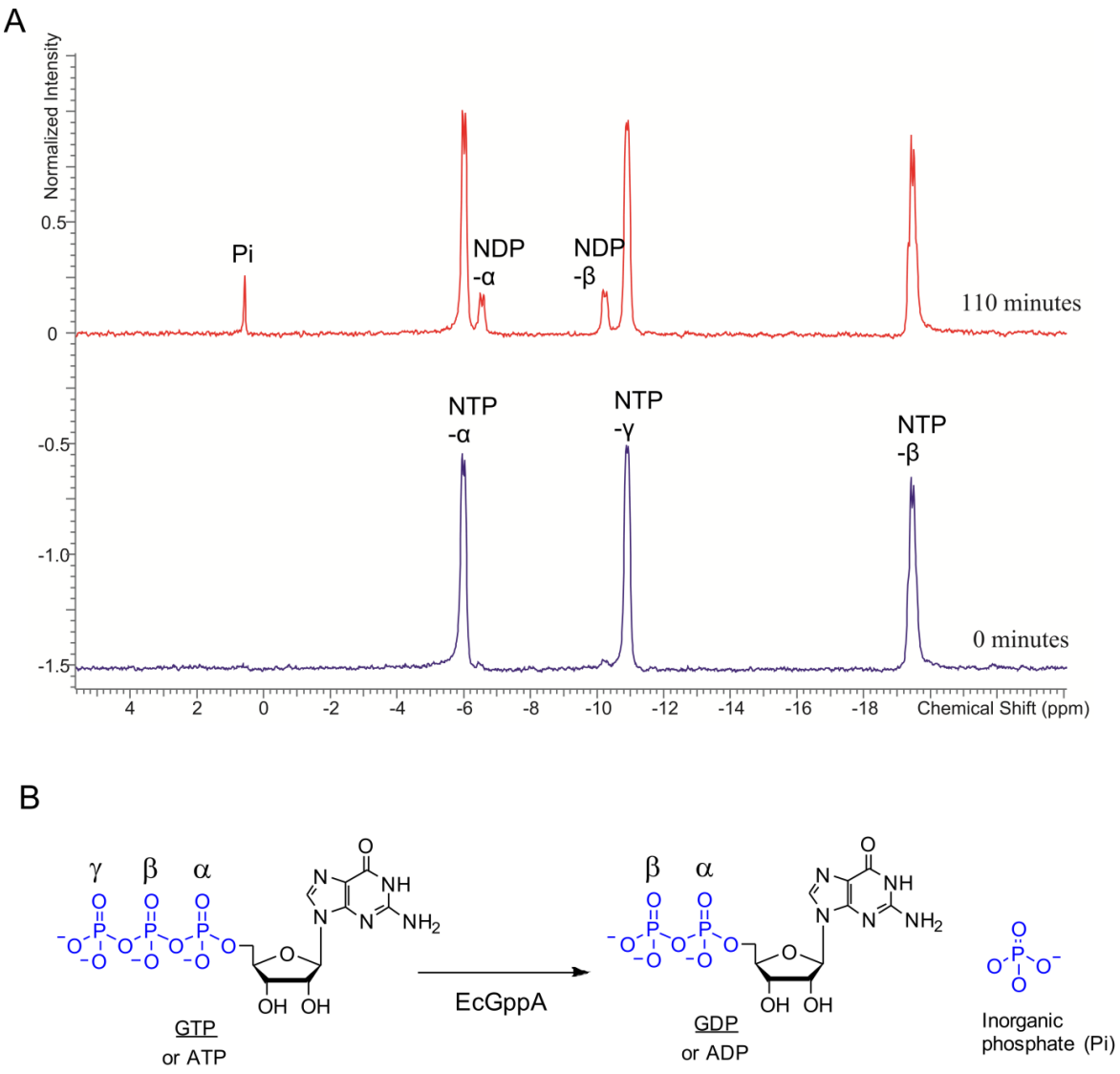

Figure 4.8. ^{31}P NMR *E. coli* RelA activity. (A) Chemical shifts observed at 0 and 110 minutes for *E. coli* GppA activity in the presence of ATP (2 mM) and GTP (2 mM). (B) Chemical schematic for the potential *E. coli* GppA activity, with phosphates of interest labelled and highlighted in blue.

The stoichiometric addition of *E. coli* GppA to a *F. tularensis* RelA activity assay resulted in the absence of measurable signal for observable peak for the 5' β phosphate of pppGpp (-19.88 ppm) (Figure 4.9). In its stead, a measurable signal for inorganic phosphate (1.94 ppm) could be observed to increase with time at a rate similar to that for AMP (3.32 ppm) (Figure 4.9). An increase in the signals at -6.13 ppm and -10.68 ppm was also observed (Figure 4.9). The increase in these signals could not be quantified due to the poor resolution of individual peaks (as discussed previously).

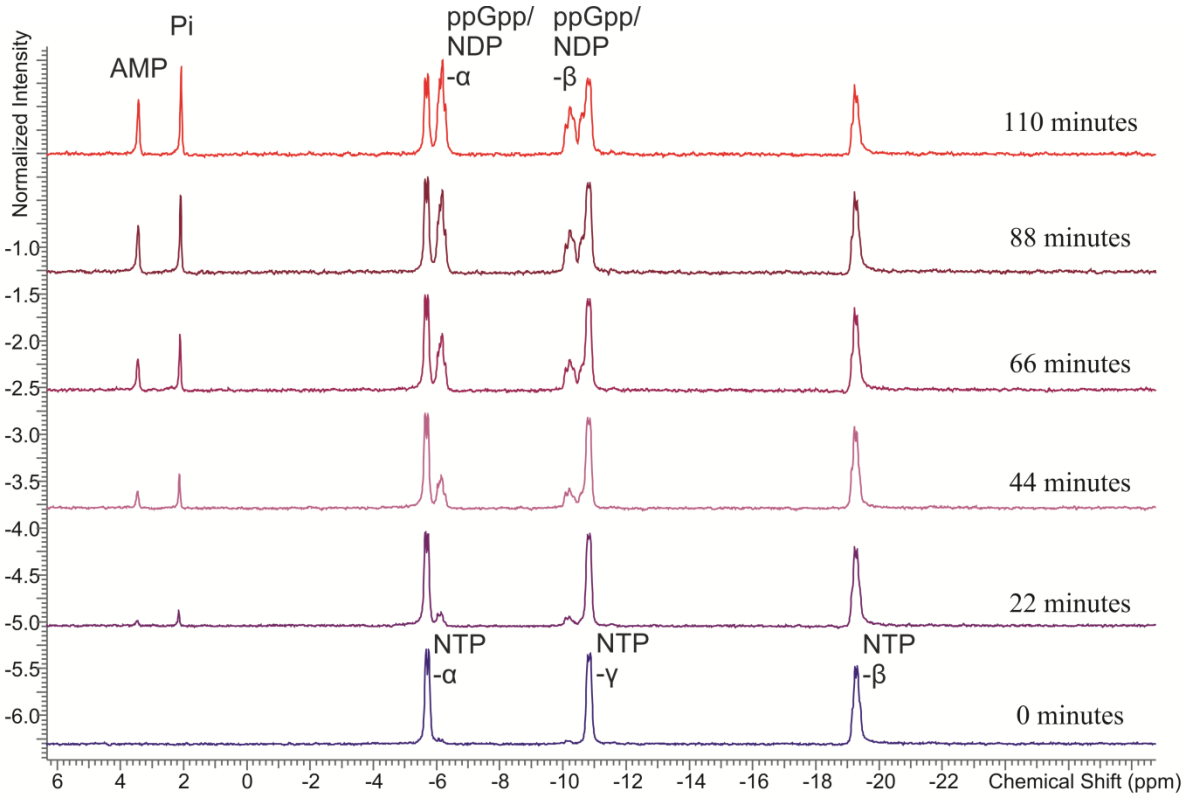

Figure 4.9. ^{31}P NMR analysis (7.6.1.5) of *F. tularensis* RelA (5 µM) activity assay coupled with *E. coli* GppA (5 µM) over time.

Further experiments, varying the concentration of *E. coli* GppA (0.05 µM to 5 µM) in coupled assays showed that no measurable signal for the 5' β phosphate of pppGpp (19.88 ppm) was observed. These concentrations of *E. coli* GppA yielded an increase in inorganic phosphate that correlated well with the increase observed for AMP (Figure 4.9a-d), as expected for an active guanosine pentaphosphatase. For the coupled assay using 5 µM *F. tularensis* RelA in the presence of 0.025 µM *E. coli* GppA, a signal for the 5' β phosphate of pppGpp (19.88 ppm) was once again measurable over time (at the apparent rate of 0.048 ± 0.009 μMs^{-1}) (Figure 4.9e).

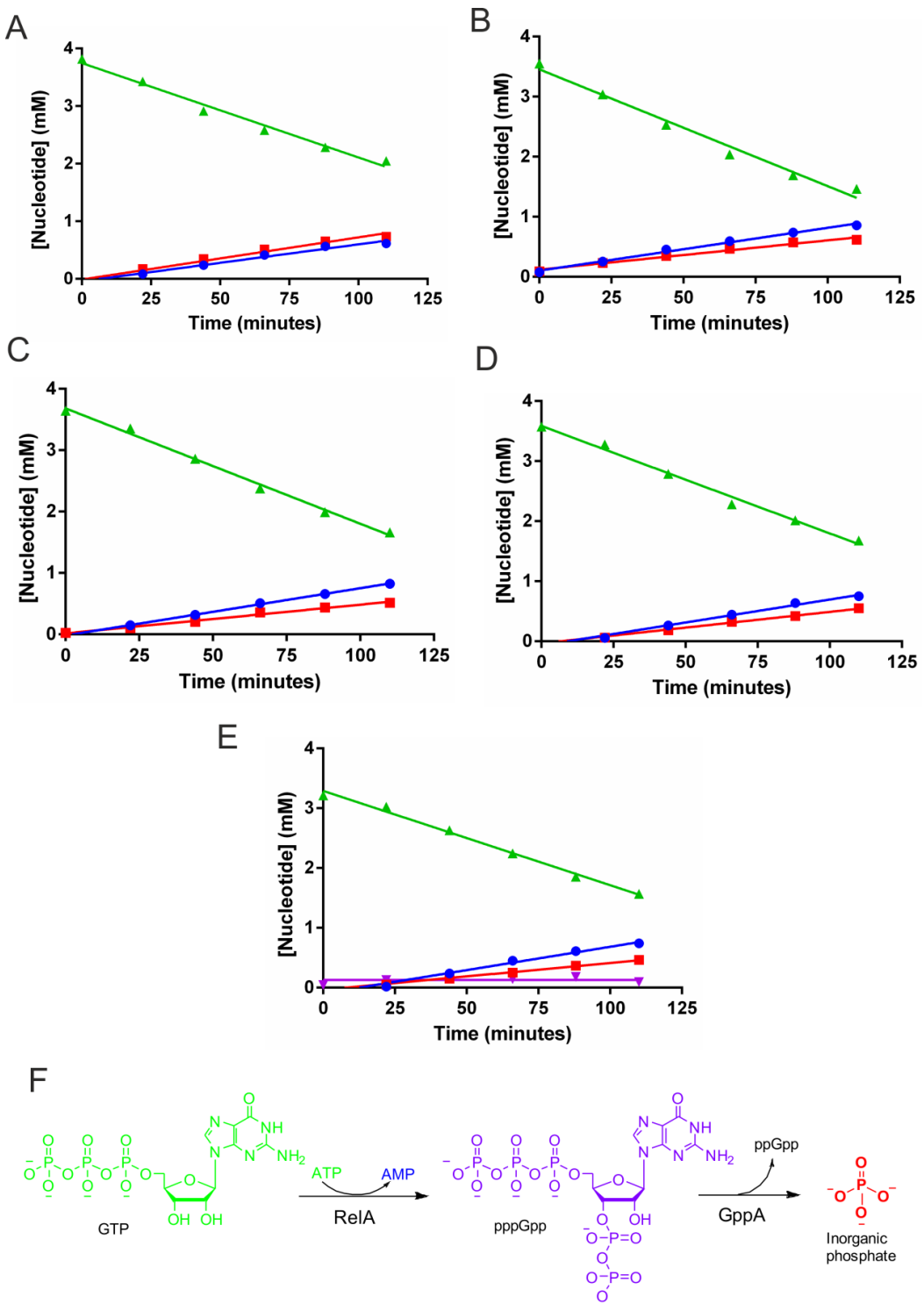

Figure 4.10. ^{31}P NMR analysis of *F. tularensis* RelA (5 µM) activity assays when coupled with *E. coli* GppA at the following concentrations; 5 µM (A), 0.5 µM (B), 0.1 µM (C), 0.05 µM (D) and 0.025 µM (E). Concentrations for AMP (blue), triphosphates (green), pppGpp (purple) and inorganic phosphate (red) were calculated from the integrals of the phosphate signals as observed for example in Figure 4.7. (F) Details a chemical schematic for the coupled reaction with phosphate containing species coloured in as described above.

4.2.3 **Substrate Specificity for *E. coli* GppA**

Previous work by Hara *et al*. described a high level of specificity for guanosine pentaphosphate as the substrate for *E. coli* GppA [372]. The observation of phosphate formation in the presence of nucleotide triphosphates (Figure 4.7a) however suggested that GppA is capable of hydrolysing the terminal phosphate from alternative substrates. The activity of *E. coli* GppA in the presence of either ATP or GTP (2 mM) was therefore investigated by ^{31}P NMR analysis. A signal for inorganic phosphate (1.94 ppm) was observed to increase over time when *E. coli* GppA was incubated with GTP but not when it was incubated with ATP (Figure 4.11).

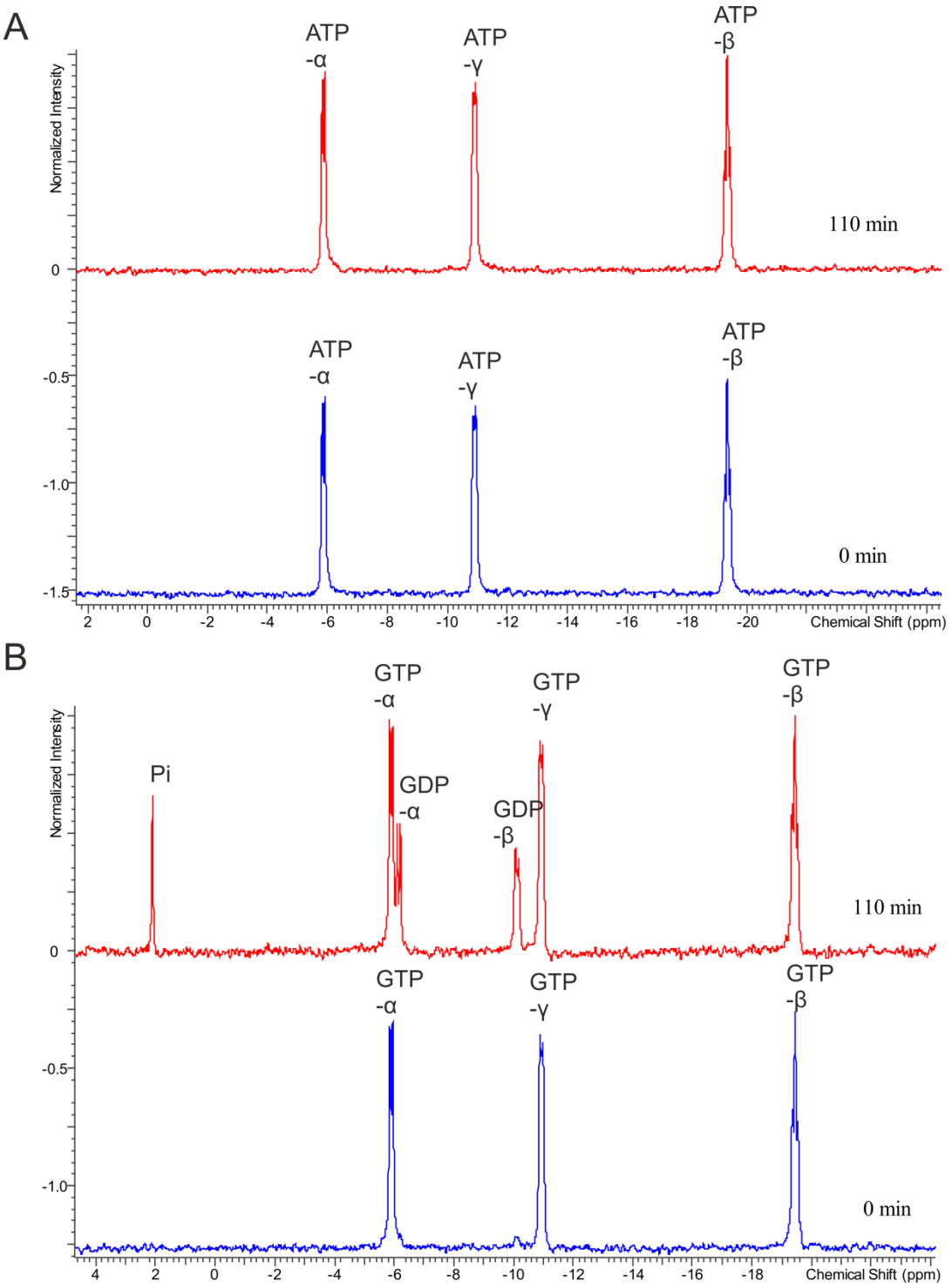

Figure 4.11. ^{31}P NMR analysis of *E. coli* GppA activity over time in the presence of 2 mM ATP (A) or GTP (B).

In the presence of GTP (2 mM) *E. coli* GppA (5 µM) hydrolyses the terminal phosphate, which in turn results in an observed increase in inorganic phosphate and GDP (Figure 4.9b). This reaction occurs at a seemingly slow rate of 0.067 μMs^{-1} (Figure 4.12).

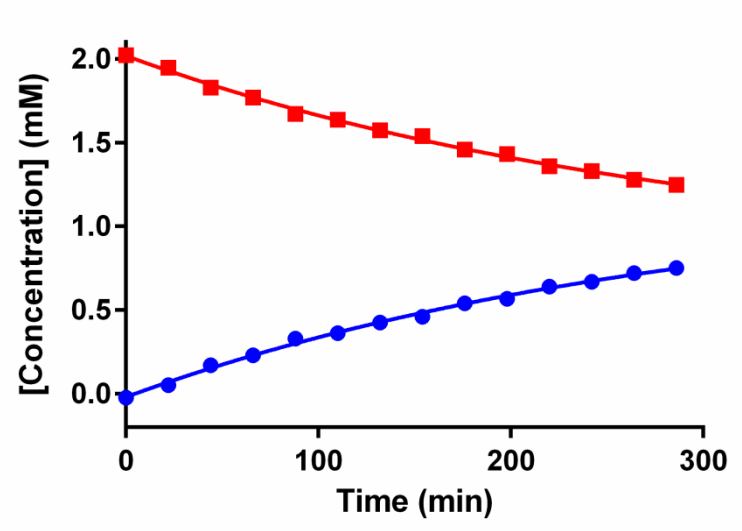

Figure 4.12. ^{31}P NMR analysis of the hydrolysis of GTP (2 mM) by *E. coli* GppA (5 µM) over time. Concentrations of phosphate species were calculated from integrals in time course experiments, yielding an increase in phosphate (blue) and corresponding reduction in GTP (red) concentrations.

Collectively, these experiments highlighted the necessity of finding the optimal enzyme concentrations for the coupled assay. Optimal conditions required a concentration of *E. coli* GppA high enough for the complete conversion of pppGpp to ppGpp, and yet low enough to minimise the unwanted hydrolysis of GTP.

4.3 Optimisation of the High Throughput Enzyme Coupled Assay

Inorganic phosphate can be measured by a wide range of standard techniques some of which are commercially available. Such techniques include, absorbance assays (malachite green [46], MESG [45]), radiolabelled assays (radiolabelled phosphate [295]), ELISA based assays, and fluorescence based assays [376]. Detection of inorganic phosphate by the addition of malachite green reagent transformed this enzyme coupled assay to a high throughput method (Figure 4.13). The spectrometric detection (620-650 nm) of the phosphomolybdate malachite green complex under acidic conditions is commonly used for phosphate detection [373, 374]. Furthermore the method has been applied to the development of spectrometric assays for characterising and screening inhibitors for enzymes [377, 378].

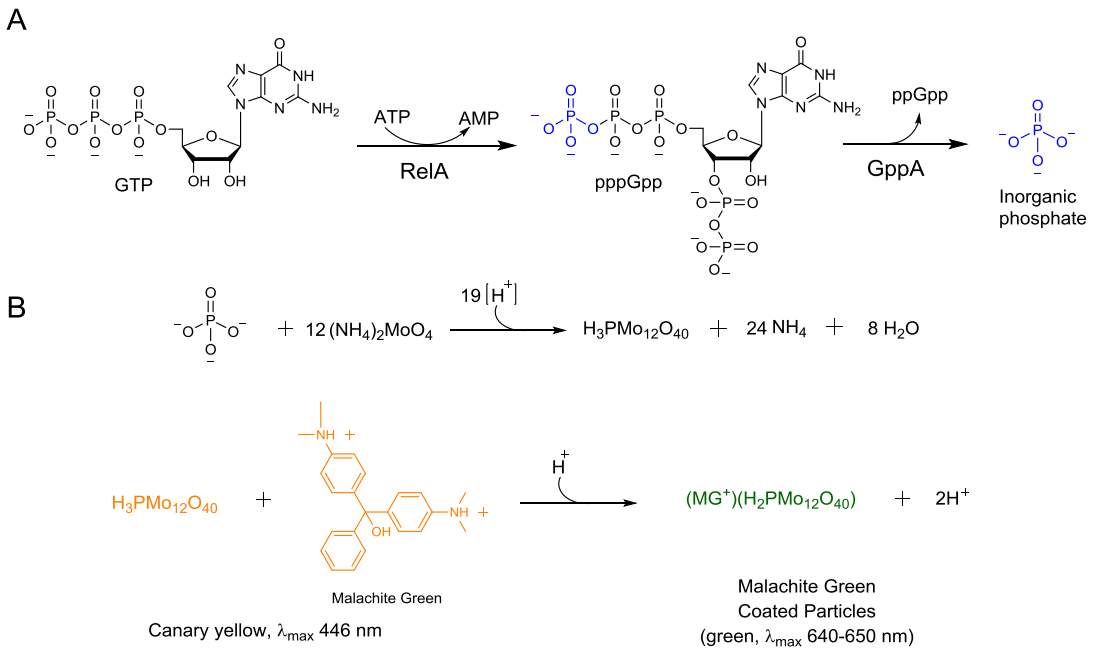

Figure 4.13. Chemical schematic outlining the detection of free phosphate from the RelA, GppA enzyme coupled assay by the addition of malachite green reagent. (A) The formation of inorganic phosphate from the coupled reaction between RelA and GppA, with GTP as the pyrophosphate acceptor for RelA. Inorganic phosphate and its origin are highlighted in blue. (B) Detection of inorganic phosphate by the addition of malachite green reagent (composed of; malachite green, ammonium molybdate, and HCl), with resultant colour change from canary yellow to green.

Addition of malachite green reagent (7.6.1.7.1) to commercially sourced nucleotides (AMP, ATP, and GTP) over a range of concentrations (7.6.1.7.3) was used to determine the background signal at 640 nm (Figure 4.14). AMP displayed no absorbance increase up to 200 µM (Figure 4.14). ATP demonstrated similarly weak increase in absorbance up to 200 µM, however an increase in absorbance could be observed for concentrations higher than this. In contrast to AMP and ATP, the nucleotide GTP generated high absorbance readings from as low as 25 µM. To identify all inhibitors modalities during high throughput screening, it is preferable to keep substrates at K_M [369]. The reason for this relates to the mode of action of the types of enzyme inhibitor. Competitive inhibitors are more easily identified at low substrate concentrations ($<K_M$), as there is a greater portion of free enzyme (E) to which they can bind [369]. Conversely, non-competitive inhibitors, which bind to the substrate bound enzyme (ES) or an equivocal complex, are more clearly observed at high substrate concentrations ($>K_M$) [369]. To achieve an optimal mixture of

ES versus E, substrate concentrations used are at K_M values. In the case of *F. tularensis* RelA substrates would therefore ideally be at the $K_{1/2}$ value (GTP at ~1 mM, ATP at ~0.4 mM). These background signal studies indicated that a compromise concentration was required for future experiments at less than the measured $K_{1/2}$ for GTP. The result of this compromise is that the high throughput screen was better adapted to identify competitive inhibitors of GTP. This was therefore well matched to the screening of nucleotide analogue libraries.

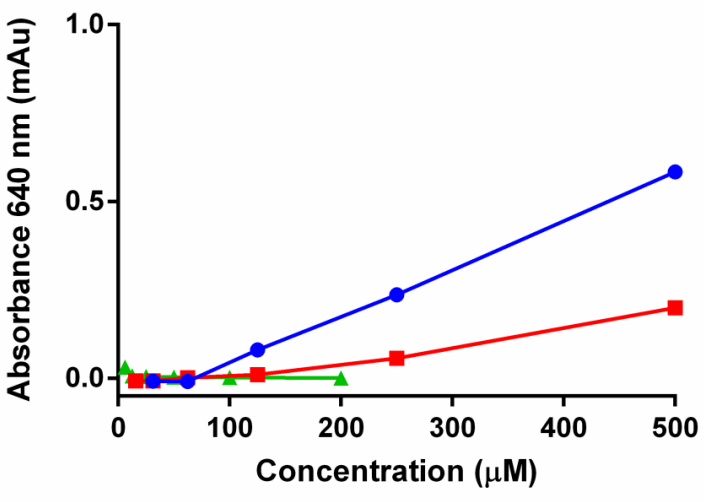

Figure 4.14. Background signal of contaminating inorganic phosphate in commercially sourced AMP (green), GTP (blue) and ATP (red) with malachite green.

The difference between calculated phosphate standard curves in the presence of water and assay buffer B (7.6.1.7.4) was however observed to be negligible (C.1).

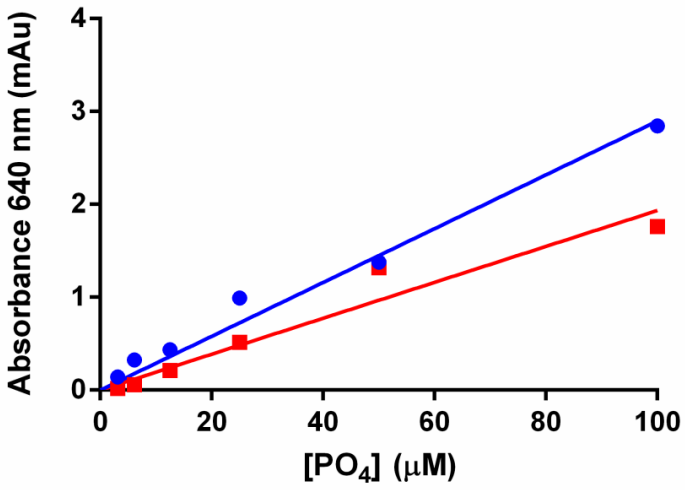

Figure 4.15. Phosphate standard curves measured by malachite green reagent, in the presence (blue, R^2 = 0.98) or absence (red, R^2 = 0.94) of 100 μM substrates (ATP and GTP).

The addition of the nucleotides GTP (200 µM) and ATP (400 µM) to phosphate standards still achieved a linear proportional relationship up to 100 µM, similar to those lacking substrates (Figure 4.15).

Analysis of absorbance values for coupled assays (*F. tularensis* RelA and *E. coli* GppA) versus control assays (*E. coli* GppA only), measuring at a range of wavelengths (600-750 nm), showed the maximal peaks were at 640-650 nm (C.2). For all further experiments absorbance was measured at 650 nm.

4.3.1 **Absorbance Measurements are Dependent on *F. tularensis* RelA Concentration.**

The high throughput screen is dependent on the measured output (i.e.; phosphate concentration) corresponding to the proportional activity of the *F. tularensis* RelA. One way of determining this dependency *in vitro* is to vary the concentration of *F. tularensis* RelA within the assay, and record the measured output. For a simple Michaelis-Menten enzyme the rate should be proportional to the concentration of enzyme (provided [enzyme] < [substrates]). The absorbance at 650 nm (A_{650}), following the addition of malachite green reagent to activity assays with a range of *F. tularensis* RelA concentrations, was measured to determine the relationship between these factors (7.6.1.7.5). Data showed a linear relationship (R^2 of 0.97) between A_{650} measurements and the concentration of *F. tularensis* RelA within the assay (Figure 4.16). Concentrations of 0.1 µM *F. tularensis* RelA were too low to yield sufficient phosphate formation in comparison to background concentrations (A_{650} of <0.0) (Figure 4.16).

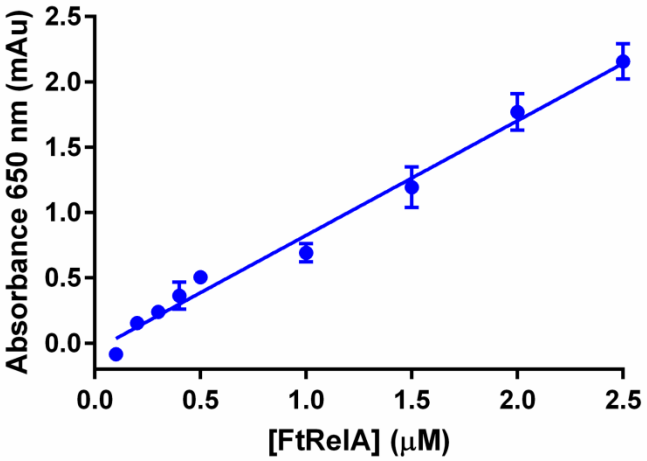

Figure 4.16. Linear relationship between measured absorbance at 650 nm (corresponding to malachite green detection of phosphate concentration) and *F. tularensis* RelA concentration (0.1 to 2.5 µM). Data fits a linear line with an R2 of 0.97.

Initial optimisation experiments for the conditions of the high throughput screen were measured using 2 µM *F. tularensis* RelA, to ensure a clear separation of coupled assays (A_{650} of ~1.6) from controls (A_{650} of ~ 0.0). A lower concentration of 0.5 µM *F. tularensis* RelA was deemed more suitable for final optimisation and the screening of *F. tularensis* RelA against small molecule compounds. In subsequent experiments A_{650} was converted into a phosphate concentration using a phosphate standard curve (0-100 µM).

4.3.2 Optimisation of *E. coli* GppA Concentration

Varying the concentration of *E. coli* GppA (0.02, 0.2, or 0.2 µM) (7.6.1.7.6) used within the coupled enzyme assay demonstrated no significant effect on measured phosphate concentrations (Figure 4.17). The higher concentration of *E. coli* GppA (2 µM) displayed an equal increase in phosphate concentration measured for the coupled assay with that of the control (GppA only) assay (Figure 4.17). These data confirm that only low levels of *E. coli* GppA were required to ensure efficient turnover of guanosine pentaphosphate. Furthermore, the observed formation of phosphate in the absence of added GppA, was consistent with the presence of residual contaminating GppA or GTPase activities within the purified *F. tularensis* RelA. Subsequent experiments and screening therefore contained 0.02 µM *E. coli* GppA. This concentration kept background phosphate

concentrations low and was sufficient to ensure full conversion of guanosine pentaphosphate to guanosine tetraphosphate and phosphate.

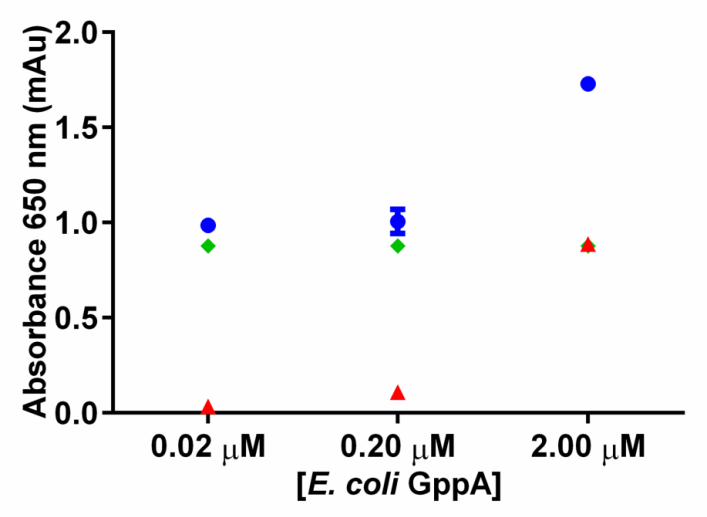

Figure 4.17. Optimisation of *E. coli* GppA concentration. Difference in absorbance at 650 nm between *F. tularensis* (2 μM) only assay (blue), *E. coli* GppA only assay, at indicated concentrations (red), and *F. tularensis* RelA (2 μM) and *E. coli* GppA, at indicated concentrations, coupled assay (green).

4.3.3 Optimisation of Buffer

There is a strong consensus throughout the literature on the buffer composition for RelA activity assays [168, 295, 296]. Additionally, a similar buffer was used for the previously described kinetic analysis of *F. tularensis* RelA (7.9.19). Optimisation of this buffer for the coupled assay was achieved by variation of individual components (7.6.1.7.9). Variation in the concentration of β-mercaptoethanol showed very little deviation in the measured phosphate production by the coupled assay, however a mild increase can be observed at 2 mM (Figure 4.18a). Work by C. Frankling (MChem project Student) demonstrated a poor stability of *F. tularensis* RelA at high concentrations of β-mercaptoethanol [337]. The requirement of long incubation periods for this enzyme coupled assay encouraged us to therefore keep the β-mercaptoethanol concentration at 1 mM.

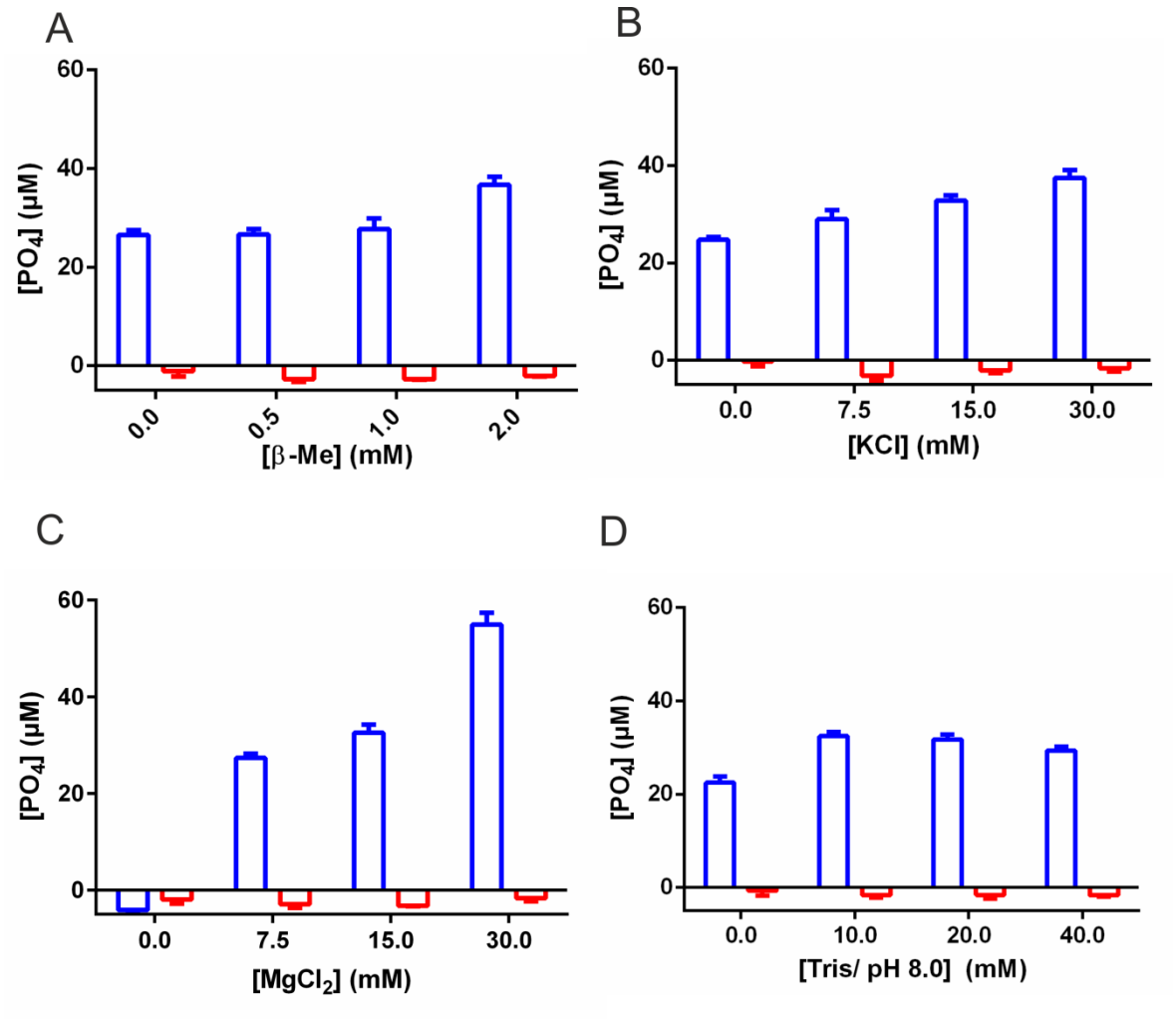

Figure 4.18. Buffer optimisation for *F. tularensis* RelA (2 µM), *E. coli* GppA (0.02 µM) coupled assay (blue bars) and *E. coli* GppA only assay (red bars). (A) Measured phosphate concentrations over a range of β-Me concentrations. (B) Measured phosphate concentrations over a range of KCl concentrations. (C). Measured phosphate concentrations over a range of Tris concentrations at pH 8.0. (D) Measured phosphate concentrations over a range of $MgCl_2$ concentrations.

The optimal concentrations of the buffer Tris were either 10 or 20 mM (Figure 4.18d), to keep a level of consistency with the *F. tularensis* RelA assay buffer, 20 mM Tris was used for subsequent assays. The determined phosphate concentration over a range of KCl concentrations showed little to no variation (Figure 4.18b), therefore for continuity 15 mM KCl was used for subsequent assays.

Perhaps unsurprisingly the concentration of $MgCl_2$ had a greater effect on measured activity (Figure 4.18c), with optimal activity observed at 30 mM $MgCl_2$ within the range tested. High concentrations (25 to 50 mM) of $MgCl_2$ have been reported to lead to an

inactivation of some bifunctional Rel enzymes [256]. Although previous analysis has suggested *F. tularensis* RelA shares various characteristics of bifunctional enzymes, this data is indicative that it does not share a similar response to Mg^{2+} ion concentration. Further analysis of the optimal $MgCl_2$ concentration for both *F. tularensis* RelA activity alone and in the coupled assay format might provide further insight into this unusual enzyme.

The use of bovine serum albumin (BSA) in high throughput screens is common practice [43]. The use of BSA in these assays can both aid in preventing the precipitation of RelA and the prevention of non-specific binding to laboratory equipment including the wells in a multi-well plate [313]. A typical concentration of BSA within these assays can range from 0.01 to 0.1 mg/mL [43]. Here a range of BSA concentrations were tested (0, 0.025, 0.05 and 0.1 mg/mL) (7.6.1.7.7). Results showed an increase in the measured phosphate concentrations for both the coupled and GppA only activity assays as the level of BSA increased (Figure 4.19). Subsequent assays all contained 0.1 mg/mL BSA final concentration.

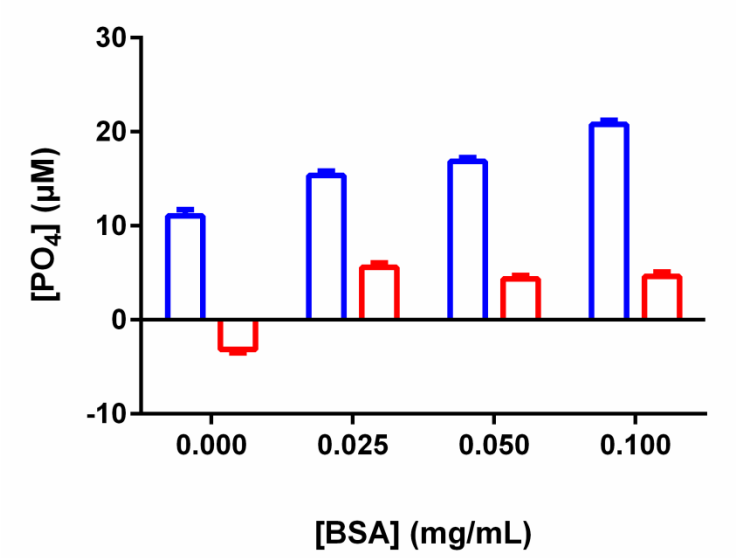

Figure 4.19. Effect of BSA on the *F. tularensis* RelA and *E. coli* GppA coupled assay (blue) and *E. coli* GppA only assay (red) on measured phosphate concentration for a 1 hour end point assay.

Dimethyl sulfoxide (DMSO) is widely used to dissolve chemical compound libraries used in high throughput screening. For this reason the effect of DMSO on the measured activity in the coupled assay and control assays was investigated (7.6.1.7.7). The coupled assay surprisingly displays a higher apparent phosphate concentration after 1 hour in the presence of DMSO (5%) than in its absence (Figure 4.20). In the presence of DMSO the recorded phosphate concentration of the control (*E. coli* GppA only) assay also appears to reduce (Figure 4.20). The inhibition of *E. coli* GppA GTP-specific hydrolytic activity, could explain this observation. This inhibition did not interfere with the coupled assay as the concentration of GppA was in excess and the efficiency of its pppGpp hydrolytic activity is greater than that for GTP. Subsequent experiments and screening could contain 5% DMSO without any negative effects on RelA activity.

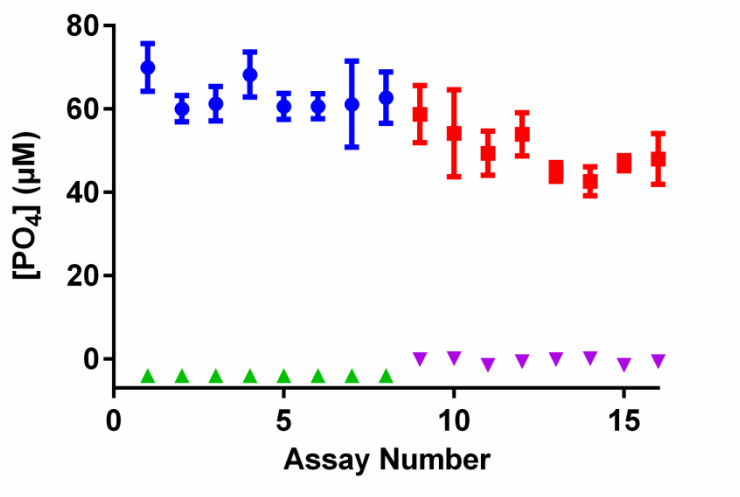

Figure 4.20. Effect of DMSO on *F. tularensis* RelA, *E. coli* GppA coupled assay on apparent phosphate concentration for a 1 hour end point assay. Assays 1 – 8, coupled enzyme assay (blue) and GppA only assay (green) are in the presence of DMSO. Assays 9-16, coupled enzyme assay (red) and GppA only assay (purple) do not contain DMSO.

4.3.4 Analysis of *F. tularensis* RelA and *E. coli* GppA Coupled Assay over Time

Time course analysis of both the coupled assay and control assay were determined to establish the optimal time point for the end-point assays (7.6.1.7.11). Analysis over time demonstrated a linear increase of signal for the coupled assay, with a near flat line observed for *E. coli* GppA activity only (Figure 4.21a). An increased activity of freshly

purified *F. tularensis* RelA prepared prior to inhibitor screening suggested a shorter incubation time (90 minutes) was required to achieve around 40 µM phosphate (Figure 4.21b). As mentioned previously a linear relationship was observed between A_{650} and phosphate concentration between 5 and 100 µM (Figure 4.14). End-point assays yielding a phosphate concentration around 40-50 µM (middle of linear range) were considered advantageous for the identification of both inhibitors and activators of *F. tularensis* RelA.

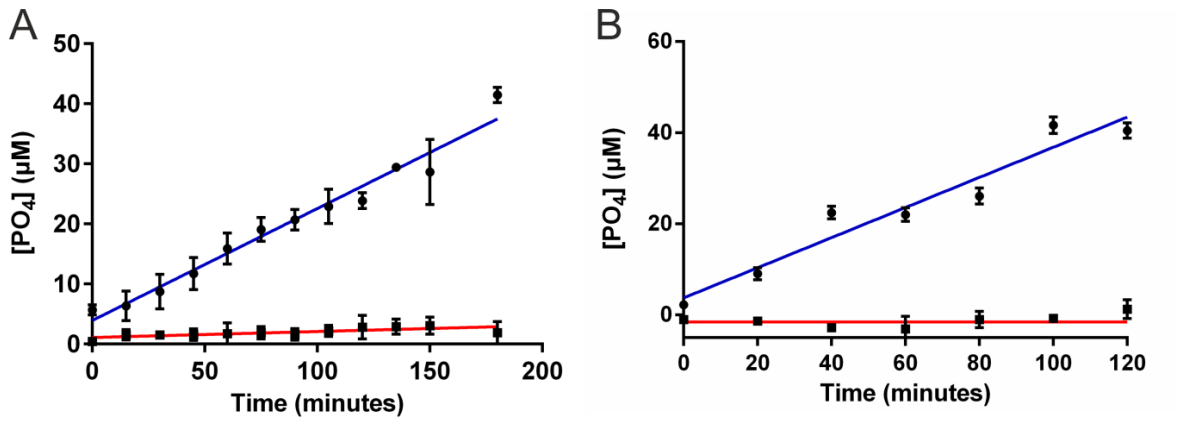

Figure 4.21. Time course analysis of *F. tularensis* RelA activity. (A) Analysis of *F. tularensis* RelA batch A (B) Analysis of *F. tularensis* RelA batch B. *F. tularensis* RelA, *E. coli* GppA enzyme coupled assay (blue), and *E. coli* GppA only assay (red).

4.3.5 Testing the Optimised High Throughput Screen

Prior to screening a library the novel enzyme coupled assay was tested with current plate layout to determine the variation in reading across the plate. Analysis showed that the positive and negative controls yielded a good screening window (Z' of 0.8) and measurements from the remaining coupled assay wells all fell within the three standard deviations of the positive control average value (Figure 4.23). The Z' value was calculated using Equation 4.1. Here σ denotes the standard deviation and µ denotes the average of positive (0% RelA activity, c+) or negative (100% RelA activity, c-) controls [44]. Calculated Z' values ≥0.5 or ≥0.7 denotes a good or excellent screening window respectively, where the separation band between controls is large (Figure 4.22) [44].

Equation 4.1

$$Z' = 1 - \left(\frac{3\sigma_{c+} + 3\sigma_{c-}}{\mu_{c-} - \mu_{c+}}\right)$$

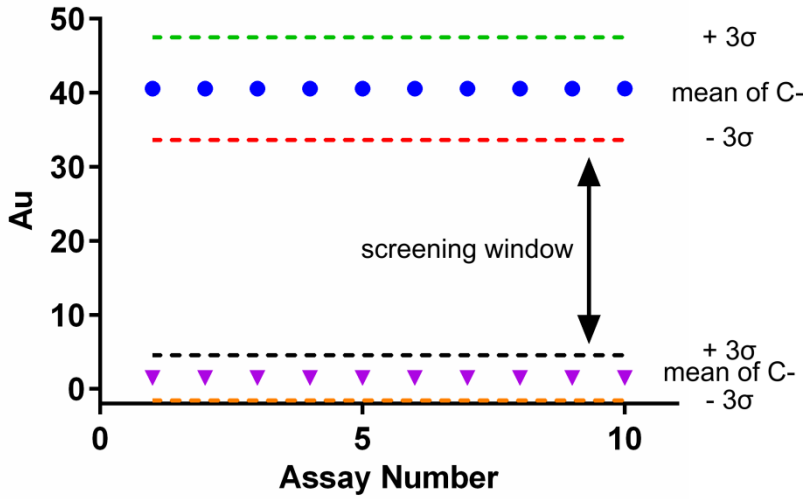

Figure 4.22. Model Screening Window. A graphical representation of high throughput screening data and the corresponding screening window (labelled as such). The mean of the positive (no RelA activity) controls (purple) and that of the negative (100% RelA activity) controls (blue) are noted. Three standard deviations either side of these means are denoted by dashed lines. The area between 3 standard deviations below the mean of the negative control (red dashed line) and 3 standard deviations above the mean of the positive controls (black dashed line) indicates the screening window. Assays yielding phosphate concentrations within the screening window are identified as inhibitors of RelA. Au stands for arbitrary units.

Calculated screening windows for test plates showed a good separation of positive and negative controls and gave a Z' value of 0.8 (Figure 4.23). Measured phosphate concentrations for all coupled assays were however higher than previously estimated by time course analysis (Figure 4.23). Although no direct explanation could be found for this observation, it was thought to relate to the combined batch to batch variation of both enzymes.

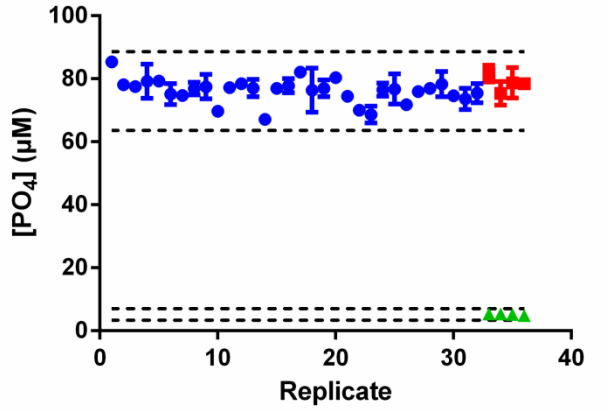

Figure 4.23. Analysis of a mock 96 well microtitre plate of malachite green treated coupled *F. tularensis* RelA and *E. coli* GppA assays (blue), positive *E. coli* GppA only controls (green) and negative *F. tularensis* RelA and *E. coli* GppA controls (red). Dashed lines indicate 3 × standard deviation of the mean for either positive or negative controls.

4.4 High Throughput Screening

Following optimisation, the designed high throughput method for measuring *F. tularensis* RelA activity was applied for experimental screening of a nucleotide analogue library. A nucleotide analogue library was chosen based on the previous success in the inhibition of *E. coli* RelA enzyme by the nucleotides AMPPNP [291], ppApp [259] and Relacin [325]. The nucleotide analogue library (838 compounds) screened was synthesised by Dr Robert Reynolds and colleagues [379, 380] and consists of a range of adenine, guanosine, uridine, thymine, and cytosine structural analogues. The library of compounds was screened using the conditions outlined in Table 4.1 by the method described in Chapter 7 (7.6.2).

Table 4.1. Conditions used for screening nucleotide analogues against *F. tularensis* RelA.

Parameter	Screening Conditions
Buffer	20 mM Tris (pH 8.0), 15 mM KCl, 30 mM $MgCl_2$, 0.1 mg/mL BSA, 1 mM β-mercaptoethanol
Substrate Concentrations	GTP (200 µM), ATP (400 µM)
Enzyme Concentrations	*F. tularensis* RelA (500 nM), *E. coli* GppA (20 nM)
Compound Concentration	10 µM
DMSO Concentration	5%
Volume	50 µL
Plate	96 well half area UV Star Microplate (Greiner Bio-One)
Quenching Method	Malachite Green Reagent (50 µL)
Temperature	Assay Incubation (30 °C)
	Malachite Green Incubation (25 °C, 30 minutes)

To improve the throughput of the screening method most compounds were tested in single assays (compounds from boxes 1, 2, 8-10), however some compounds were alternatively screened in duplicate (compounds from boxes 3-7). From the 838 compounds tested 12 were identified as primary hits, Table 4.2.

Hits were identified by the measured percentage inhibition (Equation 4.2). Here M denotes the mean of measured phosphate concentrations, signal denotes the negative control (100% RelA activity) and sample denotes the coupled enzyme assay in the presence of a compound).

Equation 4.2

$$\%\, Inhibition = 100 \times \left(\frac{M_{signal} - M_{sample}}{M_{signal}}\right)$$

These values were compared to the calculated hit statistical cut off (Equation 4.3- %Hco) for the respective microtitre plates (Table 4.2). SD here denotes the standard deviation for the signal (negative control- 100% RelA activity).

Equation 4.3

$$\%Hco = 100 \times \left(\frac{3 \times SD_{signal}}{M_{signal} - M_{Background}} \right)$$

Table 4.2. Primary hits from the screening of the Reynold's nucleotide library against *F. tularensis* RelA.

Box Number	Well Number	Compound (SRI Number)	Measured Percentage Inhibition (%)	Hit Statistical Cut Off (%)
1	F2	25505	43.25	13.78
	B4	25476	23.11	
	E5	25603	15.65	
7	E11	25665	57.10	21.37
	F11	25565	55.27	
	G11	25657	59.44	
	H11	25554	53.75	
9	A4	28080	10.01	8.42
	E8	27207	13.49	
	C8	25446	17.84	
	G6	28122	15.10	
	D6	28109	15.06	

All primary hits were screened in an identical fashion to that previously described to assess the reproducibility of inhibition. The majority of potential hits subsequently demonstrated no significant inhibition (Figure 4.24). Three compounds (Figure 4.25) however demonstrated a lower level of activity that was outside of the 3× standard deviation of the positive control average (Table 4.3).

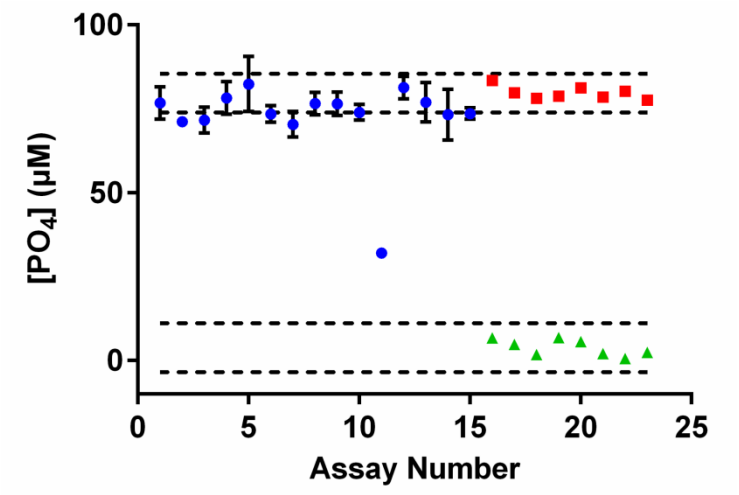

Figure 4.24. Repetition of screen for identified primary hits (Table 4.2). *F. tularensis* RelA and *E. coli* GppA assays (blue), positive *E. coli* GppA only controls (green) and negative *F. tularensis* RelA and *E. coli* GppA controls (red). Dashed lines indicate 3 × standard deviation of the mean for either positive or negative controls. Positive hits are identified as those which fall between the lower most line for the negative controls (red) and the upper most line for the positive controls (green).

Table 4.3. Secondary hits from the screening of the Reynold's nucleotide library against *F. tularensis* RelA.

Box Number	Well Number	Compound (SRI Number)	Measured Percentage Inhibition (%)	Hit Statistical Cut Off (%)
1	E5	25603	10.72	7.63
9	G7	28124	11.71	7.63
	F2	27745	59.76	7.63

Two of the compounds identified were uridine analogues (Figure 4.25b and c) and one was an adenine analogue (Figure 4.25a).

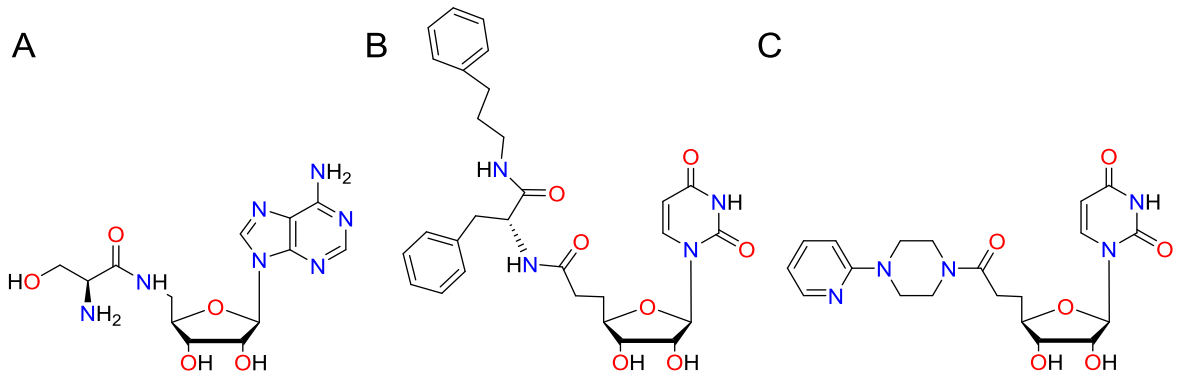

Figure 4.25. Chemical structure of the three identified secondary hits. (A) SRI number 25603 (B) SRI number 28124 (C) SRI number 27745.

The effect of the compounds 25603 and 28124 on *F. tularensis* RelA activity was further investigated at 10× the initial concentration tested (100 µM). Compound was incubated with both the coupled enzyme assay and the secondary enzyme (*E. coli* GppA) only. Activity was compared to positive controls (0% activity, corresponds to 100% inhibition) and negative controls (100% activity, corresponds to no inhibition) which contained no inhibitory compound. Neither compound displays inhibition of *F. tularensis* RelA activity

outside of the 3× deviation from the mean of negative controls (Figure 4.26). Disappointingly, these data suggest that these compounds were false positives.

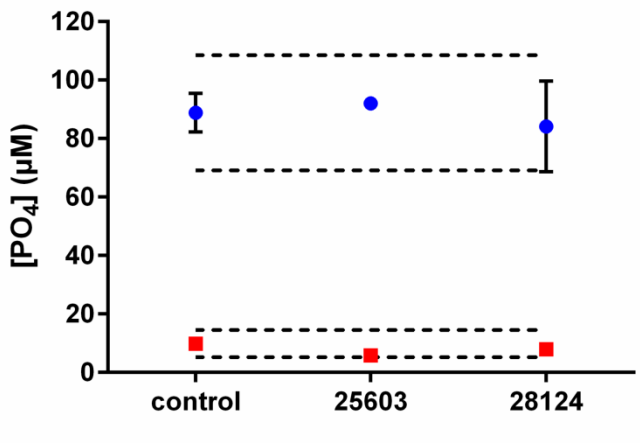

Figure 4.26. Rescreening secondary hits at a higher concentration (100 µM) against *F. tularensis* RelA. *F. tularensis* RelA, *E. coli* GppA enzyme coupled assay (blue) and *E. coli* GppA (red). Dashed lines indicate 3 × standard deviation of the mean for either coupled assay or control assay.

Analysis of the positive and negative controls across all the plates was used to obtain a generalised picture of consistency throughout the screening process (Figure 4.27a). The overall screening window had a calculated Z' value of 0.44, suggesting that this method requires further optimisation to achieve consistency across plates. Such high variability across plates could account in part for the false positive hits identified. A similar analysis of all the coupled assays in the presence of compounds showed five distinct groupings (Figure 4.27b). These groupings demonstrate a day to day variation, instead of a plate to plate variation, as the 21 plates were screened over a process of five days.

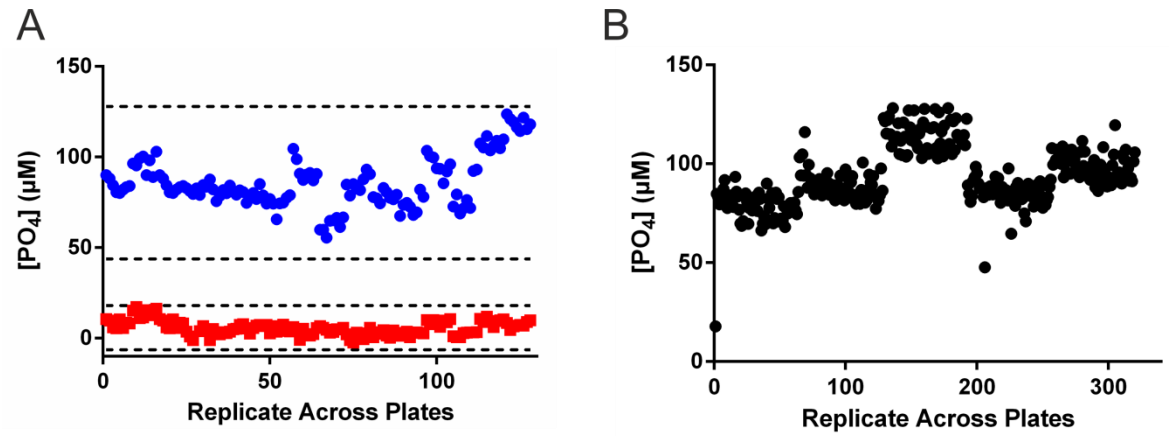

Figure 4.27. Consistency across HTS for *F. tularensis* RelA. (A) consistency of positive (red) and negative (blue) controls over time. Dashed lines indicate 3 × standard deviation of the mean for either positive (red) or negative (blue) controls. (B) Phosphate measurements of all coupled assays with test compounds.

4.5 Broadening the Application of the High Throughput Screen

With RelA enzymes from a variety of pathogenic bacteria demonstrating important roles in virulence [220, 250, 320], the possibility of broadening the parameters of this high throughput screen was of interest. Although the primary interest was to establish the potential for screening alternative RelA enzymes, the ability to interchange the secondary enzyme was equally of note. PPX enzymes have been also noted alongside Gpp enzymes for their ability to hydrolyse the terminal phosphate from pppGpp [239, 372]. The use of *E. coli* PPX as a substitute secondary enzyme for *E. coli* GppA was therefore investigated.

4.5.1 Expression and Purification of *E. coli* PPX

The *E. coli* MG1655 *ppx* gene was purchased from NBRP (ASKA Clone library, SHIGEN, Japan) in the plasmid pCA24N, carrying chloramphenicol resistance [375]. Digestion of the plasmid with the restriction SfiI (7.6.1.1) showed two bands corresponding to the vector and *ppx* gene (1.54 Kb) (Figure 4.28).

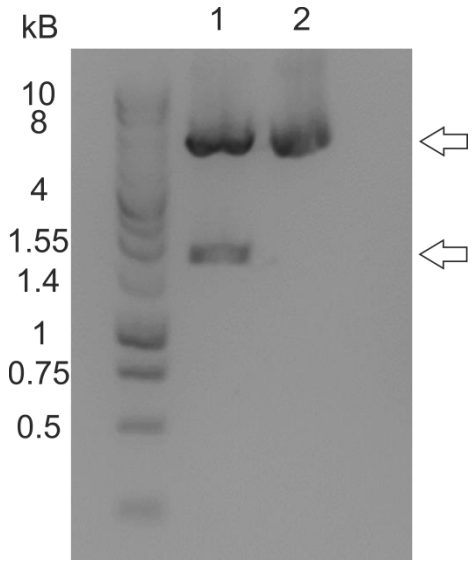

Figure 4.28. DNA gel electrophoresis of pCA24N::*Ec*ppx undigested (2) and following digestion with restriction enzyme SfiI (1). Arrows indicate the pCA24N vector (5.24 Kbp) and ppx insert (1.54 Kbp).

The *E. coli* his-tagged *ppx* gene was expressed at 27 °C for 4 hours as described by Kitagawa *et al*. [375] (7.6.3.1). Expression of PPX (5 L cell culture) yielded ~20 g cell paste. PPX was then purified initially by Nickel affinity chromatography (7.6.1.3), and further impurities removed by size exclusion chromatography (7.6.1.4).

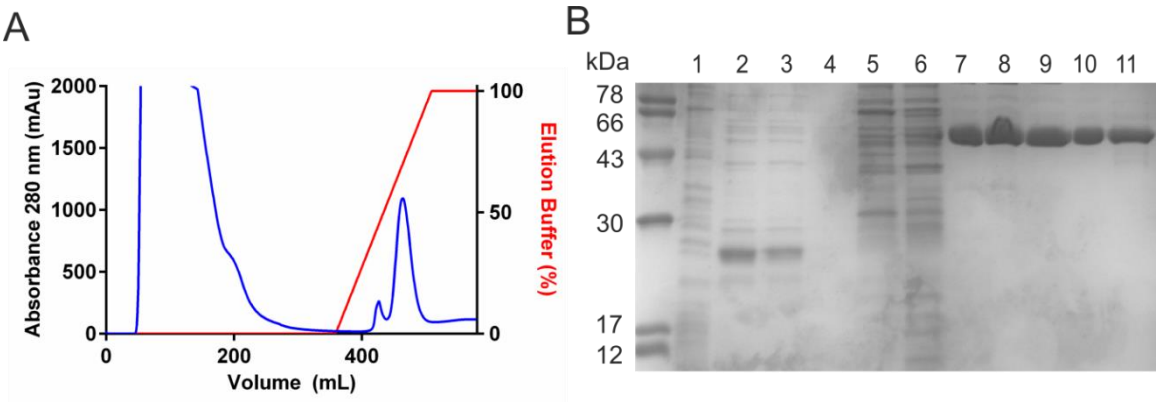

Figure 4.29. Purification of *E. coli* PPX (58 kDa) by Nickel affinity chromatography. (A) Absorbance trace at 280 nm (blue) over a gradient of elution buffer (red). (B) SDS-PAGE analysis of nickel affinity chromatography purification. Lane 1; cleared lysate, lane 2-11; fractions correlating to the eluate during gradient. Fractions 7-11 contain pure PPX (58 kDa).

SDS-PAGE analysis shows a high level of purity for PPX at both stages of purification, with histidine rich impurities eluting in a separate minor peak during nickel affinity chromatography (Figure 4.29).

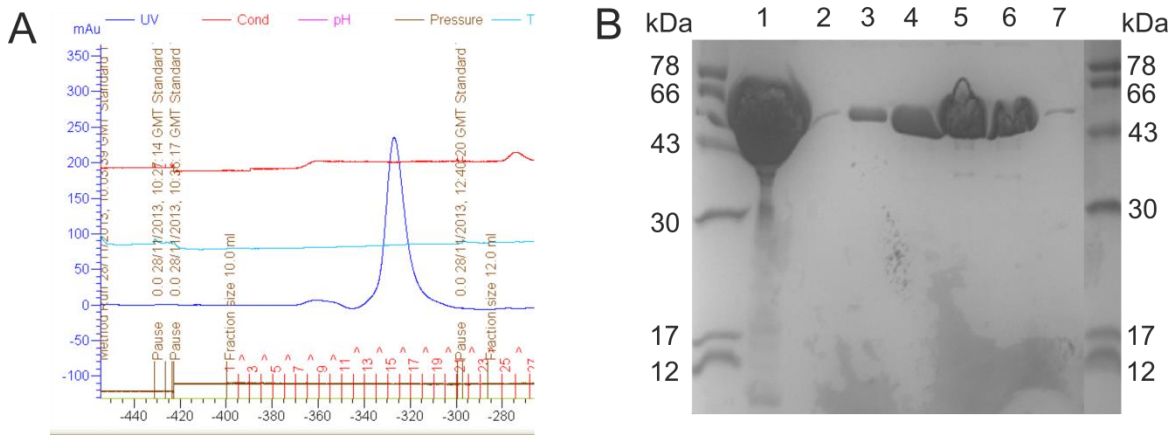

Figure 4.30. Purification of *E. coli* PPX by Size exclusion chromatography. (A) Absorbance 280 nm trace (B) SDS-PAGE analysis of fractions from size exclusion chromatography. Lanes: 1, concentrated nickel purified PPX; lane 2-7, eluate fractions. Lanes 3-6 contain purified *E. coli* PPX (58 kDa).

Final protein concentration following to both purification steps typically yielded 150-200 mg protein at a high level of purity as judged by SDS-PAGE analysis (Figure 4.30).

4.5.2 Substitution of the Secondary (Coupling) Enzyme

Substitution of *E. coli* GppA with *E. coli* PPX as a secondary enzyme (7.6.3.2) yielded similar results to previous experiments with *E. coli* GppA (Figure 4.31a) (4.3). The measured phosphate concentration for the *E. coli* PPX control however is slightly greater than that measured for *E. coli* GppA.

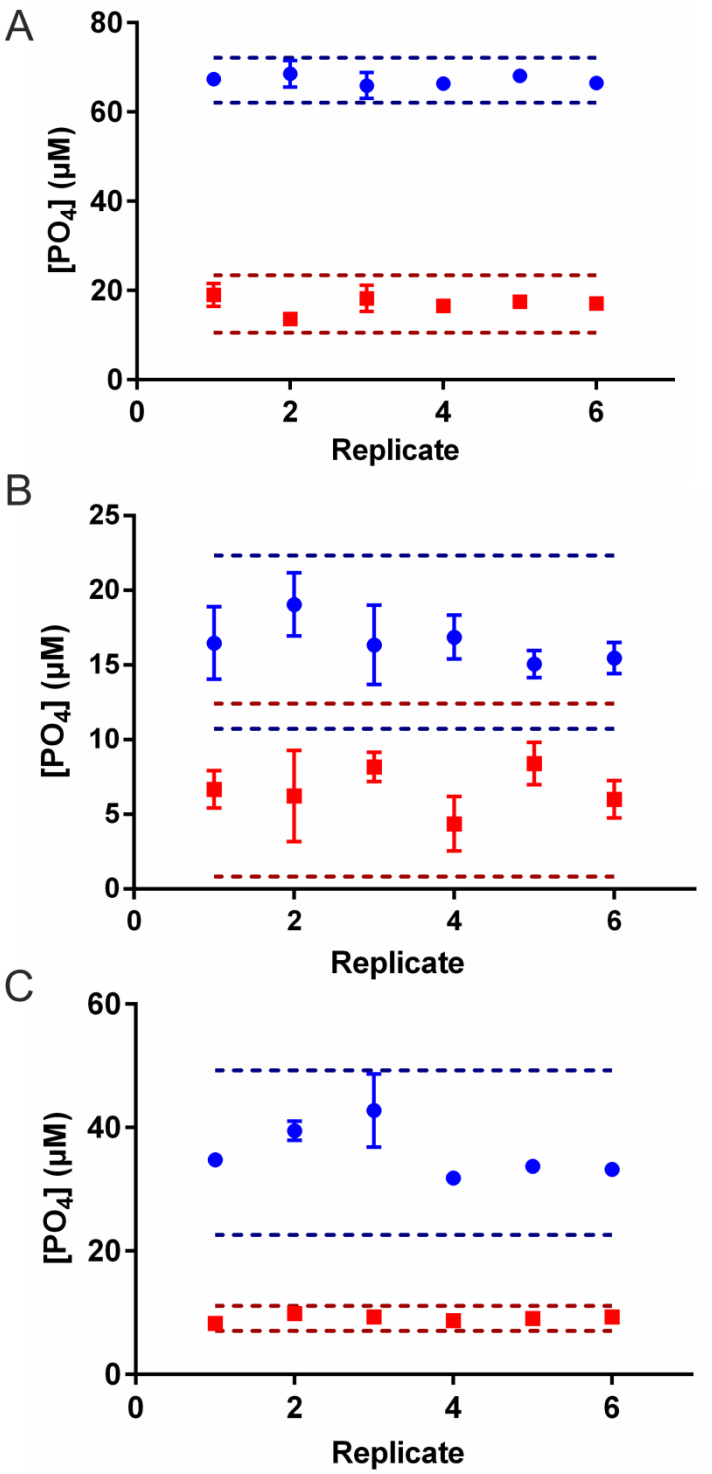

Figure 4.31. Broadening the application of the high throughput screen for RelA. (A) Activity of *F. tularensis* RelA (0.5 μM) coupled to *E. coli* PPX (0.02 μM) (blue) and *E. coli* PPX only (0.02 μM) (red). (B) Activity of *E. coli* RelA (0.5 μM) coupled to *E. coli* GppA (0.02 μM) (blue) and *E. coli* GppA only (0.02 μM) (red). (C) Activity of *B. pseudomallei* RelA (0.5 μM) coupled to *E. coli* GppA (0.02 μM) (blue) and *E. coli* PPX only (0.02 μM) (red). Dashed lines indicate 3 × standard deviation of the mean for either coupled assay or control assay.

4.5.3 **Substitution of the Primary Enzyme**

The alternative RelA enzymes from *E. coli* and *B. pseudomallei* were also substituted in the stead of *F. tularensis* RelA in a series of preliminary experiments (7.6.3.3). These coupled assays both demonstrated a greater phosphate concentration for the coupled assay than the control (Figure 4.31b and c), confirming the potential applicability of this technique for other RelA enzymes. The calculated Z' values of -0.17 and 0.43, for *E. coli* RelA and *B. pseudomallei* RelA respectively, however highlight the requirement of tailored method optimisation for individual RelA enzymes.

4.6 **Discussion**

The advent of high throughput screening has allowed the screening of large libraries of compounds for the inhibition of target enzymes. This method has distinct advantages over inhibitor design and synthesis. Such advantages include; the potential to screen many known compounds nearly simultaneously, the increased overall speed for inhibitor discovery, and an overall reduced cost. Current methods for analysing RelA activity however are all low throughput techniques [168, 295], and consequently a new detection method was required for high throughput screening of RelA enzymes. Previously identified inhibitors of RSH enzymes are only capable of inhibition when at high millimolar concentrations (1.6.6). Substrate analogues AMPPNP and ppApp have previously been shown to inhibit *E. coli* RelA [259, 291]. Following this observation we chose to investigate the effects of the nucleotide analogue AMPCPP and the dideoxy nucleotide ddGTP. The nucleotide analogue AMPCPP should not be accepted as a substrate for *F. tularensis* RelA due to the nonhydrolysable bond between the α and β phosphate. The dideoxy GTP should also not be a suitable substrate for *F. tularensis* RelA as there is no 3' hydroxyl group to attack the phosphate within ATP. We confirmed that *F. tularensis* RelA does not accept either of the substrate analogues ddGTP or AMPCPP (C.4) with neither products observed over time. Neither AMPPCP nor ddGTP however were able to competitively inhibit *F. tularensis* RelA pppGpp synthetase activity in the presence of it's substrates ATP and GTP (C.4). For this reason, these nucleotides were not suitable for use as standards for the high throughput screen in monitoring the inhibition of *F. tularensis* RelAThe advent of a high throughput technique for the screening of potential inhibitors would increase the chances of finding a more potent inhibitor which could then enter the process of drug development.

The products of RelA synthetase activity, (p)ppGpp, have been shown to both inhibit [167, 239] and activate [313] a range of targets within the cell. One such example of (p)ppGpp-mediated inhibition has been shown for the exopolyphosphatase enzyme PPX from *E. coli* [239]. The coupling of this enzyme with RelA for high throughput screening was not possible due to background levels of inorganic phosphate (the product of PPX activity) produced during *F. tularensis* RelA synthetase activity (2.5). In addition to PPX within *E. coli* the related enzyme GppA has been shown to hydrolyse the terminal 5' phosphate of the nucleotide guanosine pentaphosphate (p)ppGpp to produce ppGpp and inorganic phosphate [372]. As with the potential PPX coupled enzyme method, the GppA coupled enzyme method relies on the measurement of phosphate concentrations over time. This method however monitors the increase of phosphate concentration over time as GppA hydrolyses the pppGpp produced when RelA is active (Figure 4.1).

The enzyme GppA from *E. coli* was purified to a high level by nickel affinity and size exclusion chromatography (Figures 4.5 and 4.6) with typically high yields of ~50 mg/ L cell culture. As described by Hara *et al*. [372] the hydrolytic activity of the enzyme GppA was thought to be specific to the nucleotide pppGpp. ^{31}P NMR analysis of *E. coli* GppA incubated with RelA substrates ATP (2 mM) or GTP (2 mM) demonstrated GppA could slowly hydrolyse the terminal phosphate from GTP (0.067 μMs^{-1}) but not ATP (Figure 4.9). This is not to say that the previously published data is incorrect as the concentrations of substrates used in these assays were high. It is important however to note that the enzyme is capable of hydrolysing the substrate GTP at the relatively high concentrations that might be required in a RelA activity assay. This GppA-mediated GTP hydrolysis was shown to have an important impact on the background phosphate signal.

The hypothesised enzyme coupled assay was shown to work in practise by ^{31}P NMR analysis of *F. tularensis* RelA and *E. coli* GppA coupled assays (Figure 4.8 and 4.9). These data confirm that the enzyme GppA was capable of hydrolysing the 5' terminal phosphate of pppGpp, as shown by the disappearance of the pppGpp 5' β phosphate signal (Figure 4.8). Furthermore, the reaction occurs at low concentrations of GppA. In a reaction containing 5 µM *F. tularensis* RelA with 2 mM of each substrate as little at 0.05 µM *E. coli* GppA was required for complete turnover. With respect to the previous observation that the enzyme GppA is capable of hydrolysing the substrate GTP, utilisation of a low GppA concentration was advantageous in reducing the background signal.

4.6.1 **Development and Optimisation of the HTS**

Measurement of phosphate concentration is possible using several techniques including absorbance assays (malachite green [46], MESG [45]), radiolabelled assays (radiolabelled phosphate [295]), and fluorescence based assays [376]. The addition of malachite green reagent (7.6.1.7.1) to individual wells is suitable for end point assays as the reagent itself quenches the enzyme-catalysed reaction (by lowering the pH). The phosphate concentration is then calculated from the formation of phosphomolybdate malachite green complex, which result in a change in absorbance maxima (~ 430 - 640 nm) as the colour switches from canary yellow to green [373]. This technique is advantageous for high throughput screening as it allows for fast measurements based on a shift in the absorbance spectra of wells.

The enzyme coupled assay was therefore combined with this method of phosphate detection for further development. A linear relationship (R^2 of 0.97) was observed between A_{650} and the concentration of *F. tularensis* RelA (0.2 to 2.5 µM) (Figure 4.16). This relationship suggests that the coupled assay system is able to distinguish between different levels of *F. tularensis* RelA activity. Such a relationship is a pre-requisite for the development of a high throughput screen. Higher concentrations of *F. tularensis* RelA such as 2.5 and 5 µM displayed a greater degree of error within A_{650} measurements (C.3). This suggested an upper limit for the concentration of *F. tularensis* RelA enzyme used for high throughput screening. A lower enzyme concentration reduces the overall cost of screening. Analysis showed a good screening window for as low as 500 nM *F. tularensis* RelA (Z' of 0.72) for a single 96 well microtitre plate. Analysis of lower concentrations more akin to those usually used for high throughput screens [43] such as 100 nM *F. tularensis* RelA, yielded an absorbance value similar to that for background signals (A_{650} < 0.0) (Figure 4.16). The higher concentration of *F. tularensis* RelA (500 nM) used during screening accommodated the relatively slow rate of (p)ppGpp synthetase activity in the absence of activating factors (i.e.; ppGpp or stalled ribosomes).

As expected the variation of *E. coli* GppA concentration (0-2 µM) demonstrated little to no variation in the recorded phosphate concentration. The formation of inorganic phosphate by *F. tularensis* RelA has been observed previously (2.5). It is therefore likely that either *F. tularensis* RelA is capable of hydrolysing the 5' terminal phosphate from pppGpp itself, or that there is trace amounts of *E. coli* GppA co-purifying with the enzyme.

The latter of these explanations is supported by the observation that the activity leading to the formation of phosphate varies between batches of purified *F. tularensis* RelA. The incorporation of a low level of *E. coli* GppA into the coupled assay therefore ensured the consistency of complete pppGpp turnover across batches of purified RelA.

The buffer conditions for the enzyme coupled assay were altered for optimal activity, whilst retaining some similarity to that used for *F. tularensis* RelA kinetic characterisation for consistency. The addition of bovine serum albumin, used to prevent non-specific binding of enzymes, improved phosphate measurements for both the coupled assay and the control assay (Figure 4.19). Dimethylsulfoxide (DMSO) unexpectedly demonstrated a stabilisation of phosphate measurements for the coupled assay (Figure 4.20). DMSO is not reported to have an effect on malachite green reagent, therefore this observation must relate to the activity of *F. tularensis* RelA. Optimisation of the buffer conditions showed little to mild increase in phosphate concentration upon the increase of Tris, KCl or β- Me concentrations within the buffer (Figure 4.18). Conversely a 1.7 fold increase in phosphate production is observed when the $MgCl_2$ concentration is doubled. The high requirement of $MgCl_2$ could correlate to the requirement of both enzymes for Mg^{2+} ions, however 30 mM is greater than that typically observed within a cell (15-25 mM) [381, 382].

Time course analysis determined reproducible linearity for the coupled assay over time up to 120 minutes. Conversely the control assays demonstrated little to no variation in phosphate concentrations over time. Within this linear range, at 90 minutes there was a good difference between the coupled assay and the control assay. Optimised conditions were tested prior to the use of the developed HTS for compound screening. Analysis of these assays demonstrated that the positive control (0 % *F. tularensis* RelA activity) gave phosphate concentrations with an average of 5.9 ± 0.36 µM and negative controls (100 % *F. tularensis* RelA activity) had an average of 85.9 ± 1.24 µM yielding a screening window with an average Z' of 0.77 ± 0.012.

4.6.2 **High Throughput Screening**

A library of 838 nucleotide analogues synthesised by the laboratory of Dr. R. C. Reynolds [380] were screened against *F. tularensis* RelA using the HTS described above. The screening of compound libraries typically occurs at low concentrations of compounds

within the range 3-30 µM [383-385]. The screening of this library at 10 µM of compound demonstrated 12 primary hits, identified by the measured phosphate concentration falling outside of the 3× standard deviation from both the positive and negative controls (screening window) (Table 4.1). A repeat screen of each of these potential hits against the enzyme *F. tularensis* RelA using the HTS reduced the number of potential hits to three (Figure 4.25). A further screen of two of these compounds (28124 and 25603) at a higher concentration (100 µM) however demonstrated *F. tularensis* RelA activity within the range of the negative controls (Figure 4.26). Here we have described the screening of RelA with a focussed library, targeting nucleotide binding sites with nucleotide analogues. Screening of such focussed libraries are not guaranteed to produce initial hits, and full scale screening efforts often test hundreds of thousands of compounds [42]. It is therefore disappointing, but perhaps not too surprising that the described *F. tularensis* RelA screen produced no hits.

All 96 well plates demonstrated a good screening window from their respective controls. Further analysis of the controls as a collective however demonstrated a spread of phosphate concentrations which could be grouped into 5 sections (relating to day of analysis). This suggests that the measured phosphate concentration shows poorer consistency across days.

The detection of phosphate by the addition of malachite green reagent is commonly reported at room temperature ~ 25 °C [46, 373]. Visually the formation of precipitated malachite green however appears to increase at higher temperatures. The effect of the ambient temperature on the precipitation of malachite green is therefore a possible explanation for this day to day variation. Incubation temperature following the addition of malachite green reagent was subject to variation based on the ambient temperature due to the absence of a cooling unit within the plate reader in out laboratory (BMG POLARstar Omega, Labtech).

4.6.3 **Broadening the HTS**

F. tularensis RelA is one of many potential RelA or even RSH enzyme based antibacterial drug targets worth exploring. The novel HTS, described above, might provide a platform for the identification of inhibitors against a wide range of RSH enzymes that accept GTP as a pyrophosphate acceptor. Initial work at broadening the HTS determined the potential

use of *E. coli* PPX as an alternative secondary enzyme. This enzyme allowed a good screening window (Z' value of 0.77) to be observed when coupled with *F. tularensis* RelA but should be noted that a higher background signal was observed. This suggests that other members of the PPX/GppA family of proteins would equally work well as a secondary enzyme in this HTS system.

Initial work in broadening the use of this HTS system for other RSH enzymes looked at the use of either *E. coli* or *B. pseudomallei* RelA as primary enzymes. It should be noted that this preliminary research was completed under conditions optimised for *F. tularensis* RelA and therefore results for these alternative enzymes were likely to be suboptimal. Despite a poor screening window observed for both enzymes, with Z' values of -0.17 and 0.42, the coupled enzyme assays consistently demonstrated a higher measured phosphate concentration than control assays. The conditions described for the *F. tularensis* RelA, *E. coli* GppA coupled HTS method are therefore not currently best suited for alternative RelA enzymes. These results however suggest that with tailored method optimisation for individual RelA enzymes the HTS method described could indeed be broadened.

Chapter 5: **Initial Characterisation of *Yersinia pestis* and *Burkholderia pseudomallei* RelA Enzymes**

Further to *Francisella tularensis*, the causative agent of tularemia, the organisms *Yersinia pestis* and *Burkholderia pseudomallei* are also classed as potential biowarfare agents (1.2.1.1, 1.2.1.2). Knockout mutants in these species demonstrated attenuation in murine models [250, 320] and were considered for potential vaccine strains. Collectively these data suggest that inhibitors of the RelA enzymes from these species would be of interest. Increased understanding of a breadth of RelA enzymes will allow for a more comprehensive picture of how this class of enzyme work. This is of particular importance as current literature almost exclusively focuses on the characterisation of *E. coli* RelA (1.6). Characterisation and purification of these enzymes is therefore of interest with respect to medical applications and improving understanding of the enzyme class.

Both *Y. pestis* and *B. pseudomallei* RelA are similar in size to *E. coli* RelA at 84 and 82 kDa respectively. Furthermore the synthetase active site motifs for both *Y. pestis* and *B. pseudomallei* are EXDD, as is found in *E. coli* RelA enzymes (Figure 2.2).

5.1 ***Yersinia pestis* RelA**

5.1.1 **Gene Design for *Y. pestis relA***

The *relA* gene from *Yersinia pestis* strain CO92 was designed to encode an N-terminal hexahistidine tag (D.1). A synthetic modified gene was sourced commercially and ligated into the plasmid pET16b (D.2). Restriction analysis of the plasmid pET16b::*Yp*relA with the restriction enzymes NcoI and XhoI (7.3.7) confirmed the presence of the *YprelA* gene with bands corresponding to the expected pET16b vector (5.71 Kb) and *YprelA* gene (2.24 Kb) (Figure 5.1).

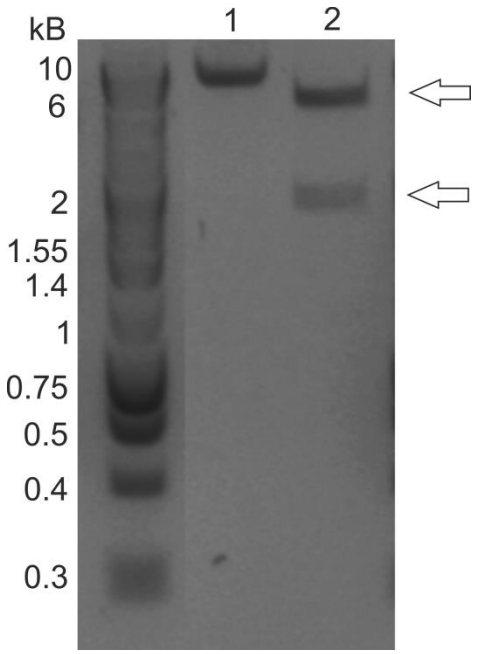

Figure 5.1. DNA gel electrophoresis of pET16b::*Yp*relA undigested (1) and following digestion with restriction enzymes NcoI and XhoI (2). Arrows indicate the pET16b vector (5.71 Kbp) and *Yp*relA insert (2.24 Kbp).

5.1.2 **Small Scale Expression Studies of *Y. pestis* RelA**

The pET16B::*Yp*relA plasmid was transformed into *E. coli* BL21 (DE3) cells by chemical transformation (7.3.4) for protein expression. To achieve maximal yield of *Y. pestis* RelA, small scale expression studies were utilised to analyse the optimal conditions for the overexpression of this protein. Parameters altered include the incubation time and temperature from induction to harvesting cells. Small scale cultures were maintained at the temperatures 37, 27 or 16 °C for either 3 hours or overnight (7.7.1), and were compared to *E. coli* BL21 (DE3) cells containing pET16B or *E. coli* BL21 (DE3) Rosetta pET16B::*Ft*relA by SDS-PAGE analysis (7.3.1). A strong band could be observed for *Y. pestis* RelA (84 kDa) within the soluble fraction when the protein was expressed at 27 °C for either 3 hours or overnight (16-20 hours) (Figure 5.2a). A discernible band for *Y. pestis* RelA could not however be observed following expression at 16 °C overnight (Figure 5.2b). When expressed at 37 °C for 3 hours the majority of the *Y. pestis* RelA appeared to be present in the insoluble fraction with only a weak band observed within the soluble fraction (Figure 5.2c).

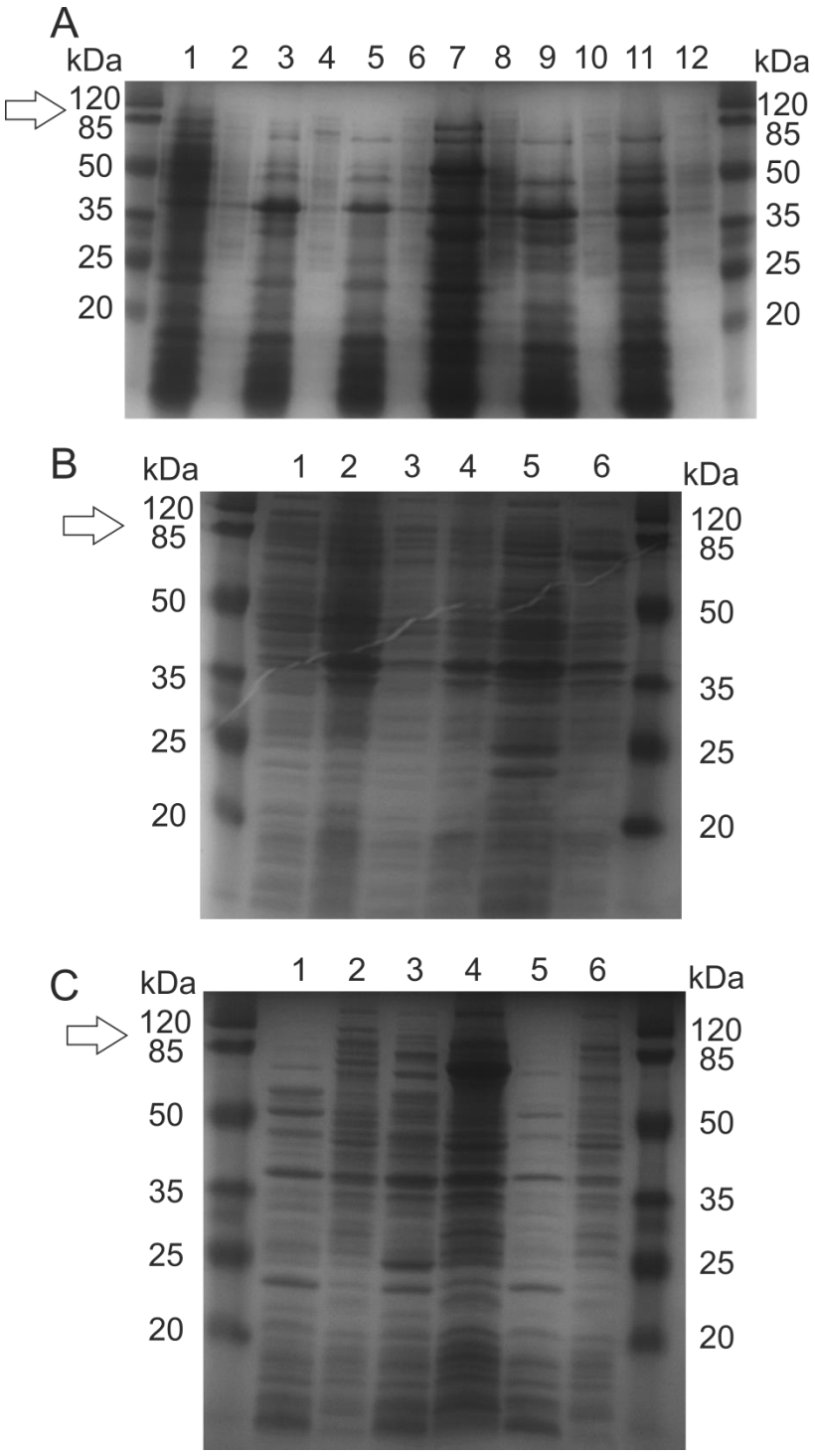

Figure 5.2. SDS-PAGE analysis of *Y. pestis* RelA small scale expression studies. (A) Lanes 1-6; expression at 27 °C for 3 hours for *Y. pestis* RelA (1 and 2), *F. tularensis* RelA (3 and 4), and the empty vector (5 and 6). Lanes 7-12; expression at 27 °C overnight for *Y. pestis* RelA (7 and 8), *F. tularensis* RelA (9 and 10), and the empty vector (11 and 12). (B) Expression at 16 °C overnight for *Y. pestis* RelA (lanes 1 and 2), the empty vector (3 and 4) and *F. tularensis* RelA (5 and 6). (C) Expression at 37 °C for 3 hours for *Y. pestis* RelA (lanes 1 and 2), the empty vector (3 and 4) and *F. tularensis* RelA (5 and 6). Odd numbered lanes correspond to soluble protein fractions and even numbered lanes correspond to insoluble protein fractions. Arrow indicates *Y. pestis* RelA (84 kDa).

The process of auto-induction in protein expression has several advantages over the alternative induction of expression with inducing factors such as IPTG. Auto-induction media monopolises the diauxic growth of *E. coli* strains, whereby they will only utilise lactose as a carbon source after consuming all other preferred carbon sources available [386]. This natural switch in carbon source results in the induction of genes under the lac promoter (i.e.; in a pET vector) [344, 386]. The overexpression of the *E. coli relA* gene with IPTG has been shown to result in the accumulation of high ppGpp levels, with 200 µM IPTG suggested to induce synthesis of similar levels to that observed during the stringent response [155]. With this in mind the use of auto-induction [386] for protein expression was of interest. SDS-PAGE analysis of small scale auto-induction (7.7.2) of *Y. pestis* RelA showed poor expression levels of this protein, (Figure 5.3).

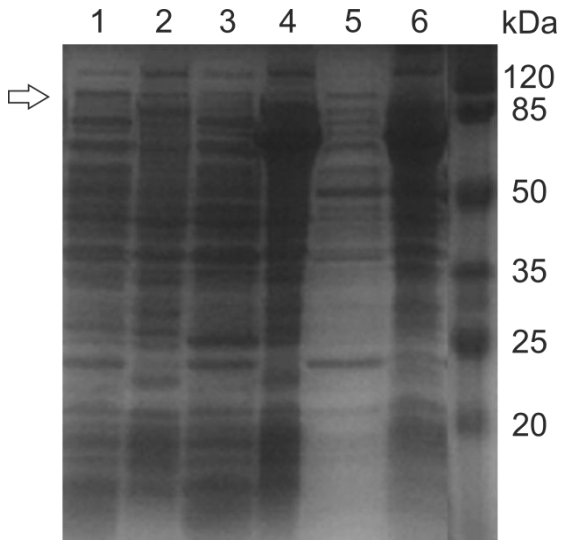

Figure 5.3. SDS-PAGE analysis of *Y. pestis* RelA small scale expression using auto induction media; the empty vector (Lanes 1 and 2), *F. tularensis* RelA (Lanes 3 and 4) and *Y. pestis* RelA (Lanes 5 and 6). Odd numbered lanes correspond to soluble protein fractions and even numbered lanes correspond to insoluble protein fractions. Arrow indicates *Y. pestis* RelA (84 kDa).

Collectively these data suggest that the expression of *Y. pestis* RelA in *E. coli* BL21 (DE3) cells is optimal when cultures are maintained at 27 °C for 3 hours.

5.1.3 Large Scale Expression and Purification of *Y. pestis* RelA

5.1.3.1 Expression of *Y. pestis* RelA

For large scale expression (5 L) of *Y. pestis* RelA cultures of *E. coli* BL21 (DE3) pET16b::*Yp*relA were incubated at 27 °C for 3-4 hours post induction (7.7.3), with a typical cell pellet of 6.08 ± 1.22 g/L cell culture.

5.1.3.2 Purification of *Y. pestis* RelA by Nickel Affinity Chromatography

Y. pestis RelA was initially purified by Ni-IDA affinity chromatography (7.7.4), utilising an imidazole gradient of 10 to 500 mM over 8 column volume, with imidazole removed by dialysis (7.4.3). The purification method resulted in the recovery of ~60 mg of purified RelA from 6.08 ± 1.22 g of cells. Similarly to that described for *E. coli* GppA previously (4.2.1) purification of *Y. pestis* RelA by this technique yielded two elution peaks (Figure 5.4a). SDS-PAGE analysis (7.3.1) revealed the initial peak contained no *Y. pestis* RelA (84 kDa) but instead contained a range of *E. coli* proteins (Figure 5.4b). The second peak however corresponded to *Y. pestis* RelA at an equal purity to that observed for *F. tularensis* RelA at this stage of purification (2.1.2, Figure 5.4). Routinely Ni-IDA purified *Y. pestis* RelA could be concentrated (7.4.4) to 3.7 mg/mL without precipitation, concentrating further however resulted in precipitation.

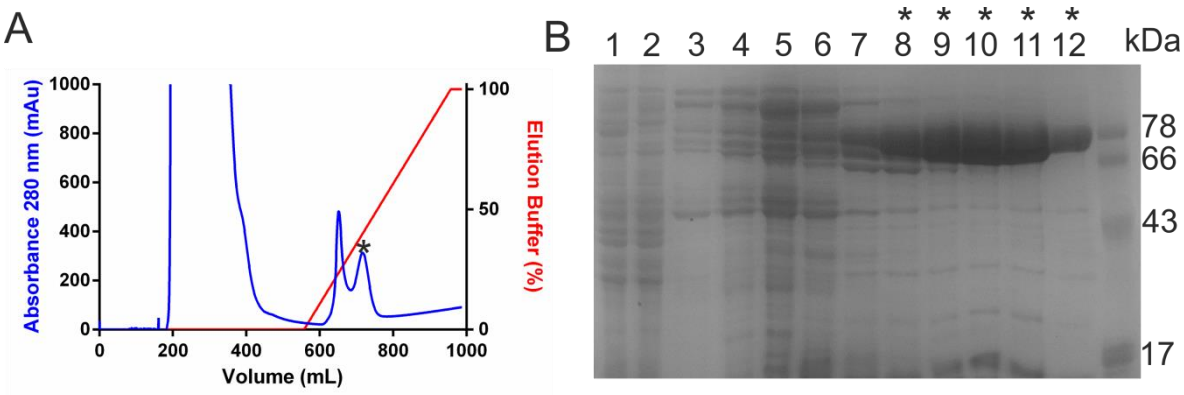

Figure 5.4. Purification of *Y. pestis* RelA (84 kDa) by nickel affinity chromatography (A) Absorbance 280 nm trace (B) SDS-PAGE analysis of fractions from nickel affinity chromatography. Lanes: 1, cleared lysate; 2, flow through; 3-12, eluate fractions from Ni-IDA chromatography. Lanes marked with * correspond to the similarly marked peak in (A).

5.1.3.3 Purification of *Y. pestis* RelA by Size Exclusion Chromatography

Y. pestis RelA was further purified by size exclusion chromatography (7.7.5) on a Superdex 200 (HiLoad 26/60, prep grade). Purification reproducibly yielded three main peaks (Figure 5.5a), with the largest peak attributable to *Y. pestis* RelA as judged by SDS-PAGE (7.7.5) (Figure 5.5b). Purified *Y. pestis* RelA (average yield ~26 mg) could be concentrated to ~1-2 mg/mL prior to the observation of any protein precipitation.

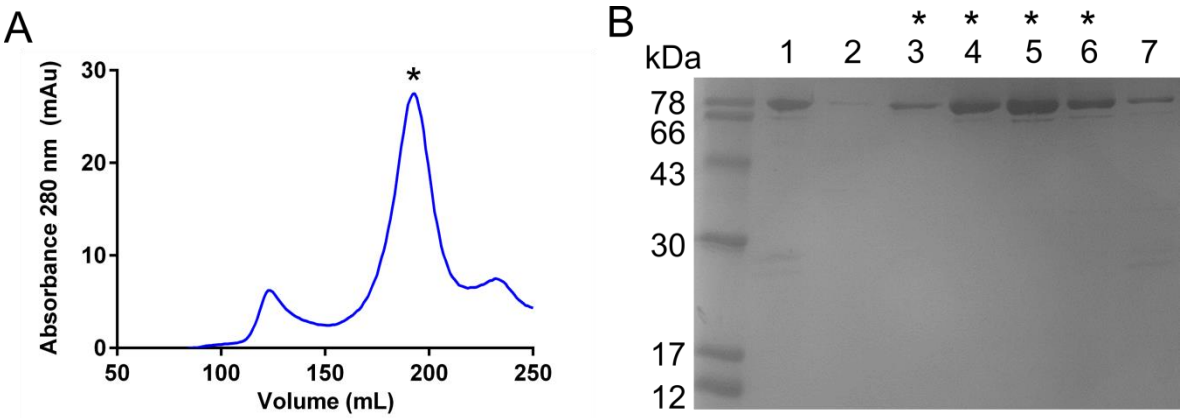

Figure 5.5. Purification of *Y. pestis* RelA (84 kDa) by size exclusion chromatography (A) Absorbance 280 nm trace (B) SDS-PAGE analysis of fractions from size exclusion chromatography. Lane 1, loaded protein, lanes 2-7, eluate fractions from size exclusion chromatography. Lanes marked with * correspond to the similarly marked peak in (A).

5.1.4 Substrate Specificity of *Y. pestis* RelA

Previous analysis of *F. tularensis* RelA revealed an absolute specificity for GTP as a pyrophosphate acceptor (2.3), making the substrate specificity of *Y. pestis* RelA of note. End-point *Y. pestis* RelA activity assays (7.7.6) were prepared with *Y. pestis* RelA, ATP and either GDP or GTP, and analysed by ion pair reverse phase HPLC. Efficient formation of AMP and the 3'-pyrophosphorylated product were observed in the presence of either GDP or GTP as a co-substrate (Figure 5.6). This demonstrated that *Y. pestis* did not have the same substrate specificity to that observed for *F. tularensis* RelA.

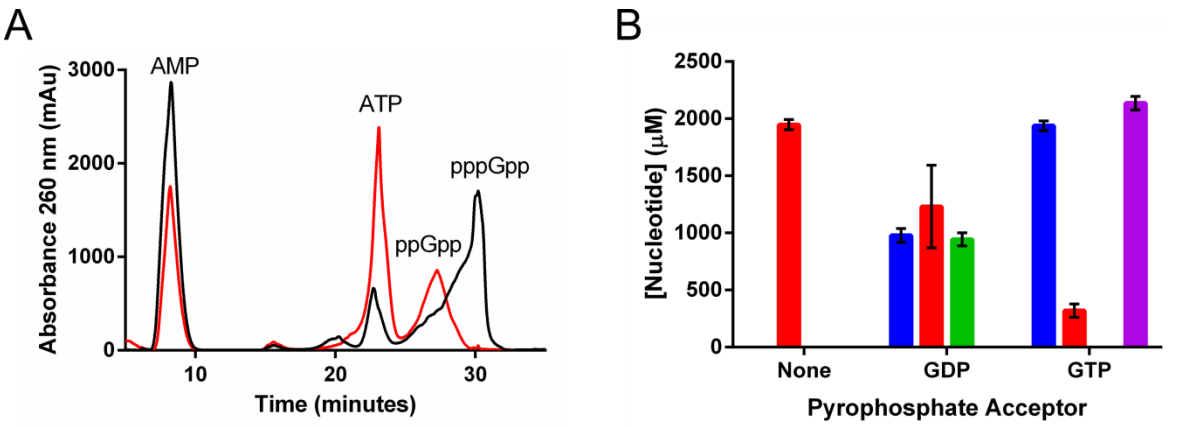

Figure 5.6. IP RP HPLC analysis (7.4.8.4) of *Y. pestis* RelA substrate specificity. (A) HPLC trace for *Y. pestis* RelA assays in the presence of GDP (red trace) or GTP (black trace) as the pyrophosphate acceptor. (B) Concentration of AMP (blue), ATP (red), ppGpp (green) and pppGpp (purple) in the presence of indicated pyrophosphate acceptor.

These end point assays were used to derive preliminary rates for the production of ppGpp and pppGpp from GDP and GTP respectively. Comparison of these rates, 0.26 µM s^{-1} and 0.59 µM s^{-1} for ppGpp and pppGpp respectively, interestingly indicates a preference for GTP as the primary pyrophosphate acceptor. Such an observation contradicts the previous claims that the RelA synthetase active site motif EXDD dictates the pyrophosphate preference. Further kinetic characterisation of the RelA enzyme from *Y. pestis*, including substrate saturation curves, could elucidate the precise nature of this bias and would provide support to this initial observation.

5.2 *Burkholderia pseudomallei* RelA

5.2.1 Gene Design for *B. pseudomallei relA*

The *relA* gene from *Burkholderia pseudomallei* was designed to encode an N-terminal hexahistidine tag (D.3). A synthetic modified gene was sourced commercially and ligated into the plasmid pET16b (D.4). Confirmation of the *Yp*relA gene was achieved by the restriction analysis of the plasmid pET16b::*Bp*relA with the restriction enzymes NcoI and XhoI (7.3.7) which yielded a band corresponding to the expected pET16b vector (5.71 Kb) and *BprelA* gene (2.24 Kb) (Figure 5.7).

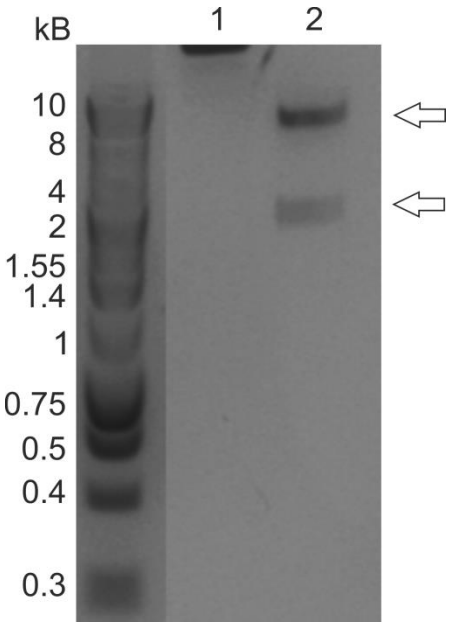

Figure 5.7. DNA gel electrophoresis (7.3.3) of pET16b::*BprelA* undigested (1) and following digestion with restriction enzymes NcoI and XhoI (2). Arrows indicate the pET16b vector (5.71 Kbp) and *BprelA* insert (2.24 Kbp).

5.2.2 **Small Scale Expression Studies of *B. pseudomallei* RelA**

The pET16B::*BprelA* plasmid was transformed into *E. coli* BL21 (DE3) cells by chemical transformation (7.3.4) for protein expression. To achieve maximal yield of *B. pseudomallei* RelA, small scale expression studies were devised to analyse the optimal conditions for the overexpression of this protein. Parameters altered included the incubation time and temperature from the point of IPTG induction to the harvesting of cells. Small scale cultures were maintained at the temperatures 37, 27 or 16 °C for either 3 hours or overnight (7.7.7), and were compared to *E. coli* BL21 (DE3) cells containing pET16B or *E. coli* BL21 (DE3) Rosetta pET16B::*Ft*relA by SDS-PAGE analysis (7.3.1).

When expressed at 16 °C overnight the resultant soluble and insoluble fractions both demonstrated very weak bands corresponding to *B. pseudomallei* RelA (82 kDa) (Figure 5.8a). No visible band was observable in either fraction when the protein was expressed at 27 °C overnight (Figure 5.8b) or by auto-induction (Figure 5.9). Alternatively soluble *B. pseudomallei* RelA could be observed when expressed at 27 °C for 3 hours (Figure 5.8b).

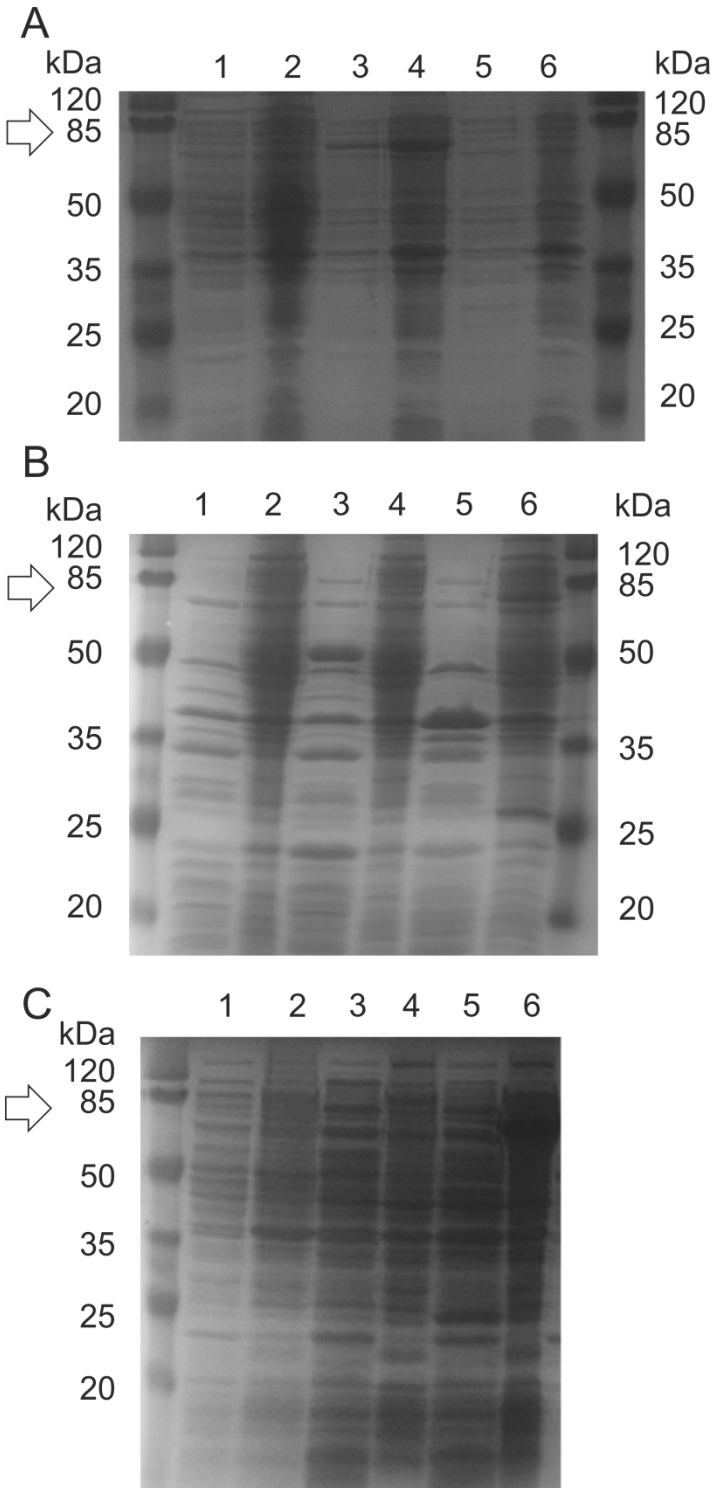

Figure 5.8. SDS-PAGE analysis of *B. pseudomallei* RelA small scale expression studies. (A) Expression at 16 °C overnight for *B. pseudomallei* RelA (1 and 2), *F. tularensis* RelA (3 and 4), and the empty vector (5 and 6). (B) Expression at 27 °C overnight for the empty vector (lanes 1 and 2), *B. pseudomallei* RelA (3 and 4) and *F. tularensis* RelA (5 and 6). (C) Expression at 37 °C for 3 hours for *B. pseudomallei* RelA (lanes 1 and 2), the empty vector (3 and 4) and *F. tularensis* RelA (5 and 6). Odd numbered lanes correspond to soluble protein fractions and even numbered lanes correspond to insoluble protein fractions. Arrow indicates *B. pseudomallei* RelA (82 kDa).

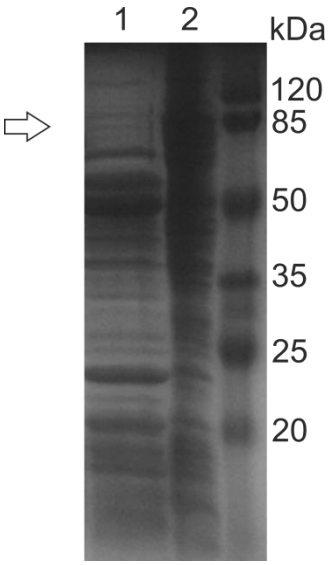

Figure 5.9. SDS-PAGE analysis of *B. pseudomallei* RelA small scale expression using auto induction media. Lane 1; soluble protein fraction, Lane 2; insoluble protein fraction. Arrow indicates *B. pseudomallei* RelA (82 kDa).

Collectively these data suggest that the expression of *B. pseudomallei* RelA in *E. coli* BL21 (DE3) cells is optimal when cultures are maintained at 27 °C for 3 hours.

5.2.3 Large Scale Expression and Purification of *B. pseudomallei* RelA

5.2.3.1 Expression of *B. pseudomallei* RelA

For large scale expression (5 L) of *B. pseudomallei* RelA cultures of *E. coli* BL21 (DE3) pET16b::*Bp*relA were incubated at 27 °C for 3-4 hours post induction (7.7.8), with a yield of 6.22 g/L cell culture.

5.2.3.2 Purification of *B. pseudomallei* RelA by Nickel Affinity Chromatography

B. pseudomallei RelA was initially purified by Ni-IDA affinity chromatography (7.7.9), utilising an imidazole gradient of 20 to 500 mM over 8 column volumes, with imidazole removed by dialysis (7.4.3). The purification method resulted in the recovery of ~26 mg of RelA from 6.22 g of cells. *B. pseudomallei* RelA was observed to co-purify with an exorbitant number of *E. coli* proteins, with no distinctly prominent band corresponding to RelA (82 kDa) (Figure 5.10). Routinely Ni-IDA purified *B. pseudomallei* RelA could be concentrated (7.4.4) to 3 mg/mL prior to the observation of protein precipitation.

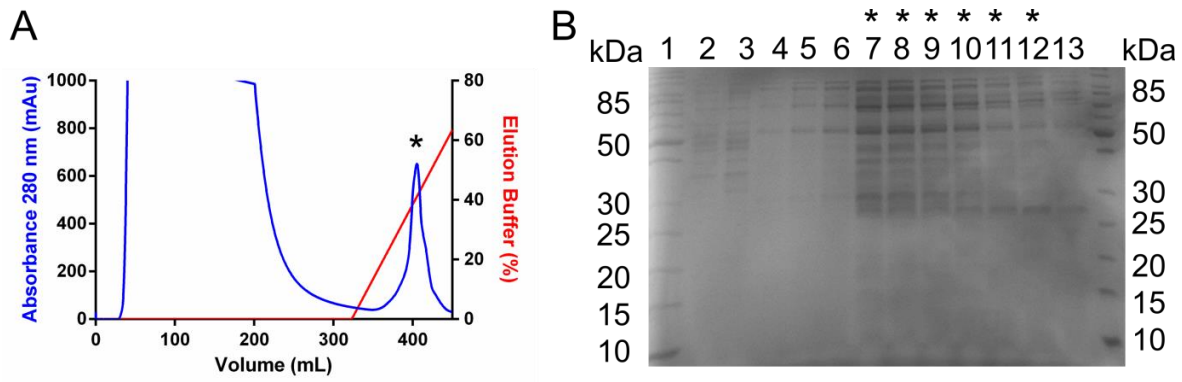

Figure 5.10. Purification of *B. pseudomallei* RelA (82 kDa) by nickel affinity chromatography (A) Absorbance 280 nm trace (B) SDS-PAGE analysis of fractions from nickel affinity chromatography. Lanes: 1, cleared lysate; 2, flow through; 3-13, eluate fractions from Ni-IDA chromatography. Lanes marked with * correspond to the similarly marked peak in (A).

5.2.3.3 Purification of *B. pseudomallei* RelA by Size Exclusion Chromatography

B. pseudomallei RelA was further purified by size exclusion chromatography (7.7.5) on a Superdex 200 (HiLoad 26/60, prep grade). Purification yielded no distinct peaks for pure *B. pseudomallei* RelA as judged by absorbance at 280 nm and SDS-PAGE analysis (7.3.1) (Figure 5.11).

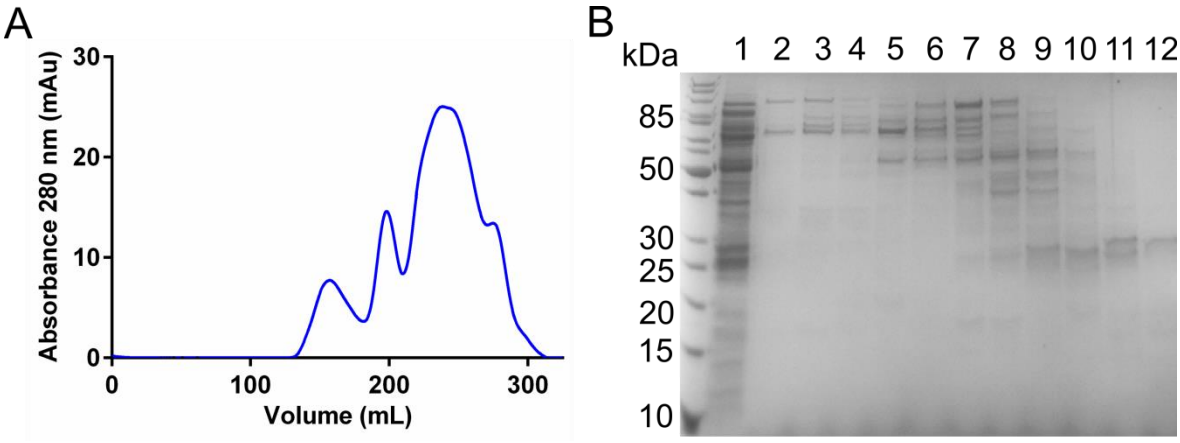

Figure 5.11. Purification of *B. pseudomallei* RelA (82 kDa) by size exclusion chromatography (A) Absorbance 280 nm trace (B) SDS-PAGE analysis of fractions from size exclusion chromatography. Lane 1, loaded protein, lanes 2-7, eluate fractions from size exclusion chromatography.

5.2.4 Substrate Specificity of *B. pseudomallei* RelA

Specificity of *B. pseudomallei* RelA for either GDP or GTP as a pyrophosphate acceptor was investigated. End-point *B. pseudomallei* RelA activity assays (7.7.10) were prepared with *B. pseudomallei* RelA, ATP and either GDP, GTP or CTP, and analysed by ion pair reverse phase HPLC (7.4.8.4). Efficient formation of AMP and the 3'-pyrophosphorylated product were observed in the presence of either GDP or GTP as a co-substrate (Figure 5.12), but not in the presence of CTP (Figure 5.12). This demonstrated that like *Y. pestis* RelA, *B. pseudomallei* RelA also did not display specificity for its pyrophosphate acceptor.

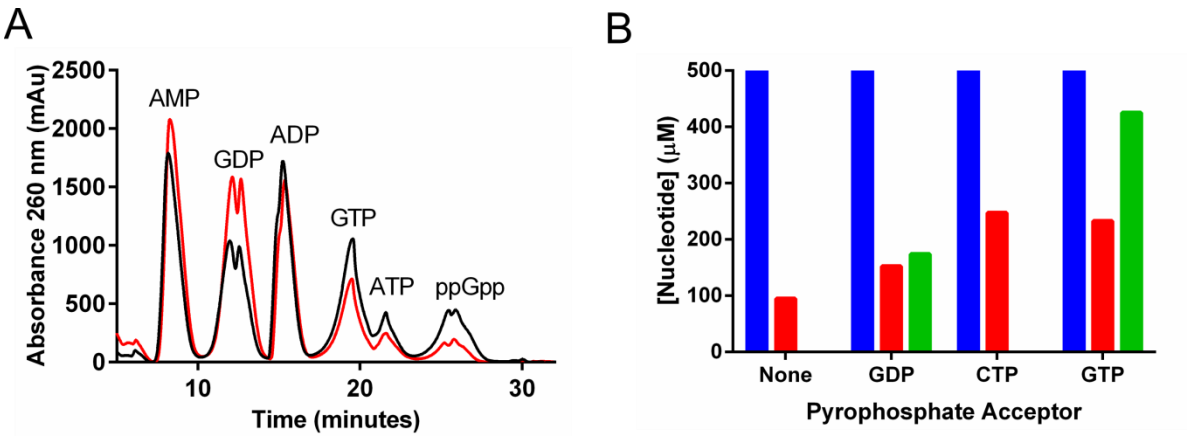

Figure 5.12. IP RP HPLC analysis (7.4.8.4) of *B. pseudomallei* RelA substrate specificity. (A) HPLC trace for *B. pseudomallei* RelA assays in the presence of GDP (red trace) or GTP (black trace) as the pyrophosphate acceptor. (B) Concentrations of the nucleotides AMP (blue), ATP (red), (p)ppGpp (green) from a 1 hour end point assay.

Following the previous observation with *Y. pestis* RelA, end point assays were used to derive primitive rates of production of ppGpp and pppGpp from GDP and GTP respectively. Comparison of these rates, 0.048 µM s^{-1} and 0.11 µM s^{-1} for ppGpp and pppGpp respectively, interestingly indicated a preference for GTP as the primary pyrophosphate acceptor. Given the high turnover of initial substrates, presumably by contaminating phosphatases, the rates determined should be treated as estimates only. Further optimisation of *B. pseudomallei* RelA purification will be required for a more accurate interpretation of its substrate bias or kinetic properties.

5.3 Discussion on the RelA enzymes from *B. pseudomallei* and *Y. pestis.*

As previously discussed (1.6.5) *relA* knockout mutants in both *B. pseudomallei* and *Y. pestis* have been investigated as potential vaccine candidates. This largely relates to the observed attenuation within these mutants of these potential biowarfare agents [250, 320]. For this reason the discovery of inhibitory compounds against these enzymes, such as for *F. tularensis* RelA, is of potential interest.

As described previously in Chapter 2, the expression and purification of *E. coli* RelA carries several complications including a high precedence for precipitation, an ability to adhere to laboratory equipment and a steep reduction of activity from freeze-thaw cycles [313]. The RelA enzymes from *Y. pestis* and *B. pseudomallei* do not contain the truncated C-terminal and unusual synthetase active site motif previously described for *F. tularensis* RelA (2.2). The small scale expression studies detailed showed optimal expression of soluble *Y. pestis* RelA at 27 °C for 4 hours, with similar levels of expression also observed for expression at 27 °C overnight. The expression of *B. pseudomallei* RelA however showed a greater degree of difficulty, with poor recovery of soluble protein under all conditions tested (Figure 5.8). Interestingly growth rates of *E. coli* BL21 (DE3) cells carrying the pET16::*Bp*relA or pET16b::*Yp*relA were consistently retarded prior to the induced expression of the gene of interest (D.5).

Purification of *Y. pestis* RelA by nickel affinity chromatography yielded ~60 mg of purified protein with a similar level of co-purifying proteins to that observed for *F. tularensis* RelA (2.1.2). A second step of purification by size exclusion chromatography proved sufficient in the separation of RelA from the majority of contaminating proteins, yielding a largely pure sample as judged by SDS-PAGE analysis (Figure 5.5). Unlike *F. tularensis* RelA (2.1.2), the ability to concentrate *Y. pestis* RelA to high levels was not successful. Maximal concentrations of purified *Y. pestis* RelA were between 1 and 2 mg/ mL (~17 µM), similar to those previously achieved for *E. coli* RelA purifications (3.2.2).

Conversely the purification of *B. pseudomallei* RelA by nickel affinity chromatography yielded ~26 mg of protein with significantly higher levels of co-purified proteins. SDS-PAGE analysis showed a weak band for *B. pseudomallei* RelA which has an observed intensity no greater than the other proteins co-eluting at the same imidazole concentration. A secondary purification step using size exclusion chromatography yielded

multiple peaks of similar absorbance intensity. SDS-PAGE analysis confirmed that no peak corresponded to purified *B. pseudomallei* RelA (Figure 5.11). The expression and purification of *B. pseudomallei* RelA requires further optimisation to achieve a highly purified enzyme preparation suitable for biochemical characterisation.

As discussed in Chapter 2, the observation of substrate specificity for GTP over GDP for *F. tularensis* RelA was deemed unusual and potentially relating to its unique active site motif. Here we demonstrate that the RelA enzymes from *B. pseudomallei* and *Y. pestis*, both containing EXDD active site motifs, showed the acceptance of both GDP and GTP as potential pyrophosphate acceptors. These data act to further support our hypothesis that *F. tularensis* RelA is an unusual RelA enzyme. Furthermore despite the suggestion that the EXDD motif in the synthetase active site determines a preference for GDP as a pyrophosphate acceptor, preliminary studies suggest that this is not the case for either *Y. pestis* or *B. pseudomallei* RelA. The high level of impurities within the purified *B. pseudomallei* RelA resulted in a high turnover of ATP and consequently observations at this stage are purely speculative. Improved purification of the enzyme will undoubtedly result in a greater understanding.

Complete turnover of all substrates within 1 hour at 30 °C for *Y. pestis* RelA demonstrates a faster rate of activity than that observed for *F. tularensis* under the same conditions. One explanation for this observation could be the difference in purification methods. The expression of *F. tularensis* RelA at 16 °C overnight yields a high level of enzyme, but this extended period of expression may also result in the artificial dimerization of the RelA enzyme. It is possible that this dimerization is consequently resulting in a decreased level of activity. Further analysis of the dimerization state of *Y. pestis* RelA could provide further insight.

Chapter 6: **Conclusions and Future Work**

6.1 Biochemical Characterisation of (p)ppGpp Synthesis by the *F. tularensis* RelA Enzyme

6.1.1 Conclusions for the Biochemical Characterisation of *F. tularensis* RelA

The heterologous expression of *F. tularensis* RelA within *E. coli* BL21 (DE3) Rosetta cells yielded 15.32 ± 1.1 g/ 5 L culture. Purification by nickel affinity followed by size exclusion chromatography yielded 75-100 mg purified *F. tularensis* RelA. *F. tularensis* RelA purified as a dimer, as shown by analytical size exclusion chromatography. The purified enzyme could be concentrated to 10 mg/ mL, a concentration higher than that previously recorded for *E. coli* RelA [168, 296]. *In vitro* experiments demonstrated strict substrate specificity of *F. tularensis* RelA for GTP as the pyrophosphate acceptor (rather than GDP which is accepted by other RSH enzymes). This specificity was also observed in ribosome-mediated activity assays, however in the presence of methanol *F. tularensis* RelA accepted GDP as an alternative pyrophosphate acceptor. Steady state kinetic characterisation of the enzyme by both IP RP HPLC and ^{31}P NMR analytical methods generated data that better fitted a sigmoidal function (R^2 = 0.95) compared to a hyperbolic function (R^2 = 0.90).This kinetic profile is expected for an enzyme that has it's activity regulated. Kinetic parameters calculated for *F. tularensis* RelA gave a V_{max} of 12.27 (± 0.37) × 10^{-3} s^{-1} and 14.02 (± 0.90) × 10^{-3} s^{-1} and $K_{1/2}$ values of 351.5 ± 15.41 µM and 1072 ± 84.43 µM for ATP and GTP respectively. The calculated GTP $K_{1/2}$ value for *F. tularensis* RelA is similar to that calculated for *M. tuberculosis* Rel (1380 ± 160 µM) [262] and yet significantly lower than that calculated for *E. coli* RelA (3703 ± 379 µM) [285].

6.1.2 Future Work for the Biochemical Characterisation of *F. tularensis* RelA

The observed dimeric state of *F. tularensis* RelA possibly results from the high protein concentration in the experiment. Analysis of the multimeric state of *F. tularensis* RelA at a concentration closer to that found within the cell [309] could provide more information about the enzymes natural state. Furthermore, light scattering could provide an

alternative method to establish the molecular weight and therefore multimeric state of *F. tularensis* RelA [387]. Analysis of the (p)ppGpp synthetase activity for an enzyme in different multimeric states would also provide insights into the physical interactions required to catalyse this reaction.

The higher concentration and purity observed for purified *F. tularensis* RelA, compared to that previously observed for other long RSH enzymes, makes it a suitable target for analysis by protein crystallography. Initial attempts to crystallise *F. tularensis* RelA using a range of commercial sparse (96 well) and narrow (24 well) screens generated a few crystals which diffracted to poor resolution (E.1). Co-crystallisation of *F. tularensis* RelA with *E. coli* GppA also yielded crystals which diffracted to a poor resolution. Further work into the optimisation of these initial crystallisation conditions to obtain a crystal that diffracts to a higher resolution, could provide the first full length crystal structure for an RSH enzyme.

Kinetic characterisation of the enzyme suggests that *F. tularensis* RelA behaves like neither a monofunctional nor bifunctional RSH enzyme based on previous definitions by Sajish *et al*. [256, 285]. Sajish *et al.* suggest the substrate preferences of these two groups of RSH enzyme are due to the synthetase active site motif EXDD/RXKD [285]. As *F. tularensis* RelA contains a previously undescribed synthetase active site motif (EXSD), mutational analysis of this motif could reveal its role in the substrate specificity observed for this enzyme. Furthermore some bifunctional enzymes are reported to be inactivated by higher concentrations of magnesium [254, 262]. Analysis of *F. tularensis* RelA over a range of magnesium concentrations would elucidate whether it responds in a similar fashion to these bifunctional RSH enzymes.

To better understand the unusual sigmoidal saturation curves observed for *F. tularensis* RelA and its substrates, the dissociation constants for ATP and GTP could be calculated using isothermal titration calorimetry. This data would also prove useful in the co-crystallisation of *F. tularensis* RelA with GTP or ATP by providing information about conditions required to achieve a homogeneous sample of the substrate complex.

6.2 Activation of the *F. tularensis* RelA Enzyme

6.2.1 Conclusions for the Activation of *F. tularensis* RelA

The activation of *F. tularensis* RelA by stalled ribosomal complexes was investigated using ribosomes from both *E. coli* MRE600 and *F. philomiragia*. Ribosomes were isolated from *E. coli* MRE600 and *F. philomiragia* culture grown to early mid-log phase, and purified by SulfoLink-cysteine chromatography. Ribosome-mediated RelA catalysed (p)ppGpp synthesis demonstrated a higher level of activity compared to that of RelA basal activity for both *E. coli* and *F. tularensis* enzymes. The activation of *F. tularensis* RelA by stalled *E. coli* MRE600 ribosomes was greater (11 fold) than that by stalled *F. philomiragia* ribosomes (1.39 fold). Under optimal conditions, ribosome-mediated activation observed for *F. tularensis* RelA was 4 fold lower than that observed for *E. coli* RelA. Sub-cloning of the *F. tularensis rplK* gene (encoding L11) into a pET16b vector and heterologous expression in *E. coli* BL21 (DE3) cells yielded 5 g/L culture. Purification of L11 by streptavidin binding affinity chromatography yielded only 10 mg of purified L11. *F. tularensis* L11 demonstrated no activation of (p)ppGpp synthesis by *F. tularensis* RelA. Conversely the addition of the RNA species, tRNA and mRNA, displayed mild activation of *F. tularensis* RelA-mediated (p)ppGpp synthesis with a 1.21 and 1.27 fold increase respectively. *F. tularensis* RelA was shown to be activated by ppGpp but not by either AMP or KH_2PO_4. An EC_{50} for ppGpp-mediated activation of *F. tularensis* RelA activity was measured at 60 ± 1.9 µM. Finally *F. tularensis* RelA was also shown to be activated by methanol containing buffers, with an optimal concentration of 15% final (v/v) and optimal temperature of 25 °C.

6.2.2 Future Work for the Activation of *F. tularensis* RelA

F. tularensis RelA unexpectedly demonstrated stronger activation by *E. coli* stalled ribosomes than stalled *F. philomiragia* ribosomes. Analysis of *F. tularensis* RelA activity over a range of tRNA concentrations would determine whether this reduced activation relates to the respective binding affinities for tRNA. Alternatively the difference in activity could relate to the requirement for an unknown additional cofactor/activating ligand. To narrow down the location of this additional factor, *E. coli* ribosomes could be further purified to yield 50S, 30S or 70S complexes by sucrose gradient ultracentrifugation. *F.*

tularensis RelA activity in the presence of each individual complex would then be compared to that in the presence of crude *F. philomiragia* ribosomal preparations.

The intriguing possibility of an RNA cofactor would also be of interest. Possible RNA-RelA interactions could be established by incubation with stalled ribosomes, followed by analysis by electrophoretic mobility shift assay (EMSA) [388]. This technique has been used previously to show the interaction between the ribosomal protein L11 and 23S rRNA [388].

Another avenue worth investigating is the possibility that SpoT is the principle enzyme required for triggering the stringent response following amino starvation within *F. tularensis*. The initial hurdle for this approach would be the expression and purification of *F. tularensis* SpoT, as it is a large enzyme (81.16 kDa). Should sufficient enzyme be purified however, analysing the stalled ribosome-mediated activation of the enzyme should provide evidence for this hypothesis.

No activation was observed from the incubation of *F. tularensis* RelA with *F. tularensis* L11. *E. coli* RelA has conversely been reported to display mild activation in the presence of *E. coli* L11 [306]. The N-terminal region of the ribosomal protein L11 is reported to bind to the C-terminal region of RelA [305, 306]. Analytical size exclusion chromatography could be used to investigate whether the lack of activation relates to an inability of the truncated RelA to bind to L11. Mild activation of *F. tularensis* RelA could be observed in the presence of either tRNA or mRNA at 25 µM. Analysis of *F. tularensis* RelA over a wider range of RNA concentrations could determine the extent and validity of this observed activation. Payoe *et al.* demonstrated that the concentration of tRNA at which activation was observed for *E. coli* RelA varied depending on the species of tRNA [295]. Further work to establish the effects of different tRNA species on *F. tularensis* RelA activity, both on its own and in complex with ribosomes, would also be worthwhile.

F. tularensis RelA is the second RelA enzyme shown to be activated by the nucleotide ppGpp [313]. The binding site for ppGpp and its mechanism of activation however still remains elusive. Several methods could be used to improve knowledge in this area. Firstly, the co-crystallisation of the enzyme RelA with the nucleotide ppGpp would provide structural evidence for where the nucleotide binds. Secondly, binding information could be obtained by the use of techniques such as isothermal titration calorimetry, which can provide an insight into the number of binding sites on the enzyme for a particular ligand.

Thirdly, binding sites could be determined by mutational analysis of sections of amino acids or areas containing likely binding sites. Removal or inactivation of the binding site would result in a reduced or removed activation of *F. tularensis* RelA by the nucleotide ppGpp. The effect of ppGpp activation on the substrate saturation curves would be of interest. Determination of whether the sigmoidal nature of substrate saturation curves altered when calculated from *F. tularensis* RelA assays pre-incubated with ppGpp (≥120 µM) could offer insights into possible mechanisms of activation.

6.3 High Throughput Screen for *F. tularensis* RelA

6.3.1 Conclusions for the *F. tularensis* RelA High Throughput Screen

The development of a novel high throughput screening method for inhibitors of the enzyme RelA has been described. This method employs an enzyme coupled assay which utilises members of the GppA/PPX family as secondary enzymes, for the conversion of pppGpp to inorganic phosphate. The coupled assay produces inorganic phosphate at concentrations stoichiometric to that of guanosine pentaphosphate, as demonstrated by ^{31}P NMR analysis. The concentration of *E. coli* GppA required to ensure the complete turnover of guanosine pentaphosphate was low (0.05 µM for 5 µM *F. tularensis* RelA with 2 mM substrates). The coupled enzyme assay was adapted for high throughput screening by the use of malachite green reagent (7.6.1.7.1.) for the determination of inorganic phosphate concentration. The concentration of inorganic phosphate was shown to increase over time with the coupled enzyme assay but not in the presence of GppA only. Optimisation of the high throughput method detailed improvements upon the addition of BSA (0.1 mg/ mL), to prevent non-specific binding of the enzymes, and an increase in $MgCl_2$ concentration to 30 mM. This method was also used to screen a library of nucleotide analogues (10 µM final concentration) against *F. tularensis* RelA (0.5 µM final concentration). From the initial round of screening twelve compounds showed inhibition of *F. tularensis* RelA. Secondary analysis of potential hits, using the aforementioned coupled enzyme assay, reduced the number of compounds demonstrating inhibition to three. Testing two of the remaining potential hits at a higher concentration of compound (100 µM) demonstrated no inhibition of *F. tularensis* RelA, suggesting they were likely false positives.

6.3.2 Future Work for the *F. tularensis* RelA High Throughput Screen

The development of a novel high throughput method for screening *F. tularensis* RelA, provides opportunities for advancement in the field of RSH enzyme inhibitor discovery. The absence of any true hits from the screening of the nucleotide analogue library (at 10 µM) described however indicates the requirement to screen a greater number of compounds or at higher concentrations. Another compound library which could be screened is the published kinase inhibitor set (PKIS) library from GlaxoSmithKline [389]. This library is a set of 367 ATP-competitive kinase inhibitors; it is possible that these compounds could therefore compete with ATP binding to RelA. Larger compound libraries with a greater diversity of chemical scaffolds could serve as a source of non-competitive or allosteric inhibitors of RelA.

The validation of compounds demonstrating a highly reproducible inhibition of RelA would be validated by a secondary enzyme assay. One possible secondary enzyme assay would be the analysis of RelA activity by IP RP HPLC, as previously described within this thesis. This technique could be used to determine the inhibition of RelA basal activity and ribosome-mediated RelA activity. Measuring the inhibition in the ribosome-mediated assay is important as previous RelA inhibitors have demonstrated drastic reductions in measured inhibition following the addition of stalled ribosomal complexes [259]. Validated compounds would be characterised by measuring their IC_{50} and K_d values for the enzyme.

The high throughput method devised could be further improved to reduce the numbers of false positives and negatives. Contaminating phosphate within commercially sourced substrates can alter the measured phosphate concentration. To remedy this, nucleotide triphosphates could be separated from inorganic phosphate by size exclusion chromatography (i.e.; Sephadex G10 column), to reduce the background signal. The use of malachite green reagent results in acidified conditions which could lead to non-enzymatic hydrolysis of phosphates from nucleotides. Further work could therefore investigate alternative methods of phosphate detection.

There are many other methods which can be utilised for phosphate detection (4.3). One example of which is a fluorescence based detection method which utilises the enzymes purine nucleoside phosphorylase, xanthine oxidase and horseradish peroxidase (Figure 6.1) [390]. The sensitivity of this method is reported down to the nanomolar range, which

could allow for shorter incubation times for the *F. tularensis* RelA coupled assay. The incorporation of three additional enzymes within this method however would result in the requirement for a greater number of controls.

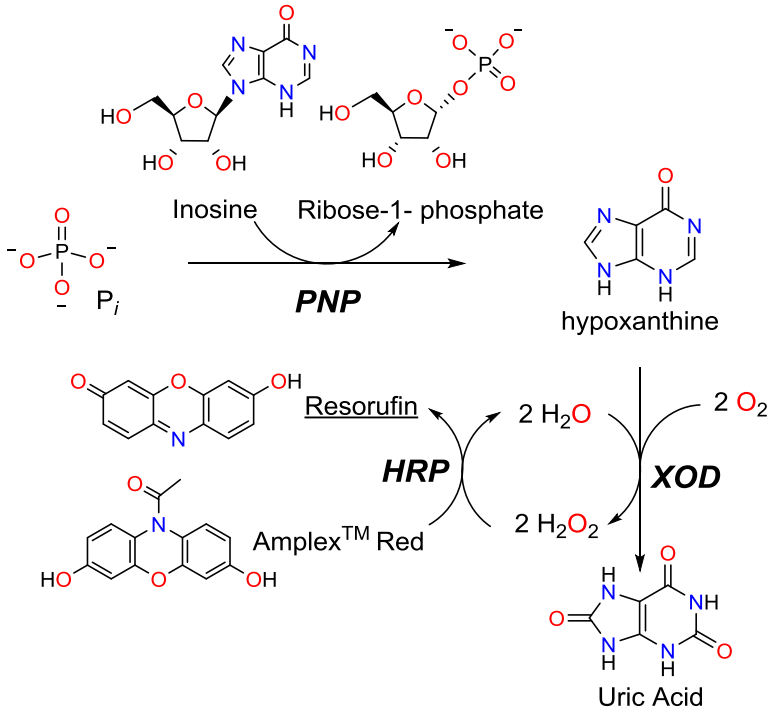

Figure 6.1. Reaction scheme for the indirect fluorescence based detection of inorganic phosphate by the formation of resorufin using the enzymes purine nucleoside phosphorylase (PNP), xanthine oxidase (XOD) and horseradish peroxidase (HRP).

6.4 Preliminary Characterisation of the RelA Enzyme from *Yersinia pestis* and *Burkholderia pseudomallei*

6.4.1 Conclusions for the Characterisation of RelA from *Y. pestis* and *B. pseudomallei*

Synthetic genes within the pET16b plasmid for codon-optimised *relA* from *B. pseudomallei* and *Y. pestis* were commercially sourced from Life Technologies. Heterologous expression of the both *B. pseudomallei* and *Y. pestis relA* were optimised by small scale expression studies. The optimal expression found for both *B. pseudomallei* RelA and *Y. pestis* RelA was 27 °C for 4 hours following induction with IPTG (1 mM final concentration). The heterologous expression of *Y. pestis* and *B. pseudomallei* RelA within *E. coli* BL21 cells yielded 6.08 ± 1.22 g/ L culture and 6.22 g/ L culture respectively. *Y. pestis* RelA were purified by nickel affinity followed by size exclusion chromatography. Purification yielded ~44 mg of *Y. pestis* RelA to a similar level of purity recorded for *F.*

tularensis. Purified *Y. pestis* RelA could only be concentrated to 1-2 mg/ mL, as attempts to concentrate it further resulted in protein precipitation. Conversely *B. pseudomallei* RelA could only be purified by nickel affinity chromatography (~26 mg) to a poor level of purity. Both enzymes were capable of (p)ppGpp synthesis, as demonstrated by IP RP HPLC analysis. Unlike *F. tularensis* RelA, neither *Y. pestis* nor *B. pseudomallei* demonstrated specificity for either GDP or GTP as the pyrophosphate acceptor.

6.4.2 Future Work for the Characterisation of RelA from *Y. pestis* and *B. pseudomallei*

The heterologous expression of *B. pseudomallei* RelA in *E. coli* BL21 (DE3) cells demonstrated poor yields across all conditions tested. The *E. coli* strain BL21 (DE3) Rosetta contains a plasmid encoding five tRNAs with rare codons for *E. coli* and is frequently used for the expression of eukaryotic proteins [343]. The use of this strain has previously been described for the successful heterologous expression of *F. tularensis* RelA (2.1.1) [391]. Further work with *B. pseudomallei* RelA might therefore benefit from expression within this strain. Growth of *E. coli* BL21 (DE3) containing pET16b::*Bp*relA showed retarded progression to mid-log phase compared to *E. coli* BL21 (DE3) containing pET16b empty vector. This slowed growth rate could relate to the leaky expression of *B. pseudomallei* RelA, as high pppGpp levels are associated with growth arrest [184]. Transferring the *BprelA* gene to an alternative plasmid such as a pBAD vector could result in reduced leaky expression [392] and higher yields of cell pellet and ultimately purified protein. Recovery could be improved from the use of either a glutathione S-transferase (GST) tag, to improve stability, or maltose-binding protein (MBP), to improve protein solubility [393].

Future work with *Y. pestis* RelA should include further investigation into the substrate preference of the enzyme. To establish the substrate preference the dissociation constants of each substrate for *Y. pestis* RelA should be determined both in the presence and absence of ATP by ITC analysis. In addition the K_M/ $K_{1/2}$ for all the potential substrates should be determined from the analysis of saturation curves as described previously for *F. tularensis* RelA. An ultimate end goal for this line of research would be to use the kinetic parameters to adapt the high throughput screening method previously described, for the discovery of inhibitors of RelA enzymes from *B. pseudomallei* and *Y. pestis*.

Chapter 7: **Materials and Methods**

7.1 Materials and Reagents

DTT, BSA and antibiotics were purchased from Melford Laboratories (Suffolk, UK); polyacrylamide-bis polyacrylamide (30% w/v, 37:5:1), Bacto tryptone and yeast extract for culture media were purchased from Oxoid (Hampshire, UK). Chelating fast flow resin and Superdex 200 resin were purchased from GE Healthcare (Buckinghamshire, UK); primers were purchased from Eurofins (London, UK); restriction enzymes and *E. coli* strain K12 JM109 were purchased from New England Biolabs (Hertfordshire, UK); pET16b plasmid was purchased from Merck Chemicals (Middlesex, UK); *E. coli* RelA, PPX, and GppA were expressed using a strain from the ASKA Clone library purchased from Shigen (Japan); *E. coli* MRE600 (C6) strain was purchased from NCTC (Hertfordshire, UK). *Francisella philomiragia* (ATCC 25015) was obtained from ATCC (Middlesex, UK); mRNA was purchased from ATDBio (Hampshire, UK). Unless stated otherwise all other reagents were purchased from Sigma Aldrich (Dorset, UK) or Fisher Scientific (Leicestershire, UK). Graphpad Prism version 6 for Windows was obtained from Graphpad Software, San Diego, California, USA.

7.2 Equipment

Fast Protein Liquid Chromatography (FPLC). All purification chromatography methods described were carried out on an ÄKTAPrime plus system (GE Healthcare). Chromatography data was analysed using Primeview software (GE Healthcare).

High Performance Liquid Chromatography (HPLC). All described HPLC methods were carried out on a Gilson System WorkCentre including 321 pumps and a 234 Gilson Autoinjector connected to a Gilson UV/vi-155 detector. Liquid chromatography data was analysed using Unipoint software (Gilson).

Liquid Chromatography Mass Spectrometry (LCMS). All described LCMS methods were carried out on a Gilson System WorkCentre (as described above) coupled to a Surveyor MSQ single quadrupole mass spectrometer (Thermo Finnigan), with electrospray

ionisation. Liquid chromatography data were analysed using Unipoint software, and mass spectrometry data were analysed using XCalibur software.

Bacterial Cell Culture. All small bacterial cultures (≤ 200 mL) were incubated in an Innova 4230 shaking incubator (New Brunswick Scientific). Large scale bacterial cultures (1-5 L) were incubated in an Innova 44 shaking incubator (New Brunswick Scientific).

Centrifugation. Cell cultures and cell lysates were pelleted by centrifugation in a Sorvall Evolution RC (Kendro Laboratory Products). Protein precipitate in quenched enzyme assays was pelleted by centrifugation in a Biofuge Fresco (Heraeus).

pH Determination. All solutions were made to the correct pH using a Mettler Toledo Seven Compact pH meter. Acids were used at the following concentrations; HOAc (20%), HCl (5 M). Bases were used at the following concentrations; KOH (2.5 M), NaOH (5 M).

High Throughput Screening Methods. Components and mixtures were added to wells using a Biomek 3000 laboratory automation workstation (Beckmann Coulter) at room temperature. Absorbance/luminescence measurements were taken using a POLARstar Omega platereader (BMG Labtech).

Cell Lysis. Category 1 bacterial cells were lysed on ice in a MSE Soniprep 150. Category 2 bacterial cells were lysed on ice using a Vibracell VCX130 Ultrasonic High Intensity Processor (Jencons, VWR) in a class II microbial safety cabinet (Herasafe, Heraeus).

7.3 General Laboratory Protocols

All bacterial cultures in the presence of antibiotics contained antibiotics at the following concentrations; chloramphenicol (30 μg/mL), ampicillin (100 μg/mL).

7.3.1 Sodium Dodecyl Sulphate Polyacrylamide Gel Electrophoresis (SDS-PAGE)

15% SDS-PAGE gels were prepared using the following:

Table 7.1. Table detailing composition for 15% resolving and stacking gel.

Component	Resolving Gel	Stacking Gel
Water (deionised)	4.6 mL	2.7 mL
30% Acrylamide	10 mL	0.67 mL
1.5 M Tris pH 8.8	5 mL	-
1 M Tris pH 6.8	-	0.5 mL
10% Sodium Dodecyl Sulphate (SDS)	200 µL	40 µL
10% Ammonium persulphate (APS)	200 µL	40 µL
Tetramethylethylenediamine (TEMED)	8 µL	4 µL

The resolving gel was made initially and left to set prior to the addition of the stacking gel. Once the gel was prepared, protein samples were prepared by mixing appropriate volumes (determined by Bradford assay, 7.3.2) with 2 x SDS loading buffer (7.9.1: 0.1 M Tris pH 6.8, 139 mM SDS, 3 mM bromophenol blue, 20% glycerol) and were then heat denatured at 95 °C for 5 min. Samples were run at 180 V for 45-55 min, in SDS tank buffer (7.9.2: 250 mM Glycine, 25 mM Tris base, 3.5 mM SDS). Gels were stained in coomassie brilliant blue stain (7.9.3, microwaved for 20 s) and destained (7.9.4) on a rocker for 2-18 hours. Gels were imaged using SynGene Genius Imager.

7.3.2 Bradford Assay

To 750 µL Bradford reagent (Pierce, Thermo Scientific), 20 µL of protein sample was added and mixed by gentle pipetting. The resultant solution was incubated at room

temperature for 10-15 min before measuring the absorbance at 595 nm. Absorbance values for samples were compared with that of a known standard (1 mg/mL BSA) to estimate protein concentration.

7.3.3 Agarose Gel Electrophoresis

For a 1% agarose gel, 1× TAE buffer (7.9.5, 40 mL) was added to agarose (0.4 g) and heated (microwave), until solution was clear. The heated agarose solution was left to cool slightly prior to the addition of Nancy 520 (2 µL). The resultant solution was poured into a secure tray and a comb carefully placed into the solution, before leaving to set.

Samples (10 µL) were prepared with 2 µL 6× DNA loading buffer (7.9.6: 30% glycerol, 150 mM EDTA pH 8.0, 0.45 mM bromophenol blue, 0.56 mM xylene cyanol) prior to loading into the set gel. Gel electrophoresis was carried out at 90 V until the samples had travelled two thirds of the gel (~30 min). The gel was then imaged using a SynGene Genius Imager.

7.3.4 Chemical Transformation

Competent *E. coli* cells (7.3.8) (50 µL) were defrosted on ice and gently resuspended. Plasmid (1 µL) was added and gently mixed via pipetting prior to 30 minute incubation on ice. The cells were then transferred to a water bath for heat shock (42 °C, 30 s). Cells were further incubated on ice for 2 min before the addition of SOC media (7.9.7, 250 µL) and gentle resuspension by pipetting. Cells were subsequently incubated at 37 °C, 180 rpm for 1 hour. Agar plates (7.9.8) containing appropriate antibiotics were also warmed at this time. After the hour incubation, cells (30-60 µL) were spread onto appropriate agar plates and incubated at 37 °C overnight.

7.3.5 Bacterial Glycerol Stocks

To bacterial culture (500 µL), typically grown overnight, sterile 75% glycerol (500 µL) was added and gently mixed by pipetting prior to flash freezing and storage at -80 °C.

7.3.6 **Overnight Bacterial Growths**

To 2×YT media (7.9.9, 10 mL for small growths, and 100 mL for large scale growths) appropriate antibiotics and a loop of glycerol stock (7.3.5) or a single bacterial colony were added. Cultures were then grown overnight (14-18 hours) at 37 °C, 180 rpm.

7.3.7 **Restriction Digest of pET16b Plasmids**

Double digestion of plasmids by the restriction enzymes NcoI and XhoI were set up as described by NEB, typically using the following composition. Restriction enzymes were always added last.

Table 7.2. Composition for restriction digest (NcoI and XhoI).

Component	Volume (µL)
Plasmid	5
NEBuffer 4 (NEB)	1
BSA (10×)	1
NcoI	0.5
XhoI	0.5
Sterile Water	2
Total Volume	10

Restriction digests were incubated at 37 °C for 1 hour, after which 6× DNA loading buffer (2 µL) was added. Samples were analysed by DNA agarose gel electrophoresis (7.3.3).

7.3.8 **Competent *E. coli* cells**

2×YT media (7.9.9, 100 mL) plus appropriate antibiotics was inoculated with an overnight growth (1 mL). Cells were incubated at 37 °C, 180 rpm to an OD_{600} of 0.6. The culture was then cooled on ice for 10 min prior to centrifugation at 4,000 rpm, 4 °C for 10 min. The supernatant was discarded and cell pellets resuspended by pipetting into TBF I buffer (7.9.10, 10 mL), prior to further centrifugation (4,000 rpm, 4 °C for 10 min). Supernatant was discarded as before and at 4 °C the cell pellet was resuspended in TBF II (7.9.11, 1.5 mL) buffer. Resuspended cells were aliquoted (100 µL), flash frozen in liquid nitrogen and stored at -80 °C.

7.4 Experimental for Chapter 2

7.4.1 **Expression of *F. tularensis* RelA**

The plasmid pET16b::*Ft*relA was chemically transformed into *E. coli* BL21 (DE3) Rosetta competent cells (7.3.4). Single colonies were used to inoculate 2×YT media (7.9.9, 10 mL, containing 100 µg/mL ampicillin and 30 µg/mL chloramphenicol) and cultured overnight at 37 °C. The overnight culture was used as a 1% inoculum for flasks of 2×YT (7.9.9, 4 × 1.25 L) which were induced with IPTG (final concentration of 0.4 mM) when the optical density at 600 nm (OD_{600}) reached 0.6 and then cultured overnight at 16 °C. The cell pellet was then collected by centrifugation (average yield of 15.05 g/ 5 L of culture) and stored at -80 °C.

7.4.2 **Purification of *F. tularensis* RelA by Nickel Affinity Chromatography**

Frozen cell pellet (typically 15 g) was resuspended (3 x v/w cell pellet) in RelA Purification Buffer A (7.9.12: 50 mM Tris pH 8.0, 500 mM NaCl, 3 mM β-mercaptoethanol, 15% v/v glycerol and 20 mM imidazole). Lysozyme (5-15 mg) and a Roche protease inhibitor tablet (1 per 50 mL) were added to the cell suspension and left to stir (4 °C, 30 min). Cells were lysed by sonication (4 °C, 20 × 30 s with 30 s rest), and cellular debris removed by centrifugation (Sorvall evolution, SS-34 rotor, 14000 rpm, 4 °C, 30 min). The resultant cleared lysate was applied (4 mL min^{-1}) to a Ni-IDA Sepharose Fast Flow Column (50 mL bed volume). The column was then washed (4 mL min^{-1}) with Buffer A until the absorption of the eluate at 280 nm (A_{280}) returned to baseline. Elution (4 mL min^{-1}) of *F. tularensis* RelA was achieved using a gradient of imidazole from 20 to 500 mM (RelA

Purification Buffer B 7.9.13, as Buffer A but with 500 mM imidazole) over 5 column volumes.

7.4.3 Removal of Imidazole by Dialysis

Fractions containing *F. tularensis* RelA were pooled and dialysed against RelA Purification Buffer C (2 x 1 L, 7.9.14: 50 mM Tris pH 8.0, 300 mM NaCl, 1 mM DTT, 15% v/v glycerol). Dialysis tubing, saturated in water, was secured using clips and filled with water to test for leaks. Supposing no leaks were observed, water was removed from the tubing and was instead filled with pooled protein fractions. The contained protein solution was then placed into a beaker of RelA Purification Buffer C (1 L) and left gently stirring for 1 hour. The buffer was removed and replaced with fresh RelA Purification Buffer C and left to gently stir for a further hour.

7.4.4 Protein Concentration by Ultrafiltration

Proteins were concentrated in an Amicon Pressure Cell (30 kDa PES filter, Sartorius) under pressure of nitrogen gas, before overnight storage at 4 °C (between RelA nickel affinity chromatography and size exclusion chromatography steps) or -80 °C [after size exclusion chromatography or ribosome purification (7.5.4)].

7.4.5 Purification of *F. tularensis* RelA by Size Exclusion Chromatography

The concentrated *F. tularensis* RelA (3 mL) was applied (2 mL min^{-1}) to a gel filtration column (HiLoad 26/60, Superdex 200, prep grade) pre-equilibrated in RelA Purification Buffer C. The purest fractions of *F. tularensis* RelA, as judged by SDS-PAGE, were pooled and concentrated (7.4.4) to ~4 mg/mL (~50 µM), then aliquoted (typically 0.2 mL) and stored at -80 °C. For biochemical experiments, *F. tularensis* RelA aliquots were defrosted and used only once. Each batch of *F. tularensis* RelA was used within 8 weeks of freezing.

7.4.6 Multimeric State by Analytical Size Exclusion Chromatography

A Superdex 200 column (10 mm x 300 mm) was used to estimate the apparent molecular weight of purified *F. tularensis* RelA. Protein samples were applied (1 mL min^{-1}) to a pre-equilibrated column in Analytical Gel Filtration Buffer (7.9.15: 50 mM Tris – HCl pH 7.5, 100 mM KCl). Cytochrome C, carbonic anhydrase, BSA, alcohol dehydrogenase and β-

amylase (Sigma Aldrich) were used as protein standards for calibration of the column. Elution of the protein samples were monitored by absorbance at 280 nm and SDS-PAGE.

For experiments at 30 °C, Analytical Gel Filtration Buffer (7.9.15) was heated to temperature by incubation in a Function line incubator (Heraeus). *F. tularensis* RelA was incubated at 30 °C for 20 min prior to injection onto a Superdex 200 column pre-equilibrated in pre-warmed Analytical Gel Filtration Buffer (7.9.15).

7.4.7 **HPLC Analysis of RelA Activity**

F. tularensis RelA activity assays, substrate specificity assays and assays to identify and quantify activating factors were all analysed by IP RP HPLC, using methods adapted from Cordell *et al*. [338]. Injected samples (40 µL) were chromatographed on a reverse phase column [Gemini C18, 150 x 4.6 mm 5 micron (Phenomenex)] at a flow rate of 0.8 mL min^{-1} with UV detection at 260 nm. The mobile aqueous phase (7.9.16) was 95% water with 5% methanol and organic phase (7.9.17) was 20% water with 80% methanol. Both phases contained DMHA (15 mM) and were adjusted to pH 7.0 with acetic acid.

7.4.8 **Optimisation of Gradient**

Gradients were adapted from method A (see below). The gradient starting percentage was optimised by analysis with a starting organic phase at 5% (Method 2J), 6% (Method 2I), 7% (Method 2H), 8% (Method 2G), 9 % (Method 2F), 10% (Method 2E), 11% (Method 2D), 12% (Method 2C), 13% (Method 2B), 14% (Method 2A), 15% (Method 2). The end point of the gradient was optimised by analysis with the final organic phase at 45% (Method 3), 47% (Method 3A), 49% (Method 3B), 51% (Method 3C), 53% (Method 3D), 55% (Method 3E).

7.4.8.1 **Method A**

Nucleotides were eluted with the following gradient: 0-5 min, isocratic, 25% organic buffer; 5-32 min, gradient 15-45% organic buffer; 32-42 min, isocratic, 45% organic buffer; 42-43 min, gradient, 45-25%.

7.4.8.2 **Method B (METH3C.GCT)**

Nucleotides were eluted with the following gradient: 0-5 min, isocratic, 9% organic buffer; 5-32 min, gradient 9-51% organic buffer; 32-42 min, isocratic, 51% organic buffer; 42-43 min, gradient, 51-9%.

7.4.8.3 **Method C (METH4C1.GCT)**

Nucleotides were eluted with the following gradient: 0-5 min, isocratic, 9% organic buffer; 5-59.1 min, gradient 9-80%; 59.1-60.1 min, gradient 80-100%; 60.1-65.1 min, isocratic, 100%; 65.1 – 67.1 min, gradient 100-9%; 67.1-76.1 min, isocratic 9%.

7.4.8.4 **Method D (METH3.GCT)**

Nucleotides were eluted with the following gradient: 0-5 min, isocratic, 25% organic buffer; 5-27 min, gradient 25-60%; 27-28 min, gradient 60-100%; 28-33 min, isocratic, 100%; 33-34 min, gradient 100-25%; 34-44 min, isocratic 25%.

7.4.9 **Substrate Specificity End Point Assays**

7.4.9.1 **RelA Only Activity Assays**

Reaction mixtures (100 µL) were prepared with components at the following final concentrations: ribonucleotide di- or triphosphates (2 mM, either G or C), ATP (2 mM), and *F. tularensis* RelA (10 µM) in 1× RelA Assay Buffer B [7.9.19 (10×): 20 mM Tris pH 8.0, 15 mM KCl, 15 mM $MgCl_2$, 1 mM β-mercaptoethanol]. Reactions were incubated at 30 °C for 60 min, prior to quenching by heating (80 °C, 2 min). The reaction mixtures were then kept on ice to ensure full protein precipitation (typically 10 min), before clearing by centrifugation (Biofuge Fresco microfuge, 12000 rpm, 4 °C, 5 min). Supernatant was then stored at -20 °C awaiting IP RP HPLC analysis (40 µL).

7.4.9.2 **Methanol Activated RelA Activity Assays**

Reaction mixtures (100 µL) were prepared with components at the following final concentrations: guanosine di- or triphosphates (2 mM), ATP (2 mM), and *F. tularensis* RelA (10 µM) in RelA Assay Buffer A (7.9.18) [317]. Reactions were incubated at 30 °C for

1 h, prior to quenching with formic acid (1 M final concentration). The reaction mixtures were then kept on ice to ensure full protein precipitation (typically 10 min), before clearing by centrifugation (Biofuge Fresco microfuge, 12000 rpm, 4 °C, 5 min). Supernatant was then stored at -20 °C awaiting IP RP HPLC analysis (40 µL).

7.4.9.3 Ribosome Activated RelA Activity Assays

Reaction mixtures (100 µL) were prepared with components at the following final concentrations: guanosine di- or triphosphates (2 mM), ATP (2 mM), *F. tularensis* RelA (0.18 µM), and RAC as described by Payoe *et al.* [295] (7.5.9.1) in 1× RelA Assay Buffer B (7.9.19). Reactions were incubated at 22 °C for 1 hour, prior to quenching with formic acid (1 M final concentration). The reaction mixtures were then kept on ice to ensure full protein precipitation (typically 10 min), before clearing by centrifugation (Biofuge Fresco microfuge, 12000 rpm, 4 °C, 5 min). Supernatant was then stored at -20 °C awaiting IP RP HPLC analysis (40 µL).

7.4.10 Temperature Optimisation of *F. tularensis* RelA Activity

Reaction mixtures (100 µL) were prepared with components at the following final concentrations: *F. tularensis* RelA (10 µM), ATP (2 mM), GTP (2 mM) in 1× RelA Assay Buffer B (7.9.19). Reactions were incubated at 17, 22, 27, 32, or 37 °C for 1 hour. Reactions were quenched by the addition of formic acid (1 M final concentration). Protein was precipitated by incubation at 4 °C for 10 min before removal by centrifugation at 12 000 rpm, 4 °C, for 5 min. Supernatant was stored at -20 °C awaiting IP RP HPLC analysis (40 µL).

7.4.11 Liquid Chromatography Mass Spectrometry (LCMS) Analysis of *F. tularensis* RelA Activity

Injected samples (40 µL) were chromatographed on a reverse phase column [Gemini C18, 150 x 4.6 mm 5 micron (Phenomenex)] at a flow rate of 0.8 mL min^{-1} with UV detection at 260 nm. The mobile aqueous phase (7.9.21) was 95% water with 5% methanol (pH 8.7) and organic phase (7.9.22) was 20% water with 80% methanol (pH 8.0); both phases were adjusted to pH with acetic acid (LCMS grade, Fluka). Both phases contained DMHA (15 mM), and the aqueous phase contained hexafluoroisopropanol (HFIP) (100 mM). LCMS analysis make up buffer contained a 50/50 mixture of acetonitrile and water (7.9.22).

7.4.11.1 **LCMS method (MC4_MS.GCT)**

Nucleotides were eluted with the following gradient: 0-5 min, isocratic, 20% organic buffer; 5-25 min, gradient 20-100%; 25-30 min, isocratic, 100%; 30-35 min, gradient 100-20%; 35-45 min, isocratic 20%. Mass spectrometry of nucleotides was carried out on a Surveyor MSQ (Thermo Finnigan). The probe temperature was set at 350 °C with the cone voltage at 200 V, in negative ion electrospray mode. LCMS analysis covered molecules within the mass range of 100 to 700 amu.

7.4.12 **Steady State Kinetics for *F. tularensis* RelA and substrates**

Reaction mixtures for time course experiments (1 mL) contained *F. tularensis* RelA (10 µM) and were made up in 1× RelA Assay Buffer B (7.9.19). When saturating, nucleotides (GTP or ATP) were included at 2 mM. Reactions were incubated at 30 °C and at selected time points, aliquots (100 µL) were withdrawn and the reaction quenched by heating (80 °C, 2 min). Precipitated protein was removed as described previously and a sample (40 µL) was analysed by IP RP HPLC. The concentrations of nucleotides were quantified by comparison with a standard calibration curve. The formation of product nucleotides over time (never more than 15% substrate turnover) was fitted to a linear function to determine initial rates. Initial rates, *v*, were fitted to an allosteric sigmoidal function (Equation 7.1) using Graphpad Prism software where V_{max} is the rate of reaction at substrate saturation, $K_{1/2}$ is the concentration of substrate giving a rate of half of V_{max} and h is the apparent Hill coefficient.

Equation 7.1.

$$v = \frac{V_{max}\mathrm{S}^{\mathrm{h}}}{\left(K_{½}^{\mathrm{h}} + \mathrm{S}^{\mathrm{h}}\right)}$$

7.4.13 **^{31}P NMR Analysis**

All data were recorded on a Bruker AVII400 FT-NMR Spectrometer using a 10 mm auto-tune and match broadband probe tuned to the sample prior to data collection (TD = 64k points; sweep width = 395 ppm; 512 scans using 90° pulse with a total acquisition time of 2.5 s per scan; chemical shifts referenced to H_3PO_4).

7.4.13.1 Analysis of Nucleotides

Nucleotides AMP, GTP and ATP (Sigma Aldrich) at 20 mg/mL in concentration were prepared in 1× RelA Assay Buffer B (7.9.19) and 10% (v/v) deuterium oxide (D_2O). Samples (750 µL) were analysed in 5 mm diameter NMR tubes. Potassium dihydrogen phosphate (KH_2PO_4) at 20 mg/ mL was prepared as described above to determine the chemical shift for inorganic phosphate.

7.4.13.2 ^{31}P NMR Analysis of *F. tularensis* RelA Activity

Reaction mixtures (3 mL) were prepared in 1× RelA Assay Buffer B and contained GTP (2 mM), ATP (2 mM), and 10% (v/v) D_2O. The reaction was initiated through the addition of *F. tularensis* RelA (10 µM), thoroughly mixed and then data collected at 25 °C for 22 min followed by 22 min bins for the duration of the experiment (typically 110 min). Peak integrals were calibrated against a spectrum recorded prior to initiation. At each substrate concentration the formation of product nucleotides over time was fitted to a linear function to determine the rate of product formation. These rates were then fitted to an allosteric sigmoidal curve (Equation 8.1).

7.5 Experimental for Chapter 3

7.5.1 Bacterial Growth Curves

Cultures were grown in appropriate media with a 1% inoculum at 37 °C, 180 rpm. At regular time points samples (1 mL) of culture was removed and the OD_{600} of the sample determined by UV-spectroscopy (Biomate3, Thermo Scientific). At key points, i.e.; start, middle and the end of the log phase, further samples were taken for viable counts. A dilution series of bacterial culture (100 µL) into the appropriate media (9.9 mL) was followed by a further five 1 in 10 dilutions. Each dilution (100 µL) was then plated onto appropriate agar plates, which were incubated overnight at 37 °C. The following day colony counts were taken.

7.5.2 **Expression of Ribosomes**

Ribosomes were isolated from both *F. philomiragia* and *E. coli* MRE600. For the purification of ribosomes from *E. coli*, overnight cultures of *E. coli* MRE600 (LB media, 10 mL) were used to inoculate flasks of LB media (7.9.23, 1 L) supplemented with $MgSO_4$ (10 mM). Cultures were grown at 37 °C to an OD_{600} of 0.4; cells were then pelleted by centrifugation (Sorvall evolution, SLC 6000 rotor, 4000 rpm, 4 °C, 30 min). For the purification of ribosomes from *F. philomiragia*, overnight cultures of *F. philomiragia* (Trypticase Soy Broth (TSB), 10 mL) were used to inoculate flasks of TSB (7.9.24, 1 L) supplemented with L-cysteine (1 g/L). Culture was grown at 37 °C to an OD_{600} of 1.0, and the cells collected by centrifugation as described above. Cell pellets recovered from *F. philomiragia* cultures were 6.86 ± 2.28 g/ L, whereas those from *E. coli* MRE600 were 6.61 ± 0.77 g/L. All cell pellets were washed in THM buffer (7.9.25) before pelleting again by centrifugation (4000 rpm, 4 °C, 30 min) prior to storage at -80 °C.

7.5.3 **Reaction of SulfloLink Resin with L-cysteine**

SulfoLink resin (Pierce Inc.) was coupled with L-cysteine hydrochloride using a manual peptide synthesis bubbler. Storage buffer was removed from the resin by vacuum filtration. 3× resin volume of coupling buffer was added to dry resin and gently agitated for 30 min. The coupling buffer (7.9.26) was then removed as described previously and replaced with 1x resin volume of coupling buffer with 50 mM L-cysteine hydrochloride. This was followed by gentle agitation for 1-2 hours. The coupling buffer with L-cysteine hydrochloride was removed by vacuum filtration, prior to a series of washing steps with 1 M NaCl solution. Each step consisted of gentle agitation by nitrogen for a couple of minutes followed by vacuum filtration. Finally the resin was resuspended in 0.1 M phosphate buffered saline (PBS) solution (Sigma Aldrich) and stored at 4 °C.

The success of the coupling reaction was analysed using the Kaiser test for primary amine groups. To a small sample of dried resin solution A (7.9.27, 100 µL) was added and the resin mixed before the addition of solution B (7.9.28, 25 µL). The mixture was then incubated at 95 °C for 5 min. The colour of the mixture indicates the presence or absence of free amines, blue colouration denotes the presence of free amines and straw colouration indicates the absence.

7.5.4 Purification of Ribosomes by SulfoLink-cysteine Chromatography

SulfoLink-cysteine resin was prepared, and ribosomes purified as described for *E. coli* ribosomes by Maguire *et al.* [359]. Frozen cell pellet (typically 5 g) was resuspended (2 x v/w of cell pellet) in Ribosome Purification Buffer A (7.9.29: 20 mM Tris pH 7.5, 10.5 mM $Mg(OAc)_2$, 100 mM NH_4Cl, 0.5 mM EDTA, disodium salt). Cells were lysed by sonication (4 °C, 6 x 15 s, 2 x 20 s with 1 min rests) and cellular debris removed by centrifugation (Sorvall Evolution, SS-34 rotor, 12000 rpm, 4 °C, 30 min). The resultant supernatant was filtered (Millipore 0.45 µm PES syringe filter), then applied (2 mL min^{-1}) to a SulfoLink-cysteine column (30 mL bed volume). The column was washed (2 mL min^{-1}) with Ribosome Buffer A until absorption of eluate at 280 nm returned to baseline. Ribosomes were eluted (2 mL min^{-1}) with a gradient of 100 to 300 mM NH_4Cl (Ribosome Buffer B, 7.9.30; same as A by with 300 mM NH_4Cl) over 15 column volumes. Fractions (10 mL) containing ribosomes, as assessed by absorption at 260 nm, SDS-PAGE and measurement of protein content by the method of Bradford [394], were pooled and concentrated to 4.96 and 8.93 µM for *F. philomiragia* and *E. coli* respectively in an Amicon Pressure Cell (30 kDa PES filter, Sartorius). Concentrated ribosomes were aliquoted (200 µL) and stored at -80 °C.

The concentration of purified ribosomes was calculated by measuring the absorbance at 254 nm. Absorbance values ≤ 1 were achieved by serial dilution of the concentrated purified ribosomes and were measured using a POLARstar Omega plate reader (BMG Labtech). Absorbance readings under 1.0 for a single dilution were then averaged and multiplied by the dilution factor. Using Beer's Law (Equation 7.2) the concentration could then be calculated, where ε is equal to the accumulative mass extinction coefficients of all the rRNA for that species, 4.81×10^7 for *E. coli* MRE600 ribosomes and 4.74×10^7 for *F. philomiragia* ribosomes, c is equal to concentration, A is absorbance and l is equal to the path length.

Equation 7.2

$$A = \varepsilon\, l\, c$$

7.5.5 RNA Analysis by Bleach Gel Electrophoresis

RNA was isolated from ribosomal samples using the GeneJet RNA purification kit (Thermo Scientific). Bleach gel electrophoresis was carried out as described by Aranda *et al*. in 2012 [395]. For a 1% agarose gel, 1× TAE buffer (7.9.5, 40 mL) was added to agarose (Sigma Aldrich) (0.4 g). Bleach (500 µL, sodium hypochlorite) was added and the solution incubated at room temperature for 5 min with occasional stirring. The agarose bleach solution was then heated (microwave), until clear and left to cool slightly before the addition of Syber Gold stain (2.5 µL in 50 mL). The solution was then poured into a secure tray and a comb carefully placed into the solution. The gel was left to solidify at room temperature.

Samples (6 µL) were prepared with 6× DNA loading buffer (2 µL) prior to loading into the set gel. Gel electrophoresis was carried out at 90 V until the samples travelled for two thirds of the gel. Gels were imaged using a SynGene Genius Imager.

7.5.6 Expression of *E. coli* W3110 RelA

The plasmid pCA24N::*Ec*relA was chemically transformed into *E. coli* BL21 (DE3) competent cells (7.3.8). Single colonies were used to inoculate 2×YT media (7.9.9, 10 mL, containing 30 µg/mL chloramphenicol) and cultured overnight at 37 °C. The overnight culture was used as a 1% inoculum for flasks of 2×YT (7.9.9, 4 x 1.25 L) which were induced with IPTG (final concentration of 0.4 mM) when the OD_{600} reached 0.6 and then cultured for 4 hours at 27 °C. The cell pellet was then collected by centrifugation (average yield of 22.3 ± 3 g/ 5 L of culture) and stored at -80 °C.

7.5.7 Purification of *E. coli* W3110 RelA by Nickel Affinity Chromatography

Frozen cell pellet (typically 22 g) was resuspended (3 x v/w cell pellet) in RelA Purification Buffer A (7.9.12). Lysozyme (5-15 mg) and a Roche protease inhibitor tablet (1 per 50 mL) were added to the cell suspension and left to stir (4 °C, 30 min). Cells were lysed by sonication (4 °C, ~20 x 30 s with 30 s rest), and cellular debris removed by centrifugation (Sorvall evolution, SS-34 rotor, 14000 rpm, 4 °C, 30 min). The resultant cleared lysate was applied (3 mL min^{-1}) to a Ni-IDA Sepharose Fast Flow Column (50 mL bed volume). The column was then washed (3 mL min^{-1}) with Buffer A until the absorption of the eluate at

280 nm (A_{280}) returned to baseline. Elution (3 mL min^{-1}) of *E. coli* RelA was achieved using a gradient of imidazole from 20 to 500 mM (Buffer B, 7.9.13, as Buffer A but with 500 mM imidazole) over 5 column volumes. Fractions containing *E. coli* RelA, as judged by Bradford assay and SDS-PAGE analysis were pooled, dialysed (7.4.3) and concentrated (7.4.4).

7.5.8 Purification of *E. coli* W3110 RelA by Size Exclusion Chromatography

The concentrated *E. coli* RelA (3 mL) was then applied (2 mL min^{-1}) to a gel filtration column (HiLoad 26/60, Superdex 200, prep grade) pre-equilibrated in RelA Purification Buffer C. The purest fractions of *E. coli* RelA, as judged by SDS-PAGE, were pooled and concentrated (7.4.4) to ~4 mg/mL (~50 µM), then aliquoted (typically 0.2 mL) and stored at -80 °C. For biochemical experiments, *E. coli* RelA aliquots were defrosted and used only once.

7.5.9 Activation of RelA by *In vitro* Stalled Ribosomal Complexes

7.5.9.1 Method 1

A 10× RelA Activating Complex (RAC) was prepared as follows; 8.93 µM ribosomes (10 µL) were heat activated by incubation at 42 °C for 2 min and then slowly cooled to 22 °C (2 °C/30 s) in a PCR machine (Eppendorf). Activated ribosomes were then programmed with mRNA (5.8 µL, 25 µM stock) and incubated at 22 °C for 2 min. To the complex $tRNA^{fmet}$ (5.8 µL, 25 µM stock) was added, followed by incubation at 22 °C for 10 min. Finally $tRNA^{val}$ (5.8 µL, 25 µM stock) was added to the complex followed by incubation at 22 °C for 1 hour. All added solutions contained 1× RelA Assay Buffer B (7.9.19).

Reaction mixtures (100 µL) were prepared with components at the following final concentrations: RelA (0.18 µM), ATP (2 mM), GTP (2 mM), 1× RAC. Reactions were incubated at 37 °C for 1 hour prior to quenching with formic acid (1 M final concentration). Precipitated protein was removed by centrifugation at 12 000 rpm, 4 °C, for 5 min. Supernatant was stored at -20 °C awaiting IP RP HPLC analysis (40 µL).

7.5.9.2 Method 2

Reaction mixtures containing stalled ribosomal complexes were prepared in 1× RelA Assay Buffer B (7.9.19) with purified ribosomes (0.2 µM), purified RelA (0.5 µM), ATP (2

mM) and each RNA species (0.3 µM). RNA species include: mRNA (5'-caaggagguaaaaauggucgucgcacgu) [295], $tRNA^{fmet}$ (from *E. coli* MRE600), and $tRNA^{val}$ (from *E. coli* MRE600). Reaction mixtures were incubated at 30 °C for 5 min prior to initiation by the addition of GTP (2 mM final concentration). Reaction mixtures were incubated for 1 hour at 30 °C prior to quenching by heating (80 °C, 2 min). Precipitated protein was removed as described previously (7.4.9.1). Supernatant was stored at -20 °C awaiting IP RP HPLC analysis (40 µL).

7.5.9.3 **Varying RelA Concentration**

Reaction mixtures containing RelA Activating Complex (RAC) as described in method 1 (at 1×), *F. tularensis* RelA (0-6 µM; 0.045, 0.09, 0.18, 0.36, 0.72, 1.44, 2.88, 5.76 µM), GTP (2 mM), ATP (2 mM) were prepared in 1× RelA Assay Buffer B (7.9.19). Reaction mixtures were incubated for 1 hour at 22 °C prior to quenching by the addition of formic acid (1 M final concentration). Precipitated protein was removed as described previously (7.4.9.1). Supernatant was stored at -20 °C awaiting IP RP HPLC analysis (40 µL).

7.5.9.4 **RelA Activation by Stalled Ribosomal Complexes**

Reaction mixtures containing stalled ribosomal complexes (method 2) were prepared in 1× RelA Assay Buffer B (7.9.19) with purified ribosomes (0.2 µM), purified RelA (0.5 µM), ATP (2 mM) and each RNA species (0.3 µM). Reaction mixtures were incubated at 30 °C for 5 min prior to initiation by the addition of GTP (2 mM final concentration). Reaction mixtures were incubated for 1 hour at 30 °C prior to quenching by heating (80 °C, 2 min). Precipitated protein was removed as described previously and a sample (40 µL) was analysed by IP RP HPLC.

7.5.10 **Subcloning of *F. tularensis rplK* Gene**

The *rplK* gene from *F. tularensis* (FTT_0140) was designed to have an N-terminal strep II tag and was purchased from Eurofins.

7.5.10.1 **Preparatory Restriction Digest**

Double digestion of plasmid pEX::rplk by restriction enzymes (NcoI and XhoI) was prepared using the following composition (Table 7.3), with restriction enzymes always added last.

Table 7.3. Composition for a preparatory scale restriction digest (NcoI and XhoI)

Component	Quantity
DNA	1 µg
NEBuffer 4 (NEB)	5 µL
BSA (10×)	1×
NcoI	10 units
XhoI	10 units
Sterile Water	Up to 50 µL

Restriction digests were incubated at 37 °C for 1 hour, after which 6× DNA loading buffer (10 µL) was added. Samples were analysed by DNA agarose gel electrophoresis (7.3.3).

7.5.10.2 **Gel Extraction**

Following DNA agarose gel electrophoresis (7.3.3) of the preparatory scale restriction digest (7.5.10.2) bands of interest were extracted from the 1% agarose gel. The bands on the gel were illuminated on a UV plate; bands of interest were excised with the use of a sharp Stanley knife. The excised bands were weighed and DNA purified using a gel extraction kit (Qiagen). Purified DNA was quantified by UV/vis analysis (Nanodrop).

7.5.10.3 **Ligation of *FtrplK* into a pET16b Vector**

Ligation of the *FtrplK* gene into pET16b vector was prepared by mixing the following together (Table 7.4), with the addition of the T4 DNA ligase at the end.

Table 7.4. Composition for the ligation of *FtrplK* gene into the pET16b vector.

Component	NEB Guidelines	Vector: Insert (1:1)	Vector: Insert (~1:2)
Vector (pET16b, 4.2 ng/µL)	50 ng	12.5 µL	12.5 µL
Insert (rplK, 22.8 ng/ µL)	50 ng	2.2 µL	4.4 µL
T4 Ligase Buffer	2 µL	2 µL	2 µL
ATP (10 mM)	1 mM	2 µL	2 µL
T4 DNA Ligase	1 µL	1 µL	1 µL
Sterile Water	To volume	0.3 µL	-
Total Volume	-	20 µL	21.9 µL

Ligations were incubated at 25 °C for 2 hours and then incubated on ice for 10-15 min before chemical transformation (7.3.4) into competent *E. coli* XL10-Gold cells.

7.5.11 **Small Scale Expression Studies for *F. tularensis* L11**

The vector pET16b::*Ft*rplK was transformed into *E. coli* BL21 (DE3) cells (7.3.4). Cultures (100 mL) of transformed cells were grown at 37 °C, 180 rpm to an OD_{600} of 0.6, before induction with IPTG (1 mM final concentration). Expression of L11 at 27 °C or 16 °C for 2, 4, and 16 hours was monitored using samples of culture (25 mL) and analysis by Bradford assay (7.3.2) and SDS-PAGE (7.3.1).

7.5.12 **Expression of *F. tularensis* L11**

Single colonies of *E. coli* BL21 (DE3) pET16b::*Ft*rplK were used to inoculate 2×YT media (7.9.9, 10 mL, containing 100 µg/mL ampicillin) and cultured overnight at 37 °C. The

overnight culture was used as a 1% inoculum for flasks of 2×YT (7.9. 9, 4 x 1.25 L) that were induced with IPTG (final concentration of 1 mM) when the optical density at 600 nm (OD_{600}) reached 0.6 and then cultured for 4 hours at 27 °C. The cell pellet was then collected by centrifugation (yield of 4.94 g/ 1 L of culture) and stored at -80 °C.

7.5.13 Purification of Strep-tagged *F. tularensis* L11 by Affinity Chromatography

Frozen cell pellet (typically 22 g) was resuspended in cold L11 Lysis Buffer (7.9.31, 3 x v/w cell pellet). Lysozyme (5-15 mg) and a Roche protease inhibitor tablet (1 per 50 mL) were added to the cell suspension and left to stir (4 °C, 30 min). Cells were lysed by sonication (4 °C, ~20 x 20 s with 40 s rest), and cellular debris removed by centrifugation (Sorvall evolution, SS-34 rotor, 14000 rpm, 4 °C, 30 min). The resultant cleared lysate was applied (3 mL min^{-1}) to a high capacity StrepTactin column (25 mL bed volume). The column was then washed (3 mL min^{-1}) with L11 Purification Buffer A (7.9.32) until the absorption of the eluate at 280 nm (A_{280}) returned to baseline. Elution (3 mL min^{-1}) of *F. tularensis* L11 was achieved using a gradient of desthiobiotin (DTB) from 0 to 2.5 mM (Buffer B, 7.9.33, as Buffer A but with 2.5 mM DTB) over 4 column volumes. Fractions (7 mL) were collected throughout the purification and were analysed by Bradford Assay (7.3.2) and SDS-PAGE analysis (7.3.1). Following purification the column was regenerated by an initial wash in 1 mM 2-(4-hydroxyazobenzene) benzoic acid (HABA) solution until the resin became deep red in colour. The column was then washed in L11 Purification Regeneration Buffer (7.9.34) until the column returned to a white colour.

7.5.14 *F. tularensis* L11 Supplemented *F. tularensis* RelA Activity Assays

Reaction mixtures (100 µL) were prepared with components at the following final concentrations: *F. tularensis* RelA (5 µM), *F. tularensis* L11 (0.5, 5, or 10 µM) ATP (2 mM), GTP (2 mM) in 1× RelA Assay Buffer B (7.9.19). Reactions were incubated at 30 °C in a water bath for 1 hour. Reactions were quenched by heating (80 °C, 2 min). Protein was precipitated by incubation at 4 °C for 10 min before removal by centrifugation at 12 000 rpm, 4 °C, for 5 min. Supernatant was stored at -20 °C awaiting IP RP HPLC analysis (40 µL).

7.5.15 RNA Supplemented *F. tularensis* RelA Activity Assays

Reaction mixtures (1000 µL) were prepared with components at the following final concentrations: *F. tularensis* RelA (5 µM), when indicated tRNA/mRNA (2.5 µM) ATP (400

µM), GTP (1 mM) in 1× RelA Assay Buffer B (7.9.19). Reactions were incubated at 30 °C in a water bath with aliquots (100 µL) taken at 0, 10, 20, 40 and 60 min. Reactions were quenched by heating (80 °C, 2 min). Protein was precipitated by incubation at 4 °C for 10 min before removal by centrifugation at 12 000 rpm, 4 °C, for 5 min. Supernatant was stored at -20 °C awaiting IP RP HPLC analysis (40 µL).

7.5.16 **Effect of amino acids on the synthetase activity of RelA enzymes**

Reaction mixtures (100 µL) were prepared with components at the following final concentrations: *F. tularensis*/ *Y. pestis*/ *E. coli* RelA (5 µM), ATP (2 mM), GTP (2 mM), serine/N-formylmethione (1 mM, or at concentration indicated) in 1× RelA Assay Buffer B (7.9.19). Reactions were incubated at 30 °C in a water bath for 1 hour. Reactions were quenched by heating (80 °C, 2 min). Protein was precipitated by incubation at 4 °C for 10 min before removal by centrifugation at 12 000 rpm, 4 °C, for 5 min. Supernatant was stored at -20 °C awaiting IP RP HPLC analysis (40 µL).

7.5.17 **Biosynthesis and Purification of ppGpp**

Reaction mixtures (5 mL) were prepared with components at the following final concentrations: GDP (5 mM), ATP (5 mM), and *Ec*RelA (33 µM) in RelA Assay Buffer A (7.9.18) [317]. Reactions were incubated at 25 °C for 16 hours, prior to quenching by heating (80 °C, 2 min). The reaction mixtures were then kept on ice to ensure full protein precipitation (typically 10 min), before clearing by centrifugation (Biofuge Fresco microfuge, 12 000 rpm, 4 °C, 5 min). The supernatant was loaded (1 mL min^{-1}) onto a DEAE sepharose column (25 mL bed volume) pre-equilibrated in ppGpp purification buffer A (7.9.35: 50 mM Tris pH 7.4, 100 mM LiCl). Elution (1 mL min^{-1}) of ppGpp was achieved using a gradient of LiCl from 100 to 1000 mM (0-100% ppGpp purification buffer B, 7.9.36) over 10 column volumes. Fractions were analysed by thin layer chromatography (TLC) using polyethylenimine (PEI) cellulose plates with KH_2PO_4 (0.75 M, pH 3.4) as the eluent. Fractions containing ppGpp were pooled and lyophilized (PowerDry LL3000, Heto). LiCl was removed by dissolving the lyophilized mixture in water and application (1 mL min^{-1}) to a G10 sephadex column pre-equilibrated in water. Elution of ppGpp was monitored by absorbance at 260 nm and LiCl elution was monitored by conductivity mS/cm. Fractions containing ppGpp were pooled and lyophilized prior to storage at -80 °C.

7.5.18 NMR Analysis of Purified ppGpp

Purified ppGpp at ~1 mg/mL in concentration was prepared in 1× RelA Assay Buffer B (7.9.19) and 10% (v/v) D_2O. Samples (750 µL) were analysed in 5 mm diameter NMR tubes on a Bruker AVIIIHD 500 MHz FT-NMR Spectrometer. Chemical shifts for purified ppGpp were referenced against phosphoric acid (H_3PO_4) for ^{31}P NMR analysis.

7.5.19 Small Molecule Activation of *F. tularensis* RelA

Reaction mixtures (100 µL) were prepared in 1× RelA Assay Buffer B (7.9.19) with components at the following final concentrations: ribonucleotide triphosphates (2 mM, both A and G), *F. tularensis* RelA (5 µM) and purified ppGpp, AMP or KH_2PO_4 (at indicated concentrations). Assays were prepared alongside a negative control containing no additional small molecular component. Reactions were incubated at 30 °C for 1 hour prior to quenching by heating (80 °C, 2 min). Protein was precipitated and removed from samples as detailed previously (7.4.9.1). Supernatant was stored at -20 °C awaiting IP RP HPLC analysis (40 µL).

7.5.20 Activation of *F. tularensis* RelA by ppGpp – EC_{50} Curve

Reaction mixtures (100 µL) were prepared in 1× RelA Assay Buffer B (7.9.19) with components at the following final concentrations: ribonucleotide triphosphates (2 mM, both A and G), *F. tularensis* RelA (5 µM) and purified ppGpp (at indicated concentrations). Assays were prepared alongside a negative control containing no additional small molecular component. Reactions were incubated at 30 °C for 60 min prior to quenching by heating (80 °C, 2 min). Protein was precipitated and removed from samples as detailed previously (7.4.9.1). Supernatant was stored at -20 °C awaiting IP RP HPLC analysis (40 µL). The EC_{50} value was calculated with a sigmoidal dose-response (variable slope) curve (Equation 7.3), using Graphpad Prism software where Y is the rate, Y_{max} is the maximum rate, Y_{min} is the basal rate and EC_{50} is the concentration of ligand required to give 50% of full activation and h is the apparent Hill slope.

Equation 7.3.

$$Y = Y_{min} + \frac{(Y_{max} - Y_{min})}{1 + 10^{(LogEC_{50} - X) - h}}$$

7.5.21 **Activation of *F. tularensis* by Methanol**

7.5.21.1 **Optimal Methanol Concentration**

Reaction mixtures (100 µL) were prepared with components at the following final concentrations: GDP (2 mM), ATP (2 mM), and *F. tularensis* RelA (10 µM) in RelA Assay Buffer A (7.9.18; 15, 30, 45, 60, and 75% v/v methanol). Reactions were incubated at 30 °C for 1 hour, prior to quenching with formic acid (1 M final concentration). The reaction mixtures were then kept on ice to ensure full protein precipitation (typically 10 min), before clearing by centrifugation (Biofuge Fresco microfuge, 12 000 rpm, 4 °C, 5 min). Supernatant was stored at -20 °C awaiting IP RP HPLC analysis (40 µL).

7.5.21.2 **Optimal Temperature**

Reaction mixtures (100 µL) were prepared with components at the following final concentrations: GDP (2 mM), ATP (2 mM), and *F. tularensis* RelA (10 µM) in 1× RelA Assay Buffer A (7.9.18; 45% v/v methanol). Reactions were incubated at 25, 30, or 40 °C for 1 hour, prior to quenching with formic acid (1 M final concentration). The reaction mixtures were then kept on ice to ensure full protein precipitation (typically 10 min), before clearing by centrifugation (Biofuge Fresco microfuge, 12 000 rpm, 4 °C, 5 min). Supernatant was stored at -20 °C awaiting IP RP HPLC analysis (40 µL).

7.6 Experimental for Chapter 4

7.6.1 Development of *F. tularensis* RelA *E. coli* GppA Coupled Enzyme Assay

7.6.1.1 Restriction Digestion of pCA24N Plasmids with SfiI

Digestion of pCA24N plasmids by the restriction enzyme SfiI was set up as described by NEB, typically using the following composition (Table 7.5). The restriction enzyme was always added last.

Table 7.5. Composition for a restriction digest (SfiI).

Component	Volume (µL)
Plasmid	5
CutSmart Buffer (NEB)	1
SfiI	1
Sterile Water	3
Total Volume	10

Restriction digests were incubated at 50 °C for 1 hour, after which 6× DNA loading buffer (2 µL) was added. Samples were analysed by DNA agarose gel electrophoresis (7.3.3).

7.6.1.2 Expression of *E. coli* GppA

The plasmid pCA24N::*Ec*gpp was chemically transformed into *E. coli* BL21 (DE3) competent cells (7.3.4). Single colonies were used to inoculate 2×YT media (7.9.9, 10 mL, containing 30 µg/mL chloramphenicol) and cultured overnight at 37 °C. The overnight culture was used as a 1% inoculum for flasks of 2×YT (7.9.9, 4 x 1.25 L) that were induced with IPTG (final concentration of 0.4 mM) when the OD_{600} reached 0.6 and then cultured for 4 hours at 27 °C. The cell pellet was collected by centrifugation (average yield of 14.6 g/ 5 L of culture) and stored at -80 °C.

7.6.1.3 **Purification of *E. coli* GppA/PPX by Nickel Affinity Chromatography**

Frozen cell pellet (typically ~15 g) was resuspended (3 x v/w cell pellet) in GppA Purification Buffer A (7.9.37: 50 mM Tris pH 8.0, 500 mM NaCl, 3 mM β-mercaptoethanol, 15% v/v glycerol and 10 mM imidazole). Lysozyme (5-15 mg) and a Roche protease inhibitor tablet (1 per 50 mL) were added to the cell suspension and left to stir (4 °C, 30 min). Cells were lysed by sonication (4 °C, 20 x 30 s with 30 s rest) and cellular debris removed by centrifugation (Sorvall evolution, SS-34 rotor, 14 000 rpm, 4 °C, 30 min). The resultant cleared lysate was applied (4 mL min^{-1}) to a Ni-IDA Sepharose Fast Flow Column (50 mL bed volume). The column was then washed (4 mL min^{-1}) with Buffer A until the absorption of the eluate at 280 nm (A_{280}) returned to baseline. Elution (4 mL min^{-1}) of *E. coli* GppA was achieved using a gradient of imidazole from 10 to 500 mM (Buffer B, as Buffer A but with 500 mM imidazole, 7.9.38) over 5 column volumes. Fractions containing *E. coli* GppA, as judged by Bradford assay and SDS-PAGE analysis were pooled, dialysed into Purification Buffer C (7.4.3) and concentrated (7.4.4) as described previously for *F. tularensis* RelA.

7.6.1.4 **Purification of *E. coli* GppA/PPX by Size Exclusion Chromatography**

The concentrated *E. coli* GppA (3 mL) was applied (2 mL min^{-1}) to a gel filtration column (HiLoad 26/60, Superdex 200, prep grade) pre-equilibrated in Purification Buffer C (7.9.14). The purest fractions of *E. coli* GppA, as judged by SDS-PAGE (7.3.1), were pooled and concentrated (7.4.4) to ~3 mg/mL (~50 µM), then aliquoted (typically 0.2 mL) and stored at -80 °C. For biochemical experiments, *E. coli* GppA aliquots were defrosted and used only once.

7.6.1.5 **^{31}P NMR Analysis of the *E. coli* GppA coupled *F. tularensis* RelA Activity Assay**

All data were recorded on a Bruker AVII400 FT-NMR Spectrometer using a 10 mm auto-tune and match broadband probe tuned to the sample prior to data collection (TD = 64k points; sweep width = 395 ppm; 512 scans using 90° pulse with a total acquisition time of 2.5 s per scan; chemical shifts referenced to H_3PO_4).

Reaction mixtures (3 mL) were prepared in 1× RelA Assay Buffer B (7.9.19) and contained GTP (2 mM), ATP (2 mM), and 10% D_2O (Table 7.6). The reaction was initiated through the

addition of; *F. tularensis* RelA (5 µM), *E. coli* GppA (5 µM) or both enzymes where applicable (at indicated concentrations). Following thorough mixing data was collected at 25 °C for 22 min followed by 22 min bins for the duration of the experiment (typically 110 min). Peak integrals were calibrated against a spectrum recorded prior to initiation.

Table 7.6. Composition of coupled enzyme activity and control assays for ^{31}P NMR analysis.

Component	Activity Assay	Time Point Zero
*Ft*RelA (47 µM)	5 µM	-
*Ec*GppA (14/ 144 µM)	0.025 – 5 µM	-
ATP (50 mM)	400 µM	400 µM
GTP (50 mM)	1000 µM	1000 µM
Assay Buffer B (10×)	1×	1 x
D_2O	10%	10%
Gel Filtration Buffer	-	Equivalent volume of enzymes
Sterile Water	Up to 3 mL	Up to 3 mL

7.6.1.6 ^{31}P NMR Analysis of the *E. coli* GppA Substrate Specificity

Reaction mixtures (3 mL) were prepared in 1× RelA Assay Buffer B (7.9.19) with 10% D_2O and contained either GTP (2 mM) or ATP (2 mM). The reaction was initiated through the addition of *E. coli* GppA (5 µM). Following thorough mixing data was collected at 25 °C for 22 min followed by 22 min bins for the duration of the experiment (typically 110 min). Peak integrals were calibrated against a spectrum recorded prior to initiation.

7.6.1.7 Malachite Green Detection of *E. coli* GppA and *F. tularensis* RelA Coupled Assay

Z' factor values used to assess the data produced by methods described in this section were calculated using Equation 7.4.; where σ denotes the standard deviation and μ denotes the average.

Equation 7.4.

$$Z' = 1 - \frac{(3\sigma_{c+} + 3\sigma_{c-})}{(\mu_{c+} - \mu_{c-})}$$

7.6.1.7.1 Synthesis of Malachite Green Reagent

In a round bottom flask malachite green carbinol base (13.5 mg) was dissolved into 30 mL of distilled water and 1 mL hydrochloric acid (4 M) forming a blue/green solution. Separately, in a glass vial, ammonium molybdate tetrahydrate (420 mg) was dissolved into 10 mL of hydrochloric acid (4 M). This acidic solution was slowly added to the dissolved malachite green carbinol base, resulting in an almost immediate colour change from blue/green to canary yellow. The combined solution (malachite green reagent) was stirred for 30 min, before filtration (Whatman filter paper) to remove any precipitate. The malachite green reagent was aliquoted (1.5 mL) and stored at -80 °C. Prior to use, each aliquot was defrosted and 10% Tween20 (1.5 μL) was added and thoroughly mixed by pipetting.

7.6.1.7.2 Platereader and Automated Workstation Protocols

Absorbance measurements were recorded with a POLARstar Omega microplate reader (BMG Labtech). A script (MG in plate assay 2.btc) was used for absorbance measurements at 0, 10, 20 and 30 min after the addition of malachite green reagent. Absorbance measurements (RW MGScurvespectra) were taken with the following parameters: positioning delay, 0.5, Number of flashes per well, 100; wavelength, spectra, 600-750 nm (resolution 1); path length correction, on, 100 μL (5.09); additional shaking, before plate reading, 10 s, double orbital 500 rpm.

The nucleotide analogue library (Reynolds) was dispensed using the laboratory automation workstation (Biomek 3000) using a designed protocol (RCW Inhibitor Dispense Whole Plate, Table 7.7).

Table 7.7. Parameters for dispensing nucleotide library.

Step	
Load Tool	MP20
Aspirate	Mix 20 µL (1×) at 100 µL/s (2 mm from bottom)
	Aspirate **5** µL at 2 mm from bottom
Dispense	Mix 10 µL (3×) at 100 µL/s (2 mm from bottom)
	Dispense **5** µL at 2 mm from bottom

Assays were initiated with GTP dispensed by the laboratory automation workstation (Biomek 3000) using a designed protocol (RCW GTP Dispense, Table 7.8).

Table 7.8. Parameters for dispensing GTP.

Step	
Load Tool	MP20
Aspirate	Mix 30 µL (1×) at 100 µL/s (5 mm from bottom)
	Aspirate **10** µL at 3.5 mm from bottom
Dispense	Mix 20 µL (3×) at 100 µL/s (2 mm from bottom)
	Dispense **10** µL at 5 mm from bottom

Assays were quenched with malachite green dispensed by the laboratory automation workstation (Biomek 3000) using a designed protocol (RCW MG Dispense, Table 7.9).

Table 7.9. Parameters for dispensing malachite green reagent.

Step	
Load Tool	MP200
Aspirate	Mix 30 µL (1×) at 100 µL/s (5 mm from bottom)
	Aspirate **50** µL at 5 mm from bottom
Dispense	Mix 40 µL (1×) at 100 µL/s (2 mm from bottom)
	Dispense **50** µL at 2 mm from bottom

7.6.1.7.3 **Background absorbance values for nucleotides in the presence of malachite green reagent.**

Commercially source nucleotides (AMP, GTP and ATP) were prepared in water over a range of concentrations (as indicated). To each well (50 µL nucleotide solution), malachite green reagent (50 µL) was injected using the laboratory automation workstation (Biomek 3000). Absorbance spectra (600-750 nm) were measured using a POLARstar Omega (BMG) platereader at 10, 20 and 30 min after the addition of malachite green reagent.

7.6.1.7.4 **Phosphate standard curves**

Phosphate standard curves were prepared with potassium phosphate (KH_2PO_4) at the the indicated concentrations in either water or 1× RelA Assay Buffer B (7.9.19). To each well (50 µL KH_2PO_4 solution), malachite green reagent (50 µL) was injected using the laboratory automation workstation (Biomek 3000). Absorbance spectra (600-750 nm) were measured using a POLARstar Omega (BMG) platereader at 10, 20 and 30 min after the addition of malachite green reagent.

7.6.1.7.5 **Optimisation of *F. tularensis* RelA Concentration.**

Stock reaction mixtures (1000 µL) were prepared containing: ATP (800 µM), GTP (200 µM) in 1× RelA Assay Buffer B (7.9.19), *F. tularensis* RelA at one of the following final concentrations: 2.5, 2, 1.5, 1, 0.5, 0.4, 0.3, 0.2, 0.1 µM and *E. coli* GppA at concentrations around 0.02 µM). Control reaction mixtures (1000 µL) were prepared containing; ATP (800 µM), GTP (200 µM) in 1× RelA Assay Buffer B (see above), and *E. coli* GppA at around 0.02 µM (see table below). Phosphate standard curves were prepared with potassium phosphate (KH_2PO_4) at the following concentrations: 0, 10, 20, 40, 50, 60, 80, 100 µM. To a 96 well UV star microplate, 50 µL of the appropriate reaction mixture was added to each well. The microplate was incubated at 30 °C for 2 hours (standing incubator). To each well, malachite green reagent (50 µL) was injected using the laboratory automation workstation (Biomek 3000). Absorbance spectra (600-750 nm) were measured using a POLARstar Omega (BMG) platereader at 10, 20 and 30 min after the addition of malachite green reagent.

7.6.1.7.6 **Optimisation of *E. coli* GppA Concentration**

Stock reaction mixtures (1000 µL) were prepared containing the following: ATP (800 µM), GTP (200 µM), *F. tularensis* RelA (2 µM) in 1× RelA Assay Buffer B (7.9.19) and *E. coli* GppA at 0.02, 0.2 or 2 µM. Control reaction mixtures (1000 µL) were prepared containing: ATP (800 µM), GTP (200 µM) in 1× RelA Assay Buffer B (see above), and *E. coli* GppA at either 0.02, 0.2 or 2 µM. Phosphate standard curves were prepared with potassium phosphate (KH_2PO_4) at the following concentrations; 0, 10, 20, 40, 50, 60, 80, 100 µM. To a 96 well UV star microplate, 50 µL of the appropriate reaction mixture was added to each well. The microplate was incubated at 30 °C for 2 hours (Function line incubator, Heraeus). To each well, malachite green reagent (50 µL) was injected using the laboratory automation workstation (Biomek 3000). Absorbance spectra (600-750 nm) were measured using a POLARstar Omega (BMG) platereader at 10, 20 and 30 min after the addition of malachite green reagent.

7.6.1.7.7 **DMSO Effect on *F. tularensis* RelA and *E. coli* GppA Coupled Assays**

Stock reaction mixtures (2000 µL) were prepared containing the following; ATP (500 µM), GTP (200 µM), *F. tularensis* RelA (2.5 µM), and *E. coli* GppA (0.025 µM) in 1× RelA Assay Buffer B (7.9.19). Control reaction mixtures (2000 µL) were prepared containing; ATP (500

μM), and GTP (200 μM) in assay buffer (see above) containing *E. coli* GppA only. Phosphate standard curves were prepared with potassium phosphate (KH_2PO_4) at the following concentrations: 0, 10, 20, 40, 50, 60, 80, 100 μM. Another set of reaction mixtures were set up as described above but with the addition of DMSO (5% final concentration). To a 96 well UV star microplate, 50 μL of the appropriate reaction mixture was added to each well. The microplate was incubated at 30 °C for 2 hours (Function line incubator, Heraeus). To each well, malachite green reagent (50 μL) was injected using the laboratory automation workstation (Biomek 3000). Absorbance spectra (600-750 nm) were measured using a POLARstar Omega (BMG) platereader at 10, 20 and 30 min after the addition of malachite green reagent.

7.6.1.7.8 **BSA Effect on *F. tularensis* RelA and *E. coli* GppA Coupled Assay**

Stock reaction mixtures (2000 μL) were prepared containing the following: ATP (500 μM), GTP (200 μM), *F. tularensis* RelA (2.5 μM), *E. coli* GppA (0.025 μM), and 5% DMSO in 1× RelA Assay Buffer B (7.9.19). Control reaction mixtures (2000 μL) were prepared containing: ATP (500 μM), GTP (200 μM), and 5% DMSO in 1× RelA Assay Buffer B (see above) containing *E. coli* GppA only. Phosphate standard curves were prepared with potassium phosphate (KH_2PO_4) at the following concentrations; 0, 10, 20, 40, 50, 60, 80, 100 μM. Reaction mixtures were set up with the addition of 0, 0.025, 0.5, or 1 mg/mL BSA. To a 96 well UV star microplate, 50 μL of the appropriate reaction mixture was added to each well. The microplate was incubated at 30 °C for 2 hours (standing incubator). To each well, malachite green reagent (50 μL) was injected using the laboratory automation workstation (Biomek 3000). Absorbance spectra (600-750 nm) were measured using a POLARstar Omega (BMG) platereader at 10, 20 and 30 min after the addition of malachite green reagent.

7.6.1.7.9 **Buffer Optimisation for Coupled Enzyme Assay**

Variations, detailed in Table 7.10, of the 1× RelA Assay Buffer B (7.9.19) were made to establish optimal conditions. At each variation all other components were kept at the original concentration.

Table 7.10. Concentrations used for buffer optimisation experiments.

Component	0	0.5×	1×	2×
Tris pH 8.0	-	10 mM	20 mM	40 mM
β-mercaptoethanol	-	0.5 mM	1 mM	2 mM
KCl	-	7.5 mM	15 mM	30 mM
$MgCl_2$	-	7.5 mM	15 mM	30 mM

Reaction mixtures (500 µL) were prepared with the following: ATP (500 µM), GTP (200 µM), *F. tularensis* RelA (2 µM), and *E. coli* GppA (0.02 µM). Control reaction mixtures (500 µL) were prepared containing; ATP (500 µM) and GTP (200 µM) in the appropriate assay buffer (see above) containing *E. coli* GppA only. Phosphate standard curves were prepared with potassium phosphate (KH_2PO_4) at the following concentrations; 0, 10, 20, 40, 50, 60, 80, 100 µM. To a 96 well UV star microplate, 50 µL of the appropriate reaction mixture was added to each well. The microplate was incubated at 30 °C for 2 hours (Function line incubator, Heraeus). To each well, malachite green reagent (50 µL) was injected using the laboratory automation workstation (Biomek 3000). Absorbance spectra (600-750 nm) were measured using a POLARstar Omega (BMG) platereader at 10, 20 and 30 min after the addition of malachite green reagent.

7.6.1.7.10 **Effect of DMSO and BSA on the Coupled Assay**

Reaction mixtures (500 µL) were prepared with the following: ATP (500 µM), GTP (200 µM), *F. tularensis* RelA (2 µM), and *E. coli* GppA (0.02 µM) in 1× RelA Buffer B (7.9.19). Control reaction mixtures (500 µL) were prepared containing; ATP (500 µM) and GTP (200 µM) in 1× RelA Buffer B (7.9.19). Both control and coupled assays were set up either with BSA (0, 0.025, 0.05, 0.1 mg/mL) or DMSO (0 or 5 %). Phosphate standard curves in both the presence and absence of the different additives were prepared with potassium phosphate (KH_2PO_4) at the following concentrations; 0, 10, 20, 40, 50, 60, 80, 100 µM. To a 96 well UV star microplate, 50 µL of the appropriate reaction mixture was added to each well. The microplate was incubated at 30 °C for 2 hours (Function line incubator, Heraeus). To each well, malachite green reagent (50 µL) was injected using the laboratory

automation workstation (Biomek 3000). Absorbance spectra (600-750 nm) were measured using a POLARstar Omega (BMG) platereader at 10, 20 and 30 min after the addition of malachite green reagent.

7.6.1.7.11 **Time Course analysis of *F. tularensis* RelA Coupled Assay**

Stock reaction mixtures (3000 µL) were prepared containing the following: ATP (500 µM), GTP (200 µM), *F. tularensis* RelA (as indicated at either 0.3, 0.5 or 2.5 µM), and *E. coli* GppA (0.015, 0.02, 0.025 µM respectively) in 1× HTS Buffer (7.9.39) High Throughput Screen (HTS) Assay Buffer (7.9.39; 20 mM Tris pH 8.0, 15 mM KCl, 30 mM $MgCl_2$, 1 mM β-mercaptoethanol, 1 mg/mL BSA, 5% DMSO). Control reaction mixtures (3000 µL) were prepared containing: ATP (500 µM) and GTP (200 µM) in HTS Assay Buffer (7.9.39) containing *E. coli* GppA only. Reaction mixtures and Control mixtures were incubated at 30 °C (water bath) with aliquots withdrawn (300 µL) at indicated time points (i.e.; 0, 15, 30, 45, 60, 75, 90, 105, 120, 135, 150 and 180 min). Reactions were quenched by heating (80 °C, 2 min) and then protein precipitated by incubation on ice (4 °C, 10 min) and removed by centrifugation (12 000 rpm, 4 °C, 5 min). To a 96 well UV star microplate, 50 µL of the appropriate reaction mixture was added to each well. Phosphate standard curves were prepared with potassium phosphate (KH_2PO_4) at the following concentrations; 0, 10, 20, 40, 50, 60, 80, 100 µM. To each well, malachite green reagent (50 µL) was injected using the laboratory automation workstation (Biomek 3000). Absorbance spectra (600-750 nm) were measured using a POLARstar Omega (BMG) platereader at 10, 20 and 30 min after the addition of malachite green reagent.

7.6.2 **Screening of Nucleotide Libraries**

7.6.2.1 **Preparation of Nucleotide Analogue Library**

From a stock (10 mM) previously aliquoted by M. Giurrandino a lower stock concentration (100 µM) was prepared. To 297 µL of DMSO (100%) 3 µL of a nucleotide analogue (10 mM) was added using the laboratory automation workstation (Biomek 3000). Stocks were stored at -80 °C, and defrosted by incubation at 30 °C for 1 hour prior to use.

7.6.2.2 **Screening the Nucleotide Analogue Library**

Compounds were screened against *F. tularensis* RelA in a UV star 96 well microtitre plate. To each assay well, a reaction mixture (35 µL) was added containing: ATP (500 µM), *F. tularensis* RelA (500 nM) and *E. coli* GppA (20 nM) in HTS Assay Buffer (7.9.39). Negative control (100% activity) reaction mixtures (50 µL) were prepared as described above. Positive controls (0% activity) were prepared containing ATP (500 µM) and *E. coli* GppA (20 nM) in 1× HTS Assay Buffer (7.9.39). All control reaction mixtures contained 5% DMSO. Standard curves were set up for the following phosphate concentrations 100, 60, 20 and 0 µM.

To each assay well, 5 µL of a nucleotide analogue (100 µM stock) and 10 µL GTP (1 mM stock) were injected into wells using the laboratory automation workstation (Biomek 3000). The plate was incubated at 30 °C for 90 min in a Function line incubator, Heraeus. Assays were quenched by the addition of malachite green reagent (50 µL) using the laboratory automation workstation (Biomek 3000). Absorbance spectra (600-750 nm) were measured using a POLARstar Omega (BMG) platereader at 10, 20 and 30 min after the addition of malachite green reagent.

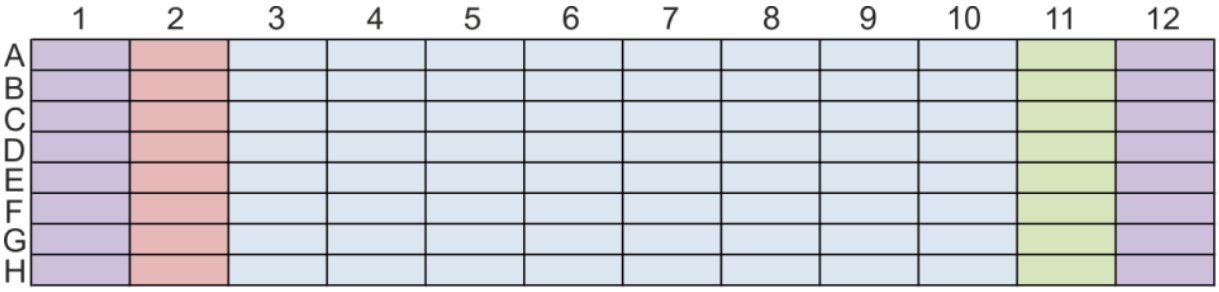

Figure 7.1. Plate layout for the screening of *F. tularensis* RelA against a nucleotide library; negative (*F. tularensis* RelA and *E. coli* GppA) control wells (green), positive control (*E. coli* GppA only) wells (red), phosphate standard curves (purple), assays containing nucleotide analogue compounds (blue).

Verification assays were set up as described above but with a higher concentration of 100 µM (1 mM stock) of potential inhibitors added to individual wells.

7.6.3 Broadening the application of the high throughput screen

7.6.3.1 Expression of *E. coli* PPX

The plasmid pCA24N::*Ec*ppx was chemically transformed into *E. coli* BL21 (DE3) competent cells (7.3.4). Single colonies were used to inoculate 2×YT media (7.9.9, 10 mL, containing 30 µg/mL chloramphenicol) and cultured overnight at 37 °C. The overnight culture was used as a 1% inoculum for flasks of 2×YT (7.9.9, 4 x 1.25 L) that were induced with IPTG (final concentration of 1 mM) when the OD_{600} reached 0.6 and then cultured for 4 hours at 27 °C. The cell pellet was collected by centrifugation (average yield of ~20 g / 5 L of culture) and stored at -80 °C.

7.6.3.2 Substitution of the secondary (Coupling) enzyme

Reaction mixtures (500 µL) were prepared with the following: ATP (500 µM), GTP (200 µM), *F. tularensis* RelA (2 µM), and *E. coli* PPX (0.02 µM) in 1× RelA Buffer B (7.9.19). Control reaction mixtures (500 µL) were prepared containing; ATP (500 µM) and GTP (200 µM) in 1× HTS Assay Buffer (7.9.39). Phosphate standard curves were prepared with potassium phosphate (KH_2PO_4) at the following concentrations; 0, 10, 20, 40, 50, 60, 80, 100 µM. To a 96 well UV star microplate, 50 µL of the appropriate reaction mixture was added to each well. The microplate was incubated at 30 °C for 90 minutes in a Function line incubator (Heraeus). To each well, malachite green reagent (50 µL) was injected using the laboratory automation workstation (Biomek 3000). Absorbance spectra (600-750 nm) were measured using a POLARstar Omega (BMG) platereader at 10, 20 and 30 min after the addition of malachite green reagent.

7.6.3.3 Substitution of the primary enzyme (RelA)

Reaction mixtures (500 µL) were prepared with the following: ATP (500 µM), GTP (200 µM), *E. coli* GppA (0.02 µM) in 1× RelA Buffer B (7.9.19) and either *Y. pestis* or *E. coli* RelA (2 µM). Control reaction mixtures (500 µL) were prepared containing; ATP (500 µM) and GTP (200 µM) in 1× RelA Buffer B (7.9.19). Phosphate standard curves were prepared with potassium phosphate (KH_2PO_4) at the following concentrations; 0, 10, 20, 40, 50, 60, 80, 100 µM. To a 96 well UV star microplate, 50 µL of the appropriate reaction mixture was added to each well. The microplate was incubated at 30 °C for 90 minutes in a Function

line incubator (Heraeus). To each well, malachite green reagent (50 µL) was injected using the laboratory automation workstation (Biomek 3000). Absorbance spectra (600-750 nm) were measured using a POLARstar Omega (BMG) platereader at 10, 20 and 30 min after the addition of malachite green reagent.

7.7 Experimental for Chapter 5

7.7.1 Small Scale Expression of *Y. pestis* RelA

The vector pET16b::*Yp*relA was transformed into *E. coli* BL21 (DE3) cells (7.3.4). Cultures (100 mL) of transformed cells were grown at 37 °C, 180 rpm to an OD_{600} of 0.6, before induction with IPTG (1 mM final concentration). Expression of *Y. pestis* RelA at 27 °C or 16 °C for 2, 4, and 16 hours was monitored using samples of culture (100 mL) and analysis by Bradford assay (7.3.2) and SDS-PAGE (7.3.1).

7.7.2 Small Scale Expression by Auto-induction

The plasmid of interest (i.e.; pET16b::*Yp*relA/ pET16b::*Bp*relA) was chemically transformed into *E. coli* BL21 (DE3) competent cells (7.3.4). Single colonies were used to inoculate 2×YT media (7.9.9, 10 mL, containing 100 µg/mL ampicillin and 30 µg/mL chloramphenicol) and cultured overnight at 37 °C. The overnight culture was used as a 1% inoculum for flasks of auto-induction media (7.9.40, 100 mL) which were cultured overnight at 27 °C. The cell pellet was then collected by centrifugation and stored at -80 °C.

7.7.3 Expression of *Y. pestis* RelA

The plasmid pET16b::*Yp*relA was chemically transformed into *E. coli* BL21 (DE3) competent cells (7.3.4). Single colonies were used to inoculate 2×YT media (7.9.9, 10 mL, containing 100 µg/mL ampicillin) and cultured overnight at 37 °C. The overnight culture was used as a 1% inoculum for flasks of 2×YT (4 x 1.25 L) which were induced with IPTG (final concentration of 1 mM) when the OD_{600} reached 0.6 and then cultured for 4 hours at 27 °C. The cell pellet was then collected by centrifugation (average yield of 30.4 ±6.1 g/ 5 L of culture) and stored at -80 °C.

7.7.4 **Purification of *Y. pestis* RelA by Nickel Affinity Chromatography**

Frozen cell pellet (typically ~30 g) was resuspended (3 x v/w cell pellet) in RelA Purification Buffer A (7.9.12: with 10 mM Imidazole instead of 20 mM). Lysozyme (5-15 mg) and a Roche protease inhibitor tablet (1 per 50 mL) were added to the cell suspension and left to stir (4 °C, 30 min). Cells were lysed by sonication (4 °C, ~20 x 30 s with 30 s rest) and cellular debris removed by centrifugation (Sorvall evolution, SS-34 rotor, 14000 rpm, 4 °C, 30 min). The resultant cleared lysate was applied (3 mL min^{-1}) to a Ni-IDA Sepharose Fast Flow Column (30 mL bed volume). The column was then washed (3 mL min^{-1}) with Buffer A until the absorption of the eluate at 280 nm (A_{280}) returned to baseline. Elution (3 mL min^{-1}) of *Y. pestis* RelA was achieved using a gradient of imidazole from 10 to 500 mM (7.9.13, Buffer B, as Buffer A but with 500 mM imidazole) over 10 column volumes. Fractions containing *Y. pestis* RelA, as judged by Bradford assay and SDS-PAGE analysis were pooled, dialysed (7.4.3) and concentrated (7.4.4).

7.7.5 **Purification of *Y. pestis* / *B. pseudomallei* RelA by Size Exclusion Chromatography**

The concentrated *Y. pestis/ B. pseudomallei* RelA (3 mL) was then applied (2 mL min^{-1}) to a gel filtration column (HiLoad 26/60, Superdex 200, prep grade) pre-equilibrated in RelA Purification Buffer D (7.9.40). The purest fractions of *Y. pestis/ B. pseudomallei* RelA, as judged by SDS-PAGE, were pooled and concentrated (7.4.4) to 1-2 mg/mL (~18 µM), then aliquoted (typically 0.2 mL) and stored at -80 °C. For biochemical experiments, *Y. pestis / B. pseudomallei* RelA aliquots were defrosted and used only once.

7.7.6 **Substrate Specificity of *Y. pestis* RelA**

Reaction mixtures (100 µL) were prepared with components at the following final concentrations: guanosine di- or triphosphates (2 mM), ATP (2 mM), and *Y. pestis* RelA (5 µM) in 1× RelA Assay Buffer B (7.9.19). Reactions were incubated at 30 °C for 1 hour, prior to quenching by heating (80 °C, 2 min). The reaction mixtures were then kept on ice to ensure full protein precipitation (typically 10 min), before clearing by centrifugation (Biofuge Fresco microfuge, 12000 rpm, 4 °C, 5 min). Supernatant was stored at -20 °C awaiting IP RP HPLC analysis (40 µL).

7.7.7 Small Scale Expression of *B. pseudomallei* RelA

The vector pET16b::*Bp*relA was transformed into *E. coli* BL21 (DE3) cells (7.3.4). Cultures (100 mL) of transformed cells were grown at 37 °C, 180 rpm to an OD_{600} of 0.6, before induction with IPTG (1 mM final concentration). Expression of *B. pseudomallei* RelA at 27 °C or 16 °C for 2, 4, and 16 hours was monitored using samples of culture (100 mL) and analysis by Bradford assay (7.3.2) and SDS-PAGE (7.3.1).

7.7.8 Expression of *B. pseudomallei* RelA (Carried out by C. Frankling)

The plasmid pET16b::*Bp*relA was chemically transformed into *E. coli* BL21 (DE3) competent cells. Single colonies were used to inoculate 2×YT media (7.9.9, 10 mL, containing 30 μg/mL chloramphenicol) and cultured overnight at 37 °C. The overnight culture was used as a 1% inoculum for flasks of 2×YT (7.9.9, 4 x 1.25 L) which were induced with IPTG (final concentration of 0.4 mM) when the OD_{600} reached 0.6 and then cultured for 4 hours at 27 °C. The cell pellet was then collected by centrifugation (yield of 31.12 g/ 5 L of culture and stored at -80 °C.

7.7.9 Purification of *B. pseudomallei* RelA by Nickel Affinity Chromatography (carried out by C. Frankling)

Frozen cell pellet (typically 31.12 g) was resuspended (3 x v/w cell pellet) in RelA Purification Buffer A (7.9.12). Lysozyme (5-15 mg) and a Roche protease inhibitor tablet (1 per 50 mL) were added to the cell suspension and left to stir (4 °C, 30 min). Cells were lysed by sonication (4 °C, 30 x 30 s with 30 s rest), and cellular debris removed by centrifugation (Sorvall evolution, SS-34 rotor, 14,000 rpm, 4 °C, 30 min). The resultant cleared lysate was applied (4 mL min^{-1}) to a Ni-IDA Sepharose Fast Flow Column (50 mL bed volume). The column was then washed (4 mL min^{-1}) with Buffer A until the absorption of the eluate at 280 nm (A_{280}) returned to baseline. Elution (4 mL min^{-1}) of *B. pseudomallei* RelA was achieved using a gradient of imidazole from 20 to 500 mM (Buffer B, as Buffer A but with 500 mM imidazole, 7.9.13) over 5 column volumes. Fractions containing *B. pseudomallei* RelA, as judged by Bradford assay and SDS-PAGE analysis were pooled, dialysed (7.4.3) into RelA Purification Buffer D (7.9.41) and concentrated (7.4.4).

7.7.10 Substrate Specificity of *B. pseudomallei* RelA

Reaction mixtures (100 µL) were prepared with components at the following final concentrations: guanosine di- or triphosphates (2 mM), ATP (2 mM), and *B. pseudomallei* RelA (5 µM) in 1× RelA Assay Buffer B (7.9.19). Reactions were incubated at 30 °C for 1 hour, prior to quenching by heating (80 °C, 2 min). The reaction mixtures were then kept on ice to ensure full protein precipitation (typically 10 min), before clearing by centrifugation (Biofuge Fresco microfuge, 12000 rpm, 4 °C, 5 min). Supernatant was stored at -20 °C awaiting IP RP HPLC analysis (40 µL).

7.8 Experimental for Appendices

7.8.1 Effect of nucleotide analogues (ddGTP or AMPCPP) on *F. tularensis* RelA synthetase activity.

Reaction mixtures (100 µL) were prepared with components at the following final concentrations: GTP (1 mM, 2 mM), ATP (0.4 mM, or 1 mM), *F. tularensis* RelA (5 µM) and either AMPCPP (Synthesised by C. Frankling [337]) or ddGTP (Sigma Aldrich) at indicated concentrations (0, 10, 100, or 1000 µM) in 1× RelA Assay Buffer B (7.9.19). Experiments with ddGTP contained GTP at $K_{1/2}$ concentrations (1 mM) and ATP at saturating concentrations (1 mM). Experiments with AMPCPP contained ATP at $K_{1/2}$ concentrations (0.4 mM) and GTP at saturating concentrations (2 mM). Control reactions were prepared as above but with GTP (2 mM) and AMPCPP (0.4 mM) or ATP (1 mM) and ddGTP (1 mM). Reactions were incubated at 30 °C for 1 hour, prior to quenching by heating (80 °C, 2 min). The reaction mixtures were then kept on ice to ensure full protein precipitation (typically 10 min), before clearing by centrifugation (Biofuge Fresco microfuge, 12000 rpm, 4 °C, 5 min). Supernatant was stored at -20 °C awaiting IP RP HPLC analysis (40 µL).

7.8.2 Crystallisation of *F. tularensis* RelA

7.8.2.1 Sparse Screens for *F. tularensis* RelA

Sparse crystallisation screens for *F. tularensis* RelA (10 mg/mL) were prepared either using a Gryphon robot (Art Robbins Instruments) or set up by hand, in a sitting drop format [396]. A 96-well MRC 3 drop LP plate (Molecular Dimensions) was set up using a pre-prepared 96-well screens, with reservoir (40 µL) and 3 sitting drops (0.5 µL reservoir

buffer, 0.5 µL protein complex). Commercial 96 well screens tested were PactPremier, JCSG$^+$, Morpheus, MemGold I and II, Midas (Molecular Dimensions). The plate was sealed with a ClearVue sheet (Molecular Dimensions) before incubation at 25 °C, 15 °C or 4 °C. Wells were monitored for crystal growth using a Leica M165 C microscope with images taken on the program Leica Application Suite. Alternatively wells were monitored for crystal growth using CrystalTrak v2 (Rigaken) linked to a Crystalmation hotel suite (Rigaken). Plates maintained at 15 °C were incubated in an Unichromat 1700 incubator (Avant).

7.8.2.2 **Co-crystallisation of *F. tularensis* RelA and *E. coli* GppA**

Sparse crystallisation screens for *F. tularensis* RelA (18.7 mg/ mL) coupled with *E. coli* GppA (12.3 mg/ mL) were set up by hand in a sitting drop format [396]. A 96-well MRC 3 drop LP plate (Molecular Dimensions) was set up using a pre-prepared 96-well screens, with reservoir (40 µL) and 3 sitting drops (0.5 µL reservoir buffer, 0.5 µL protein complex). Commercial 96 well screens tested were Midas, Proplex (Molecular Dimensions). The plate was sealed with a ClearVue sheet (Molecular Dimensions) before incubation at 25 °C. Wells were monitored for crystal growth using a Leica M165 C microscope with images taken on the program Leica Application Suite.

7.8.2.3 **Narrow Screens**

Narrow crystallisation screens for *F. tularensis* RelA were set up by hand in 24-well XRL plates using the hanging drop method [396]. Narrow screens were set up around conditions for wells G1 and E2 from the Proplex screen (Molecular Dimension) (Table E.1 and E.2).

7.9 Preparation of Buffers

Composition and preparation of buffers are listed below, following the order in which they first appear in the text.

7.9.1 SDS Loading Buffer (250 mL)

Component	Quantity	Concentration
0.2 M Tris HCl pH 6.8	125 mL	100 mM
Sodium Dodecyl Sulphate (SDS)	10 g	139 mM
Bromophenol Blue	500 mg	3 mM
Glycerol	50 mL	20%
SDS Tank Buffer (7.9.3)	75 mL	-

7.9.2 SDS Tank Buffer (5 L)

Component	Quantity	Concentration
Glycine	94 g	250 mM
Tris base	15.1 g	25 mM
SDS	5 g	3.5 mM
Deionised water	To 5 L	-

7.9.3 **Coomassie Brilliant Blue Stain**

Component	Quantity	Concentration
Coomassie Blue	2.5 g	3 mM
Methanol: Water (1:1)	900 mL	45% Methanol
Acetic Acid	100 mL	10%

7.9.4 **Destain Solution**

Component	Quantity	Concentration
Methanol	250 mL	5%
Acetic Acid	375 mL	7.5%
Deionised Water	4375 mL	-

7.9.5 **50× TAE Buffer (pH 8, 1 L)**

Component	Quantity	Concentration
Tris acetate	242 g	2 M
EDTA (500 mM)	100 mL	50 mM
Deionised water	To 1 L	-

7.9.6 **DNA Loading Dye (10 mL)**

Component	Quantity	Concentration
Glycerol	3 mL	30%
0.5 M Ethylenediaminetetraacetic Acid (EDTA) pH 8.0	3 mL	150 mM
Bromophenol Blue	3 mg	0.45 mM
Xylene Cyanol	3 mg	0.56 mM
Sterile Water	4 mL	-

7.9.7 **SOC media (1 L)**

The following was dissolved:

Component	Quantity
Tryptone	20 g
Yeast Extract	5 g
NaCl	0.5 g
Deionised water	965 mL

To the above solution the following was added:

Component	Quantity
KCl (250 mM)	10 mL
$MgCl_2$ (2 M)	5 mL

The solution was autoclaved (121 °C, 15 min) and then the following added:

Component	Quantity
Sterile Filtered glucose (1 M)	20 mL

SOC media was stored at 4 °C in sealed sterile 15 mL falcon tubes until use.

7.9.8 **Agar Plates**

7.9.8.1 **2×YT media Agar Plates (500 mL) (For *E. coli* K12- and BL21-derived strains)**

Agar was prepared as described below and autoclaved for sterilisation (121 °C, 15 min). Sterilised agar was left to cool to ~50 °C prior to the addition of any antibiotics followed by pouring into triple vented petri dishes and leaving to set.

Component	Quantity
Tryptone	8 g
Yeast Extract	5 g
NaCl	2.5 g
Agar	7.5 g
Deionised water	To 1 L

Agar plates were sealed with Parafilm before storage upside down at 4 °C.

7.9.8.2 **Blood Agar Plates (250 mL) (For *F. philomiragia*)**

Agar was prepared as described below and autoclaved for sterilisation (121 °C, 15 min). Sterilised agar was left to cool to ~50 °C prior to the addition of defibrinated horse blood (12.5 mL, Sigma Aldrich) followed by pouring into triple vented petri dishes and leaving to set.

Component	Quantity
Cysteine Heart Agar Powder	25.5 g
Deionised water	237.5 mL

Agar plates were sealed with Parafilm before storage upside down at 4 °C in a locked cupboard.

7.9.8.3 **Luria Broth (LB) supplemented with 10 mM $MgSO_4$ agar plates (For *E. coli* MRE600)**

Agar was prepared as described below and autoclaved for sterilisation (121 °C, 15 min). Sterilised agar was left to cool to ~50 °C prior to pouring into triple vented petri dishes and then left to set.

Component	Quantity
Tryptone	10 g
Yeast Extract	5 g
NaCl	10 g
$MgSO_4$	2.465 g
Agar	7.5 g
Deionised water	To 1 L

Agar plates were sealed with Parafilm before storage upside down at 4 °C.

7.9.9 **2×YT media (1 L)**

Media was prepared as described below and autoclaved for sterilisation (121 °C, 15 min).

Component	Quantity
Tryptone	16 g
Yeast Extract	10 g
NaCl	5 g
Deionised water	To 1 L

7.9.10 **TBF I Buffer (pH 5.8, 1 L)**

The following was prepared and sterile filtered before storage at -80 °C.

Component	Quantity	Concentration
$RbCl_2$	12.1 g	100 mM
$MnCl_2$	9.9 g	50 mM
KOAc	2.9 g	30 mM
$CaCl_2$	1.1 g	10 mM
Deionised water	985 mL	-

Buffer was made to the correct pH with acetic acid (HOAc).

7.9.11 **TBF II Buffer (pH 7.0, 1 L)**

The following was prepared and sterile filtered before storage at -80 °C.

Component	Quantity	Concentration
MOPS	2.1 g	10 mM
$RbCl_2$	1.2 g	10 mM
$CaCl_2$	8.3 g	75 mM
Glycerol	15 mL	15%
Deionised water	985 mL	-

7.9.12 **(RelA) Purification (Nickel Affinity Chromatography) Buffer A (pH 8.0, 1 L)**

Component	Quantity	Concentration
Tris Base	6.07 g	50 mM
NaCl	29.22 g	500 mM
Imidazole	1.36 g	20 mM
Glycerol	150 g	15% (w/v)
β-mercaptoethanol	200 µL	3 mM
Deionised water	To 1 L	-

Buffer was made to the correct pH with hydrochloric acid (HCl). Buffer was stored at 4 °C prior to and during use.

7.9.13 **(RelA) Purification (Nickel Affinity Chromatography) Buffer B (pH 8.0, 1 L)**

Component	Quantity	Concentration
Tris Base	6.07 g	50 mM
NaCl	29.22 g	500 mM
Imidazole	34 g	500 mM
Glycerol	150 g	15% (w/v)
β-mercaptoethanol	200 µL	3 mM
Deionised water	To 1 L	-

Buffer was made to the correct pH with hydrochloric acid (HCl). Buffer was stored at 4 °C prior to and during use.

7.9.14 **(RelA) Purification Buffer C (pH 8.0, 2 L)**

Component	Quantity	Concentration
Tris Base	12.7 g	50 mM
Tris HCl	2.36 g	-
NaCl	35.16 g	300 mM
Glycerol	300 g	15% (w/v)
Dithiothreitol (DTT)	154 mg	1 mM
Deionised water	To 1 L	-

Buffer was made to the correct pH with hydrochloric acid (HCl) or sodium hydroxide (NaOH). Buffer was stored at 4 °C prior to and during use.

7.9.15 **Analytical Gel Filtration Buffer (pH 7.5, 1 L)**

Component	Quantity	Concentration
Tris HCl	7.88 g	50 mM
KCl	7.45 g	100 mM
Deionised water	To 1 L	-

Buffer was made to the correct pH using hydrochloric acid (HCl) or potassium hydroxide (KOH). Buffer was stored at 4 °C prior to and during use.

7.9.16 **HPLC Aqueous Phase (pH 7.0, 1 L)**

Aqueous phase solution, see below, was made to the correct pH with acetic acid (HOAc) in a fume hood.

Component	Quantity	Concentration
N,N-Dimethylethylamine (DMHA)	2.6 mL	15 mM
Methanol (HPLC grade)	50 mL	5%
Deionised water	To 1 L	-

The solution was prepared and then filtered via passage through a glass sinter filter. The buffer was degassed in a sonication bath (5 min) before use. Solution was stored at room temperature during and prior to use.

7.9.17 **HPLC Organic Phase (pH 7.0, 1 L)**

Organic phase solution, see below, was made to the correct pH with acetic acid (HOAc) in a fume hood.

Component	Quantity	Concentration
N,N-Dimethylethylamine (DMHA)	2.6 mL	15 mM
Methanol (HPLC grade)	800 mL	80 %
Deionised water	To 1 L	-

The solution was prepared and then filtered via passage through a glass sinter filter. The buffer was degassed in a sonication bath (5 min) before use. Solution was stored at room temperature during and prior to use.

7.9.18 **1× RelA Assay Buffer A (pH 8.0, 100 mL)**

Component	Quantity	Concentration
Tris Acetate	905.9 mg	50 mM
$Mg(OAc)_2$ (tetrahydrate)	321.7 mg	15 mM
KOAc	588.7 mg	60 mM
NH_4OAc	231.5 mg	30 mM
EDTA	5.845 mg	0.2 mM
Methanol	30 mL	30 %
Deionised water	To 100 mL	-

Variations of this buffer were made with methanol concentrations ranging from 5 to 60%. Buffer was made to the correct pH using either acetic acid (HOAc) or potassium hydroxide (KOH).

7.9.19 **10× RelA Assay Buffer B (pH 8.0, 100 mL)**

Component	Quantity	Concentration
Tris Base	2.423 g	200 mM
$MgCl_2$ (hexahydrate)	3.045 g	150 mM
KCl	1.118 g	150 mM
β-mercaptoethanol	66.6 µL	10 mM
Deionised water	To 100 mL	-

Assay buffer was made to the correct pH using hydrochloric acid (HCl). Aliquots (1 mL) were prepared and stored at -20 °C prior to use.

7.9.20 **LCMS Aqueous Phase (pH 8.7, 1 L)**

Aqueous phase solution, see below, was made to the correct pH with acetic acid (HOAc) in a fume hood.

Component	Quantity	Concentration
N,N-Dimethylethylamine (DMHA)	2.6 mL	15 mM
Hexafluoroisopropanol (HFIP)	4.21 mL	100 mM
Methanol (LCMS grade)	50 mL	5%
Deionised water	To 1 L	-

The solution was prepared and then filtered via passage through a glass sinter filter. The buffer was degassed in a sonication bath (5 min) before use. Solution was stored at room temperature during and prior to use.

7.9.21 **LCMS Organic Phase (pH 8.0, 1 L)**

Organic phase solution, see below, was made to the correct pH with acetic acid (HOAc) in a fume hood.

Component	Quantity	Concentration
N,N-Dimethylethylamine (DMHA)	2.6 mL	15 mM
Methanol (LCMS grade)	50 mL	5%
Deionised water	To 1 L	-

The solution was prepared and then filtered via passage through a glass sinter filter. The buffer was degassed in a sonication bath (5 min) before use. Solution was stored at room temperature during and prior to use.

7.9.22 **LCMS Make-up Buffer (pH 10, 1 L)**

Make-up buffer, see below, was made to the correct pH with ammonia (NH_3) in a fume hood.

Component	Quantity	Concentration
Acetonitrile (LCMS grade)	500 mL	50%
Deionised water	500 mL	50%

7.9.23 **Luria Broth (LB) media supplemented with 10 mM $MgSO_4$ (1 L)**

Media was prepared as described below and autoclaved for sterilisation (121 °C, 15 min).

Component	Quantity
Tryptone	10 g
Yeast Extract	5 g
NaCl	10 g
$MgSO_4$	2.465 g
Deionised Water	To 1 L

7.9.24 **Trypticase Soy Broth (TSB) supplemented with L-cysteine (6.3 mM) (1 L)**

Media was prepared as described below and autoclaved for sterilisation (121 °C, 15 min).

Component	Quantity
TSB Powder (Becton Dickinson)	30 g
L-cysteine (Sigma Aldrich)	1 g
Deionised	To 1 L

7.9.25 **THM Buffer (pH 7.4, 500 mL)**

Buffer was prepared as described below and autoclaved for sterilisation (121 °C, 15 min).

Component	Quantity	Concentration
Tris HCl	661 mg	10 mM
Tris Base	97 mg	-
$Mg(OAc)_2$	1.072 g	10 mM
Deionised water	To 500 mL	-

7.9.26 **Coupling Buffer (pH 8.0, 1 L)**

Component	Quantity	Concentration
Tris Base	2.21 g	50 mM
Tris HCl	4.36 g	-
Disodium Ethylenediaminetetraacetic Acid (Na_2-EDTA)	1.86 g	5 mM
Deionised water	To 1 L	-

7.9.27 **Kaiser Test Solution A (55 mL)**

Component	Quantity
9.81 mM Potassium Cyanide (KCN)	1 mL
Pyridine	49 mL
Phenol	20 g
Ethanol	5 mL

7.9.28 **Kaiser Test Solution B (25 mL)**

Component	Quantity
Ninhydrin	1.25 g
Ethanol	25 L

7.9.29 **Ribosome Purification Buffer A (pH 7.5, 1 L)**

Buffer was prepared as described below and autoclaved for sterilisation (121 °C, 15 min). Once cooled the buffer was stored at 4 °C until use.

Component	Quantity	Concentration
Tris HCl	6.35 g	20 mM
Tris Base	1.18 g	-
NH_4Cl	5.39 g	100 mM
Na_2-EDTA	0.186 g	0.5 mM
$Mg(OAc)_2$	2.252 g	10.5 mM
Deionised water	To 1 L	-

7.9.30 **Ribosome Purification Buffer B (pH 7.5, 1 L)**

Buffer was prepared as described below and autoclaved for sterilisation (121 °C, 15 min). Once cooled the buffer was stored at 4 °C until use.

Component	Quantity	Concentration
Tris HCl	6.35 g	20 mM
Tris Base	1.18 g	-
NH_4Cl	16.05 g	300 mM
Na_2-EDTA	0.186 g	0.5 mM
$Mg(OAc)_2$	2.252 g	10.5 mM
Deionised water	To 1 L	-

7.9.31 **L11 Purification Lysis Buffer (pH 8.0, 1L)**

Component	Quantity	Concentration
Tris Base	6.07 g	50 mM
NaCl	29.22 g	500 mM
Glycerol	150 mL	15%
Deionised water	To 1 L	-

Buffer was stored at 4 °C prior to and during use.

7.9.32 **L11 Purification Lysis Buffer (pH 8.0, 1L)**

Component	Quantity	Concentration
Tris Base	6.07 g	50 mM
NaCl	29.22 g	500 mM
Glycerol	150 mL	15%
Deionised water	To 1 L	-

Buffer was stored at 4 °C prior to and during use.

7.9.33 **L11 Purification (Streptactin) Buffer B (pH 8.0, 1 L)**

Component	Quantity	Concentration
Tris HCl	8.88 g	100 mM
Tris Base	5.30 g	-
KCl	37.28 g	500 mM
Glycerol	50 mL	5%
Desthiobiotin (DTB)	536 mg	2.5 mM
Deionised water	To 1 L	-

Buffer was made to the correct pH with hydrochloric acid (HCl) or potassium hydroxide (KOH). Buffer was stored at 4 °C prior to and during use.

7.9.34 **L11 Purification Regeneration Buffer (pH 10.5, 1 L)**

Component	Quantity	Concentration
Tris HCl	8.88 g	100 mM
Tris Base	5.30 g	-
KCl	37.28 g	500 mM
Glycerol	50 mL	5%
Deionised water	To 1 L	-

Buffer was made to the correct pH with potassium hydroxide (KOH). Buffer was stored at 4 °C prior to and during use.

7.9.35 **ppGpp Ion Exchange Purification Buffer A (pH 7.4, 1 L)**

Component	Quantity	Concentration
Tris HCl	6.61 g	50 mM
Tris Base	0.97 g	-
LiCl	423.9 mg	100 mM
Deionised water	To 1 L	-

Buffer was made to the correct pH using hydrochloric acid (HCl). Buffer was stored at 4 °C prior to and during use.

7.9.36 **ppGpp Ion Exchange Purification Buffer B (pH 7.4, 1 L)**

Component	Quantity	Concentration
Tris HCl	6.61 g	50 mM
Tris Base	0.97 g	-
LiCl	21.195 g	1000 mM
Deionised water	To 1 L	-

Buffer was made to the correct pH using hydrochloric acid (HCl). Buffer was stored at 4 °C prior to and during use.

7.9.37 **GppA Purification (Nickel Affinity Chromatography) Buffer A (pH 8.0, 1 L)**

Component	Quantity	Concentration
Tris Base	6.07 g	50 mM
NaCl	29.22 g	500 mM
Imidazole	0.68 g	10 mM
Glycerol	150 g	15% (w/v)
β-mercaptoethanol	200 µL	3 mM
Deionised water	To 1 L	-

Buffer was made to the correct pH with hydrochloric acid (HCl). Buffer was stored at 4 °C prior to and during use.

7.9.38 **GppA Purification (Nickel Affinity Chromatography) Buffer B (pH 8.0, 1 L)**

Component	Quantity	Concentration
Tris Base	6.07 g	50 mM
NaCl	29.22 g	500 mM
Imidazole	34 g	500 mM
Glycerol	150 g	15% (w/v)
β-mercaptoethanol	200 µL	3 mM
Deionised water	To 1 L	-

Buffer was made to the correct pH with hydrochloric acid (HCl). Buffer was stored at 4 °C prior to and during use.

7.9.39 **10× High Throughput Screen Buffer (pH 8.0, 100 mL)**

Component	Quantity	Concentration
Tris Base	2.423 g	200 mM
$MgCl_2$ (hexahydrate)	6.09 g	300 mM
KCl	1.118 g	150 mM
β-mercaptoethanol	66.6 µL	10 mM
BSA (10 mg/mL)	10 mL	1 mg/ mL
Deionised water	To 100 mL	-

Assay buffer was made to the correct pH using hydrochloric acid (HCl). Aliquots (1 mL) were prepared and stored at -20 °C prior to use.

7.9.40 **Auto-induction Media**

The following was dissolved and made to pH 7.2 with HCl:

Component	Quantity
Tryptone	20 g
Yeast Extract	5 g
NaCl	5 g
Na_2HPO_4	6 g
Deionised water	965 mL

The solution was autoclaved (121 °C, 15 min) and then the following added:

Component	Quantity
Sterile filtered glucose (10% w/v)	5 mL
Sterile filtered glycerol (60% w/v)	10 mL
Sterile filtered lactose (8% w/v)	25 mL

7.9.41 **RelA Purification Buffer D (pH 8.0, 2 L)**

Component	Quantity	Concentration
Tris Base	12.7 g	50 mM
Tris HCl	2.36 g	-
NaCl	58.44 g	500 mM
Glycerol	300 g	15% (w/v)
Dithiothreitol (DTT)	154 mg	1 mM
Deionised water	To 1 L	-

Buffer was made to the correct pH with hydrochloric acid (HCl) or sodium hydroxide (NaOH). Buffer was stored at 4 °C prior to and during use.

Appendix A

A.1 Conservation of the EXSD motif across different *Francisella* species RelA sequences (Figure A.1).

Francisella tularensis RelA	I P E E F S D Y I A
Francisella holarctica RelA	I P E E F S D Y I A
Francisella novicida RelA	I P E E F S D Y I A
Francisella philomiragia RelA	I P E E F S D Y I A
Consensus	I P E E F S D Y I A

Figure A.1. Alignment of synthetase active site motifs of RelA enzymes across four *Francisella* species. Key residues are boxed, with the unusual serine residue highlighted in red.

A.2 Substrate Specificity of *F. tularensis* RelA. *F. tularensis* RelA does not accept CTP or GDP as a pyrophosphate acceptor (Figure A.2).

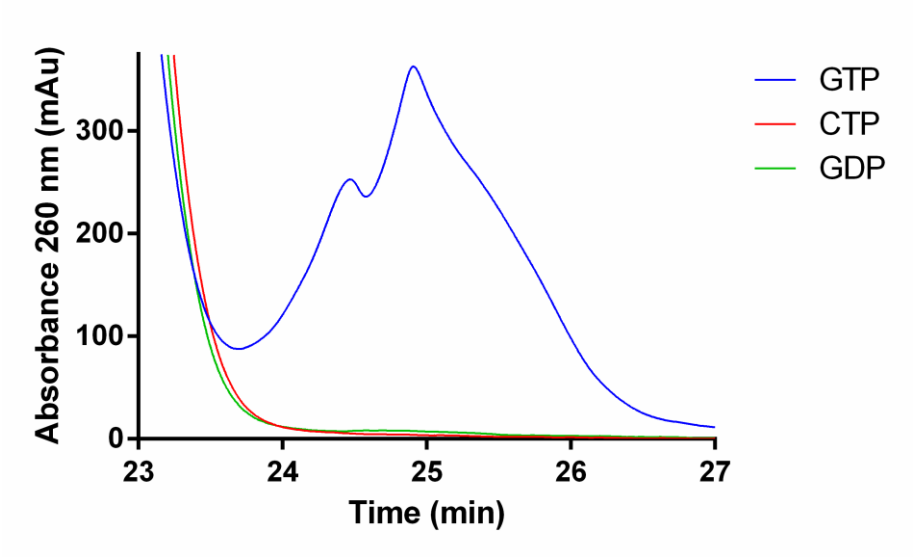

Figure A.2. Substrate specificity of *F. tularensis* RelA. HPLC chromatograph which shows no hyperphosphorylated product is formed in the presence of GDP or CTP.

A.3 Separation of guanosine tetraphosphate and pentaphosphate by IP RP HPLC analysis using Method C (7.3.8.3) (Figure A.3).

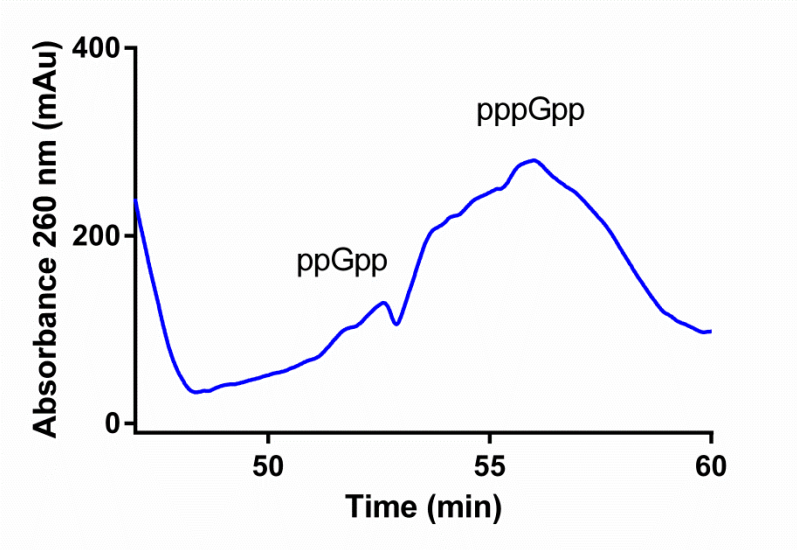

Figure A.3. HPLC analysis of *F. tularensis* RelA activity using Method C. Separation of peaks for ppGpp and pppGpp is minimal and both peaks are broad.

A.4 Initial rates from (p)ppGpp production at varying substrate concentrations as quantified by IP RP HPLC (Table A.1).

Table A.1. Table of initial rates for *F. tularensis* RelA synthetase activity over a range of substrate concentrations as measured by IP RP HPLC. The concentration of the non-variable substrate was 2 mM for all experiments. R^2 values are a measure of goodness of fit for the linear plots.

[GTP] /μM	Initial rate/ nM s^{-1}	R^2	[ATP]/ μM	Initial rate/ nM s^{-1}	R^2
3750	41.0 ± 9.4	0.73	2000	82.5 ± 13	0.89
2750	64.5 ± 18	0.64	1500	117 ± 10	0.93
2250	205 ± 93	0.41	1000	86.4 ± 12	0.96
2000	87.8 ± 13	0.87	800	64.7 ± 13	0.71
1750	65.6 ± 2.8	0.99	600	84.8 ± 8.0	0.92
1250	42.9 ± 3.8	0.95	400	117 ± 42	0.80
1000	46.0 ± 8.3	0.81	350	52.2 ± 9.9	0.73
750	22.9 ± 1.3	0.98	250	29.4 ± 3.8	0.86
400	22.2 ± 4.9	0.75	200	19.9 ± 2.4	0.87
250	3.61 ± 1.9	0.33	100	10.2 ± 2.7	0.59
0	0.00	-	0	0.000	-

A.5 Initial rates from (p)ppGpp production at varying substrate concentrations as quantified by NMR (Table A.2).

Table A.2. Table of initial rates for *F. tularensis* RelA synthetase activity over a range of substrate concentrations, as measured by ^{31}P NMR analysis. The concentration of the non-variable substrate was 2 mM for all experiments. R^2 values are a measure of goodness of fit for the linear plots.

[GTP] /μM	Initial rate/ nM s^{-1}	R^2	[ATP]/ μM	Initial rate/ nM s^{-1}	R^2
4000	211 ± 25	0.97	1750	168 ± 10	0.99
3000	191 ± 15	0.99	1500	170 ± 11	0.99
2000	238 ± 14	0.99	1250	158 ± 3.2	1.00
1500	120 ± 8.6	0.99	1000	158 ± 14	0.98
1000	72.1 ± 12	0.95	750	126 ± 9.0	0.99
750	67.6 ± 6.7	0.95	500	92.9 ± 3.7	1.00
500	40.6 ± 24	0.59	250	31.9 ± 17	0.54
250	22.4 ± 10	0.71	125	26.7 ± 13	0.58
0	0.00	-	0	0.000	-

A.6 Amino acid sequence for *Francisella tularensis* subspecies *tularensis* SCHU S4 RelA (UniprotKB – Q5NEV0).

This protein is 647 amino acids in length, has a molecular weight of 74, 079.8 kDa and isoelectric point of 6.77.

1 MQVIDSKLLDSDGQIKDELLISELKSFYTSDKFEIIAAALELLKNKSAESVRHPTGISSF

61 LYAIEMAYVLFKIRADEESVSAGILYELYNFGDISDEDIEQATNQTVLKILQGTRKMSAI

121 RMYRSDNISLEQIDIFRKMLLTIIEDVRIVLVKIVDKLCTIRHLKSLSSNTQRVIARETL

181 DIYAPLANRLGLGAIKWELEDRAFFFLQQDEYKRIAKSLGVTRKQREDFLHQVIQELKST

241 LKKYNLHAGIQGRVKHIYSIYKKFKNKGYQELDDLYDITAVRVITNNVDECYKVLAEVNN

301 LYSPIPEEFSDYIAHPKPNGYKSIHTVVKVGEQNIEVQIRTQQMHEESELGFAAHWRYKE

361 GVKFDASYEARVAWLRSLLEWEKEINEDDSQITKELNKKLYVFTPANELIDLAEGSTVLD

421 FAYSVHTMVGHRTKGAKLNGKIVPLTTKLKTGDKVEILTGKEPNPSKDWASENLGYLTSA

481 RNRSRVTKWFNEQNKEDNIALGKDRLLKELRGYDLKEVDFVEVAAKFNMKTSDSLFAAIE

541 GGSLKTNSVVNYIIDTYSAEEKLIKKKHKVTNLKAKAPKVLVSGFDGMKYEMAKCCHPVY

601 PDQIQGYMSVSKGVVIHTTNCPNLNHLKEKSPEKFIEVNWDDNEEVS

Appendix B

B.1 Plasmid map for pET16b::*Ft*rplK (compiled with pDraw32 software) (Figure B.1).

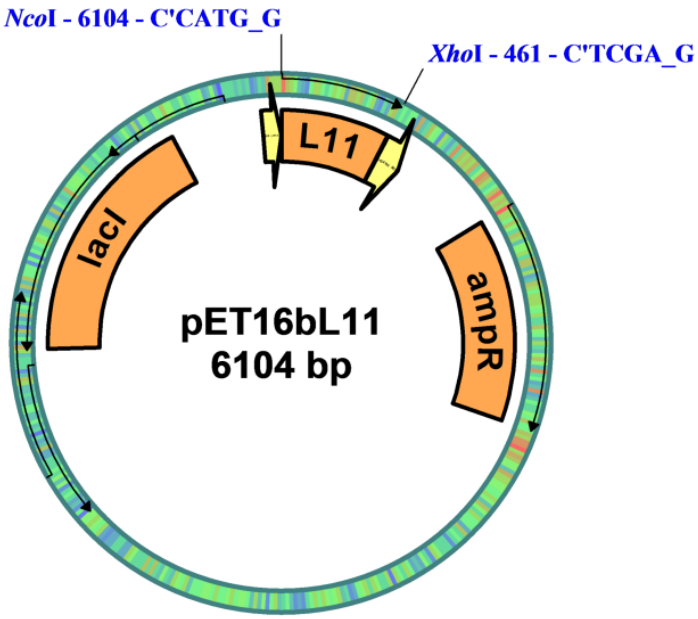

Figure B.1. Vector map for the plasmid pET16b containing *F. tularensis* rplK (L11) (pDraw32).

B.2 ^{31}P NMR analysis (Bruker, 500 MHz) of purified ppGpp in RelA Assay Buffer B, 10% D_2O (7.4.17).

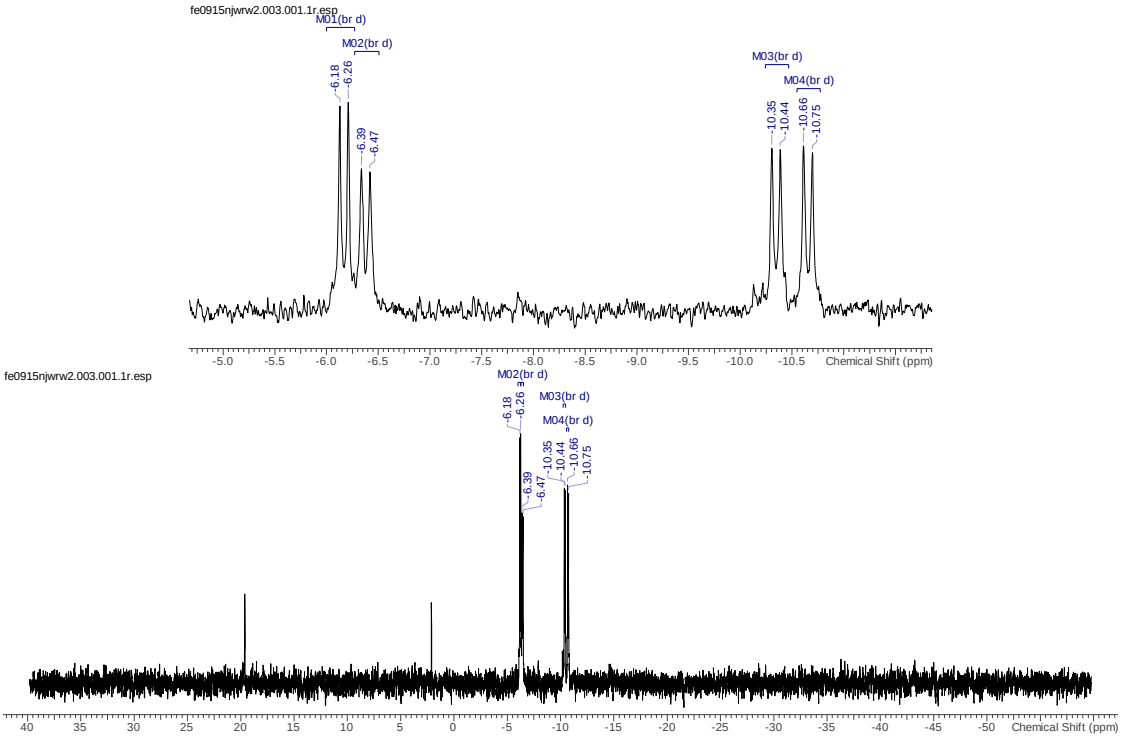

Figure B.2. 1D ^{31}P NMR analysis of ppGpp in 1× RelA Assay Buffer B and 10% D_2O.

B.3 ^{31}P- ^{31}P COSY analysis (Bruker, 500 MHz) of purified ppGpp in RelA Assay Buffer B, 10% D2O (7.4.17).

^{31}P NMR (202 MHz, H2O-D2O) δ ppm 10.70 (d, *J* =17.23 Hz, 1 P), 10.40 (d, *J* =16.61 Hz, 1 P), 6.43 (d, *J* =16.61 Hz, 1 P), 6.22 (d, *J* =17.23 Hz, 1 P), 2.11 (s, 1 P).

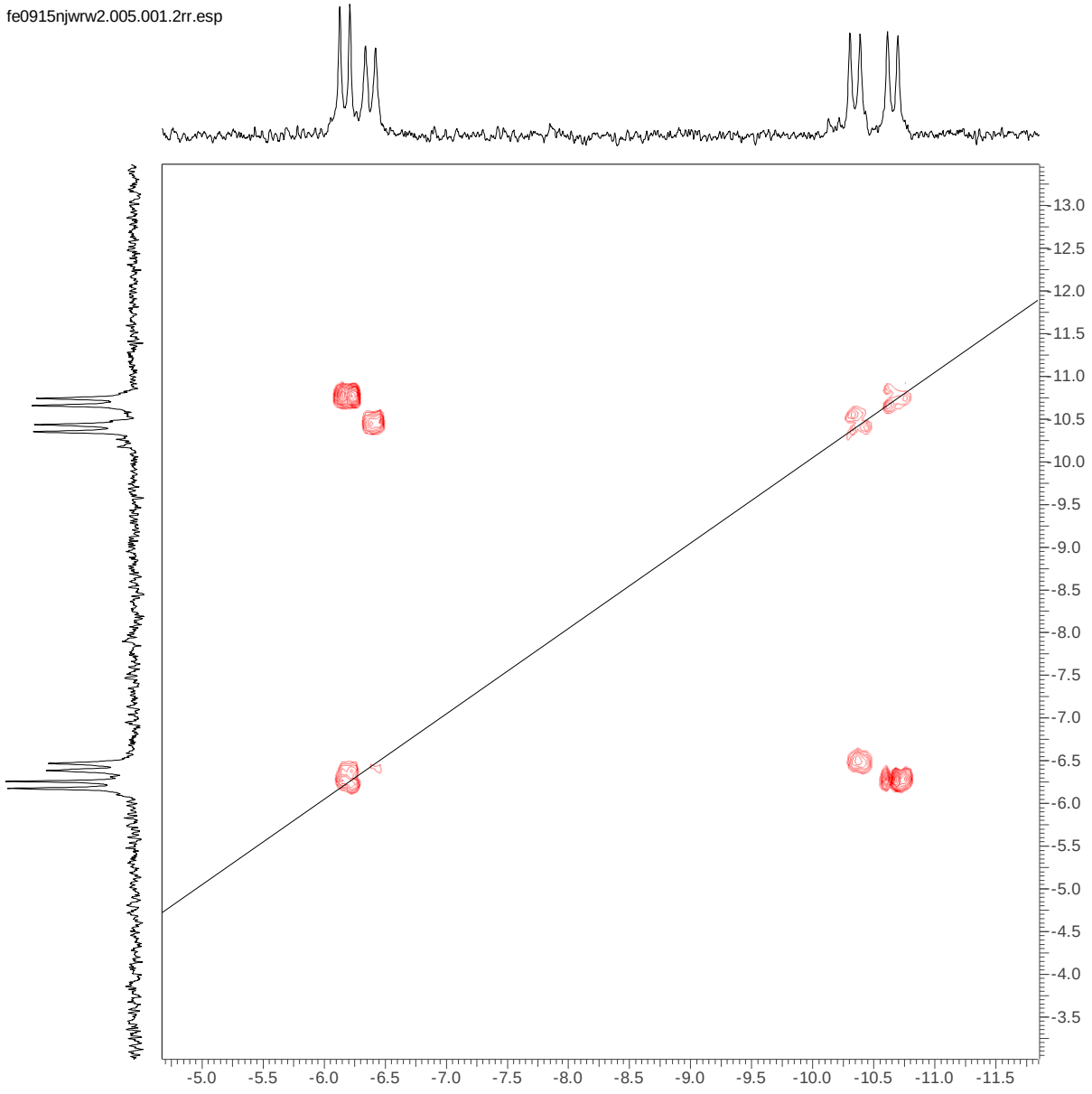

Figure B.3. 2D ^{31}P-^{31}P NMR COSY analysis of ppGpp in 1× RelA Assay Buffer B and 10% D_2O.

B.4 ^{1}H-NMR 1D NOESY (Bruker, 500 MHz) analysis of purified ppGpp in RelA Assay Buffer B, 10% D_2O (7.4.17).

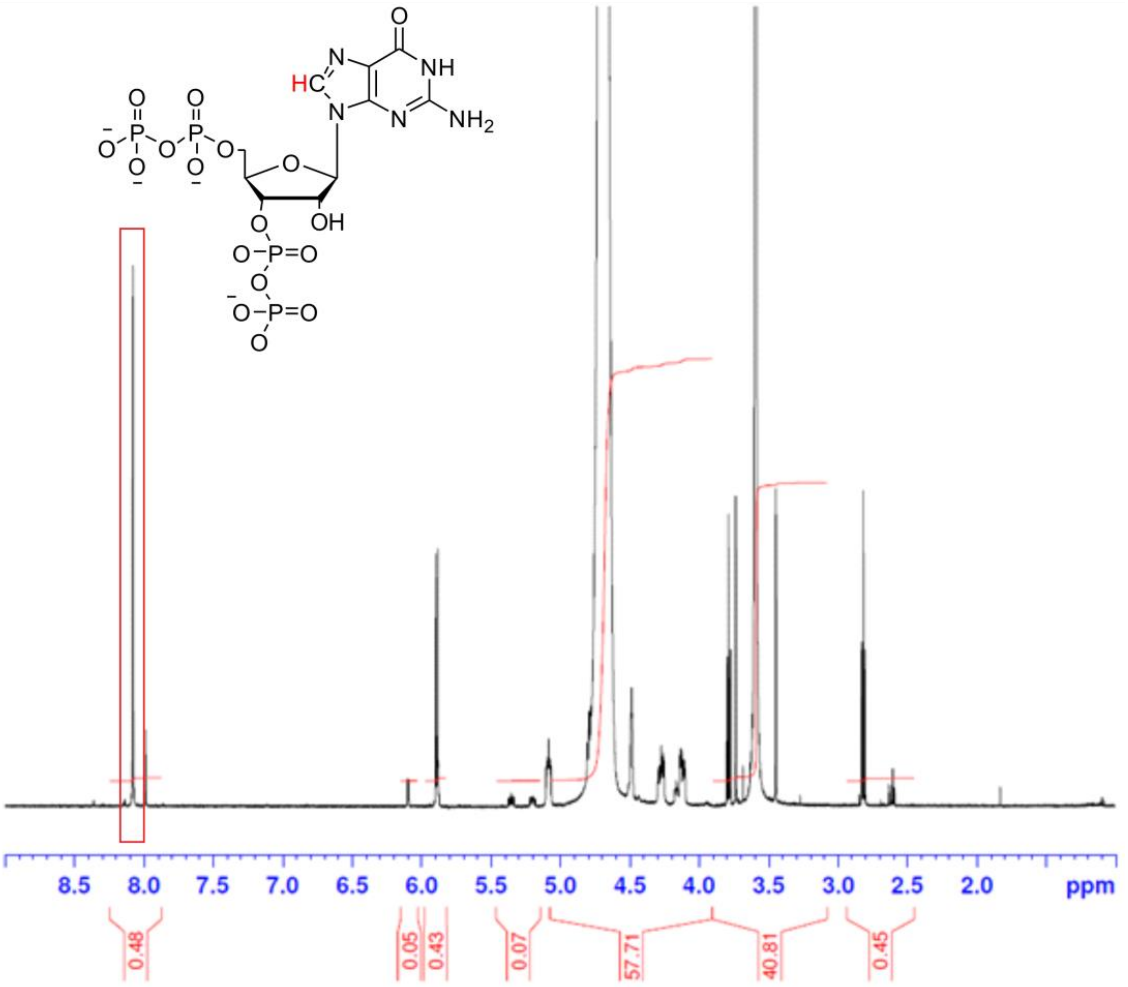

Figure B.4. ^{1}H NOESY NMR spectrum (water subtracted) for ppGpp in 1× RelA Assay Buffer B and 10% D_2O. Highlighted peak at 8.08 ppm (red box) corresponds to the highlighted proton in the guanine base of ppGpp.

B.5 The effect of serine and N-formylmethionine on the activity of *F. tularensis* RelA (blue), *E. coli* RelA (red) and *Y. pestis* RelA (green).

Initial amino acids investigated were serine and N-formylmethionine. Artificial depletion of serine, by the addition of the serine analogue serine hydroxamate, of cells growing in culture induces the stringent response. Alternatively, N-formylmethionine is required for the initiation of protein synthesis within bacteria. Neither serine nor N-formylmethionine exhibited an effect on *F. tularensis* RelA activity (Figure B5a). A reduction in measured AMP concentrations was observed for *E. coli* RelA in the presence of N-formylmethionine. Further investigation into the effect of N-formylmethionine on regulating RelA activity, highlighted that no significant effect was observed for *F. tularensis*, *E. coli* or *Y. pestis* RelA.

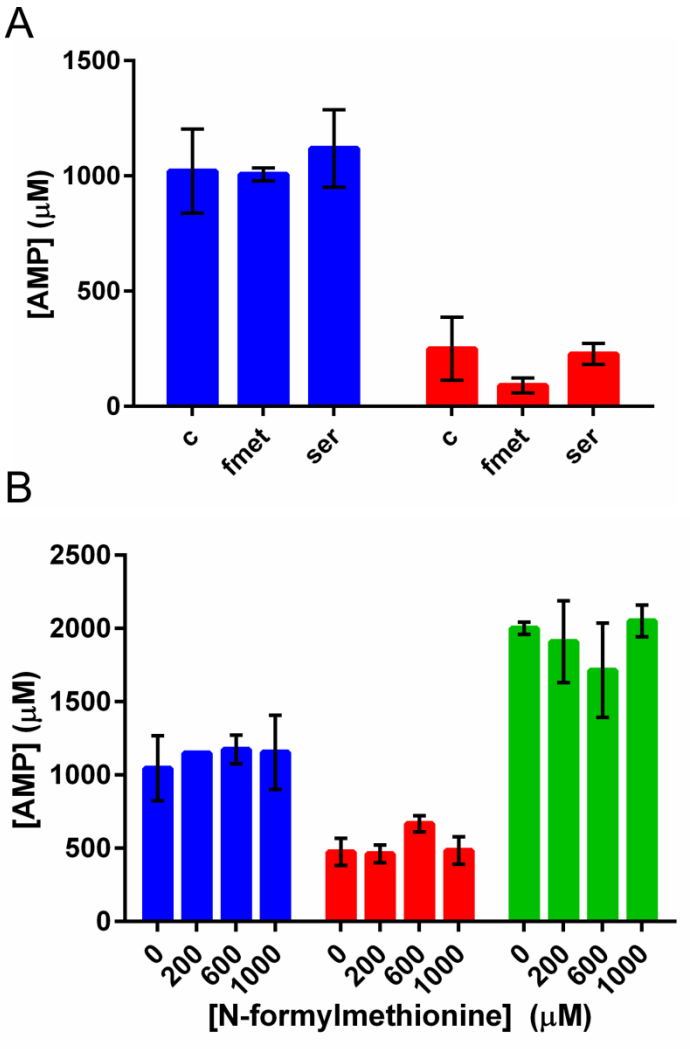

Figure B.5. IP RP HPLC analysis of the effect of serine or N-formylmethionine on the activity of RelA enzymes. (A) AMP production from a 1 hour end point assay in the presence of only substrates (c), substrates and 1 mM N-formylmethionine (fmet), substrates and 1 mM serine (ser) for either *F. tularensis* RelA (blue) or *E. coli* RelA (red). (B) AMP production from a 1 hour end point assay in the presence of substrates (2 mM) and 0-1000 μM N-formylmethionine for *F. tularensis* RelA (blue), *E. coli* RelA (red), or *Y. pestis* RelA (green).

Appendix C

C.1 The alteration in A_{640} for phosphate standards dissolved in water versus those dissolved in RelA Assay Buffer B.

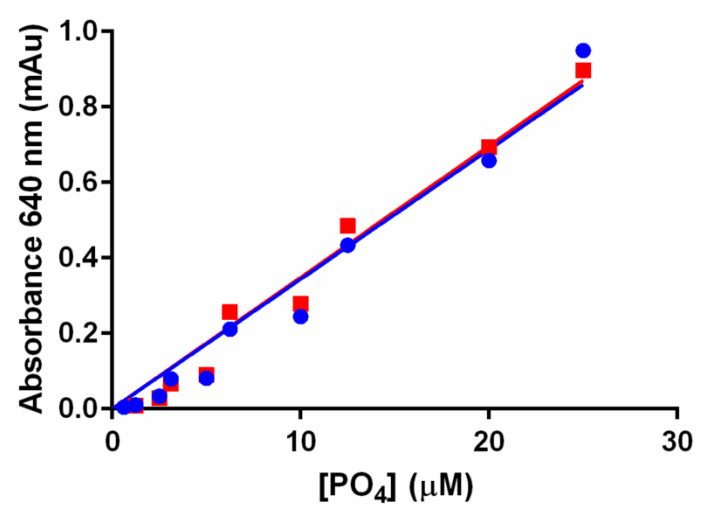

Figure C.1. Linear relationship between the absorbance at 640 nm versus phosphate (KH2PO4) concentration (0-30 μM) when dissolved in water (red) or in 1× RelA Assay Buffer B (blue).

C.2 Absorbance spectra for malachite green detection of phosphate in coupled assays versus control assays.

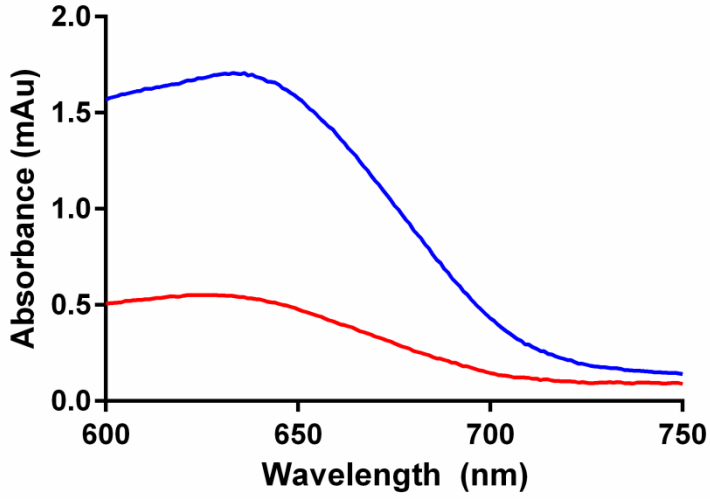

Figure C.2. Absorbance spectra for malachite green phosphate detection of end point coupled *F. tularensis* RelA (2 μM), *E. coli* GppA (0.02 μM) assay (blue) or control *E. coli* GppA (0.02 μM) only assay (red).

C.3 A_{650} for *F. tularensis* RelA at either 2.5 or 5 µM in a coupled enzyme assay format.

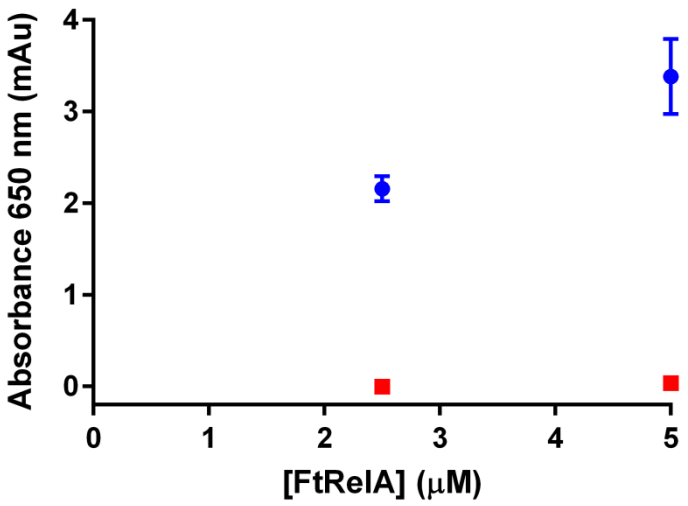

Figure C.3. Concentration of phosphate measured by malachite green detection for *F. tularensis* RelA (2.5 or 5 µM), *E. coli* GppA (0.02 µM) coupled assay (blue), or control *E. coli* GppA assay (red).

C.4 The Effect of Nucleotide Analogues (ddGTP or AMPCPP) on *F. tularensis* RelA Synthetase Activity.

The nucleotide analogue AMPCPP was synthesised by C. Frankling [337] and the nucleotide analogue ddGTP was purchased from Sigma Aldrich. Preliminary experiments demonstrated that as expected *F. tularensis* RelA could not turnover either AMPCPP or ddGTP (Figure C4a). In the presence of substrates neither AMPCPP nor ddGTP were inhibitory against *F. tularensis* RelA at concentrations ranging from 0-1000 µM (Figure C4b and c).

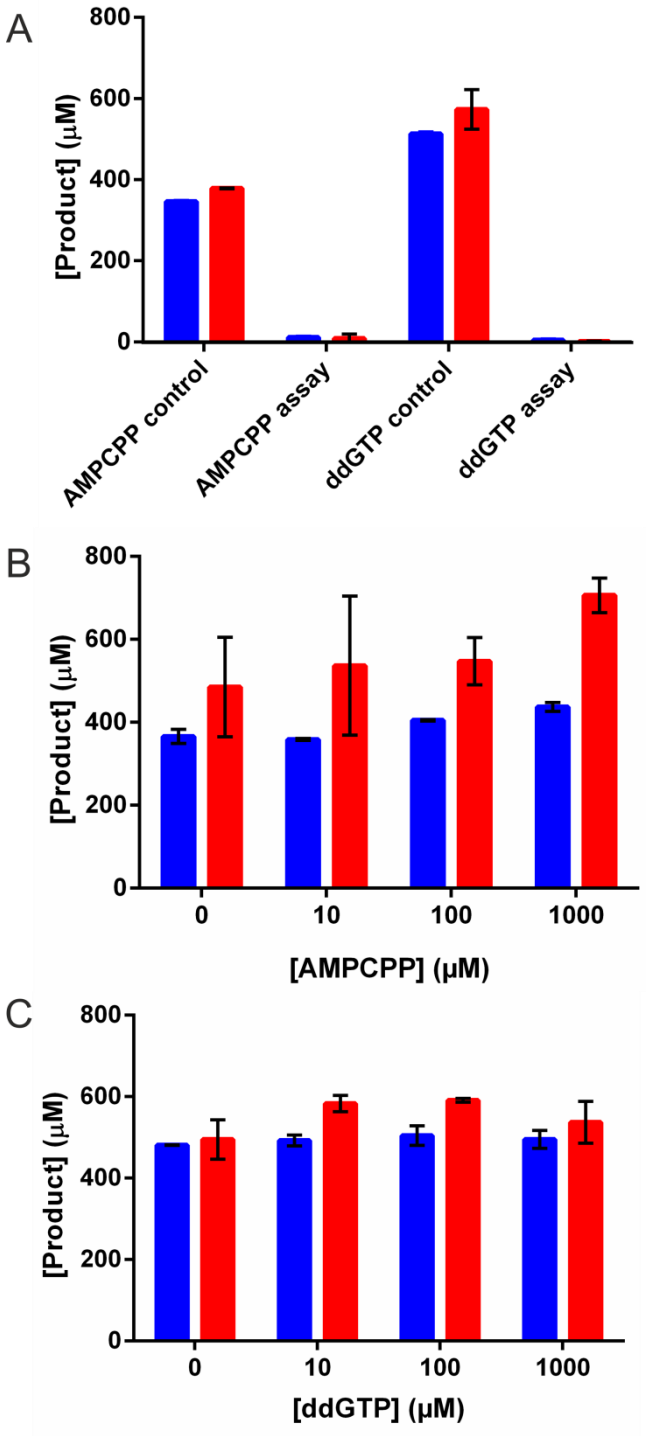

Figure C.4. Effect of the nucleotide analogues AMPCPP and ddGTP on *F. tularensis* RelA activity as measured by the concentration of products AMP (blue) or pppGpp (red) after 1 hour end point assay. (A) *F. tularensis* RelA activity in the presence of its substrates ATP and GTP (AMPCPP and ddGTP controls), or in the presence of ATP and ddGTP (ddGTP assay), or in the presence of GTP and AMPCPP (AMPCPP assay). (B) Effect of varying AMPCPP concentrations on the activity of *F. tularensis* RelA in the presence of its substrates (ATP and GTP). (C) Effect of varying ddGTP concentrations on the activity of *F. tularensis* RelA in the presence of its substrates (ATP and GTP).

Appendix D

D.1 Gene Design for a C-terminal hexahistidine (highlighted in yellow) tagged *Y. pestis* RelA.

Restriction sites are in bold and the stop codon is highlighted in red.

CCATGGTGGCAGTCCGAAGTGCCCACCTCAACCCTGCCGGGGAATTCGCACTGGATGATTGGATAGCCAGTCTAGGTC
TGGCCAACCCGCAGAGCAGCGAGCGGCTGGCAGAAACTTGGCGTTACTGCGAACAACAGACCCAGAATCACCCGGAT
GCGTCCCTGCTGCTGTGGCGGGGCTTAGAGATGGTTGAGATCCTCAGTACACTGTCGATGGATAACGATTCTATGCGA
GCGGCACTTTTGTTTCCTCTTGTGGATGCCAACATAGTAGATGAGACGACGCTGACCGAGCAGTTTGGCAAGGGAATT
ACTTACCTTGTTCACGGCGTTCGAGATATGGACGCCATTAGGCAGCTCAAGGCGACGCACAATGATTCTATGTCCAGT
GAGCAAGTTGATAATGTACGTAGAATGCTGCTGGCTATGGTAGAGGATTTCCGTTGTGTCGTCATCAAGCTGGCAGAG
CGCATCGCTCATCTGAGAGAAGTCAAGGACGCACCAGAGGACGAGCGAGTTTTGGCTGCTAAAGAATGCTCAAACAT
CTATGCACCACTGGCCAACCGCCTGGGAATAGGCCAGATCAAGTGGGAGCTAGAAGACTTTTGTTTTCGTTACCTGCA
CCCGGATGAATATAAAAAAATCGCGAAGCTCCTCCATGAGCGCCGTATCGACCGCGAACAATTCATTGATGACTTCGT
CGCAAGTCTGCATAAAGCAATGGCAGATGAGGGTATCAAGGCAGATATATACGGGCGTCCGAAACATATATATTCAAT
CTGGCGCAAGATGCAAAAAAAATCTCTCGCATTTGATGAATTATTTGACGTACGCGCAGTACGGGTGGTTGTAGAGCG
CTTGCAAGACTGTTATGCGGCGTTAGGCATTGTGCATACTCATTTCCGTCACTTGCCCGACGAGTTCGACGATTACGTG
GCGAACCCGAAACCGAACGGCTACCAGTCCATCCATACGGTAGTATTAGGGCCTCGCGGGAAAACCCTGGAGATTCA
GATTCGCACACGGCAAATGCATGAAGACGCTGAATTGGGTGTGGCTGCGCATTGGAAATATAAAGAAGGCGCCGTCG
CGGCGGGTCGCAGTTCTTACGAGGGTCGGATCGCTTGGCTTCGTAAATTAATCGCTTGGCAGGAAGAAATGGCCGAT
AGCGGCGAAATGCTGGATGAAGTTCGGTCGCAGGTGTTTGACGACCGTGTCTATGTGTTCACCCCAAAAGGCGATGTC
ATTGATCTGCCAGCTGGTTCAACGCCGCTGGATTTTGCCTATCATATTCACTCTGATGTGGGTCATCGTTGTATTGGTGC
GAAAATCTCCGGCCGCATCGTCCCGTTCACCTACCAACTGCAGATGGGGGATCAAATCGAAATCATCACCCAAAAACA
ACCGAATCCGTCGCGTGACTGGTTGAATCCCAACCTTGGTTACATTACCACCTCACGCGGCCGCAGCAAAATCCATAAT
TGGTTTCGCAAACAGGATCGTGACAAAAACATCCTGGCTGGTCGCCAGATGCTGGATGACGAACTAGAACATCTGGAT
ATTAGCCTTAAAGAAGCCGAAAAACTGTTGGTCCCGCGCTATAACATGAACAGCATGGATGAAGTGCTGGCTGCCATT
GGAGGTGGTGATATTCGTCTGAACCAAATGGTCAATTTTCTTCAGGGTAAATTGAATAAACCAACTGCCGAGGAAGCG
GACCTGGAAGCGTTACGTCATCTCAATAATAAACATCAGCCGGCCCCGCGCAACGCGTCAAAAGATTCGGGCCGTATT
GTTGTTGAAGGAGTCGGCAATCTGATGCATCACATTGCGCGCTGCTGCCAGCCCATTCCTGGTGACCAGATCATCGGC
TTTATTACCCAGGGACGTGGTATTAGCATTCACCGTGCGGACTGCGAACAGCTGGCCGAATTAGAAAGCCACGCCCCG
GAACGTATTGTGGATGCGGTTTGGGGCGAATCCTATTCCTCGGGCTATAGCCTGGTTGTTCGCGTGACAGCGAACGAC
CGCTCGGGGCTTTTGCGCGATATTACCACGATTTTAGCGAACGAAAAAGTGAATGTGCTGGGCGTGGCGAGCCGTAG
CGATACGAAAAAAATGGTGGCGACCATTGATATGGATATTGAAATTTATAACTTACAGGTGCTGGGGCGCGTGCTGG
CGAAACTGAATCAGCTGCCCGATGTGATTGATGCGCGTCGTTTGCACGGCAAT**CATCATCATCATCATCAT**TAA**CTCG
AG**

D.2 Plasmid map for pET16b::*Yp*relA (compiled with pDraw32 software).

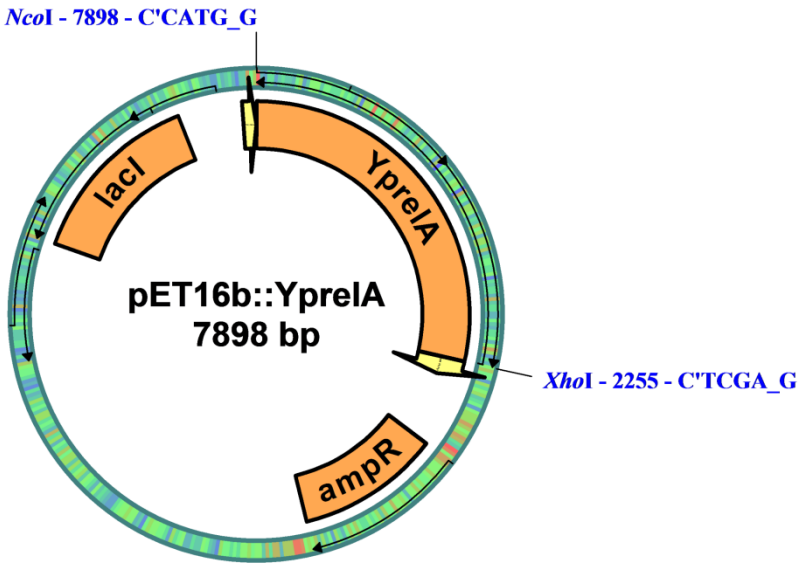

Figure D.1. Vector map for the plasmid pET16b containing the *relA* gene from *Y. pestis*.

D.3 Gene Design for a C-terminal hexahistidine (highlighted in yellow) tagged *B. pseudomallei* RelA.

Restriction sites are in bold and start and end codons are highlighted in red.

CCATGGCUACGGCAGACAGTGCCAGTACCGCTGCGGCGCCCTCACTCGACGATGTGCTTGCCTTCGTGCGGGAACAC
GCGGGAGACGCACGGTTAAGCTCTGGCGAGCGGCTGGCCGATCACGCGGCCGGTACCTCTACTATCATGCAACGTTT
AAACGTCGATCCACCTGCTACTCAGGCGGCCGCACTGTTTGCCCTTGCTCCTTACTTGTCTGATCCCGATAAACAAATCG
CAGAGCATTTCGGCGATGAAGTTGCCCATCTTGTTGCGGACGTAAGGAAGTTGTTGCGCTTGGGCACGGTTTCCCTCC
GCGCAGCGCAATCTGCTCCCGTTGATGCGGGCCGTGACGCACAGGCGGAGCGTCGTGCCCAAATTGAAGCGCTTCGA
AAAATGTTATTAGCTTTTGCGCAGGACATCCGTGTAGTCCTTATTCGGTTGGCGTCGCGCCTTCAGTCATTACGTTATTA
CGCGGCCGCAAAAATCGAACCCCCGCCGGACGTAGCCCGAGAGACCCTTGAAATTTATGCGCCGCTAGCGAACCGCC
TAGGGATCTGGCAGCTGAAATGGGAACTGGAAGATCTCGCCTTTCGCTTCGAGGACCCAGTAACCTATAAACGTATTG
CAAAATTGTTAGACGAAAAAAGAGTTGAGCGTGAAGCCTATGTGGCAGGTGCAATCGAAAGATTGCAACACGAGCTC
GCGGCTGCACACATTCAAGCCGAAGTGTCCGGTCGCCCAAAACATATTTATTCTATCTGGCGTAAAATGCGGGGCAAA
GAACTCGATTTTTCTGAACTGTACGACGTACGTGCCTTTAGAGTTATTGTTCCGGATATTAAAGACTGTTACACTGTCCT
CGGCATTGTACATCACTTATGGCAGCCAGTGCCCAAAGAATTTGATGATTATATTTCCCGCCCGAAGCCTAACGGTTAC
AAATCGTTACACACAGTTGTGATTGGTGATGATGGTCGGGCCTTTGAGGTCCAGATCCGAACACAGGAGATGCATCGT
TTTGCAGAATATGGTGTTGCAGCGCATTGGCGTTATAAGGAGGCTGGAGCCCGCGGGTATGGCGGACAGTTTTCAGC
GAGCGAAAAATATGATGAAAAAATTGCCTGGTTGCGGCAGTTGTTGGCGTGGAAAGACGAGATCGCGGACGGTGGC
GGCGCAGAGGTGTCAGGCCAGCAGGCATGGGCCCAGCTGCGCGAAGCAACGCTGGATGATGACCATATTTATGTTCT

GACCCCACAGGCACGCGTGATCGCTCTGCCTCAGGGTGCGACCCCAGTCGATTTCGCGTATCATCTGCATAGCGAACT
GGGTCACCGCTGCCGTGGAGCGCGCGTCGACGGCGCGATGGTACCACTGAACACCCAGCTGGCTAATGGCCAAACCG
TAGAGATTGTAGCAGTTAAGGAAGGCGGGCCGTCACGTGATTGGCTGAACCCTCAGCTGGGTTACCTGCATTCGTCCC
GCGCCCGCCAAAAAGTCCGTGCGTGGTTCAACGCCGTTGACCAACAGGAAAACGTGGCTCATGGCCGCGCGCTGGTG
GAGAAAACCCTGCAGCGTGAAGGCAAGACTTCGGTCAATCTGGAACATCTGGCCGCTAAGCTGGGCTTCAAAAGCCC
TGATGAACTGTTTAGTGTGGTCGGTAAGGAAGAATTTAGCCTGCGCAACGTCGAGCAGGCGCTGTCCGATGCGCCGG
CGCCGGAACCGGAGCCGGAGGCCCCGGCTAATTTCGAAAAACGTGCAAGCGGGGCGAATGTGGCACACGGAGCCTC
GGCCGGCGTTCTGGTGGTTGGTGTGGACGCCCTGCTGACCCAGCTGGCGCGTTGTTGCCGTCCGGCGCCTCCGGATCC
GATCAGTGGCTTCGTCACGCGCGGTAAGGGGATGAGCATCCACCGTAGTGATTGTGCTACATTTCGTCGTATGGCAGA
ACGTGCGCCGGAACGCGTTCTGCAAACGACGTGGAGCGCCGATGTGCTGGGTGGTCGCGGCGCGAGCGTTTACCCG
GTGGATCTGATGATTGAAGCCACCGATCGCCAAGGGCTGCTGCGCGATATCAGCGAAGTGTTCGCACGCGAAAAAAT
GAATGTCATAGGCGTCAAAACGCAATCGCGCCGCAATGCGGCGTTTATGCAGTTCACAGTGGAAGTGTCGAGTGCGA
GCCAAGTGCAGCGCGCATGCACCCTGCTGGGGGGAAATCCAGGGGGTGGTGCGCGCTGCCCGCAAGGCT**CATCATCAT**
CATCATCATTAA**CTCGAG**

D.4 Plasmid map for pET16b::*Bp*relA (compiled with pDraw32 software).

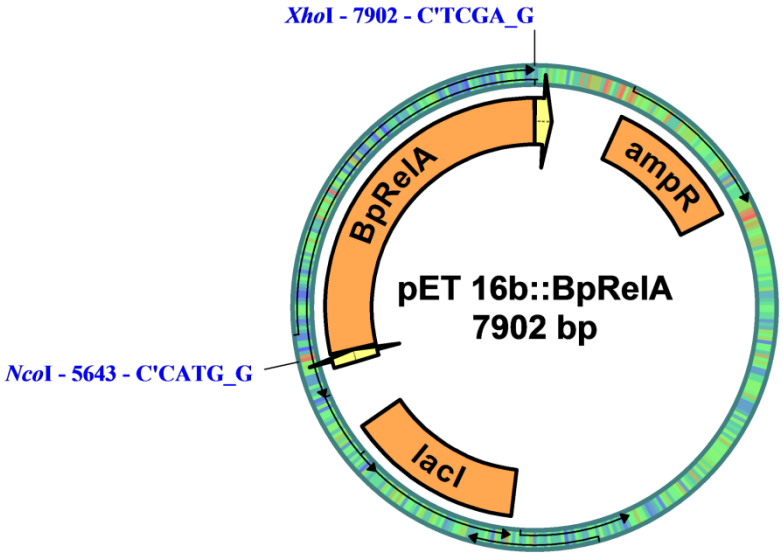

Figure D.2. Vector map for the plasmid pET16b containing the *relA* gene from *B. pseudomallei*.

D.5 Retarded growth for cultures containing pET16b::*Bp*relA or pET16b::*Yp*relA.

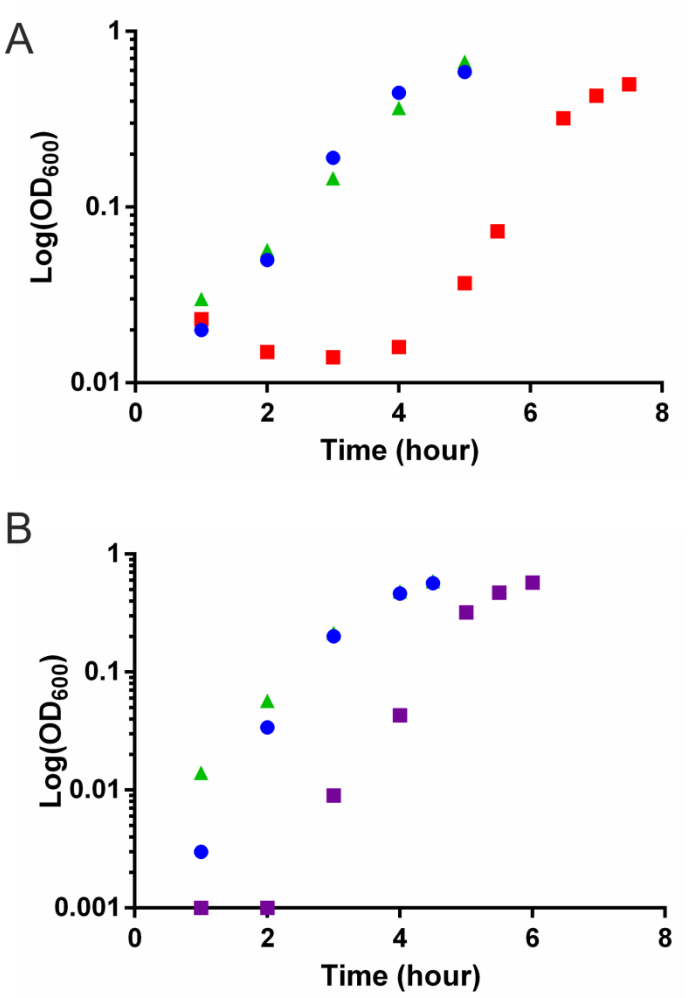

Figure D.3. Growth of *E. coli* BL21 cells at 37 °C, as established by optical density at 600 nm, for cells containing either (A) pET16b::*Bp*RelA (red) or (B) pET16b::*Yp*relA (purple) in comparison with pET16b (blue) or pET16b::*Ft*RelA (green).

Appendix E

E.1 Crystallisation of *F. tularensis* RelA

The crystallisation of *F. tularensis* RelA was attempted using a variety of commercial sparse screens (8.7.2) between 10-18 mg/mL. Crystallisation screens were set up in the presence of GTP (4 mM), ATP (4 mM), and *E. coli* GppA (12.3 mg/mL). *F. tularensis* RelA crystals were not observed in any of the conditions tested from PactPremier, Morpheus, Midas or MemGold I or II commercial screens.

F. tularensis RelA and *E. coli* GppA complex yielded crystals in a variety of wells in the Proplex screen (Figures E.1 and E.2). Following a grid scan a cyro-protected (30% glycerol) crystal grown in well E2 (Proplex screen) was diffracted to yield a resolution of 5.02 Å, but could not be solved using EDNA. Further attempts to reproduce or grow bigger crystals were not successful (Table E.1). Crystals from G1 (Proplex screen) did not diffract, narrow screens around these conditions (Table E.2) did not yield crystals.

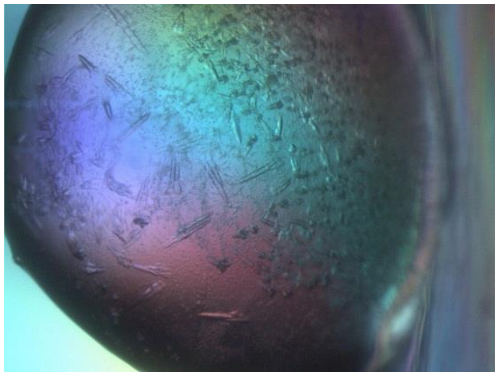

Figure E.1. Image of *F. tularensis* RelA, *E. coli* GppA crystals grown in well E2 (0.1 M sodium citrate pH 5.0, 8% PEG8000) from the Proplex screen (Molecular Dimensions).

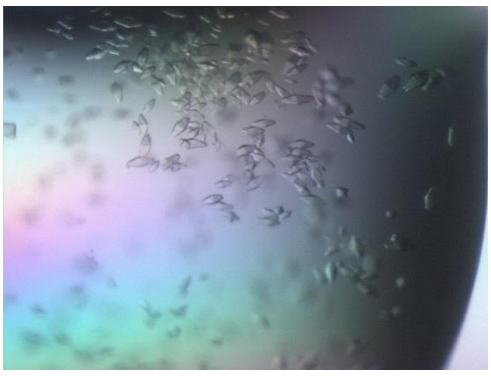

Figure E.2. Image of *F. tularensis* RelA, *E. coli* GppA crystals grown in well G1 (0.1 M Tris pH 8.0, 1.5 M NH_4SO_4) from the Proplex screen (Molecular Dimensions).

A 96 well sparse screen for *F. tularensis* RelA (10 mg/mL) purified by C. Frankling [337] using the commercially available JCSG$^+$ screen (Molecular Dimensions) yielded crystals. Small *F. tularensis* RelA crystals were observed for conditions in well B10 (0.2 M $MgCl_2$ (hexahydrate), 0.1 M sodium cacodylate pH 6.5, 50% (v/v) PEG200). Poor diffraction was observed for these crystals. Further optimisation is required to yield crystals which diffract to higher resolutions.

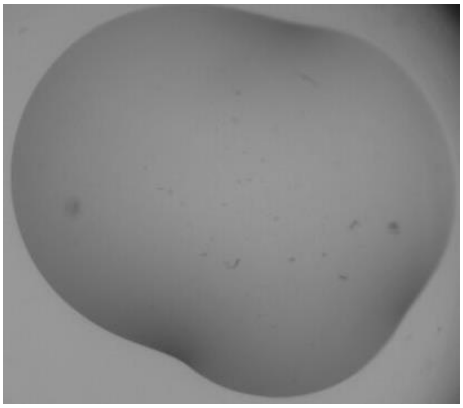

Figure E.3. Image of *F. tularensis* RelA crystals grown in well B10 (0.2 M $MgCl_2$ (hexahydrate), 0.1 M sodium cacodylate pH 6.5, 50% (v/v) PEG200) from the JCSG$^+$ screen (Molecular Dimensions).

Table E.1. Conditions for 24 well hanging drop screen based on those from well E2 from the Proplex screen.

	1	2	3	4	5	6
A	100 mM Sodium citrate pH 5.0 0 % PEG8000	100 mM Sodium citrate pH 5.0 2 % PEG8000	100 mM Sodium citrate pH 5.0 4 % PEG8000	100 mM Sodium citrate pH 5.0 6 % PEG8000	100 mM Sodium citrate pH 5.0 8 % PEG8000	100 mM Sodium citrate pH 5.0 10 % PEG8000
B	90 mM Sodium citrate pH 5.0 8 % PEG8000	95 mM Sodium citrate pH 5.0 8 % PEG8000	100 mM Sodium citrate pH 5.0 8 % PEG8000	105 mM Sodium citrate pH 5.0 8 % PEG8000	110 mM Sodium citrate pH 5.0 8 % PEG8000	115 mM Sodium citrate pH 5.0 8 % PEG8000
C	100 mM Sodium citrate pH 6.0 0 % PEG8000	100 mM Sodium citrate pH 6.0 2 % PEG8000	100 mM Sodium citrate pH 6.0 4 % PEG8000	100 mM Sodium citrate pH 6.0 6 % PEG8000	100 mM Sodium citrate pH 6.0 8 % PEG8000	100 mM Sodium citrate pH 6.0 10 % PEG8000
D	90 mM Sodium citrate pH 6.0 8 % PEG8000	95 mM Sodium citrate pH 6.0 8 % PEG8000	100 mM Sodium citrate pH 6.0 8 % PEG8000	105 mM Sodium citrate pH 6.0 8 % PEG8000	110 mM Sodium citrate pH 6.0 8 % PEG8000	115 mM Sodium citrate pH 6.0 8 % PEG8000

Table E.2. Conditions for 24 well hanging drop screen based on those from well G1 from the Proplex screen.

	1	2	3	4	5	6
A	100 mM Tris pH 8.0 1 M NH_4SO_4	100 mM Tris pH 8.0 1.2 M NH_4SO_4	100 mM Tris pH 8.0 1.4 M NH_4SO_4	100 mM Tris pH 8.0 1.6 M NH_4SO_4	100 mM Tris pH 8.0 1.7 M NH_4SO_4	100 mM Tris pH 8.0 1.8 M NH_4SO_4
B	90 mM Tris pH 8.0 1.5 M NH_4SO_4	95 mM Tris pH 8.0 1.5 M NH_4SO_4	100 mM Tris pH 8.0 1.5 M NH_4SO_4	105 mM Tris pH 8.0 1.5 M NH_4SO_4	110 mM Tris pH 8.0 1.5 M NH_4SO_4	115 mM Tris pH 8.0 1.5 M NH_4SO_4
C	100 mM Tris pH 8.0 1 M NH_4SO_4	100 mM Tris pH 8.0 1.2 M NH_4SO_4	100 mM Tris pH 8.0 1.4 M NH_4SO_4	100 mM Tris pH 8.0 1.6 M NH_4SO_4	100 mM Tris pH 8.0 1.7 M NH_4SO_4	100 mM Tris pH 8.0 1.8 M NH_4SO_4
D	90 mM Tris pH 8.0 50 mM NH_4SO_4	95 mM Tris pH 8.0 1.5 M NH_4SO_4	100 mM Tris pH 8.0 1.5 M NH_4SO_4	105 mM Tris pH 8.0 1.5 M NH_4SO_4	110 mM Tris pH 8.0 1.5 M NH_4SO_4	115 mM Tris pH 8.0 1.5 M NH_4SO_4

References

1. Madigan, M.T.M., J.M. Dunap, P.V. and Clark, D.P., *Brock Biology of Microorganisms*. Twelfth ed2009, San Francisco: Pearson, Benjamin Cummings.

2. Domagk, G., *Twenty-five years of sulfonamide therapy.* Ann N Y Acad Sci, 1957. **69**(3): p. 380-384.

3. Fleming, A., *On the specific antibacterial properties of penicillin and potassium tellurite. Incorporating a method of demonstrating some bacterial antagonisms.* J Pathol Bacteriol, 1932. **35**(6): p. 831-842.

4. Ling, L.L., et al., *A new antibiotic kills pathogens without detectable resistance.* Nature, 2015. **517**(7535): p. 455-459.

5. Kali, A., *Teixobactin: A Novel Antibiotic in Treatment of Gram Positive Bacterial Infections.* J Clin Diagn Res, 2015. **9**(3): p. DL01-DL01.

6. Walsh and Wright, *Introduction: Antibiotic Resistance.* Chemical Reviews, 2005. **105**(2): p. 391-394.

7. Harvey, A.L., *Natural products in drug discovery.* Drug Discovery Today, 2008. **13**(19–20): p. 894-901.

8. Donadio, S., et al., *Antibiotic discovery in the twenty-first century: current trends and future perspectives.* J Antibiot, 2010. **63**(8): p. 423-430.

9. Greer, N.D., *Tigecycline (Tygacil): the first in the glycylcycline class of antibiotics.* Proceedings (Baylor University. Medical Center), 2006. **19**(2): p. 155-161.

10. Bush, K., et al., *Tackling antibiotic resistance.* Nat Rev Micro, 2011. **9**(12): p. 894-896.

11. Landers, T.F., et al., *A review of antibiotic use in food animals: perspective, policy, and potential.* Public Health Rep, 2012. **127**(1): p. 4-22.

12. Bin Abdulhak, A., et al., *Non prescribed sale of antibiotics in Riyadh, Saudi Arabia: A Cross Sectional Study.* BMC Public Health, 2011. **11**(1): p. 538.

13. Safrany, N. and D.L. Monnet, *Antibiotics obtained without a prescription in Europe.* Lancet Infect Dis, 2012. **12**(3): p. 182-183.

14. Golan, D.E., et al., *Principles of Pharmacology. The pathophysiologic basis of drug therapy*. second ed2008: Wolters Kluwer, Lippincott Williams and Wilkins.

15. Alberts, B.J., A. Lewis, J. Raff, M. Roberts, K. and Walter P., *Molecular Biology of the Cell* 4th ed2002: Garland Science.

16. McKeegan, K.S., M.I. Borges-Walmsley, and A.R. Walmsley, *Microbial and viral drug resistance mechanisms.* Trends Microbiol, 2002. **10**(10): p. s8-s14.

17. Friedman, L., J.D. Alder, and J.A. Silverman, *Genetic Changes That Correlate with Reduced Susceptibility to Daptomycin in Staphylococcus aureus.* Antimicrob Agents Ch, 2006. **50**(6): p. 2137-2145.

18. Dowson, C.G., et al., *Penicillin-binding protein 2 genes of non-β-lactamase-producing, penicillin-resistant strains of Neisseria gonorrhoeae.* Mol Microbiol, 1989. **3**(1): p. 35-41.

19. Georgopapadakou, N.H. and F.Y. Liu, *Penicillin-binding proteins in bacteria.* Antimicrob Agents Chemother, 1980. **18**(1): p. 148-57.

20. Hartman, B.J. and A. Tomasz, *Low-affinity penicillin-binding protein associated with beta-lactam resistance in Staphylococcus aureus.* J Bacteriol, 1984. **158**(2): p. 513-516.

21. Bush, K. and R.B. Sykes, *Methodology for the study of beta-lactamases.* Antimicrob Agents Chemother, 1986. **30**(1): p. 6-10.

22. Livermore, D.M., *beta-Lactamases in laboratory and clinical resistance.* Clin Microbiol Rev, 1995. **8**(4): p. 557-84.

23. Holden, M.T.G., et al., *Genomic plasticity of the causative agent of melioidosis, Burkholderia pseudomallei.* PNAS, 2004. **101**(39): p. 14240-14245.

24. Antunes, N.T., et al., *The class A beta-lactamase FTU-1 is native to Francisella tularensis.* Antimicrob Agents Chemother, 2012. **56**(2): p. 666-71.

25. Palzkill, T., *Metallo-β-lactamase structure and function.* Ann N Y Acad Sci, 2013. **1277**: p. 91-104.

26. Saier, M.H., et al., *Evolutionary origins of multidrug and drug-specific efflux pumps in bacteria.* The FASEB Journal, 1998. **12**(3): p. 265-274.

27. Piddock, L.J.V., *Clinically Relevant Chromosomally Encoded Multidrug Resistance Efflux Pumps in Bacteria.* Clin Microbiol Rev, 2006. **19**(2): p. 382-402.

28. Tseng, S.-P., et al., *The Contribution of Antibiotic Resistance Mechanisms in Clinical Burkholderia cepacia Complex Isolates: An Emphasis on Efflux Pump Activity.* PLoS One, 2014. **9**(8): p. e104986.

29. Peters, S. *Cost to Develop and Win Marketing Approval for a New Drug Is $2.6 Billion*. 2014.

30. Li, J.W.-H. and J.C. Vederas, *Drug Discovery and Natural Products: End of an Era or an Endless Frontier?* Science, 2009. **325**(5937): p. 161-165.

31. Singh, S.B. and J.F. Barrett, *Empirical antibacterial drug discovery--foundation in natural products.* Biochem Pharmacol, 2006. **71**(7): p. 1006-15.

32. Donadio, S., et al., *Targets and assays for discovering novel antibacterial agents.* Journal of Biotechnology, 2002. **99**(3): p. 175-185.

33. Kohanski, M.A., D.J. Dwyer, and J.J. Collins, *How antibiotics kill bacteria: from targets to networks.* Nat Rev Microbiol, 2010. **8**(6): p. 423-435.

34. Clatworthy, A.E., E. Pierson, and D.T. Hung, *Targeting virulence: a new paradigm for antimicrobial therapy.* Nat Chem Biol, 2007. **3**(9): p. 541-548.

35. Kuhn, P., et al., *The genesis of high-throughput structure-based drug discovery using protein crystallography.* Current Opinion in Chemical Biology, 2002. **6**(5): p. 704-710.

36. Ealick, S.E., *Advances in multiple wavelength anomalous diffraction crystallography.* Current Opinion in Chemical Biology, 2000. **4**(5): p. 495-499.

37. Cain, R., et al., *Applications of structure-based design to antibacterial drug discovery.* Bioorg Chem, 2014. **55**(0): p. 69-76.

38. Johansson, D., et al., *Design, synthesis and ribosome binding of chloramphenicol nucleotide and intercalator conjugates.* Bioorganic & Medicinal Chemistry Letters, 2005. **15**(8): p. 2079-2083.

39. Schneider, G. and U. Fechner, *Computer-based de novo design of drug-like molecules.* Nat Rev Drug Discov, 2005. **4**(8): p. 649-663.

40. Chen, Y. and B.K. Shoichet, *Molecular docking and ligand specificity in fragment-based inhibitor discovery.* Nature chemical biology, 2009. **5**(5): p. 358-364.

41. Hu, X., et al., *3-Substituted Indole Inhibitors Against Francisella tularensis FabI Identified by Structure-Based Virtual Screening.* Journal of Medicinal Chemistry, 2013. **56**(13): p. 5275-5287.

42. Hertzberg, R.P. and A.J. Pope, *High-throughput screening: new technology for the 21st century.* Current Opinion in Chemical Biology, 2000. **4**(4): p. 445-451.

43. Acker, M.G. and D.S. Auld, *Considerations for the design and reporting of enzyme assays in high-throughput screening applications.* Perspectives in Science, 2014. **1**(1–6): p. 56-73.

44. Zhang, J.-H., T.D.Y. Chung, and K.R. Oldenburg, *A Simple Statistical Parameter for Use in Evaluation and Validation of High Throughput Screening Assays.* Journal of Biomolecular Screening, 1999. **4**(2): p. 67-73.

45. Webb, M.R., *A continuous spectrophotometric assay for inorganic phosphate and for measuring phosphate release kinetics in biological systems.* PNAS, 1992. **89**(11): p. 4884-4887.

46. Sherwood, A.R., et al., *A Malachite Green-Based Assay to Assess Glucan Phosphatase Activity.* Anal Biochem, 2013. **435**(1): p. 54-56.

47. Liu, H., et al., *Development of Multichannel Devices with an Array of Electrospray Tips for High-Throughput Mass Spectrometry.* Anal Chem, 2000. **72**(14): p. 3303-3310.

48. Wilkins, M.R., et al., *High-throughput mass spectrometric discovery of protein post-translational modifications1.* J Mol Biol, 1999. **289**(3): p. 645-657.

49. Mere, L., et al., *Miniaturized FRET assays and microfluidics: key components for ultra-high-throughput screening.* Drug Discovery Today, 1999. **4**(8): p. 363-369.

50. Mezna, M., et al., *Development of a high-throughput screening method for LIM kinase 1 using a luciferase-based assay of ATP consumption.* Journal of Biomolecular Screening, 2012. **17**(4): p. 460-468.

51. Fan, F. and K.V. Wood, *Bioluminescent Assays for High-Throughput Screening.* ASSAY and Drug Development Technologies, 2007. **5**(1): p. 127-136.

52. Barras, V. and G. Greub, *History of biological warfare and bioterrorism.* Clinical Microbiology and Infection, 2014. **20**(6): p. 497-502.

53. Rotz, L.D., et al., *Public health assessment of potential biological terrorism agents.* Emerg Infect Dis, 2002. **8**(2): p. 225-30.

54. Kaufmann, S.H., *Immunity to intracellular bacteria.* Annual review of immunology, 1993. **11**(1): p. 129-163.

55. Aderem, A., *Phagocytosis and the Inflammatory Response.* J Infect Dis, 2003. **187**(Supplement 2): p. S340-5.

56. Geisow, M.J., P. D'Arcy Hart, and M.R. Young, *Temporal changes of lysosome and phagosome pH during phagolysosome formation in macrophages: studies by fluorescence spectroscopy.* The Journal of Cell Biology, 1981. **89**(3): p. 645-652.

57. Garcia-del Portillo, F. and B.B. Finlay, *The varied lifestyles of intracellular pathogens within eukaryotic vacuolar compartments.* Trends Microbiol, 1995. **3**(10): p. 373-380.

58. Gorvel, J.P. and E. Moreno, *Brucella intracellular life: from invasion to intracellular replication.* Veterinary Microbiology, 2002. **90**(1–4): p. 281-297.

59. Pujol, C. and J.B. Bliska, *Turning Yersinia pathogenesis outside in: subversion of macrophage function by intracellular yersiniae.* Clinical Immunology, 2005. **114**(3): p. 216-226.

60. Jones, A.L., T.J. Beveridge, and D.E. Woods, *Intracellular survival of Burkholderia pseudomallei.* Infect Immun, 1996. **64**(3): p. 782-90.

61. Chong, A. and J. Celli, *The Francisella Intracellular Life Cycle: Toward Molecular Mechanisms of Intracellular Survival and Proliferation.* Front Microbiol, 2010. **1**: p. 138.

62. Inglesby Tv, D.D.T.H.D.A. and et al., *Plague as a biological weapon: Medical and public health management.* JAMA, 2000. **283**(17): p. 2281-2290.

63. Achtman, M., et al., *Microevolution and history of the plague bacillus, Yersinia pestis.* PNAS, 2004. **101**(51): p. 17837-17842.

64. Parkhill, J., et al., *Genome sequence of Yersinia pestis, the causative agent of plague.* Nature, 2001. **413**(6855): p. 523-527.

65. Perry, R.D. and J.D. Fetherston, *Yersinia pestis--etiologic agent of plague.* Clin Microbiol Rev, 1997. **10**(1): p. 35-66.

66. Spinner, J.L., J.A. Cundiff, and S.D. Kobayashi, *Yersinia pestis Type III Secretion System-Dependent Inhibition of Human Polymorphonuclear Leukocyte Function.* Infect Immun, 2008. **76**(8): p. 3754-3760.

67. Du, Y., R. Rosqvist, and Å. Forsberg, *Role of Fraction 1 Antigen of Yersinia pestis in Inhibition of Phagocytosis.* Infect Immun, 2002. **70**(3): p. 1453-1460.

68. Perry, R.D. and J.D. Fetherston, *Yersinia pestis--etiologic agent of plague.* Clinical Microbiology Reviews, 1997. **10**(1): p. 35-66.

69. Finegold, M.J., *Pneumonic plague in monkeys. An electron microscopic study.* The American Journal of Pathology, 1969. **54**(2): p. 167-185.

70. Straley, S.C. and P.A. Harmon, *Yersinia pestis grows within phagolysosomes in mouse peritoneal macrophages.* Infect Immun, 1984. **45**(3): p. 655-659.

71. Pujol, C., et al., *Yersinia pestis Can Reside in Autophagosomes and Avoid Xenophagy in Murine Macrophages by Preventing Vacuole Acidification.* Infect Immun, 2009. **77**(6): p. 2251-2261.

72. Ogawa, M., et al., *Manipulation of autophagy by bacteria for their own benefit.* Microbiology and Immunology, 2011. **55**(7): p. 459-471.

73. Ponnusamy, D. and K.D. Clinkenbeard, *<italic>Yersinia pestis</italic> Intracellular Parasitism of Macrophages from Hosts Exhibiting High and Low Severity of Plague.* PLoS One, 2012. **7**(7): p. e42211.

74. Stevens, D.L., et al., *Practice Guidelines for the Diagnosis and Management of Skin and Soft Tissue Infections: 2014 Update by the Infectious Diseases Society of America.* Clinical Infectious Diseases, 2014.

75. Wendte, J.M., et al., *In Vitro Efficacy of Antibiotics Commonly Used To Treat Human Plague against Intracellular Yersinia pestis.* Antimicrob Agents Chemother, 2011. **55**(8): p. 3752-3757.

76. Rasolomaharo, M., et al., *Plague in Majunga, Madagascar.* The Lancet, 1995. **346**(8984): p. 1234.

77. Galimand, M., et al., *Multidrug Resistance in Yersinia pestis Mediated by a Transferable Plasmid.* New England Journal of Medicine, 1997. **337**(10): p. 677-681.

78. Lazar Adler, N.R., et al., *The molecular and cellular basis of pathogenesis in melioidosis: how does Burkholderia pseudomallei cause disease?* FEMS Microbiology Reviews, 2009. **33**(6): p. 1079-1099.

79. Chaowagul, W., et al., *Melioidosis: a major cause of community-acquired septicemia in northeastern Thailand.* J Infect Dis, 1989. **159**(5): p. 890-9.

80. Barnes, J.L. and N. Ketheesan, *Route of infection in melioidosis.* Emerg Infect Dis, 2005. **11**(4): p. 638-9.

81. Shams, A.M., et al., *Survival of Burkholderia pseudomallei on Environmental Surfaces.* Applied and Environmental Microbiology, 2007. **73**(24): p. 8001-8004.

82. Chaowagul, W., et al., *Melioidosis: A Major Cause of Community-Acquired Septicemia in Northeastern Thailand.* J Infect Dis, 1989. **159**(5): p. 890-899.

83. Peacock, S.J., *Melioidosis.* Current Opinion in Infectious Diseases, 2006. **19**(5): p. 421-428 10.1097/01.qco.0000244046.31135.b3.

84. McGovern Tw, C.G.W.E.E.M., *CUtaneous manifestations of biological warfare and related threat agents.* Archives of Dermatology, 1999. **135**(3): p. 311-322.

85. Chaowagul, W., et al., *Relapse in Melioidosis: Incidence and Risk Factors.* J Infect Dis, 1993. **168**(5): p. 1181-1185.

86. Pruksachartvuthi, S., N. Aswapokee, and K. Thankerngpol, *Survival of Pseudomonas pseudomallei in human phagocytes.* J Med Microbiol, 1990. **31**(2): p. 109-114.

87. Harley, V.S., et al., *Interaction of Pseudomonas pseudomallei with macrophages.* Biochemical Society transactions, 1994. **22**(2): p. 88S.

88. Ekchariyawat, P., et al., *Burkholderia pseudomallei-Induced Expression of Suppressor of Cytokine Signaling 3 and Cytokine-Inducible Src Homology 2-Containing Protein in Mouse Macrophages: a Possible Mechanism for Suppression of the Response to Gamma Interferon Stimulation.* Infect Immun, 2005. **73**(11): p. 7332-7339.

89. Utaisincharoen, P., et al., *Burkholderia pseudomallei Interferes with Inducible Nitric Oxide Synthase (iNOS) Production: A Possible Mechanism of Evading Macrophage Killing.* Microbiology and Immunology, 2001. **45**(4): p. 307-313.

90. Lengwehasatit, I., et al., *Involvement of B. pseudomallei RpoS in apoptotic cell death in mouse macrophages.* Microbial Pathogenesis, 2008. **44**(3): p. 238-245.

91. Kespichayawattana, W., et al., *Burkholderia pseudomallei Induces Cell Fusion and Actin-Associated Membrane Protrusion: a Possible Mechanism for Cell-to-Cell Spreading.* Infect Immun, 2000. **68**(9): p. 5377-5384.

92. Stevens, M.P., et al., *Identification of a bacterial factor required for actin-based motility of Burkholderia pseudomallei.* Mol Microbiol, 2005. **56**(1): p. 40-53.

93. Attree, O. and I. Attree, *A second type III secretion system in Burkholderia pseudomallei: who is the real culprit?* Microbiology, 2001. **147**(12): p. 3197-3199.

94. Stevens, M.P., et al., *A Burkholderia pseudomallei Type III Secreted Protein, BopE, Facilitates Bacterial Invasion of Epithelial Cells and Exhibits Guanine Nucleotide Exchange Factor Activity.* J Bacteriol, 2003. **185**(16): p. 4992-4996.

95. Stevens, M.P., et al., *An Inv/Mxi-Spa-like type III protein secretion system in Burkholderia pseudomallei modulates intracellular behaviour of the pathogen.* Mol Microbiol, 2002. **46**(3): p. 649-659.

96. Cullinane, M., et al., *Stimulation of autophagy suppresses the intracellular survival of Burkholderia pseudomallei in mammalian cell lines.* Autophagy, 2008. **4**(6): p. 744-753.

97. Wiersinga, W.J., et al., *Melioidosis: insights into the pathogenicity of Burkholderia pseudomallei.* Nat Rev Micro, 2006. **4**(4): p. 272-282.

98. Thibault, F.M., et al., *Antibiotic susceptibility of 65 isolates of Burkholderia pseudomallei and Burkholderia mallei to 35 antimicrobial agents.* Journal of Antimicrobial Chemotherapy, 2004. **54**(6): p. 1134-1138.

99. Peacock, S.J., et al., *Management of Accidental Laboratory Exposure to Burkholderia pseudomallei and B. mallei.* Emerg Infect Dis, 2008. **14**(7): p. e2-e2.

100. Sarovich, D.S., et al., *Characterization of Ceftazidime Resistance Mechanisms in Clinical Isolates of <italic>Burkholderia pseudomallei</italic> from Australia.* PLoS One, 2012. **7**(2): p. e30789.

101. Livermore, D.M., et al., *beta-Lactamase of Pseudomonas pseudomallei and its contribution to antibiotic resistance.* J Antimicrob Chemother, 1987. **20**(3): p. 313-21.

102. Larsson, P., et al., *The complete genome sequence of Francisella tularensis, the causative agent of tularemia.* Nat Genet, 2005. **37**(2): p. 153-159.

103. Oyston, P.C., *Francisella tularensis: unravelling the secrets of an intracellular pathogen.* J Med Microbiol, 2008. **57**(Pt 8): p. 921-30.

104. Jellison, W.L., *Tularemia: Dr. Edward Francis and His First 23 Isolates of "Francisella tularensis".* Bulletin of the history of medicine, 1972. **46**(5).

105. Sjodin, A., et al., *Genome characterisation of the genus Francisella reveals insight into similar evolutionary paths in pathogens of mammals and fish.* BMC Genomics, 2012. **13**: p. 268.

106. Tarnvik, A., *WHO Guidelines on Tularaemia.* Geneva: World Health Organisation, 2007.

107. Kim, D.Y., et al., *Rabbit tularemia and hepatic coccidiosis in wild rabbit.* Emerg Infect Dis, 2010. **16**(12): p. 2016-7.

108. Tärnvik, A. and L. Berglund, *Tularaemia.* European Respiratory Journal, 2003. **21**(2): p. 361-373.

109. Matyas, B.T., H.S. Nieder, and S.R. Telford, *Pneumonic Tularemia on Martha's Vineyard.* Ann N Y Acad Sci, 2007. **1105**(1): p. 351-377.

110. Berrada, Z.L. and S.R. Telford, *Survival of Francisella tularensis Type A in brackish-water.* Arch microbiol, 2011. **193**(3): p. 223-226.

111. Sjostedt, A., *Intracellular survival mechanisms of Francisella tularensis, a stealth pathogen.* Microbes Infect, 2006. **8**(2): p. 561-7.

112. McLendon, M.K., M.A. Apicella, and L.A. Allen, *Francisella tularensis: taxonomy, genetics, and Immunopathogenesis of a potential agent of biowarfare.* Annu Rev Microbiol, 2006. **60**: p. 167-85.

113. Dennis, D.T., et al., *Tularemia as a biological weapon: medical and public health management.* JAMA, 2001. **285**(21): p. 2763-73.

114. Long, G.W., et al., *Detection of Francisella tularensis in blood by polymerase chain reaction.* J Clin Microbiol, 1993. **31**(1): p. 152-154.

115. Saslaw, S., et al., *Tularemia vaccine study: I. intracutaneous challenge.* Arch Intern Med, 1961. **107**(5): p. 689-701.

116. Saslaw, S., et al., *Tularemia vaccine study: Ii. respiratory challenge.* Arch Intern Med, 1961. **107**(5): p. 702-714.

117. Anthony, L.D., R.D. Burke, and F.E. Nano, *Growth of Francisella spp. in rodent macrophages.* Infect Immun, 1991. **59**(9): p. 3291-3296.

118. Fortier, A.H., et al., *Growth of Francisella tularensis LVS in macrophages: the acidic intracellular compartment provides essential iron required for growth.* Infect Immun, 1995. **63**(4): p. 1478-83.

119. Celli, J. and T.C. Zahrt, *Mechanisms of Francisella tularensis Intracellular Pathogenesis.* Cold Spring Harbor Perspectives in Medicine, 2013. **3**(4).

120. Oyston, P.C.F., A. Sjostedt, and R.W. Titball, *Tularaemia: bioterrorism defence renews interest in Francisella tularensis.* Nat Rev Micro, 2004. **2**(12): p. 967-978.

121. McCaffrey, R.L. and L.A. Allen, *Francisella tularensis LVS evades killing by human neutrophils via inhibition of the respiratory burst and phagosome escape.* J Leukoc Biol, 2006. **80**(6): p. 1224-30.

122. Hall, J.D., et al., *Francisella tularensis Replicates within Alveolar Type II Epithelial Cells In Vitro and In Vivo following Inhalation.* Infect Immun, 2007. **75**(2): p. 1034-1039.

123. Balagopal, A., et al., *Characterization of the Receptor-Ligand Pathways Important for Entry and Survival of Francisella tularensis in Human Macrophages.* Infect Immun, 2006. **74**(9): p. 5114-5125.

124. Schulert, G.S. and L.-A.H. Allen, *Differential infection of mononuclear phagocytes by Francisella tularensis: role of the macrophage mannose receptor.* J Leukoc Biol, 2006. **80**(3): p. 563-571.

125. Pierini, L.M., *Uptake of serum-opsonized Francisella tularensis by macrophages can be mediated by class A scavenger receptors.* Cell Microbiol, 2006. **8**(8): p. 1361-1370.

126. Geier, H. and J. Celli, *Phagocytic Receptors Dictate Phagosomal Escape and Intracellular Proliferation of Francisella tularensis.* Infect Immun, 2011. **79**(6): p. 2204-2214.

127. Barel, M., et al., *A novel receptor – ligand pathway for entry of Francisella tularensis in monocyte-like THP-1 cells: interaction between surface nucleolin and bacterial elongation factor Tu.* BMC Microbiology, 2008. **8**: p. 145-145.

128. Clemens, D.L., B.-Y. Lee, and M.A. Horwitz, *Francisella tularensis Enters Macrophages via a Novel Process Involving Pseudopod Loops.* Infect Immun, 2005. **73**(9): p. 5892-5902.

129. Checroun, C., et al., *Autophagy-mediated reentry of Francisella tularensis into the endocytic compartment after cytoplasmic replication.* PNAS, 2006. **103**(39): p. 14578-14583.

130. Clemens, D.L., B.-Y. Lee, and M.A. Horwitz, *Virulent and Avirulent Strains of Francisella tularensis Prevent Acidification and Maturation of Their Phagosomes and Escape into the Cytoplasm in Human Macrophages.* Infect Immun, 2004. **72**(6): p. 3204-3217.

131. Chong, A., et al., *The Early Phagosomal Stage of Francisella tularensis Determines Optimal Phagosomal Escape and Francisella Pathogenicity Island Protein Expression.* Infect Immun, 2008. **76**(12): p. 5488-5499.

132. Bönquist, L., et al., *MglA and Igl Proteins Contribute to the Modulation of Francisella tularensis Live Vaccine Strain-Containing Phagosomes in Murine Macrophages.* Infect Immun, 2008. **76**(8): p. 3502-3510.

133. Kinchen, J.M. and K.S. Ravichandran, *Phagosome maturation: going through the acid test.* Nat Rev Mol Cell Biol, 2008. **9**(10): p. 781-795.

134. Eskelinen, E.-L., *Roles of LAMP-1 and LAMP-2 in lysosome biogenesis and autophagy.* Mol Aspects Med, 2006. **27**(5–6): p. 495-502.

135. Pechous, R., et al., *Construction and Characterization of an Attenuated Purine Auxotroph in a Francisella tularensis Live Vaccine Strain.* Infect Immun, 2006. **74**(8): p. 4452-4461.

136. Pechous, R.D., et al., *A Francisella tularensis Schu S4 Purine Auxotroph Is Highly Attenuated in Mice but Offers Limited Protection against Homologous Intranasal Challenge.* PLoS One, 2008. **3**(6): p. e2487.

137. Alkhuder, K., et al., *Glutathione Provides a Source of Cysteine Essential for Intracellular Multiplication of Francisella tularensis.* PLoS Pathog, 2009. **5**(1): p. e1000284.

138. Ikäheimo, I., et al., *In vitro antibiotic susceptibility of Francisella tularensis isolated from humans and animals.* Journal of Antimicrobial Chemotherapy, 2000. **46**(2): p. 287-290.

139. Oyston, P.C.F., *Francisella tularensis vaccines.* Vaccine, 2009. **27, Supplement 4**(0): p. D48-D51.

140. Marohn, M.E. and E.M. Barry, *Live Attenuated Tularemia Vaccines: Recent Developments and Future Goals.* Vaccine, 2013. **31**(35): p. 3485-3491.

141. Gilbert, P., P.J. Collier, and M.R. Brown, *Influence of growth rate on susceptibility to antimicrobial agents: biofilms, cell cycle, dormancy, and stringent response.* Antimicrob Agents Chemother, 1990. **34**(10): p. 1865-8.

142. Seyfzadeh, M., J. Keener, and M. Nomura, *spoT-dependent accumulation of guanosine tetraphosphate in response to fatty acid starvation in Escherichia coli.* PNAS, 1993. **90**(23): p. 11004-11008.

143. Spira, B., N. Silberstein, and E. Yagil, *Guanosine 3',5'-bispyrophosphate (ppGpp) synthesis in cells of Escherichia coli starved for Pi.* J Bacteriol, 1995. **177**(14): p. 4053-8.

144. Sarmientos, P. and M. Cashel, *Carbon starvation and growth rate-dependent regulation of the Escherichia coli ribosomal RNA promoters: differential control of dual promoters.* PNAS, 1983. **80**(22): p. 7010-7013.

145. Traxler, M.F., D.-E. Chang, and T. Conway, *Guanosine 3´,5´-bispyrophosphate coordinates global gene expression during glucose-lactose diauxie in Escherichia coli.* PNAS, 2006. **103**(7): p. 2374-2379.

146. Durfee, T., et al., *Transcription profiling of the stringent response in Escherichia coli.* J Bacteriol, 2008. **190**(3): p. 1084-96.

147. Magnusson, L.U., A. Farewell, and T. Nyström, *ppGpp: a global regulator in Escherichia coli.* Trends Microbiol, 2005. **13**(5): p. 236-242.

148. Gentry, D.R., et al., *Synthesis of the stationary-phase sigma factor sigma s is positively regulated by ppGpp.* J Bacteriol, 1993. **175**(24): p. 7982-7989.

149. Gustavsson, N., A. Diez, and T. Nyström, *The universal stress protein paralogues of Escherichia coli are co-ordinately regulated and co-operate in the defence against DNA damage.* Mol Microbiol, 2002. **43**(1): p. 107-117.

150. Dalebroux, Z.D., et al., *ppGpp Conjures Bacterial Virulence.* Microbiol Mol Biol R, 2010. **74**(2): p. 171-199.

151. Maisonneuve, E., M. Castro-Camargo, and K. Gerdes, *(p)ppGpp Controls Bacterial Persistence by Stochastic Induction of Toxin-Antitoxin Activity.* Cell, 2013. **154**(5): p. 1140-1150.

152. Wu, J., Q. Long, and J. Xie, *(p)ppGpp and drug resistance.* J Cell Physiol, 2010. **224**(2): p. 300-304.

153. Eichel, J., et al., *Effect of ppGpp on Escherichia coliCyclopropane Fatty Acid Synthesis Is Mediated through the RpoS Sigma Factor (çS).* J Bacteriol, 1999. **181**(2): p. 572-576.

154. Kanjee, U., K. Ogata, and W.A. Houry, *Direct binding targets of the stringent response alarmone (p)ppGpp.* Mol Microbiol, 2012. **85**(6): p. 1029-1043.

155. Schreiber, G.R., E. and Glaser, G., *ppGpp-mediated regulation of DNA replication and cell division in Escherichia coli.* Current Microbiology, 1995. **30**: p. 27-32.

156. Magnusson, L.U., et al., *Identical, Independent, and Opposing Roles of ppGpp and DksA in Escherichia coli.* J Bacteriol, 2007. **189**(14): p. 5193-5202.

157. Traxler, M.F., et al., *The global, ppGpp-mediated stringent response to amino acid starvation in Escherichia coli.* Mol Microbiol, 2008. **68**(5): p. 1128-1148.

158. Hernandez, V.J. and H. Bremer, *Characterization of RNA and DNA synthesis in Escherichia coli strains devoid of ppGpp.* J Biol Chem, 1993. **268**(15): p. 10851-62.

159. Lemke, J.J., et al., *Direct regulation of Escherichia coli ribosomal protein promoters by the transcription factors ppGpp and DksA.* PNAS, 2011. **108**(14): p. 5712-5717.

160. Svitil, A.L., M. Cashel, and J.W. Zyskind, *Guanosine tetraphosphate inhibits protein synthesis in vivo. A possible protective mechanism for starvation stress in Escherichia coli.* J Biol Chem, 1993. **268**(4): p. 2307-11.

161. Milon, P., et al., *The nucleotide-binding site of bacterial translation initiation factor 2 (IF2) as a metabolic sensor.* PNAS, 2006. **103**(38): p. 13962-13967.

162. Pao, C.C. and B.T. Dyess, *Stringent control of RNA synthesis in the absence of guanosine 5'-diphosphate-3'-diphosphate.* J BiolChem, 1981. **256**(5): p. 2252-2257.

163. Höltje, J.V., *Regulation of polyamine and streptomycin transport during stringent and relaxed control in Escherichia coli.* J Bacteriol, 1979. **137**(1): p. 661-663.

164. Polakis, S.E., R.B. Guchhait, and M.D. Lane, *Stringent Control of Fatty Acid Synthesis in Escherichia coli : Possible Regulation of Acetyl Coenzyme A Carboxylase by ppGpp.* J Biol Chem, 1973. **248**(22): p. 7957-7966.

165. Chang, D.-E., D.J. Smalley, and T. Conway, *Gene expression profiling of Escherichia coli growth transitions: an expanded stringent response model.* Mol Microbiol, 2002. **45**(2): p. 289-306.

166. Bougdour, A. and S. Gottesman, *ppGpp regulation of RpoS degradation via anti-adaptor protein IraP.* PNAS, 2007. **104**(31): p. 12896-901.

167. Maciąg, M., et al., *ppGpp inhibits the activity of Escherichia coli DnaG primase.* Plasmid, 2010. **63**(1): p. 61-67.

168. Wendrich, T.M., et al., *Dissection of the Mechanism for the Stringent Factor RelA.* Mol Cell, 2002. **10**(4): p. 779-788.

169. Vance, D., et al., *Inhibition of fatty acid synthetases by the antibiotic cerulenin.* Biochem Bioph Res Co, 1972. **48**(3): p. 649-656.

170. Xiao, H., et al., *Residual guanosine 3',5'-bispyrophosphate synthetic activity of relA null mutants can be eliminated by spoT null mutations.* J Biol Chem, 1991. **266**(9): p. 5980-5990.

171. Battesti, A. and E. Bouveret, *Acyl carrier protein/SpoT interaction, the switch linking SpoT-dependent stress response to fatty acid metabolism.* Mol Microbiol, 2006. **62**(4): p. 1048-1063.

172. Heath, R.J. and C.O. Rock, *Regulation of Fatty Acid Elongation and Initiation by Acyl-Acyl Carrier Protein in Escherichia coli.* J Biol Chem, 1996. **271**(4): p. 1833-1836.

173. Ostling, J., L. Holmquist, and S. Kjelleberg, *Global analysis of the carbon starvation response of a marine Vibrio species with disruptions in genes homologous to relA and spoT.* J Bacteriol, 1996. **178**(16): p. 4901-8.

174. Peterson, C.N., M.J. Mandel, and T.J. Silhavy, *Escherichia coli Starvation Diets: Essential Nutrients Weigh in Distinctly.* J Bacteriol, 2005. **187**(22): p. 7549-7553.

175. Sokawa, Y., J. Sokawa, and Y. Kaziro, *Regulation of stable RNA synthesis and ppGpp levels in growing cells of Escherichia coli.* Cell, 1975. **5**(1): p. 69-74.

176. Kessler, D.P. and H.V. Rickenberg, *The competitive inhibition of α-methylglucoside uptake in Escherichia coli.* Biochem Bioph Res Co, 1963. **10**(6): p. 482-487.

177. Hansen, M.T., et al., *Simple downshift and resulting lack of correlation between ppGpp pool size and ribonucleic acid accumulation.* J Bacteriol, 1975. **122**(2): p. 585-591.

178. Lazzarini, R.A., M. Cashel, and J. Gallant, *On the Regulation of Guanosine Tetraphosphate Levels in Stringent and Relaxed Strains of Escherichia coli.* J Biol Chem, 1971. **246**(14): p. 4381-4385.

179. Ostling, J., K. Flärdh, and S. Kjelleberg, *Isolation of a carbon starvation regulatory mutant in a marine Vibrio strain.* J Bacteriol, 1995. **177**(23): p. 6978-82.

180. Haseltine, W.A.a.B., R. , *Synthesis of guanosine tetra- and pentaphosphate requires the presence of a codon-specific, uncharged transfer ribonucleic acid in the acceptor site of ribosomes.* Proc. Nat. Acad. Sci. USA, 1973. **70**(5): p. 1564 - 1568.

181. Ramakrishnan, V., *Ribosome structure and the mechanism of translation.* Cell, 2002. **108**(4): p. 557-72.

182. Haseltine, W.A., et al., *MSI and MSII made on Ribosome in Idling Step of Protein Synthesis.* Nature, 1972. **238**(5364): p. 381-384.

183. Dittmar, K.A., et al., *Selective charging of tRNA isoacceptors induced by amino-acid starvation.* Embo Reports, 2005. **6**(2): p. 151-7.

184. Potrykus, K. and M. Cashel, *(p)ppGpp: still magical?* Annu Rev Microbiol, 2008. **62**: p. 35-51.

185. Cashel, M. and J. Gallant, *Two compounds implicated in the function of the RC gene of Escherichia coli.* Nature, 1969. **221**(5183): p. 838-41.

186. Que, L., et al., *Guanosine 5´-Diphosphate, 3´-Diphosphate: Assignment of Structure by 13C Nuclear Magnetic Resonance Spectroscopy.* PNAS, 1973. **70**(9): p. 2563-2566.

187. Mechold, U., et al., *Differential regulation by ppGpp versus pppGpp in Escherichia coli.* Nucleic Acids Res, 2013. **41**(12): p. 6175-6189.

188. Hamel, E. and M. Cashel, *Role of guanine nucleotides in protein synthesis. Elongation factor G and guanosine 5'-triphosphate,3'-diphosphate.* PNAS, 1973. **70**(11): p. 3250-4.

189. Atkinson, G.C., T. Tenson, and V. Hauryliuk, *The RelA/SpoT homolog (RSH) superfamily: distribution and functional evolution of ppGpp synthetases and hydrolases across the tree of life.* PLoS One, 2011. **6**(8): p. e23479.

190. Kuroda, A.M., H. Cashel, M. and Kornberg, A., *Guanosine Tetra- and pentaphosphate promote accumulation of inorganic polyphosphate in Escherichia coli.* J Biol Chem, 1996. **272**(34): p. 21240-21243.

191. Mechold, U., et al., *Intramolecular Regulation of the Opposing (p)ppGpp Catalytic Activities of Rel(Seq), the Rel/Spo Enzyme from Streptococcus equisimilis.* J Bacteriol, 2002. **184**(11): p. 2878-2888.

192. Avarbock, D., et al., *Cloning and characterization of a bifunctional RelA/SpoT homologue from Mycobacterium tuberculosis.* Gene, 1999. **233**(1–2): p. 261-269.

193. Artsimovitch, I., et al., *Structural basis for transcription regulation by alarmone ppGpp.* Cell, 2004. **117**(3): p. 299-310.

194. Roberts, J.W., *Promoter-specific control of E. coli RNA polymerase by ppGpp and a general transcription factor.* Genes Dev, 2009. **23**(2): p. 143-6.

195. Perederina, A., et al., *Regulation through the secondary channel--structural framework for ppGpp-DksA synergism during transcription.* Cell, 2004. **118**(3): p. 297-309.

196. Srivatsan, A. and J.D. Wang, *Control of bacterial transcription, translation and replication by (p)ppGpp.* Curr Opin Microbiol, 2008. **11**(2): p. 100-5.

197. Dalebroux, Z.D. and M.S. Swanson, *ppGpp: magic beyond RNA polymerase.* Nat Rev Micro, 2012. **10**(3): p. 203-212.

198. Dennis, D.I., T. Henderson, D. Bartlett, J. Ascher, M. Eitzen, E. Fine, A. Friedlander, A. Hauer, J. Layton, M. Lillibridge, S. McDade, J. Osterholm, M. O'Toole, T. Parker, G. Perl, T. Russell, P. Tonat, K., *Tularemia as a biological weapon.* JAMA, 2001. **285**(21).

199. Brown, L., et al., *DksA Affects ppGpp Induction of RpoS at a Translational Level.* J Bacteriol, 2002. **184**(16): p. 4455-4465.

200. Hirsch, M. and T. Elliott, *Role of ppGpp in rpoS Stationary-Phase Regulation in Escherichia coli.* J Bacteriol, 2002. **184**(18): p. 5077-5087.

201. Zhou, Y., et al., *The RssB response regulator directly targets sigma(S) for degradation by ClpXP.* Genes Dev, 2001. **15**(5): p. 627-37.

202. Bougdour, A. and S. Gottesman, *ppGpp regulation of RpoS degradation via anti-adaptor protein IraP.* PNAS, 2007. **104**(31): p. 12896-12901.

203. Merrikh, H., A.E. Ferrazzoli, and S.T. Lovett, *Growth Phase and (p)ppGpp Control of IraD, a Regulator of RpoS Stability, in Escherichia coli.* J Bacteriol, 2009. **191**(24): p. 7436-7446.

204. Sarubbi, E., K.E. Rudd, and M. Cashel, *Basal ppGpp level adjustment shown by new spoT mutants affect steady state growth rates and rrnA ribosomal promoter regulation in Escherichia coli.* Mol Gen Genet, 1988. **213**(2-3): p. 214-22.

205. Geiger, T. and C. Wolz, *Intersection of the stringent response and the CodY regulon in low GC Gram-positive bacteria.* Int J Med Microbiol, 2014. **304**(2): p. 150-5.

206. Hauryliuk, V., et al., *Recent functional insights into the role of (p)ppGpp in bacterial physiology.* Nat Rev Micro, 2015. **13**(5): p. 298-309.

207. Krásný, L., et al., *The identity of the transcription +1 position is crucial for changes in gene expression in response to amino acid starvation in Bacillus subtilis.* Mol Microbiol, 2008. **69**(1): p. 42-54.

208. Geiger, T., et al., *Role of the (p)ppGpp Synthase RSH, a RelA/SpoT Homolog, in Stringent Response and Virulence of Staphylococcus aureus.* Infect Immun, 2010. **78**(5): p. 1873-1883.

209. Sonenshein, A.L., *CodY, a global regulator of stationary phase and virulence in Gram-positive bacteria.* Curr Opin Microbiol, 2005. **8**(2): p. 203-7.

210. Lopez, J.M., A. Dromerick, and E. Freese, *Response of Guanosine 5´-Triphosphate Concentration to Nutritional Changes and Its Significance for Bacillus subtilis Sporulation.* J Bacteriol, 1981. **146**(2): p. 605-613.

211. Krásný, L. and R.L. Gourse, *An alternative strategy for bacterial ribosome synthesis: Bacillus subtilis rRNA transcription regulation.* EMBO Journal, 2004. **23**(22): p. 4473-4483.

212. Molle, V., et al., *Additional Targets of the Bacillus subtilis Global Regulator CodY Identified by Chromatin Immunoprecipitation and Genome-Wide Transcript Analysis.* J Bacteriol, 2003. **185**(6): p. 1911-1922.

213. Rodionov, D.G. and E.E. Ishiguro, *Direct correlation between overproduction of guanosine 3',5'-bispyrophosphate (ppGpp) and penicillin tolerance in Escherichia coli.* J Bacteriol, 1995. **177**(15): p. 4224-4229.

214. Li, Y.-H. and X. Tian, *Quorum Sensing and Bacterial Social Interactions in Biofilms.* Sensors (Basel, Switzerland), 2012. **12**(3): p. 2519-2538.

215. Schafhauser, J., et al., *The Stringent Response Modulates 4-Hydroxy-2-Alkylquinoline Biosynthesis and Quorum-Sensing Hierarchy in Pseudomonas aeruginosa.* J Bacteriol, 2014. **196**(9): p. 1641-1650.

216. van Delden, C., et al., *Stringent Response Activates Quorum Sensing and Modulates Cell Density-Dependent Gene Expression in Pseudomonas aeruginosa.* J Bacteriol, 2001. **183**(18): p. 5376-5384.

217. O'Toole, G., H.B. Kaplan, and R. Kolter, *Biofilm Formation as Microbial Development.* Annu Rev Microbiol, 2000. **54**(1): p. 49-79.

218. Chávez de Paz, L.E., et al., *Role of (p)ppGpp in Biofilm Formation by Enterococcus faecalis.* Appl Environ Microb, 2012. **78**(5): p. 1627-1630.

219. Balzer, G.J. and R.J.C. McLean, *NoteThe stringent response genes relA and spoT are important for Escherichia coli biofilms under slow-growth conditions.* Can J Microbiol, 2002. **48**(7): p. 675-680.

220. Lemos, J.A.C., T.A. Brown, and R.A. Burne, *Effects of RelA on Key Virulence Properties of Planktonic and Biofilm Populations of Streptococcus mutans.* Infect Immun, 2004. **72**(3): p. 1431-1440.

221. He, H., et al., *Stringent Response Regulation of Biofilm Formation in Vibrio cholerae.* J Bacteriol, 2012. **194**(11): p. 2962-2972.

222. de la Fuente-Núñez, C., et al., *Broad-Spectrum Anti-biofilm Peptide That Targets a Cellular Stress Response.* PLoS Pathog, 2014. **10**(5): p. e1004152.

223. Lister, J.L. and A.R. Horswill, *Staphylococcus aureus biofilms: recent developments in biofilm dispersal.* Front Cell and Infect Microbiol, 2014. **4**: p. 178.

224. Reffuveille, F., et al., *A Broad-Spectrum Antibiofilm Peptide Enhances Antibiotic Action against Bacterial Biofilms.* Antimicrob Agents Chemother, 2014. **58**(9): p. 5363-5371.

225. Greenway, D.L.A. and R.R. England, *The intrinsic resistance of Escherichia coli to various antimicrobial agents requires ppGpp and σs.* Lett Appl Microbiol, 1999. **29**(5): p. 323-326.

226. Pomares, M.F., et al., *Protective Action of ppGpp in Microcin J25-Sensitive Strains.* J Bacteriol, 2008. **190**(12): p. 4328-4334.

227. Wilson, K.-A., et al., *Structure of Microcin J25, a Peptide Inhibitor of Bacterial RNA Polymerase, is a Lassoed Tail.* J Am Chem Soc, 2003. **125**(41): p. 12475-12483.

228. Bharathiraja, R., et al., *Factors affecting antibiotic prescribing pattern in pediatric practice.* Indian J Pediatr, 2005. **72**(10): p. 877-879.

229. Col, N.F. and R.W. O'Connor, *Estimating Worldwide Current Antibiotic Usage: Report of Task Force 1.* Rev Infect Dis, 1987. **9**(Supplement 3): p. S232-S243.

230. Waxman, D.J. and J.L. Strominger, *Penicillin-Binding Proteins and the Mechanism of Action of Beta-Lactam Antibiotics1.* Annu Rev Biochem, 1983. **52**(1): p. 825-869.

231. Smith, T.J., S.A. Blackman, and S.J. Foster, *Autolysins of Bacillus subtilis: multiple enzymes with multiple functions.* Microbiology, 2000. **146**(2): p. 249-262.

232. Betzner, A.S., et al., *Control of the activity of the soluble lytic transglycosylase by the stringent response in Escherichia coli.* FEMS Microbiology Letters, 1990. **67**(1-2): p. 161-164.

233. Bigger, J., *The bactericidal action of penicillin on Staphylococcus pyogenes.* Ir J Med Sci 1944. **19**(11): p. 553-568.

234. Fauvart, M., V.N. De Groote, and J. Michiels, *Role of persister cells in chronic infections: clinical relevance and perspectives on anti-persister therapies.* J Med Microbiol, 2011. **60**(6): p. 699-709.

235. Moyed, H.S. and K.P. Bertrand, *hipA, a newly recognized gene of Escherichia coli K-12 that affects frequency of persistence after inhibition of murein synthesis.* J Bacteriol, 1983. **155**(2): p. 768-775.

236. Korch, S.B., T.A. Henderson, and T.M. Hill, *Characterization of the hipA7 allele of Escherichia coli and evidence that high persistence is governed by (p)ppGpp synthesis.* Mol Microbiol, 2003. **50**(4): p. 1199-1213.

237. Keren, I., et al., *Specialized Persister Cells and the Mechanism of Multidrug Tolerance in Escherichia coli.* J Bacteriol, 2004. **186**(24): p. 8172-8180.

238. Kuroda, A., *A Polyphosphate-Lon Protease Complex in the Adaptation of Escherichia coli to Amino Acid Starvation.* Biosci Biotech Bioch, 2006. **70**(2): p. 325-331.

239. Kuroda, A., et al., *Guanosine Tetra- and Pentaphosphate Promote Accumulation of Inorganic Polyphosphate in Escherichia coli.* J Biol Chem, 1997. **272**(34): p. 21240-21243.

240. de Lima Procópio, R.E., et al., *Antibiotics produced by Streptomyces.* Braz J Infect Dis, 2012. **16**(5): p. 466-471.

241. Raaijmakers, J., M. Vlami, and J. de Souza, *Antibiotic production by bacterial biocontrol agents.* Antonie van Leeuwenhoek, 2002. **81**(1-4): p. 537-547.

242. Gomez-Escribano, J.P., et al., *Streptomyces clavuligerus relA-null mutants overproduce clavulanic acid and cephamycin C: negative regulation of secondary metabolism by (p)ppGpp.* Microbiology, 2008. **154**(3): p. 744-755.

243. Déziel, E., et al., *Analysis of Pseudomonas aeruginosa 4-hydroxy-2-alkylquinolines (HAQs) reveals a role for 4-hydroxy-2-heptylquinoline in cell-to-cell communication.* PNAS, 2004. **101**(5): p. 1339-1344.

244. Mitchell, G., et al., *Staphylococcus aureus sigma B-dependent emergence of small-colony variants and biofilm production following exposure to Pseudomonas aeruginosa 4-hydroxy-2-heptylquinoline-N-oxide.* BMC Microbiology, 2010. **10**: p. 33-33.

245. Kaper, J.B., J.P. Nataro, and H.L.T. Mobley, *Pathogenic Escherichia coli.* Nat Rev Micro, 2004. **2**(2): p. 123-140.

246. Jerse, A.E., et al., *A genetic locus of enteropathogenic Escherichia coli necessary for the production of attaching and effacing lesions on tissue culture cells.* PNAS, 1990. **87**(20): p. 7839-7843.

247. Nakanishi, N., et al., *ppGpp with DksA controls gene expression in the locus of enterocyte effacement (LEE) pathogenicity island of enterohaemorrhagic Escherichia coli through activation of two virulence regulatory genes.* Mol Microbiol, 2006. **61**(1): p. 194-205.

248. Hu, P., et al., *Structural Organization of Virulence-Associated Plasmids of Yersinia pestis.* J Bacteriol, 1998. **180**(19): p. 5192-5202.

249. Coburn, B., I. Sekirov, and B.B. Finlay, *Type III Secretion Systems and Disease.* Clin Microbiol Rev, 2007. **20**(4): p. 535-549.

250. Sun, W., et al., *The role of relA and spoT in Yersinia pestis KIM5 pathogenicity.* PLoS One, 2009. **4**(8): p. e6720.

251. Charity, J.C., et al., *Small molecule control of virulence gene expression in Francisella tularensis.* PLoS Pathog, 2009. **5**(10): p. e1000641.

252. Fuller, J., et al., *Environmental and intracellular regulation of Francisella tularensis ripA.* BMC Microbiology, 2009. **9**(1): p. 216.

253. Charity, J.C., et al., *Twin RNA polymerase-associated proteins control virulence gene expression in Francisella tularensis.* PLoS Pathog, 2007. **3**(6): p. e84.

254. Hogg, T., et al., *Conformational Antagonism between Opposing Active Sites in a Bifunctional RelA/SpoT Homolog Modulates (p)ppGpp Metabolism during the Stringent Response.* Cell, 2004. **117**(1): p. 57-68.

255. Avarbock, A., et al., *Functional Regulation of the Opposing (p)ppGpp Synthetase/Hydrolase Activities of RelMtb from Mycobacterium tuberculosis†.* Biochemistry, 2005. **44**(29): p. 9913-9923.

256. Sajish, M., et al., *A Charge Reversal Differentiates (p)ppGpp Synthesis by Monofunctional and Bifunctional Rel Proteins.* J Biol Chem, 2007. **282**(48): p. 34977-34983.

257. Metzger, S., et al., *Protein sequences encoded by the relA and the spoT genes of Escherichia coli are interrelated.* J Biol Chem, 1989. **264**(16): p. 9122-5.

258. Zhang, J., *Evolution by gene duplication: an update.* Trends Ecol Evol, 2003. **18**(6): p. 292-298.

259. Richter, D., S. Fehr, and R. Harder, *The Guanosine 3',5'-Bis(diphosphate) (ppGpp) Cycle.* European Journal of Biochemistry, 1979. **99**(1): p. 57-64.

260. Cochran, J.W. and R.W. Byrne, *Isolation and Properties of a Ribosome-bound Factor Required for ppGpp and pppGpp Synthesis in Escherichia coli.* J Biol Chem, 1974. **249**(2): p. 353-360.

261. Tozawa, Y., et al., *Calcium-activated (p)ppGpp synthetase in chloroplasts of land plants.* J Biol Chem, 2007. **282**(49): p. 35536-45.

262. Avarbock, D., A. Avarbock, and H. Rubin, *Differential Regulation of Opposing RelMtb Activities by the Aminoacylation State of a tRNA·Ribosome·mRNA·RelMtb Complex†.* Biochemistry, 2000. **39**(38): p. 11640-11648.

263. Zheng, R., T.M. Jenkins, and R. Craigie, *Zinc folds the N-terminal domain of HIV-1 integrase, promotes multimerization, and enhances catalytic activity.* PNAS, 1996. **93**(24): p. 13659-13664.

264. Mildvan, A.S., D.J. Weber, and C. Abeygunawardana, *Solution Structure and Mechanism of the MutT Pyrophosphohydrolase*, in *Adv Enzymol Ramb*2006, John Wiley & Sons, Inc. p. 183-207.

265. Frick, D.N., et al., *Dual divalent cation requirement of the MutT dGTPase. Kinetic and magnetic resonance studies of the metal and substrate complexes.* J Biol Chem, 1994. **269**(3): p. 1794-1803.

266. Sawaya, M.R., et al., *Crystal Structures of Human DNA Polymerase β Complexed with Gapped and Nicked DNA: Evidence for an Induced Fit Mechanism.* Biochemistry, 1997. **36**(37): p. 11205-11215.

267. Xiao, H., et al., *Residual guanosine 3',5'-bispyrophosphate synthetic activity of relA null mutants can be eliminated by spoT null mutations.* J Biol Chem, 1991. **266**(9): p. 5980-90.

268. Gentry, D.R. and M. Cashel, *Mutational analysis of the Escherichia coli spoT gene identifies distinct but overlapping regions involved in ppGpp synthesis and degradation.* Mol Microbiol, 1996. **19**(6): p. 1373-1384.

269. Laffler, T. and J. Gallant, *spoT, a new genetic locus involved in the stringent response in E. coli.* Cell, 1974. **1**(1): p. 27-30.

270. Murray, K.D. and H. Bremer, *Control of spoT-dependent ppGpp synthesis and degradation in Escherichia coli.* J Mol Biol, 1996. **259**(1): p. 41-57.

271. Gentry, D.R. and M. Cashel, *Cellular localization of the Escherichia coli SpoT protein.* J Bacteriol, 1995. **177**(13): p. 3890-3.

272. Heinemeyer, E.A. and D. Richter, *Mechanism of the in vitro breakdown of guanosine 5'-diphosphate 3'-diphosphate in Escherichia coli.* PNAS, 1978. **75**(9): p. 4180-3.

273. Hernandez, V.J. and H. Bremer, *Escherichia coli ppGpp synthetase II activity requires spoT.* J Biol Chem, 1991. **266**(9): p. 5991-9.

274. Aravind, L. and E.V. Koonin, *The HD domain defines a new superfamily of metal-dependent phosphohydrolases.* Trends Biochem Sci, 1998. **23**(12): p. 469-72.

275. De Boer, H.A., et al., *Synthesis of guanosine 5´-diphosphate, 3´-diphosphate in spot mutants of Escherichia coli.* Biochim Biophys Acta Nucl Acids Protein Synth, 1977. **474**(2): p. 165-172.

276. Seyfzadeh, M., J. Keener, and M. Nomura, *spoT-dependent accumulation of guanosine tetraphosphate in response to fatty acid starvation in Escherichia coli.* PNAS, 1993. **90**(23): p. 11004-11008.

277. Vinella, D., et al., *Iron limitation induces SpoT-dependent accumulation of ppGpp in Escherichia coli.* Mol Microbiol, 2005. **56**(4): p. 958-970.

278. Battesti, A. and E. Bouveret, *Acyl carrier protein/SpoT interaction, the switch linking SpoT-dependent stress response to fatty acid metabolism.* Mol Microbiol, 2006. **62**(4): p. 1048-63.

279. Angelini, S., L. My, and E. Bouveret, *Disrupting the Acyl Carrier Protein/SpoT Interaction In Vivo: Identification of ACP Residues Involved in the Interaction and Consequence on Growth.* PLoS One, 2012. **7**(4): p. e36111.

280. Cashel, M., *Regulation of Bacterial ppGpp and pppGpp.* Annu Rev Microbiol, 1975. **29**(1): p. 301-318.

281. Stent, G.S. and S. Brenner, *A genetic locus for the regulation of ribonucleic acid synthesis.* PNAS, 1961. **47**: p. 2005-14.

282. Yang, X. and E.E. Ishiguro, *Dimerization of the RelA protein of Escherichia coli.* Biochem Cell Biol, 2001. **79**(6): p. 729-736.

283. Gropp, M., et al., *Regulation of Escherichia coli RelA requires oligomerization of the C-terminal domain.* J Bacteriol, 2001. **183**(2): p. 570-9.

284. Steinchen, W., et al., *Catalytic mechanism and allosteric regulation of an oligomeric (p)ppGpp synthetase by an alarmone.* PNAS, 2015.

285. Sajish, M., et al., *The Significance of EXDD and RXKD Motif Conservation in Rel Proteins.* J Biol Chem, 2009. **284**(14): p. 9115-9123.

286. Yang, W., J.Y. Lee, and M. Nowotny, *Making and Breaking Nucleic Acids: Two-Mg2+-Ion Catalysis and Substrate Specificity.* Mol Cell, 2006. **22**(1): p. 5-13.

287. Wendrich, T.M. and M.A. Marahiel, *Cloning and characterization of a relA/spoT homologue from Bacillus subtilis.* Mol Microbiol, 1997. **26**(1): p. 65-79.

288. Jain, V., M. Kumar, and D. Chatterji, *ppGpp: stringent response and survival.* J Microbiol, 2006. **44**(1): p. 1-10.

289. Ramagopal, S. and B.D. Davis, *Localization of the stringent protein of Escherichia coli on the 50S ribosomal subunit.* PNAS, 1974. **71**(3): p. 820-4.

290. LIENERT, I. and D. RICHTER, *Sringent Control in an Extreme Thermophilic Bacterium. Preliminary Characterization of a Guanosine 3',5'-Polyphosphate [(p)ppGpp] Synthesizing Enzyme from Thermus thermophilus.* J Gen Microbiol, 1981. **123**(2): p. 383-386.

291. Richter, D., *Formation of guanosine tetraphosphate (magic spot I) in homologous and heterologous systems.* FEBS Letters, 1973. **34**(2): p. 291-294.

292. Fehr, S. and D. Richter, *Stringent response of Bacillus stearothermophilus: evidence for the existence of two distinct guanosine 3',5'-polyphosphate synthetases.* J Bacteriol, 1981. **145**(1): p. 68-73.

293. Sy, J., Y. Ogawa, and F. Lipmann, *Nonribosomal Synthesis of Guanosine 5',3'-Polyphosphates by the Ribosomal Wash of Stringent Escherichia coli.* PNAS, 1973. **70**(7): p. 2145-2148.

294. Block, R. and A.W. Haseltine, *Purification and properties of stringent factor.* J Biol Chem, 1975. **250**(4): p. 1212-1217.

295. Payoe, R. and R.P. Fahlman, *Dependence of RelA-mediated (p)ppGpp formation on tRNA identity.* Biochemistry, 2011. **50**(15): p. 3075-83.

296. Knutsson Jenvert, R.M. and L. Holmberg Schiavone, *Characterization of the tRNA and ribosome-dependent pppGpp-synthesis by recombinant stringent factor from Escherichia coli.* FEBS J, 2005. **272**(3): p. 685-95.

297. English, B.P., et al., *Single-molecule investigations of the stringent response machinery in living bacterial cells.* PNAS, 2011. **108**(31): p. E365-73.

298. Friesen, J.D., et al., *A new relaxed mutant of Escherichia coli with an altered 50S ribosomal subunit.* PNAS, 1974. **71**(9): p. 3465-9.

299. Parker, J., et al., *A relaxed mutant with an altered ribosomal protein L11.* Mol Gen Genet MGG, 1976. **144**(1): p. 111-114.

300. Nierhaus, K.H. and D.N. Wilson, *Protein Synthesis and Ribosome Structure: Translating the Genome*2004, Weinheim, Germany: Wiley-VCH.

301. Wimberly, B.T., et al., *A Detailed View of a Ribosomal Active Site: The Structure of the L11–RNA Complex.* Cell, 1999. **97**(4): p. 491-502.

302. Agrawal, R.K., et al., *Localization of L11 protein on the ribosome and elucidation of its involvement in EF-G-dependent translocation1.* J Mol Biol, 2001. **311**(4): p. 777-787.

303. Rawat, U., et al., *Interactions of the release factor RF1 with the ribosome as revealed by cryo-EM.* J Mol Biol, 2006. **357**(4): p. 1144-1153.

304. Harms, J.M., et al., *Translational Regulation via L11: Molecular Switches on the Ribosome Turned On and Off by Thiostrepton and Micrococcin.* Mol Cell, 2008. **30**(1): p. 26-38.

305. Yang, X. and E.E. Ishiguro, *Involvement of the N terminus of ribosomal protein L11 in regulation of the RelA protein of Escherichia coli.* J Bacteriol, 2001. **183**(22): p. 6532-7.

306. Jenvert, R.M. and L.H. Schiavone, *The flexible N-terminal domain of ribosomal protein L11 from Escherichia coli is necessary for the activation of stringent factor.* J Mol Biol, 2007. **365**(3): p. 764-72.

307. Li, W., et al., *Functional conformations of the L11–ribosomal RNA complex revealed by correlative analysis of cryo-EM and molecular dynamics simulations.* RNA, 2006. **12**(7): p. 1240-1253.

308. Schrier, P.I. and W. Möller, *The involvement of 50S ribosomal protein L11 in the EF-G dependent GTP hydrolysis of E. coli ribosomes.* FEBS Letters, 1975. **54**(2): p. 130-134.

309. Pedersen, F.S. and N.O. Kjeldgaard, *Analysis of the relA gene product of Escherichia coli.* Eur J Biochem, 1977. **76**(1): p. 91-7.

310. Lund, E. and N.O. Kjeldgaard, *Metabolism of Guanosine Tetraphosphate in Escherichia coli.* European Journal of Biochemistry, 1972. **28**(3): p. 316-326.

311. Agirrezabala, X., et al., *The ribosome triggers the stringent response by RelA via a highly distorted tRNA.* Embo Reports, 2013. **14**(9): p. 811-816.

312. Mittelstaet, J., A.L. Konevega, and M.V. Rodnina, *Distortion of tRNA upon Near-cognate Codon Recognition on the Ribosome.* J Biol Chem, 2011. **286**(10): p. 8158-8164.

313. Shyp, V., et al., *Positive allosteric feedback regulation of the stringent response enzyme RelA by its product.* Embo Reports, 2012. **13**(9): p. 835-839.

314. Coleman, K.J., A. Cornish-Bowden, and J.A. Cole, *Activation of nitrite reductase from Escherichia coli K12 by oxidized nicotinamide-adenine dinucleotide.* Biochem J, 1978. **175**(2): p. 495-499.

315. Massey, V. and C. Veeger, *Studies on the reaction mechanism of lipoyl dehydrogenase.* Biochimica et Biophysica Acta, 1961. **48**(1): p. 33-47.

316. Jishage, M., et al., *Regulation of sigma factor competition by the alarmone ppGpp.* Genes Dev, 2002. **16**(10): p. 1260-70.

317. Carmona, M., et al., *In vivo and in vitro effects of (p)ppGpp on the sigma(54) promoter Pu of the TOL plasmid of Pseudomonas putida.* J Bacteriol, 2000. **182**(17): p. 4711-8.

318. Vogt, S.L., et al., *The stringent response is essential for Pseudomonas aeruginosa virulence in the rat lung agar bead and Drosophila melanogaster feeding models of infection.* Infect Immun, 2011. **79**(10): p. 4094-104.

319. Klinkenberg, L.G., et al., *The stringent response is required for full virulence of Mycobacterium tuberculosis in guinea pigs.* J Infect Dis, 2010. **202**(9): p. 1397-404.

320. Muller, C.M., et al., *Role of RelA and SpoT in Burkholderia pseudomallei virulence and immunity.* Infect Immun, 2012. **80**(9): p. 3247-55.

321. Dean, R.E., et al., *RelA regulates virulence and intracellular survival of Francisella novicida.* Microbiology, 2009. **155**(Pt 12): p. 4104-13.

322. Connell, S.R., et al., *Ribosomal Protection Proteins and Their Mechanism of Tetracycline Resistance.* Antimicrob Agents Chemother, 2003. **47**(12): p. 3675-3681.

323. Verbist, L., *The antimicrobial activity of fusidic acid.* Journal of Antimicrobial Chemotherapy, 1990. **25**(suppl B): p. 1-5.

324. Porse, B.T., et al., *The antibiotic thiostrepton inhibits a functional transition within protein L11 at the ribosomal GTPase centre1.* J Mol Biol, 1998. **276**(2): p. 391-404.

325. Wexselblatt, E., et al., *Relacin, a Novel Antibacterial Agent Targeting the Stringent Response.* PLoS Pathog, 2012. **8**(9): p. e1002925.

326. Ezequiel, W., et al., *ppGpp analogues as antibacterial compounds.* Nucleic Acids Symp Ser (Oxf), 2008(52): p. 633-4.

327. Wexselblatt, E., et al., *ppGpp analogues inhibit synthetase activity of Rel proteins from Gram-negative and Gram-positive bacteria.* Bioorg Med Chem, 2010. **18**(12): p. 4485-97.

328. Wermuth, C.G., et al., *The Practice of Medicinal Chemistry*. 4th ed2015: Elsevier Ltd.

329. Rhee, H.-W., et al., *Selective Fluorescent Chemosensor for the Bacterial Alarmone (p)ppGpp.* JACS, 2008. **130**(3): p. 784-785.

330. Zhang, P., et al., *Highly selective detection of bacterial alarmone ppGpp with an off–on fluorescent probe of copper-mediated silver nanoclusters.* Biosensors and Bioelectronics, 2013. **49**: p. 433-437.

331. Zheng, L.L. and C.Z. Huang, *Selective and sensitive colorimetric detection of stringent alarmone ppGpp with Fenton-like reagent.* Analyst, 2014. **139**(23): p. 6284-6289.

332. Lebbink, J.H.G., et al., *Magnesium Coordination Controls the Molecular Switch Function of DNA Mismatch Repair Protein MutS.* J Biol Chem, 2010. **285**(17): p. 13131-13141.

333. Batten, L.E., *Bacterial Kinases as Potential Targets for Broad-spectrum Antibiotics*, 2013, University of Southampton.

334. Fortier, A.H., et al., *Activation of macrophages for destruction of Francisella tularensis: identification of cytokines, effector cells, and effector molecules.* Infect Immun, 1992. **60**(3): p. 817-825.

335. Abd, H., et al., *Survival and Growth of Francisella tularensis in Acanthamoeba castellanii.* Appl Environ Microb, 2003. **69**(1): p. 600-606.

336. Lauriano, C.M., et al., *MglA regulates transcription of virulence factors necessary for Francisella tularensis intraamoebae and intramacrophage survival.* PNAS, 2004. **101**(12): p. 4246-4249.

337. Frankling, C.L., *Studies of RelA as an Antibacterial Target*, in *Faculty of Natural and Environmental Sciences*2015, University of Southampton.

338. Cordell, R.L., et al., *Quantitative profiling of nucleotides and related phosphate-containing metabolites in cultured mammalian cells by liquid chromatography tandem electrospray mass spectrometry.* Journal of Chromatography B, 2008. **871**(1): p. 115-124.

339. Apffel, A., et al., *Analysis of oligonucleotides by HPLC-electrospray ionization mass spectrometry.* Anal Chem, 1997. **69**(7): p. 1320-1325.

340. Segel, I.H., *Enzyme kinetics : behavior and analysis of rapid equilibrium and steady state enzyme systems*1975: Wiley, New York.

341. Hammes, G.G. and C.W. Wu, *Kinetics of Allosteric Enzymes.* Annual Review of Biophysics and Bioengineering, 1974. **3**(1): p. 1-33.

342. Copeland, R.A., *Enzymes: A practical Introduction to Structure, Mechanism, and Data Analysis*2000: Wiley.

343. Terpe, K., *Overview of bacterial expression systems for heterologous protein production: from molecular and biochemical fundamentals to commercial systems.* Applied Microbiology and Biotechnology, 2006. **72**(2): p. 211-222.

344. Sambrook, J. and D.W. Russell, *Molecular Cloning: A laboratory Manual*. Third edition ed2001: Cold Spring Harbor Laboratory Press.

345. Ng, H., *Effect of Decreasing Growth Temperature on Cell Yield of Escherichia coli.* J Bacteriol, 1969. **98**(1): p. 232-237.

346. Baneyx, F. and M. Mujacic, *Recombinant protein folding and misfolding in Escherichia coli.* Nat Biotech, 2004. **22**(11): p. 1399-1408.

347. Gaberc-Porekar, V. and V. Menart, *Potential for Using Histidine Tags in Purification of Proteins at Large Scale.* Chem Eng Technol, 2005. **28**(11): p. 1306-1314.

348. Structural Genomics, C., et al., *Protein production and purification.* Nat methods, 2008. **5**(2): p. 135-146.

349. Hwang, S., et al., *Methanol Strengthens Hydrogen Bonds and Weakens Hydrophobic Interactions in Proteins – A Combined Molecular Dynamics and NMR study.* J Phys Chem B, 2011. **115**(20): p. 6653-6660.

350. Buckstein, M.H., J. He, and H. Rubin, *Characterization of Nucleotide Pools as a Function of Physiological State in Escherichia coli.* J Bacteriol, 2008. **190**(2): p. 718-726.

351. Ratnayake-Lecamwasam, M., et al., *Bacillus subtilis CodY represses early-stationary-phase genes by sensing GTP levels.* Genes Dev, 2001. **15**(9): p. 1093-1103.

352. Kriel, A., et al., *Direct Regulation of GTP Homeostasis by (p)ppGpp: A Critical Component of Viability and Stress Resistance.* Mol Cell, 2012. **48**(2): p. 231-241.

353. Krásný, L. and R.L. Gourse, *An alternative strategy for bacterial ribosome synthesis: Bacillus subtilis rRNA transcription regulation*. Vol. 23. 2004. 4473-4483.

354. Reeh, S., S. Pedersen, and J. Friesen, *Biosynthetic regulation of individual proteins in relA + and relA strains of Escherichia coli during amino acid starvation.* Mol Gen Genet, 1976. **149**(3): p. 279-289.

355. O'Farrell, P.H., *The suppression of defective translation by ppGpp and its role in the stringent response.* Cell, 1978. **14**(3): p. 545-557.

356. Schreiber, G., et al., *Overexpression of the relA gene in Escherichia coli.* J Biol Chem, 1991. **266**(6): p. 3760-3767.

357. Chipman, D.M. and B. Shaanan, *The ACT domain family.* Current Opinion in Structural Biology, 2001. **11**(6): p. 694-700.

358. Wade, H.E. and H.K. Robinson, *Magnesium ion-independent ribonucleic acid depolymerases in bacteria.* Biochem J, 1966. **101**(2): p. 467-79.

359. Maguire, B.A., et al., *A novel chromatography system to isolate active ribosomes from pathogenic bacteria.* RNA, 2008. **14**(1): p. 188-95.

360. Lancaster, L., et al., *Orientation of Ribosome Recycling Factor in the Ribosome from Directed Hydroxyl Radical Probing.* Cell, 2002. **111**(1): p. 129-140.

361. Dunkle, J.A., et al., *Structures of the Escherichia coli ribosome with antibiotics bound near the peptidyl transferase center explain spectra of drug action.* PNAS, 2010. **107**(40): p. 17152-17157.

362. Spedding, G., *Ribosomes and protein synthesis: a practical approach*1990: IRL Press at Oxford University Press.

363. Meskauskas, A., J.A. Leshin, and J.D. Dinman, *Chromatographic Purification of Highly Active Yeast Ribosomes.* J Vis Exp, 2011(56): p. 3214.

364. Piir, K., et al., *Ribosome degradation in growing bacteria.* Embo Reports, 2011. **12**(5): p. 458-462.

365. Fersht, A., *Enzyme Structure and Mechanism*. second ed1977, New York: W.H. Freeman and Company.

366. Grant, G.A., *The ACT Domain: A Small Molecule Binding Domain and Its Role as a Common Regulatory Element.* J Biol Chem, 2006. **281**(45): p. 33825-33829.

367. Copeland, R.A., *Evaluation of Enzyme Inhibitors in Drug Discovery*. second ed2013, New Jersey: John Wiley and Sons Inc.

368. Berg, J.M., J.L. Tymoczko, and S. L., *Biochemistry*. 5th ed2002, New York: W H Freeman.

369. Copeland, R.A., *Mechanistic considerations in high-throughput screening.* Anal Biochem, 2003. **320**(1): p. 1-12.

370. Izaki, K., M. Matsuhashi, and J.L. Strominger, *Glycopeptide transpeptidase and D-alanine carboxypeptidase: penicillin-sensitive enzymatic reactions.* PNAS, 1966. **55**(3): p. 656-663.

371. Poulin, R., et al., *Mechanism of the irreversible inactivation of mouse ornithine decarboxylase by alpha-difluoromethylornithine. Characterization of sequences at the inhibitor and coenzyme binding sites.* J Biol Chem, 1992. **267**(1): p. 150-158.

372. Hara, A. and J. Sy, *Guanosine 5'-triphosphate, 3'-diphosphate 5'-phosphohydrolase. Purification and substrate specificity.* J Biol Chem, 1983. **258**(3): p. 1678-83.

373. Carter, S.G. and D.W. Karl, *Inorganic phosphate assay with malachite green: An improvement and evaluation.* J Biochem Bioph Meth, 1982. **7**(1): p. 7-13.

374. Itaya, K. and M. Ui, *A new micromethod for the colorimetric determination of inorganic phosphate.* Clin Chim Acta, 1966. **14**(3): p. 361-366.

375. Kitagawa, M., et al., *Complete set of ORF clones of Escherichia coli ASKA library (A Complete Set of E. coli K-12 ORF Archive): Unique Resources for Biological Research.* DNA Research, 2006. **12**(5): p. 291-299.

376. Okoh, M.P., et al., *A Biosensor for Inorganic Phosphate Using a Rhodamine-Labeled Phosphate Binding Protein†.* Biochemistry, 2006. **45**(49): p. 14764-14771.

377. McConnell, J.L. and B.E. Wadzinski, *Targeting Protein Serine/Threonine Phosphatases for Drug Development.* Mol Pharmacol, 2009. **75**(6): p. 1249-1261.

378. Newton, G.L., et al., *A coupled spectrophotometric assay for l-cysteine:1-d-myo-inosityl 2-amino-2-deoxy-α-d-glucopyranoside ligase and its application for inhibitor screening.* Anal Biochem, 2006. **353**(2): p. 167-173.

379. Crooks, P.A., et al., *Nucleoside sultones: synthons for the preparation of novel nucleotide analogs. 1. Synthesis and ring-opening reactions.* J Org Chem, 1992. **57**(10): p. 2830-2835.

380. Moukha-chafiq, O. and R.C. Reynolds, *Parallel Solution-Phase Synthesis of an Adenosine Antibiotic Analog Library.* ACS Comb Sci, 2013. **15**(3): p. 147-152.

381. Romani, A. and A. Scarpa, *Regulation of cell magnesium.* Arch Biochem Biophys, 1992. **298**(1): p. 1-12.

382. Moomaw, A.S. and M.E. Maguire, *The Unique Nature of Mg(2+) Channels.* Physiology (Bethesda, Md.), 2008. **23**: p. 275-285.

383. Gupta, P.B., et al., *Identification of Selective Inhibitors of Cancer Stem Cells by High-Throughput Screening.* Cell, 2009. **138**(4): p. 645-659.

384. Baldwin, J., et al., *High-throughput Screening for Potent and Selective Inhibitors of Plasmodium falciparum Dihydroorotate Dehydrogenase.* J Biol Chem, 2005. **280**(23): p. 21847-21853.

385. von Ahsen, O. and U. Bömer, *High-Throughput Screening for Kinase Inhibitors.* ChemBioChem, 2005. **6**(3): p. 481-490.

386. Studier, F.W., *Stable Expression Clones and Auto-Induction for Protein Production in E. coli*, in *Structural Genomics*, Y.W. Chen, Editor 2014, Humana Press. p. 17-32.

387. Debye, P., *Molecular-weight Determination by Light Scattering.* J Phys Colloid Chem, 1947. **51**(1): p. 18-32.

388. Shcherbakov, D. and W. Piendl, *A novel view of gel-shifts: Analysis of RNA–protein complexes using a two-color fluorescence dye procedure.* Electrophoresis, 2007. **28**(5): p. 749-755.

389. Dranchak, P., et al., *Profile of the GSK Published Protein Kinase Inhibitor Set Across ATP-Dependent and-Independent Luciferases: Implications for Reporter-Gene Assays.* PLoS One, 2013. **8**(3): p. e57888.

390. Vazquez, M.J., et al., *Determination of phosphate in nanomolar range by an enzyme-coupling fluorescent method.* Anal Biochem, 2003. **320**(2): p. 292-298.

391. Batten, L.E., *Bacterial kinases as potential targets for broad spectrum antibiotics*, in *Faculty of Natural and Environmental Sciences*2013, University of Southampton.

392. Rosano, G.L. and E.A. Ceccarelli, *Recombinant protein expression in Escherichia coli: advances and challenges.* Front Microbiol, 2014. **5**: p. 172.

393. Terpe, K., *Overview of tag protein fusions: from molecular and biochemical fundamentals to commercial systems.* Appl Microbiol Biot, 2003. **60**(5): p. 523-533.

394. Kruger, N.J., *The Bradford Method For Protein Quantitation*, in *The Protein Protocols Handbook*. p. 17-24.

395. Aranda, P.S., D.M. LaJoie, and C.L. Jorcyk, *Bleach gel: a simple agarose gel for analyzing RNA quality.* Electrophoresis, 2012. **33**(2): p. 366-9.

396. McPherson, A., *Current approaches to macromolecular crystallization.* Eur J Biochem, 1990. **189**(1): p. 1-23.